Titre: Title:	Evolution of the Hydrogeotechnical Properties of Paste Tailings Deposited on the Surface
Auteur: Author:	Vincent Martin
Date:	2018
Type:	Mémoire ou thèse / Dissertation or Thesis
Référence: Citation:	Martin, V. (2018). Evolution of the Hydrogeotechnical Properties of Paste Tailings Deposited on the Surface [Thèse de doctorat, École Polytechnique de Montréal]. PolyPublie. https://publications.polymtl.ca/3097/

UNIVERSITÉ DE MONTRÉAL

EVOLUTION OF THE HYDROGEOTECHNICAL PROPERTIES OF PASTE TAILINGS DEPOSITED ON THE SURFACE

VINCENT MARTIN

DÉPARTEMENT DES GÉNIES CIVIL, GÉOLOGIQUE ET DES MINES

ÉCOLE POLYTECHNIQUE DE MONTRÉAL

THÈSE PRÉSENTÉE EN VUE DE L'OBTENTION

DU DIPLÔME DE PHILOSOPHIAE DOCTOR

(GÉNIE MINÉRAL)

AVRIL 2018

UNIVERSITÉ DE MONTRÉAL

ÉCOLE POLYTECHNIQUE DE MONTRÉAL

Cette thèse intitulée :

EVOLUTION OF THE HYDROGEOTECHNICAL PROPERTIES OF PASTE TAILINGS DEPOSITED ON THE SURFACE

présentée par : MARTIN Vincent

en vue de l'obtention du diplôme de : Philosophiae Doctor

a été dûment acceptée par le jury d'examen constitué de :

M. BUSSIÈRE Bruno, Ph. D., président

M. PABST Thomas, Ph. D., membre et directeur de recherche

M. AUBERTIN Michel, Ph. D., membre et codirecteur de recherche

M. LI Li, Ph. D., membre

M. SIMMS Paul H., Ph. D., membre externe

CITATION

“Unless someone like you cares a whole awful lot,

Nothing is going to get better.

It's not.”

- Dr. Seuss, The Lorax

“One need not hope in order to undertake, nor succeed in order to persevere”

- William the Silent

ACKNOWLEDGEMENTS

After so many years working on this project, there are many people to whom I am grateful.

First and foremost, thank you to Michel Aubertin. He is an exceptional professor, wonderful mentor, and outstanding individual, it has been a pleasure to study and work under his supervision. Thank you for everything.

Thank you to Thomas Pabst. You went from lab colleague and friend, to work colleague and thesis advisor. I am proud to be your student and thankful for your help. Thank you for your generosity, your time, your Sundays, your good and crazy ideas. I always look forward to our discussions (work related or not).

Thank you to the partners of the Research Institute on Mines and the Environment (RIME), to Barrick Gold Corporation, to the Natural Sciences and Engineering Research Council of Canada (NSERC) and to the Fonds de recherche nature et technologies Québec (FRQNT) for the funding and financial support that made this project possible.

Thank you to Jacques McMullen for his vision and belief that I could do this.

Thank you to Guosheng Zhan and John Meyer for teaching me how to integrate research data in the real world.

Thank you to Étienne Bélanger for all the technical support and ideas, and to Noura El Harrak for the help in the laboratory.

Thank you to Mostafa Benzaazoua for his support and involvement in many stages of this project.

Thank you to the students and colleagues who, throughout the years, were present and supported me. I will probably forget some, but must name a few: Véronique, Daniel, Romain, Dominic, Nicolas, Richard, Lincar, Abtin, Monica, Marie-Lin, Julien, Adrien, Gabrielle, Lucette, Manon, Monique and many more.

Thank you to my friends outside of Polytechnique, who through smiles, hugs, questions, discussions, babysitting, and so much more, have contributed to my happiness and making my life so gratifying. A special shout out to Marie-Andrée, Philippe, David (×2), Emmanuelle, Martin, Magalie and Pierre.

Thank you to François, for the tips and the suggestions.

Thank you to Michèle and Jean-Baptiste, for the presence in good and tough times, and for the priceless friendship. I will always be grateful for your presence in my life.

Thank you to my family, Olivier, Catherine, Jean-Philippe, Marie-Ève, Bertille, Thierry and Paule for their belief that I would endure, that I would eventually succeed in finishing this project. A special thanks to Jean-Philippe. You are an inspiration, and your insights and comments are always relevant and useful.

Thank you to my parents, Michèle and Raymond, for the unconditional love, the reassuring presence, the wise words, and all the help (and cookies) necessary to bring this project to an end.

Thank you to Éloïse and Victor. You were a light in the dark times. You remind me of what is important and will always be my greatest accomplishment. My weekends are yours now.

Finally, thank you to Caroline. Thank you for believing in me. Thank you for supporting me throughout the years. Thank you for keeping me sane. Thank you for your strength, your determination, your kindness, your patience, and your love. I would not have made it here without you.

RÉSUMÉ

Les résidus miniers sont généralement produits et transportés à des teneurs en eau élevées (teneurs en solides inférieures à 45%) et entreposés en surface dans des parcs à résidus. La stabilité géotechnique des ouvrages de retenue constitue un défi pour l'industrie, notamment en raison des quantités d'eau importantes en amont des digues. De plus, les minéraux sulfureux (ex. pyrite) parfois contenus dans les résidus peuvent s'oxyder et générer du drainage minier acide (DMA) ou du drainage neutre contaminé (DNC). Plusieurs solutions ont été proposées ces dernières années afin de tenter de minimiser l'impact environnemental des rejets de concentrateur pendant l'opération de la mine et à sa fermeture. L'épaississement des résidus miniers et en particulier la production de résidus en pâte (avec une teneur en solides entre 70% - 85%), fait partie des solutions potentielles visant à favoriser la gestion intégrée des rejets.

Les résidus en pâte contiennent moins d'eau interstitielle, ce qui favorise leur consolidation et améliore leur comportement géotechnique. Ils se désaturent cependant plus rapidement que des résidus en pulpe et pourraient donc être plus susceptibles de générer du drainage contaminé s'ils sont réactifs. Les mécanismes qui contribuent à la désaturation des résidus en pâte déposés en surface doivent donc être étudiés afin d'évaluer et d'optimiser cette approche de déposition. Les mouvements de l'eau dans un empilement de résidus en pâte sont principalement influencés par les propriétés hydrogéologiques des résidus, les conditions climatiques, et d'autres facteurs opérationnels.

La présente étude porte sur l'évaluation du comportement hydrogéotechnique des résidus en pâte de la mine Bulyanhulu (Tanzanie). Cette mine a déposé des résidus en pâte en surface pendant 15 ans, du début de l'opération, en mars 2001, jusqu'à 2016. Des essais de terrain ont été réalisés sur le parc à résidus de la mine au cours de l'automne 2004 afin d'évaluer les flux d'oxygène à la surface de ces résidus pour des degrés de saturation variables. Des échantillons de résidus ont aussi été prélevés et envoyés au laboratoire à Polytechnique Montréal.

Ces matériaux ont été caractérisés afin de déterminer leurs propriétés géotechniques (granulométrie, densité relative des grains, limites d'Atterberg), minéralogiques et hydrogéologiques (conductivité hydraulique saturée et courbe de rétention d'eau). Les courbes de rétention d'eau ont été mesurées en cellules Tempe et au moyen d'une cellule de pression (ou

pressure plate extractor) avec deux porosités initiales différentes, représentant respectivement un état relativement dense et lâche.

Deux types de modèles physiques ont aussi été développés au laboratoire afin d'étudier, dans des conditions contrôlées, le comportement hydrogéotechnique des résidus en pâte déposés en surface. Des colonnes d'environ 30 cm de diamètre ont permis d'étudier l'effet de l'épaisseur des couches de résidus en pâte sur leur désaturation progressive (pour des épaisseurs initiales de 10 cm, 20 cm et 30 cm). Deux essais en colonnes ont également été réalisés afin d'étudier l'effet de la teneur en eau gravimétrique initiale (w0 ≈ 40% et ≈ 50%) sur la désaturation des résidus. La durée de ces essais était d'environ 60 jours. Les pertes d'eau par drainage et évaporation, l'épaisseur des couches et la succion dans les résidus ont été mesurées en continu. Des images de la surface ont également permis de quantifier l'évolution des fractures à la surface des résidus.

Des essais de déposition multicouche ont également été réalisés dans des colonnes (diamètre d'environ 30 cm) afin d'évaluer l'influence de la séquence de déposition sur le comportement hydrogéologique des résidus en pâte. Des couches de résidus en pâte étaient déposées en séquence dans les colonnes. La durée entre chaque déposition était variable (15 à 180 jours). Les pertes d'eau par drainage et évaporation, les pressions interstitielles, les teneurs en eau volumique et l'épaisseur des couches ont été suivis tout au long des essais. Plusieurs essais de consommation d'oxygène ont également été réalisés afin d'évaluer le flux d'oxygène dans les résidus en fonction de l'évolution de leur teneur en eau.

Le comportement des résidus dans les colonnes en laboratoire a été simulé au moyen du logiciel Vadose/W (GeoSlope Inc, 2007). Les simulations numériques représentaient relativement bien les résultats des essais de laboratoire et ont ensuite été extrapolées pour des conditions plus représentatives du terrain. Un empilement de résidus en pâte déposés à la surface a été simulé en 1D et l'effet de plusieurs paramètres a été étudié numériquement : l'épaisseur des couches de résidus, le temps entre chaque déposition couches, les propriétés hydrogéologiques des résidus miniers et du sol sous-jacent, la position de la nappe phréatique, et les conditions climatiques.

Il a été observé que les résidus en pâte de la mine Bulyanhulu avaient des propriétés de base et hydrogéologiques comparables aux résidus provenant d'autres opérations minières en roches dures. Les flux d'oxygène à la surface de ces derniers augmentaient lorsque les rejets de concentrateur se désaturaient. Les essais en colonne au laboratoire ainsi que les modélisations numériques ont

indiqué que la désaturation d'un empilement de résidus en pâte se faisait principalement par évaporation pour les conditions simulées. La présence de couches de résidus partiellement saturées sous des résidus frais (initialement saturés) accélérait la désaturation initiale (par drainage) de ces derniers. En général, la désaturation par drainage se produisait le premier jour suivant la mise en place de la couche fraîche de résidus en pâte. Ensuite, le gradient hydraulique s'inversait (vers le haut) et la couche de résidus à la surface se désaturait principalement par évaporation. Une approche analytique a été développée pour évaluer la direction et la quantité d'eau qui migre entre les différentes couches de résidus miniers dans les colonnes.

La technique des résidus en pâte déposés en surface est une méthode de gestion des rejets de concentrateur prometteuse qui peut s'avérer utile dans certains cas. Mais les résidus en pâte se désaturent plus rapidement que des résidus dits « conventionnels » (car ils contiennent moins d'eau que ces derniers). La désaturation des résidus réactifs doit donc être contrôlée afin de prévenir les réactions d'oxydation qui génèrent du drainage contaminé. Il est possible de conserver un degré de saturation relativement élevé dans les résidus en s'assurant que les couches déposées ne sont pas trop minces et que le temps de repos entre le dépôt de deux couches est minimisé. La teneur en eau dans les résidus miniers est aussi influencée par la granulométrie de ces derniers puisque les matériaux plus fins retiennent habituellement plus d'eau. Finalement, les travaux menés ici ont permis de mettre en évidence l'effet des conditions climatiques et des variations saisonnières sur le degré de saturation dans un empilement de résidus en pâte.

ABSTRACT

Mine tailings are typically produced and transported at high water contents (solids content less than 45%) and stored at the surface in tailings ponds. The geotechnical stability of the retaining structures is a challenge for the mining industry, especially because of the large volumes of water stored upstream the dikes. In addition, sulphides (e.g. pyrite), sometimes present in the tailings, may oxidize and generate acid mine drainage (AMD) or contaminated neutral drainage (CND). Many solutions have been proposed in the last years to minimise the environmental impact of the tailings during the operation and after the closure of a mine. Thickening of the mine tailings, and more specifically production of paste tailings (with a solids content between 70% and 85%), is one of the solutions proposed for integrated management of tailings.

Paste tailings contain less pore water, which will favor consolidation and improve their geotechnical behaviour. However, they also desaturate more rapidly than slurry tailings and could therefore be more susceptible to generate contaminated drainage if they are reactive. The mechanisms that contribute to the desaturation of paste tailings deposited on the surface must therefore be studied to evaluate and optimise this disposal method. Water movements in a paste tailings stack are mainly influenced by the hydrogeological properties of the tailings, the climatic conditions, and other operational factors.

This project studies the evolution of the hydrogeotechnical properties of paste tailings from the Bulyanhulu mine (Tanzania). This mining operation used surface paste tailings disposal for 15 years, from the beginning of the operation, in March 2001, until 2016. Field tests were completed in the tailings storage facility during the Fall of 2004 to evaluate surface oxygen fluxes in the tailings for varying degrees of saturation. Tailings samples were also collected and sent to the laboratory at Polytechnique Montreal.

These materials were characterized to determine their main geotechnical (particle size distribution, relative density of the solid particles, Atterberg limits), mineralogical and hydrogeological (saturated hydraulic conductivity and water retention curve) properties. The water retention curves were measured at two different initial porosities (representing dense and soft tailings) in Tempe cells and using a pressure plate extractor.

Two physical models were also developed in the laboratory to study, under controlled conditions, the hydrogeotechnical behaviour of paste tailings deposited on the surface. Columns, with an

approximate diameter of 30 cm, were used to study the influence of the thickness of paste tailings layers on their progressive desaturation (for initial thicknesses of 10 cm, 20 cm and 30 cm). Two column tests were also carried out to study the influence of the initial gravimetric water content ($w0 \approx 40\%$ and $\approx 50\%$) on the desaturation behaviour of the paste tailings. These tests lasted approximately 60 days. The losses of water by drainage and evaporation, the thickness of the tailings, and the suction in the tailings were monitored during the tests. The evolution of fractures at the surface of the paste tailings was also analyzed using image analyses.

Columns with multilayer deposition (approximate diameter of 30 cm) were also used to study the influence of the deposition sequence on the hydrogeological behaviour of the paste tailings. Paste tailings layers were deposited in sequence in the columns. The time between the placement of two fresh layers was variable (15 to 180 days). The loss of water by drainage and evaporation, the pore water pressure, the volumetric water content and the thickness of the layers were recorded during the tests. Multiple oxygen consumption tests were also carried out during the tests to evaluate the evolution of the surface oxygen fluxes in the tailings with changes in the water content of the tailings layer.

The behaviour of the tailings in the laboratory columns was also simulated using the software Vadose/W (GeoSlope Inc., 2007). The numerical simulations reproduced adequately the laboratory models and were therefore extrapolated to conditions more representative of the field. A 1D paste tailings surface stack was simulated and the effect of multiple parameters was studied: the thickness of the tailings layers, the time between the deposition of two fresh paste tailings layers, the hydrogeological properties of the tailings and of the underlying soil, the position of the water table, and the climatic conditions at the site.

It was observed that the paste tailings from the Bulyanhulu mine had hydrogeological properties similar to other hard rock mines. The oxygen fluxes at the surface of the tailings increased as they were desaturating. The laboratory column tests and numerical simulation also demonstrated that the desaturation of a surface paste tailings stack in the simulated conditions was mainly by evaporation. The presence of partially saturated layers of tailings below the fresh tailings layers accelerated desaturation by drainage of the surface layer. In general, desaturation by drainage occurred during the first day following the placement of the fresh layer of surface paste tailings. Afterwards, the hydraulic gradient would reverse (towards the surface) and the surface layer of

paste tailings would mainly desaturate by evaporation. An analytical approach was developed to evaluate the direction and the amount of water migrating between the various layers of paste tailings in the laboratory columns.

The method of surface paste tailings disposal is a promising solution that may be useful in certain situations. However, surface paste tailings desaturate more rapidly than conventional (slurry) tailings (as the former contain less water initially than the latter). It is therefore necessary to ensure that desaturation of potentially reactive tailings is controlled to avoid the oxidation reactions that are responsible for the generation of contaminated mine drainage. It is possible to keep an elevated degree of saturation in the tailings by increasing layer thickness and decreasing the time between the placement of two fresh tailings layers. The water content in the tailings is also influenced by their particle size distribution, as finer materials typically retain more water. Finally, the work presented here also allowed to demonstrate the influence of climatic conditions and seasonal variations on the degree of saturation of a surface paste tailings stack.

TABLE OF CONTENTS

LIST OF TABLES

LIST OF FIGURES

LIST OF SYMBOLS AND ABBREVIATIONS

A	Area [L^2]
A'	Permeability coefficient in the Philip (1957) equation [$L \cdot T^{-1}$]
A_{col}	Cross-sectional area of the laboratory column [L^2]
A_{cracks}	Horizontal surface area of the cracks (not to the total exposed surface area in the cracks) [L^2]
A_D	Area of the cross-section [L^2]
A_{intact}	Surface area of the intact tailings [L^2]
A_{RH}	Inverse of the relative humidity at the material surface [-]
A_{total}	Total area of the tailings facility [L^2]
AE	Actual evaporation [$L \cdot T^{-1}$]
AEV	Air entry value [L] or [$M \cdot L^{-1} \cdot T^{-2}$]
AMD	Acid mine drainage
a_{fx}	Model parameter of the Fredlund and Xing model (1994) associated with the inflection point of the WRC [L] or [$M \cdot L^{-1} \cdot T^{-2}$]
a_{MK}	Smoothing coefficient in the MK model (Unitless)
a_v	Coefficient of compressibility [$L \cdot T^2 \cdot M^{-1}$]
B_{RH}	Inverse of the air relative humidity [-]
b	Pore size factor in the MK model (cm^2)
b_{fx}	$\ln(1 \times 10^6)$ (Fredlund et al. (1994) model)

C	Concentration of oxygen [$M \cdot L^{-3}$]
C_C	Coefficient of consolidation [-]
C_G	Adimensional material constant (-) in the Kozeny-Carman modified model which can be fixed at 0.1 according to Mbonimpa et al. (2002)
C_{KC}	Adimensional material constant in the Kozeny-Carman model [-]
CIF	Crack intensity factor
CMD	Contaminated mine drainage
CND	Contaminated neutral drainage
C_p	Pyrite content over mass of dry tailings [$M \cdot M^{-1}$]
C_U	Uniformity coefficient [L/L]
$C(\psi)$	Correlation function of the Fredlund and Xing (1994) model
C_ψ	Correction factor for dryness in the MK model
c_{vap}	Vapour density [$M \cdot L^{-3}$]
c'_{vap}	Saturation vapour density (0.017 kg/m^3 at 20°C)
D^*	Bulk diffusion coefficient [$L^2 \cdot T^{-1}$]
D_{10}	Grain diameter at which 10% of the material is smaller on the cumulative particle size distribution curve [L]
D_{50}	Grain diameter at which 50% of the material is smaller on the cumulative particle size distribution curve [L]
D_{60}	Grain diameter at which 60% of the material is smaller on the cumulative particle size distribution curve [L]

D_a'	Diffusion coefficient of water vapour in air (2.417×10^{-5} m^2/s at 20°C)
D_a^0	Diffusion coefficient of oxygen in air ($\approx 1.8\times10^{-5}$ m^2/s)
D_e	Effective diffusion coefficient [$L^2\cdot T^{-1}$]
D_H	Equivalent particle diameter [L]
D_r	Relative density of the solid particles [-]
D_v	Coefficient of diffusion of vapour of the material [$L^2\cdot T^{-1}$]
D_{vap}	Molecular diffusivity of water vapour in air [$L^2\cdot T^{-1}$]
D_w^0	Diffusion coefficient of oxygen in air ($\approx 2.5\times10^{-9}$ m^2/s)
d	Diameter [L]
E	Evaporation [$L^3\cdot L^{-2}$] or [L]
E_a	Potential rate of evaporation from the Dalton-type equation [$L\cdot T^{-1}$]
E_{crack}	Evaporation from the desiccation cracks [$L\cdot T^{-1}$]
E_{intact}	Evaporation from the intact tailings [$L\cdot T^{-1}$]
E_{total}	Total evaporation from the tailings facility [$L\cdot T^{-1}$]
ET	Evapotranspiration [$L^3\cdot L^{-2}$] or [L]
e	Void ratio [-]
e_0	Initial void ratio [-]
e_T	Void ratio at time t [-]
e_{T-1}	Void ratio at the previous time t-1 [-]

e_a Void ratio when the suction is equal to the AEV [-]

e_{air} Vapour pressure of the air above the evaporating surface [$M \cdot L^{-1} \cdot T^{-2}$]

e_f Final void ratio [-]

e_i Initial void ratio [-]

e_{in} Surface void ratio at crack initiation [-]

e_p Pulp void ratio [-]

e_s Final void ratio [-]

e_{sa} Saturation vapour pressure at the temperature of the water [$M \cdot L^{-1} \cdot T^{-2}$]

e_{surf} Vapour pressure at the surface of the material [$M \cdot L^{-1} \cdot T^{-2}$]

e_t Surface void ratio of the intact area [-]

e_{va} Vapour pressure of the air [$M \cdot L^{-1} \cdot T^{-2}$]

F Diffusive oxygen flux [$M \cdot L^{-2} \cdot T^{-1}$]

F_{O_2} Steady-state oxygen flux [$M \cdot L^{-2} \cdot T^{-1}$]

f_v Vapour flux [$M \cdot L^{-2} \cdot T^{-1}$]

$f(u)$ Wind mixing function

G Soil heat flux (W/m^2)

G_s Specific gravity

g Acceleration of gravity (9.81 m/s^2)

H Henry's equilibrium constant ($H \approx 0.03$ at 20°C)

H_s	Sensitive heat flux (W/m^2)
H_w	Height of water above the soil [L]
h	Hydraulic head [L]
h_L	Layer thickness [L]
h_f	Final layer thickness [L]
h_j	Hydraulic head at point j [L]
h_{co}	Average height of the capillary rise in the MK model
h_i	Initial thickness [L]
$h_{reservoir}$	Height of the reservoir in the MOC tests
I	Cumulative infiltration per surface area [$L^3 \cdot L^{-2}$] or [L]
I_{nf}	Infiltrability [$L^3 \cdot L^{-2} \cdot T^{-1}$] or [$L \cdot T^{-1}$]
I_{nt}	Interception (uptake of water by plants) [$L^3 \cdot L^{-2}$] or [L]
i	Hydraulic gradient [$L \cdot L^{-1}$]
K’	Reactivity of pyrite with oxygen (K’ $\approx 5\times10^{-10}$ $m^3O_2m^{2}⁄s$)
KC	Kozeny-Carman model
KCM	Kozeny-Carman modified model
K_r	Oxygen reactivity rate coefficient [T^{-1}]
K_r^*	Bulk oxygen reactivity rate coefficient [T^{-1}]
k_{fs}	Field saturated (satiated) hydraulic conductivity [$M \cdot L^{-1}$]

k_{KC}	Predicted saturated hydraulic conductivity with the Kozeny-Carman model [$L \cdot T^{-1}$]
k_{KCM}	Predicted saturated hydraulic conductivity with the Kozeny-Carman modified model [$L \cdot T^{-1}$]
k_{rel}	Relative hydraulic conductivity [-]
k_s or k_{sat}	Saturated hydraulic conductivity [$L \cdot T^{-1}$]
k_u	Unsaturated hydraulic conductivity [$L \cdot T^{-1}$]
L	Water leaching from waste [$L^3 \cdot L^{-2}$] or [L]
L_D	Darcy length [L]
L_f	Depth of the wetting front [L]
L_{OT}	Depth in the tailings from the surface at which the oxygen concentration becomes nil [L]
M	Mass [M]
M_L	Mass of tailings in the layer [M]
M_s	Mass of the solids [M]
M_T	Total mass (water and solids) [M]
M_{pulp}	Mass of pulp [M]
M_w	Mass of water [M]
MDC	Main drying curve
MK	Modified Kovács model
ML	Multilayer

MOC	Modified oxygen consumption
MWC	Main wetting curve
m_{MK}	Shape coefficient in the MK model
m_{fx}	Smoothing parameter of the curve in the Fredlund and Xing (1994) model linked to the residual water content and the correction function (C(ψ))
m_v	Coefficient of volumetric compressibility [$L \cdot T^2 \cdot M^{-1}$]
n	Porosity [-]
n_{consol}	Porosity of the consolidated (settled) tailings layer [-]
n_{fresh}	Initial porosity of the fresh tailings layer [-]
n_{fx}	Smoothing parameter of the Fredlund and Xing (1994) model that controls the slope of the inflection point of the WRC [-]
n_p	Pulp porosity (when S_r = 100%) [-]
P	Precipitation [$L^3 \cdot L^{-2}$] or [L]
$P_{No\ D}$	Percentage by weight smaller than size D
$P_{No\ d}$	Percentage by weight smaller than size d
P_m	Gravimetric pulp density [$M \cdot M^{-1}$]
P_v	Volumetric pulp density [$L^3 \cdot L^{-3}$]
P_{vap}	Partial pressure of water vapour [$M \cdot L^{-1} \cdot T^{-2}$]
PE	Potential evaporation [$L \cdot T^{-1}$]
PPE	Pressure plate extractor

PSD	Particle size distribution
p_a	Unitless exponent of the θ_a function [-]
p_w	Unitless exponent of the θ function [-]
Q	Total flow rate of water [$L^3 \cdot T^{-1}$]
Q_{net}	Net solar radiation [$M \cdot L \cdot T^{-2} \cdot L^{-2} \cdot T^{-1}$] or [$L \cdot T^{-1}$] water equivalent
q	Specific flux or Darcy velocity [$L \cdot T^{-1}$]
q_L	Unit flux between two tailings layers [$L \cdot T^{-1}$]
q_{fx}	Correction factor in the Fredlund et al. (1994) model
$q_{y=0\ m}$	Outflow at the tailings/sand interface in the 1D numerical simulations [$L \cdot T^{-1}$]
R	Universal gas constant (8.3143 J/mol·K)
R_{ech}	Recharge [$L^3 \cdot L^{-2}$] or [L]
RD_p	Relative pulp density [-]
RH	Relative humidity [-]
RH_a	Relative humidity in the air [-]
RH_{surf}	Relative humidity at the surface of the material [-]
SM	Snowmelt [$L^3 \cdot L^{-2}$] or [L]
S	Sorptivity (ability of the pores to absorb and release water by capillarity) in the Philip (1957) infiltration model [$L \cdot T^{-0.5}$]
S_a	Degree of saturation due to adhesion suction [-]
S_c	Degree of saturation due to capillary suction [-]

S_r	Degree of saturation [-]
S_S	Specific surface of the solid grains [$L^2 \cdot M^{-1}$]
SL	Single-layer
T	Temperature (℃ or K)
T_a	Air temperature (℃ or K)
T_{avg}	Average measured daily temperature (℃)
T_{max}	Maximum measured daily temperature (℃)
T_{min}	Minimum measured daily temperature (℃)
T_{surf}	Temperature at the surface (℃ or K)
TC	Tempe cell
TDR	Time domain reflectometry
TSF	Tailings storage facility
t	Time [T]
t_{85}	Time required to attain a degree of saturation of 85% 1 m below the surface of the tailings [T]
U_a	Wind speed [$L \cdot T^{-1}$]
USCS	United soil classification system
u	Relative water pressure [$M \cdot L^{-1} \cdot T^{-2}$]
u_a	Atmospheric pressure ($u_a \approx 101.3$ kPa)
u_j	Pressure at point j [$M \cdot L^{-1} \cdot T^{-2}$]

u_w	Water pressure [$M \cdot L^{-1} \cdot T^{-2}$]
V_L	Volume of the tailings layer [L^3]
V_T	Total volume (water, air and solids) [L^3]
V_{cracks}	Volume of the cracks in a tailings layer [L^3]
V_s	Volume of solids [L^3]
$V_{tailings}$	Volume of tailings poured in the column [L^3]
V_w	Volume of water [L^3]
v_j	Velocity of flow at point j [$L \cdot T^{-1}$]
v_w	Wind speed [$L \cdot T^{-1}$]
W	Water from the fresh waste being deposited [$L^3 \cdot L^{-2}$] or [L]
W_v	Molecular weight of water (0.018 kg/mol)
WB	Water balance [$L^3 \cdot L^{-2}$] or [L]
WB_{error}	Water balance error during the numerical simulations [-]
WEV	Water entry value [L] or [$M \cdot L^{-1} \cdot T^{-2}$]
WRC	Water retention curve
w	Gravimetric water content [-]
w_0	Initial gravimetric water content [-]
w_L	Gravimetric water content in the tailings layer [-]
w_a	Gravimetric water content when the suction is equal to the AEV [-]

w_{es}	Shrinkage limit [-]
w_i	Initial gravimetric water content [-]
w_l	Liquid limit [-]
w_p	Plastic limit [-]
w_s	Final gravimetric water content [-]
y_{fx}	Dummy variable standing for the natural logarithm of suction (Fredlund et al. (1994) model)
ZFP	Zero-flux plane
z	Measurement depth [L]
z_j	Elevation of point j with respect to datum [L]
z_{wt}	Depth from the surface to the water table [L]
Δh	Hydraulic head loss [L]
ΔST	Change in storage or $[L^3 \cdot L^{-2}]$ or [L]
$\Delta \theta$	Variation in the volumetric water content $[L \cdot L^{-1}]$
Γ	Slope of the saturation versus vapour pressure curve at the mean air temperature $[M \cdot L^{-1} \cdot T^{-2} \cdot °C^{-1}]$
γ_w	Unit weight of water (9.81 kN/m3);
ν	Psychrometric constant $[M \cdot L^{-1} \cdot T^{-2} \cdot °C]$
θ	Volumetric water content [-]
θ_L	Volumetric water content in the tailings layer [-]

θ_a	Volumetric air content [-]
θ_{eq}	Equivalent (diffusion) porosity [-]
θ_f	Final volumetric water content [-]
θ_i	Initial volumetric water content [-]
θ_r	Residual volumetric water content [-]
θ_s or θ_{sat}	Volumetric water content at saturation [-]
ρ_d	Dry density of the tailings [$M \cdot L^{-3}$]
ρ_p	Density of the tailings pulp (solid particles and water) [$M \cdot L^{-3}$]
ρ_s	Density of the material particles [$M \cdot L^{-3}$]
ρ_w	Density of water (998 kg/m^3 at 20°C) [$M \cdot L^{-3}$]
μ_w	Dynamic viscosity of water (10^{-3} Pa·s at 20°C)
ξ	Relative diffusion coefficient (-) standing for the tortuosity of the material [-]
ψ	Suction [L] or [$M \cdot L^{-1} \cdot T^{-2}$]
ψ_0	Initial suction [L] or [$M \cdot L^{-1} \cdot T^{-2}$]
ψ_a	Air entry value [L] or [$M \cdot L^{-1} \cdot T^{-2}$]
ψ_{es}	Suction at the shrinkage limit [L] or [$M \cdot L^{-1} \cdot T^{-2}$]
ψ_f	Suction head at the wetting front [L]
ψ_r	Residual suction [L] or [$M \cdot L^{-1} \cdot T^{-2}$]
ψ_T	Total suction in the liquid water phase expressed as equivalent matric suction (negative value) [L] or [$M \cdot L^{-1} \cdot T^{-2}$]

LIST OF APPENDICES

CHAPTER 1 INTRODUCTION

1.1 Description of the problem

Mining operations generate large quantities of tailings and waste rocks. Mine tailings are produced during the processing and concentration of ore. They are composed of finely grinded rocks mixed with process water and reagents. Mine tailings are typically transported hydraulically and deposited at a high water content (slurry) on the surface in tailings storage facilities (TSF), also called tailings pounds or impoundments. TSF are surrounded by engineered dikes to retain the tailings slurry and limit its footprint. Because of the high-water content of slurries, geotechnical instabilities regularly occur with tailings impoundment, as illustrated for example at the Mount Polley Mine in 2014 (British-Columbia, Canada) or at the Bento Rodrigues mine (Mariana province, Brazil) in 2015 (Morgenstern et al., 2015, 2016). Another issue of concern raised by tailings is the production of contaminated mine drainage (including acid mine drainage, AMD, characterized by a low pH and high concentration of dissolved metals) due to the oxidation of sulfidic minerals sometimes present in the rock (e.g. Kleinmann et al., 1981; Gray, 1997; Aubertin et al., 2002).

Mine operators have expressed greater interest, during the last few decades, for the development of alternative mine waste management methods. One of the main objectives is then to minimise the environmental impact of mining operations and to mitigate the potential geotechnical and geochemical risks associated with mine wastes storage facilities. The benefits of integrating mine wastes management into the mining cycle have also been demonstrated (e.g. Benzaazoua et al., 2008; Aubertin et al., 2015, 2016). Innovative disposal options have been proposed to better control potential problems and favor mine wastes integrated management such as waste rock inclusions in TSF (James et al., 2013), underground paste backfill (Hassani and Archibald, 1998; Benzaazoua 2010), and tailings desulfurization and valorization (Bussière et al., 2004; Demers, 2008).

Another management technique consists in reducing the water content in the tailings through thickening and filtration, to improve their physical stability. The use of densified tailings (thickened, paste or filtered) is common for backfilling underground stopes, to reduce surface storage of tailings and improve ore recovery and underground openings stability (Thomas et al., 1979; Hassani and Archibald, 1998; Li and Aubertin, 2014). Robinsky (1975, 1999) first proposed

thickened tailings for surface disposal, by increasing the pulp density (i.e. remove water and increase solid content) before disposition in the TSF.

Densifying tailings to obtain a paste-like consistency may provide several advantages over traditional slurry tailings, such as (e.g. Jewell et al., 2002; Johnson et al., 2005, Martin et al., 2006b; Bussière, 2007; Simms et al., 2005, 2007, 2010; Blight, 2010; Fourie, 2012a, 2012b; Jones and Boger, 2012; Simms, 2017; Fitton, 2017):

- An increased strength upon deposition;
- Improved dike stability (for example during earthquakes);
- A decreased demand for borrow materials for the construction of impoundment structures;
- A significant reduction (or elimination) of ponding;
- A more rapid consolidation, allowing traffic and progressive reclamation;
- Better leachate recovery;
- Less water to collect and treat.

Most of these advantages are site specific and depend on the processing method and site conditions. There are also some uncertainties and limitations to the use of paste tailings for surface disposal. For instance, transport of paste tailings to the TSF requires more energy than conventional slurry because of a higher viscosity, so centrifugal pumps usually cannot be used. Instead, positive displacement pumps are required to transport paste tailings in pipelines. Moreover, thickeners and/or filters are usually costly to purchase and may significantly increase operating costs. Fourie (2012b) argues that, although the capital costs are higher at the plant, they can be reduced at the TSF (i.e. smaller dikes, less water to manage). Therefore, paste tailings can become, in certain cases, an attractive option both from an economic and operational standpoint.

Another uncertainty relates to the potential water savings (recovery) from a paste tailings storage facility. For some authors (e.g. Haile, 2000; Gonzales, 2005; Boger, 2012; Fourie, 2012a, 2012b), the lower water content of paste tailings implies that more process water can be recirculated at the mill. The technique can also potentially reduce the treatment costs of the water exfiltrating from the TSF. Other authors, however, state that the water savings are negligible, compared to slurry

tailings (if water from the tailings pond is pumped back to the process plant) (Lyell et al., 2008; Blight et al., 2012).

Paste tailings deposition can also lead to an increased potential for wind erosion and dust transport outside the site (Jewell et al., 2002).

Another major concern relates to tailings that are prone to generate contaminated mine drainage (such as AMD). The risk of oxidation of sulfide minerals in paste tailings is greater since they typically desaturate more rapidly than conventional (slurry) tailings (e.g. Aubertin, 2004). In this case, deposition planning should aim at controlling the degree of saturation; this aspect is investigated in this thesis.

The use of paste tailings for surface disposal is a recent technology and it still requires investigation to better understand the effect of various influence factors and optimize disposal, particularly in the case of reactive tailings, as a function of drainage and desaturation. The objective of this thesis is to assess how tailings properties (e.g. grain size, porosity, water retention curve, hydraulic conductivity), operational constraints (e.g. layer thickness, deposition rate), and site specific (foundation soils, depth of water table) and climatic conditions (e.g. potential evaporation and precipitation) can influence the distribution and movement of water in a variably saturated surface paste tailings stack. The results of this research project provide quantitative information and general guidelines to help optimise paste tailings deposition, particularly regarding the prevention of contaminated mine drainage.

1.2 Research project

Research question

How does water move through a variably saturated stack of paste tailings on the surface? This question is addressed considering that a lower water content (and higher density) may increase geotechnical stability, while also increasing the potential for sulfide oxidation and production of contaminated mine drainage.

General objective

Assess the effect of tailings properties, operational constraints, and site specific and climatic conditions on the hydrogeotechnical behaviour of a paste tailings stack.

Specific objectives

1. Characterize the hydrogeological properties of paste tailings from the Bulyanhulu Mine (Tanzania).
2. Develop and use physical model tests in the laboratory to evaluate the hydrogeological behaviour of paste tailings under controlled conditions.
3. Evaluate and validate numerical simulations conducted with Vadose/W (GeoSlope, 2007, 2016) using the results from the physical models.
4. Assess the influence of several factors, including operational, material and climatic properties on the behaviour of a surface paste tailings stack using numerical parametric analyses.
5. Summarize and analyse the findings to provide some practical guidelines to help manage reactive paste tailings.

Scientific hypothesis

Surface paste tailings disposal can be, under specific conditions, an effective technique to manage reactive mine tailings and improve the overall geochemical and geotechnical stability of the TSF.

1.3 Thesis outline

Chapter 2 presents a detailed literature review on mine tailings management, including tailings properties, unsaturated hydrogeology, oxygen flow trough porous media, surface-atmosphere exchanges, and numerical simulations. Chapter 3 describes the field and laboratory methodology used in this study. Laboratory and field experimental results are presented in Chapter 4. Results from the physical model tests conducted in the laboratory follow in Chapter 5 (for single-layer tailings deposition) and Chapter 6 (multilayer tailings deposition). The main outcomes from the numerical simulations of laboratory and field conditions are shown and discussed in Chapter 7.

Finally, Chapter 8 summarizes the experimental and numerical results, concludes on the main findings, and proposes some recommendations for future work.

1.4 Main contributions and justification of the originality

The main contribution of this study is to contribute to a better understanding of the hydrogeological behaviour of paste tailings, with an emphasis on the reactive tailings produced at the Bulyanhulu mine. The findings show for instance the major influence of evaporation with respect to water movement in surface paste tailings. The effect of various other factors is also shown quantitatively.

Specific laboratory procedures were modified or optimised throughout this research, and an analytical approach was developed to determine interlayer flow during paste tailings deposition. Laboratory column (physical model) tests and numerical simulations also helped gain a better insight on the movement of water into a surface paste tailings storage facility, and on the operational, climatic and material parameters that may influence drainage and evaporation from surface paste tailings.

The assessment of the overall behaviour of a surface paste tailings storage facility is relatively new, and the work shown here is original in many aspects. This project combined field and laboratory work, and extensive numerical simulations. This thesis illustrates how several factors and parameters influence the short, medium and long-term behaviour of reactive paste tailings. The knowledge acquired through this doctoral project will be helpful for the planning and management of paste tailings storage facilities.

CHAPTER 2 LITTERATURE REVIEW

2.1 Properties of tailings from hard rock mines

Mine tailings are fine-grained milling wastes produced from the grinding and concentration of ore (Vick, 1983; Aubertin et al., 2002). Tailings are typically produced as a pulp consisting of finely ground rock, water and reagents. The tailings pulp (of varying density – depending on the type of process and mining operation) is pumped to a tailings storage facility TSF. They are deposited from perimeter dikes around the TSF. They may also be placed directly underwater to limit AMD generation. Another choice is to return tailings underground and to use them for backfilling of open stopes (Thomas et al., 1979; Hassani and Archibald, 1998; Benzaazoua et al., 1999; Potvin et al., 2005).

Operational factors, material properties and site conditions affect the management of mine tailings (Aubertin et al., 2002; Fahey et al., 2002; Sofra and Boger, 2002; Aubertin, 2004; Bussière, 2007; Deschamps, 2009; Blight, 2010; Boger, 2012; Simms, 2017). Some of the operational factors influencing the management of mine tailings are the production rate of the tailings, the initial pulp density (gravimetric, volumetric or relative; see below for more details), the pumping rate, distance and method, the disposal method in the TSF (e.g. use of hydrocylcones), the rate of sedimentation of the tailings, the beaching behaviour of the tailings (e.g. beach angle and segregation on the beach), the volume of water recovery (after deposition), the short-term (1-2 days after deposition) tailings density and the long-term consolidation behaviour (i.e. affecting time before the surface can support rehabilitation), and the composition of the process water (e.g. presence of flocculants).

The material properties affecting the management of tailings include the particle size distribution (PSD), the relative particle density (D_r), the hydraulic properties (saturated and unsaturated – e.g. hydraulic conductivity and water retention curve), the yield stress, and the mineralogy (Vick, 1983; Aubertin et al., 1996, 1998, 2002; Fahey et al., 2002; Blight, 2010).

Finally, some of the site conditions include the potential and actual rates of evaporation, the presence (and development time) of a surface crust on the tailings surface, the erodibility and compaction characteristics of the tailings, and the hydrogeological conditions below the TSF (e.g. depth of the water table, underlying soil properties).

The gravimetric pulp density (P_m) is sometimes used to characterize the properties of mine tailings properties and is expressed as (Jewell et al., 2002):

$$P_m = \frac{M_s}{M_T} \quad 2.1$$

where M_s = Mass of the solids in the tailings pulp [M];

M_T = Total mass of the tailings pulp [M].

The gravimetric water content of the pulp (w) can then be calculated:

$$w = \frac{M_w}{M_s} = \frac{M_T - M_s}{M_s} = \frac{1 - P_m}{P_m} = (P_m)^{-1} - 1 \quad 2.2$$

where M_w = Mass of the water in the tailings pulp [M];

The gravimetric pulp density (P_m) gives a rough estimate of the density of the tailings. The yield stress (shear stress necessary for the tailings to flow) is typically a better measurement of the texture of a tailings slurry (Boger, 2012). Tailings with different gravimetric pulp densities (P_m) may have the same shear yield stress, depending on the material type and the relative density of its solid grains (D_r).

The characteristics of thickened tailings can therefore also be defined according to volumetric properties: the pulp porosity (n_p) and the volumetric pulp density (P_v). For a pulp, the porosity for a degree of saturation (S_r) of 100% is:

$$n_p = \frac{V_w}{V_T} = \frac{w \times D_r}{w \times D_r + 1} \quad 2.3$$

where V_w = Volume of water of the sample (equal to the volume of voids V_v when S_r is 100%) [M];

V_T = Total volume of the sample [L^3];

w = Gravimetric water content of the sample (in decimal figures; $w = M_w/M_s$) [-]

The volumetric pulp density (P_v) is the ratio between the volume of solids and the total volume of a tailings slurry:

$$P_v = \frac{V_s}{V_T} = 1 - \frac{V_w}{V_T} = 1 - n_p \quad 2.4$$

The pulp relative density (RD_p) can be expressed as (Blight, 2010):

$$RD_p = \frac{\rho_p}{\rho_w} = \frac{D_r + e_p}{1 + e_p} \text{ where } e_p = w \times D_r = \frac{n_p}{1 - n_p} \quad 2.5$$

where ρ_p = Density of the tailings pulp (solid particles and water) [M/L^3];

ρ_w = Density of the process water in the slurry [M/L^3];

e_p = Pulp void ratio [-].

The previous equations of P_m, n_p, P_v, and RD_p are only valid for a saturated tailings pulp. However, the tailings begin to desaturate following their deposition in the surface tailings storage facility.

The following nomenclature, adapted from authors such as Verberg (1997), Jewell et al. (2002) and Crowder (2004), was used in this project (Martin et al., 2006a, 2006b, 2010, 2013):

1. *Slurried tailings:* are the most commonly produced tailings. The pulp has an elevated water content and a critical flow velocity (i.e. when pumping velocity is below the critical flow velocity, the solids contained in the slurry settle and segregate). Slurried tailings have a yield stress equal to 0 kPa. The gravimetric pulp density (P_m) is usually composed between 30% and 45%. The gravimetric water content can be between 120% and 230%.

2. *Thickened tailings:* tailings have a relatively low water content due to the densification process at the mill. They show a critical flow velocity but do not segregate during sedimentation. Bleed water can be observed from thickened tailings following a slump test or after disposal in a TSF. The gravimetric pulp density (P_m) is usually comprised between 45% and 70% (i.e. w between 40% and 120%). Thickened tailings have a yield stress and can be deposited from a central discharge point to form a conical stack (e.g. Kidd Creek – Robinsky, 1999) or in layers (dry stacking) (Haile et al., 2000, Sofra and Boger, 2002).

3. *Paste tailings:* have a lower water content than thickened tailings. Paste tailings do not have a critical flow velocity. The applied yield stress (during pumping) must be greater than the shear yield stress to pump a paste (i.e. minimum applied yield stress necessary to pump the paste). Paste tailings can be deposited in a surface TSF, or in underground excavations (usually mixed with a binder). The initial gravimetric water content (at saturation) of paste tailings (P_m) is typically comprised between 70% and 85% (w is

between 20% and 40%), depending on the properties of the solids (Benzaazoua et al., 2004; Potvin et al., 2005; Alkangas et al., 2013). There is almost no particle segregation during disposal. Also, paste tailings have a measurable yield stress from 10 Pa to 1000 Pa for cemented paste backfill for underground mines (Boger, 2012; Fourie, 2012a). Fourie (2012a) defines a cut-off yield stress (yield stress values above which the tailings are not considered anymore as paste tailings) between 100 Pa and 200 Pa and specifies that transport of the material may require positive displacement pumps.

4. *Filtered tailings:* When the water content is reduced even further (P_m > 85%, w < 20%), the material forms a filter cake. At this point, it is not possible to pump the tailings and they need to be transported by trucks or conveyors (e.g. Bussière, 2007; Coulombe, 2012). The material produces negligible displacement following a slump test.

However, the gravimetric pulp density (P_m) depends on the relative particle density (D_r) of the material, which influences rheology of the tailings pulp (Sofra and Boger, 2002). A more appropriate measure of the actual pulp characteristics of a tailings slurry is therefore either its volumetric pulp density (P_v), its yield stress, or its viscosity. The relationship between gravimetric and volumetric pulp densities is non-linear (Figure 2.1).

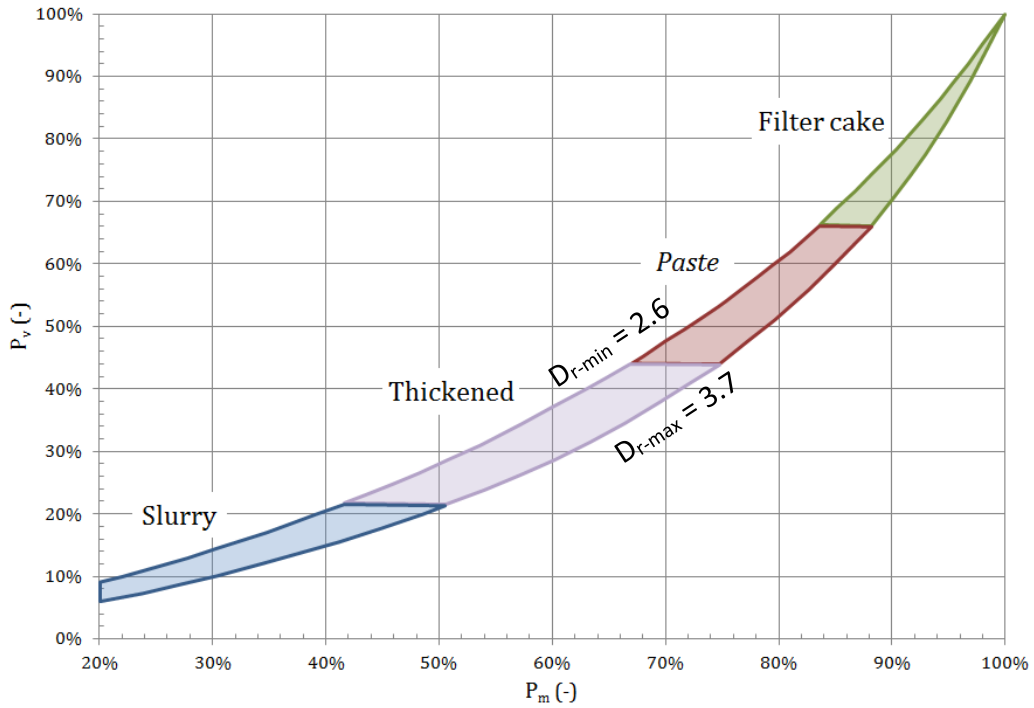

Figure 2.1: Relationship between the gravimetric and volumetric pulp densities, with varying specific gravities.

The rheology of densified tailings pulps is time-dependent (thixotropic) and sensitive to shear rate (typically shear thinning), and their viscosity and yield stress will decrease with pumping distance for a given, constant shear rate (Sofra and Boger, 2002; Mizani and Simms, 2016).

The physical properties of mine tailings may be influenced by many factors including the pulp density (gravimetric, volumetric or relative; see below for more details), the particle size distribution and relative density of the solid particles in the slurry, the pumping rate, distance and method, the composition of process water (e.g. presence of flocculants);

More information on the general properties of slurried mine tailings can be found in the literature (e.g. Vick, 1983; Aubertin et al., 1996, 1998, 2002; Bussière, 1999, 2007; Rassam and Williams, 1999b; Qiu and Sego, 2001; Fahey et al., 2002; Sofra and Boger, 2002; Blowes et al., 2003; Jambor, 2003; Gawu and Fourie, 2004; Simms et al., 2007; Henriquez and Simms, 2009; Blight, 2010; Pabst, 2011).

One of the challenges when it comes to management of mine tailings is acid mine drainage (AMD) or contaminated neutral drainage (CND). AMD and CND are the main sources of water contamination from mining operations and are most often caused when sulphur bearing minerals oxidize (SRK, 1989; Ritcey, 1989; Aubertin et al., 2002). The main sulphide mineral involved in AMD generation is pyrite (FeS_2). Sulphide oxidation leaches hydrogen (H^+), sulphate (SO_4^{-2}) and iron (Fe^{2+}) ions. The generation of AMD through the oxidation of pyrite can be expressed with these simplified equations (Kleinman et al., 1981):

$$FeS_{2(s)} + \frac{7}{2}O_2 + H_2O \rightarrow Fe^{2+} + 2SO_4^{2-} + 2H^+ \quad 2.6$$

$$Fe^{2+} + \frac{1}{4}O_2 + H^+ \rightarrow Fe^{3+} + \frac{1}{2}H_2O \quad 2.7$$

$$Fe^{3+} + 3H_2O \rightarrow Fe(OH)_{3(s)} + 3H^+ \quad 2.8$$

$$FeS_{2(s)} + 14Fe^{3+} + 8H_2O \rightarrow 15Fe^{2+} + 2SO_4^{2-} + 16H^+ \quad 2.9$$

Equation 2.6 is the direct oxidation of pyrite and shows that a sulphide mineral must be in contact with both water and oxygen to produce AMD. This reaction may occur at near-neutral pH (pH = 7.0). The phenomenon will therefore occur in the unsaturated zone of a TSF, where the pores contain both air and water. When the pH of the pore water drops below a certain value (around 3.5 - 4.0), the ferrous iron (Fe(II) or Fe^{2+}) transforms in ferric iron (Fe(III) or Fe^{3+}) (Equation 2.7). The latter can then serve as the oxidizing agent (even in anaerobic conditions) therefore leaching greater amounts of acidity (Equations 2.8 and 2.9). This indirect oxidation reaction may occur below the water table in the TSF (Aubertin et al., 2002; Pabst, 2011). Once the oxidation reactions have started, the drainage water from the TSF will become acidic. It will leach various ions (mostly sulphate and metals) in the environment (Gray, 1997). Neutralisation and precipitation reactions will also influence the quality of the leachates.

Bacterial activity may increase the rate of oxidation of the AMD reactions presented above. Iron oxidizing bacteria (IOB, such as Acidithiobacillus ferooxydans) act as a catalyst when the pore water pH is below 5. They can accelerate the oxidation rate in aerobic and/or anaerobic conditions (Equations 2.6 to 2.9). There exists a large variety of IOBs that may be involved in AMD reactions. The populations will vary with the hydrogeochemical conditions found in the TSF such as pH of the pore water, ambient temperature, oxygen concentration and availability, water content, particle size distribution of the material, and mineralogy of the tailings (Aubertin et al., 2002).

To control the generation of AMD, it is necessary to remove or isolate at least one of the reagents of Equation 2.6 (the water, the oxygen or the sulphur). Some of the available techniques include (SRK, 1989; Bussière, 1999; Zhan, 1999; Aubertin et al., 2002; Dagenais, 2005; Bois et al., 2005; Demers, 2008; Pabst, 2011): minimizing the flow of oxygen and/or water to the tailings; removal of the sulphides before disposal of the tailings (e.g. sulphur flotation or desulphurization); control of the pH of the leachate (e.g. permeable reactive barriers); and control of bacterial activity.

Another solution to help limit the risk of generation of AMD from mine tailings is to design the TSF with rehabilitation in mind from the onset, and to engineer the tailings in ways that can help achieve the closure objectives. In this regard, in some cases, thickening of tailings for surface disposal may offer some advantages from both a management and environmental standpoint (Robinsky, 1975, 1999; Jewell et al., 2002; Crowder, 2004; Simms, 2017).

2.2 Surface disposal of tailings

Mine tailings are typically produced and deposited as a slurry at the mill with a gravimetric pulp density (P_m) composed of 15% - 45% solids (e.g. Vick, 1983; Haile et al., 2000; Aubertin et al., 2002). Tailings are typically deposited sub-aerially from the crest of a dike inside a tailings storage facility (TSF). TSFs are limited by dikes, which may be permeable or have an impermeable core. They can be constructed with either borrowed natural materials and/or mine tailings (Vick, 1983; Aubertin et al., 2002).

Following end of pipe deposition, the tailings slurry flows towards a low point in the basin, with coarser particles settling closer to the discharge point forming a sandy beach. This segregation of tailings in the TSF affects the hydraulic and mechanical properties of the tailings and of the facility (Aubertin et al., 2002; Bussière, 2007; Blight, 2010). It may also raise some geotechnical and environmental concerns. For example, tailings along the beach may generate acid mine drainage (AMD) if they contain sulphidic minerals and the material is note saturated (Aubertin et al., 2002). Larger TSFs may create higher pore water pressures on containment dams, which increases the risk of dam failure (Vick, 1983; Aubertin et al., 2002; James, 2009; Pépin, 2010; James et al., 2013).

Conventional TSFs filled with low-density slurry tailings will habitually exhibit particle segregation (Aubertin et al., 2002; Bussière, 2007; Lyell et al., 2008; Blight, 2010; Blight et al., 2012) because slurry tailings have a critical velocity. The larger tailings particles will settle more

rapidly than the finer particles following disposal. Therefore, such tailings ponds tend to have coarser particles upstream (close to the deposition points) and finer particles downstream (Figure 2.2). This segregation may have the following consequences on the behaviour of the TSF (Aubertin et al., 2002; Pépin, 2010):

- Fine particles downstream create an elevated water table;
- Presence of a pond downstream of the TSF;
- Higher drainage rate upstream which creates a lower water table close to the dikes;
- "Bathtub" shape (lowest point of the facility located farthest away from the deposition point).

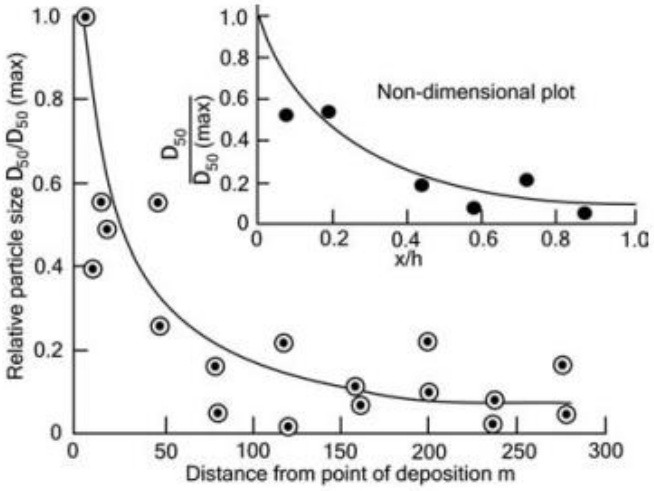

Figure 2.2: Example of particle segregation in a tailings storage facility filled with slurried tailings (Blight, 2010).

Figure 2.3 presents a schematic representation of a TSF filled with slurry tailings, including some parameters that influence its properties (i.e. rate of rise, evaporation/precipitation, seepage, recycling of water).

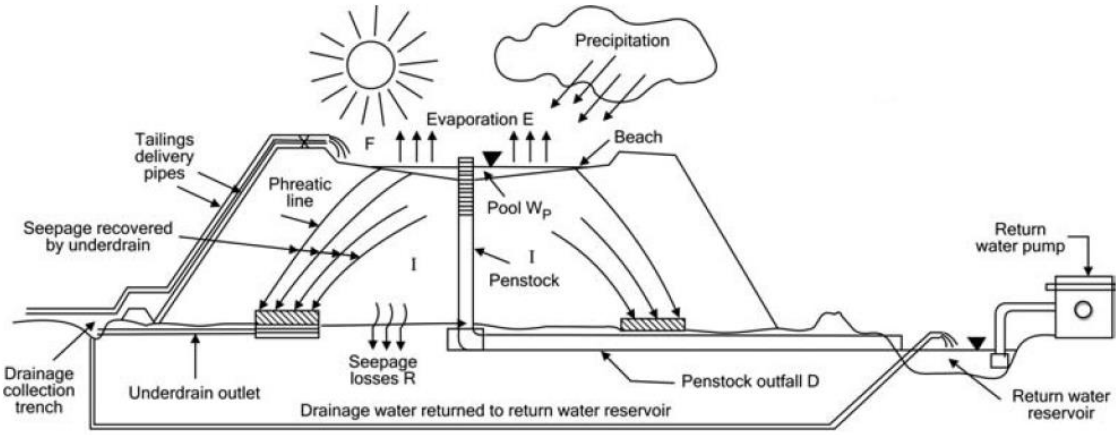

Figure 2.3: Schematic representation of tailings storage facilities for traditional (slurry) tailings (Blight, 2010).

For surface paste tailings disposal, the tailings are deposited by end of a pipe in a gently sloping stack (Mizani and Simms, 2016). They will form a cone with an outwards slope if discharged from a point inside the TSF (Mizani et al., 2013; Figure 2.4). The discharge point can also be placed on a dike upstream with paste flowing downstream. The slurry flows freely along the interface to create a lobe with a texture approaching that of concrete (Theriault et al., 2003). As the paste lobe spreads, it will lose some water (through drainage and evaporation) and its velocity will decrease until it stops flowing. The thickness of the tailings layer depends on the rheological properties of the material and the deposition sequence defined by the operator (Sofra and Boger, 2002; Shuttleworth et al., 2005).

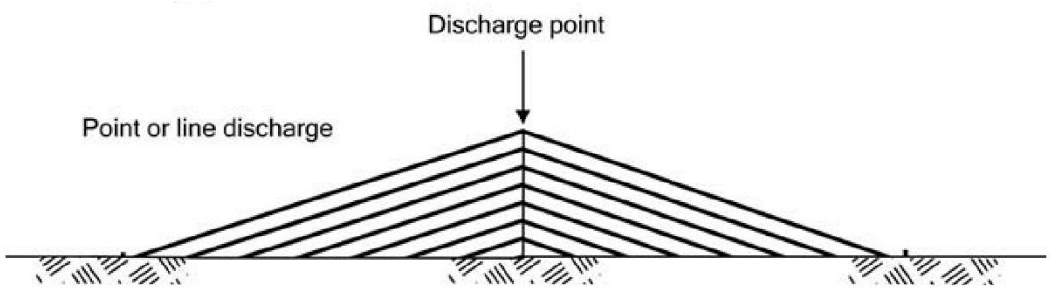

Figure 2.4: Section of a typical configuration for a tailings storage facility filled with paste tailings (not to scale; Blight, 2010).

When depositing surface paste tailings, the first goal is to allow the freshly deposited tailings to consolidate and stabilize. However, the operator should ensure that the tailings will not desaturate if they are potentially acid generating. The degree of saturation at which this occurs is typically taken as being around 85%-90% (Aubertin et al., 1995, 1999), but this may also vary depending on the tailings type (e.g. reactivity, mineralogy). Figure 2.5 shows a sketch of a section of a storage facility with potentially acid generating paste tailings. This figure illustrates some of the many factors affecting the properties of the materials under potentially acid forming conditions.

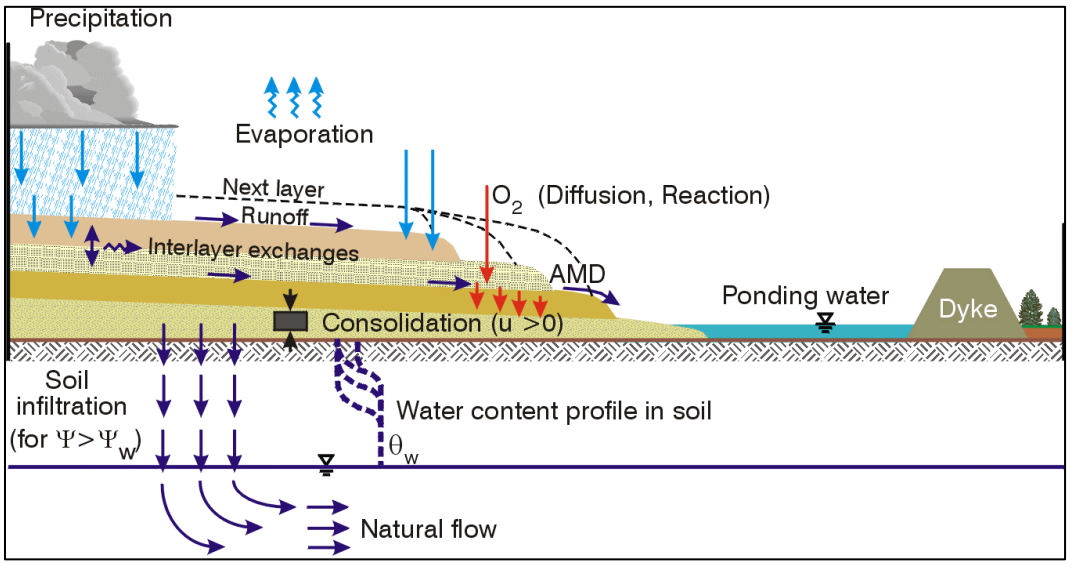

Figure 2.5: Schematic representation of reactive paste tailings deposited in successive layers (adapted from Aubertin, 2004).

The layers are thicker near the central axis of the cone in a paste tailings storage facility. Similarly, the slope angle becomes smaller near the outer limits of the facility. The slope ranges between 1.5% and 5% (Fourie, 2012a; Mizani and Simms, 2016). The slope formed by the tailings cone favors flow of runoff water towards the outside of the facility. Accumulated water can then be captured and recirculated to the mill or pumped into a polishing pond. Furthermore, the slope of the cone produced from deposition of thickened tailings will tend to decrease as the volumes of tailings deposited increases (Mizani et al., 2013).

The mechanical benefits from evaporation are maximised by placing thin layers of paste tailings, which can consolidate under the effect of evaporation before further filling takes place (Newson and Fahey, 2003; Simms et al., 2007; Dunmola, 2012; Mizani et al., 2013). Important gains in strength of the paste tailings can be observed even before the material attains its shrinkage limit (Daliri et al., 2014).

If the tailings are potentially acid generating, it is preferable to keep the layers close to saturation, to minimise the development of the oxidation reactions (Equation 2.6). In these conditions, the deposition cycle is adjusted to cover tailings with a fresh layer of paste before significant desaturation occurs. The length of this deposition cycle depends on many factors, including (Figure 2.5):

- Intensity, frequency and duration of precipitation events;
- Evaporation (and temperature gradient) at the tailings surface;
- Settlement, consolidation, and hydraulic conductivity of the tailings;
- Unsaturated properties of the tailings and evolution of the degree of saturation, and of the pore pressure (positive or negative) profile in the various layers;
- Presence, size, and density of the desiccation cracks;
- Depth to the water table and hydrogeotechnical properties of the underlying soils;
- Tailings production rate, size of the tailings storage facility and time of exposure to meteorological elements;
- Reactivity of the tailings, which control the oxygen consumption and acid mine drainage production rates; this aspect is also related to the mineralogical composition of the tailings (and their acid generating potential).

Cracking of the surface may also influence water and oxygen movement in a surface paste tailings stack (Simms et al., 2017). The size and density of shrinkage cracks must therefore be controlled. Cracks favor flow of oxygen in the tailings stack (Fujiyasu et al., 2000; Simms et al., 2007; Fisseha et al., 2010). Another issue with shrinkage cracks is the potential of creating preferential flow paths during storms that will erode significantly the tailings stack (Figure 2.6). This could cause silting of polishing ponds or tailings spills in the environment.

Figure 2.6: Example of erosion in shrinkage cracks following a storm on a paste tailings facility (Blight, 2010).

2.3 Flow in porous media

A porous medium containing water can be either saturated or unsaturated. Its voids are filled with water when it is saturated (degree of saturation, S_r, of 100%). In this case, only two phases are present: water and solids. If it is unsaturated, three phases may be present: solid, liquid (e.g. water), and gaseous (e.g. air), (Fredlund and Rahardjo, 1993). Water for the liquid phase and air for the gas phase are the only two fluids considered in this project. Water flow rate in porous media depends on the degree of saturation.

2.3.1 Flow of water in saturated media

The hydraulic head (h) at a point gives the amount of energy available per unit mass of fluid at a point in space (Hillel, 1980). The hydraulic head (h_j) is the sum of the elevation (z_j), pressure (u_j) and velocity (v_j) heads at a point (j) (Todd, 1980), and is presented using Bernoulli's equation:

$$h_j = \frac{u_j}{\gamma_w} + \frac{v_j^2}{2g} + z_j \qquad 2.10$$

where u_j = Relative water pressure at point j (kPa);

γ_w = Unit weight of water (9.81 kN/m3);

v_j = Velocity of flow at point j (m/s);

g = Acceleration of gravity (9.81 m/s^2);

z_j = Elevation of point j with respect to datum (m);

The head loss (Δh) between two points is:

$$\Delta h = \left(\frac{u_1}{\gamma_w} + \frac{v_1^2}{2g} + z_1\right) - \left(\frac{u_2}{\gamma_w} + \frac{v_2^2}{2g} + z_2\right) \qquad 2.11$$

The head loss (Δh) is the potential loss of energy within a granular material. The velocity of water in these materials is usually very small, and it can be neglected in Equation 2.11 (Todd, 1980).

The relative water pressure (u) used in Bernoulli's equation (Equation 2.11) is:

$$u = u_w - u_a \qquad 2.12$$

The water pressure (u_w) is equal to the atmospheric (or air) pressure ($u_a \approx 101.3$ kPa) at the surface of the water table. Below the water table, the porous medium is a two-phase system (water and solid), and the water pressure is greater than the air pressure (i.e. u > 0 kPa). The relative pore water pressure (u) above the water table is negative. A negative value of u can be expressed as a suction (ψ), where the suction is the absolute value of the relative pore water pressure when this value is below zero. This will be addressed in Section 2.3.2.

In a saturated material, Darcy demonstrated that the total flow rate of water (Q [$L^3 \cdot T^{-1}$]) is proportional to the head loss and inversely proportional to the distance between two measurement points, or (Todd, 1980):

$$Q = -k_s \times A_D \frac{\Delta h}{\Delta L_D} \qquad 2.13$$

The parameter k is a constant known as the saturated hydraulic conductivity [$L \cdot T^{-1}$] and it represents the ability of a porous medium to allow the flow of water. The constant A_D is the area

of the cross-section [L^2]. The parameter $\Delta h/\Delta L_D$ expresses the hydraulic gradient (i) between the two measurement points. This equation is valid if the Reynolds number is lower than 1 or does not depart seriously from 10 (Todd, 1980).

Darcy's law can also be presented in the more general form:

$$q = k \times i \tag{2.14}$$

Where q is the specific flux or Darcy velocity [$L \cdot T^{-1}$]. It is possible to generalize Darcy's equation in three dimensions if the material is heterogeneous or anisotropic:

$$q = -[k_{ij}] \times \begin{bmatrix} i_x \\ i_y \\ i_z \end{bmatrix} \tag{2.15}$$

This generalization of Darcy's law is valid for most cases of water flowing through saturated materials.

2.3.2 Determination of the hydraulic conductivity

The saturated hydraulic conductivity (k or k_s) of a material is measured (in the laboratory or in the field) or estimated using prediction models. For this project, flexible membrane permeameter (ASTM D5084) were used to obtain the k_s. In addition, the Kozeny-Carman (KC; Chapuis and Aubertin, 2003) and Modified Kozeny-Carman (KCM; Mbonimpa et al, 2002a) models were also used to predict the saturated hydraulic conductivity of the tailings studied in this project.

The Kozeny-Carman model used to predict the hydraulic conductivity, can be written as (Chapuis and Aubertin, 2003):

$$k_{KC} = C_{KC} \frac{g}{\mu_w \times \rho_w} \times \frac{e^3}{S_s^2 \times D_R^2 (1+e)} \tag{2.16}$$

where k_{KC} = Predicted saturated hydraulic conductivity with the Kozeny-Carman model (cm/s);

C_{KC} = Adimensional material constant (-) which can be fixed to 0.2 according to Chapuis and Aubertin (2002);

g = Gravitational constant (9.81 kN/m^3);

ρ_w = Density of water (998 kg/m^3 at 20°C);

μ_w = Dynamic viscosity of water (10^{-3} Pa·s at 20°C);

e = Void ratio (-).

D_R = Relative grain density (-).

The parameter S_s (m^2/kg) in Equation 2.16 is the specific surface of the material. Chapuis and Légaré (1992) propose the following expression to estimate S_s:

$$S_s = \frac{6}{\rho_s} \sum \left(\frac{P_{No\,D} - P_{No\,d}}{d} \right) \quad 2.17$$

where ρ_s = Density of the material particles (kg/m^3);

$(P_{No\,D} - P_{No\,d})$ = Percentage by weight smaller than size D ($P_{No\,D}$) and larger than the next size d ($P_{No\,d}$).

The Kozeny-Carman Modified model (or KCM model) for non-plastic soils (Mbonimpa et al., 2002a) is expressed as:

$$k_{KCM} = C_G \frac{\rho_w}{\mu_w} \times \frac{e^{3+x}}{1+e} \times C_u^{1/3} \times D_{10}^2 \quad 2.18$$

where k_{KCM} = Predicted saturated hydraulic conductivity (cm/s);

C_G = Adimensional material constant (-) which can be fixed at 0.1 according to Mbonimpa et al. (2002);

D_{10} = Grain diameter at which 10% of the material is smaller on the cumulative particle size distribution curve.

The KCM model has often been used to predict (with good precision) the saturated hydraulic conductivity of tailings (Bussière, 2007; Pabst, 2011; Toussaint, 2016).

2.3.3 Flow of water in unsaturated media

The relative pore water pressure can be negative in unsaturated conditions when the degree of saturation of the material is less than 100% (i.e. some of the pores are filled with air instead of water). The hydraulic conductivity in these conditions does not remain constant and decreases as the degree of saturation (S_r) decreases.

A unit volume can be used to better understand water flow in unsaturated conditions (see Figure 2.7). The sides of this volume are Δx, Δy and Δz; for a total volume equal to Δx×Δy×Δz. On Figure 2.7 the flow of water is in the x-direction.

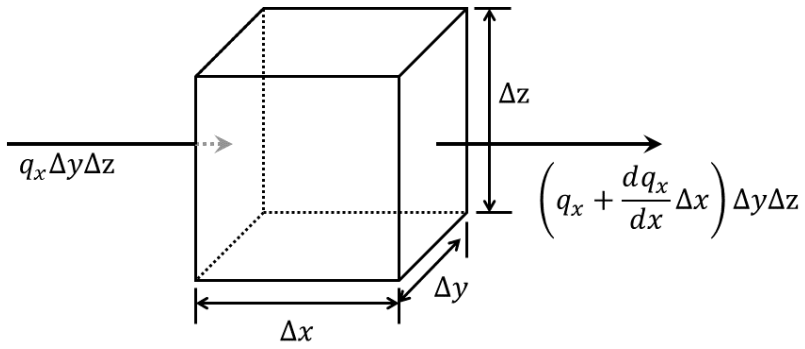

Figure 2.7: Schematic view of a unit volume of granular material (adapted from Hillel, 1980).

The rate of change in the flow rate (difference between water entering and exiting) in the x-direction is (Bussière, 1999):

$$\Delta q_x = q_x \Delta y \Delta z - \left[q_x + \left(\frac{dq_x}{dx}\right)\Delta x\right]\Delta y \Delta z \qquad 2.19$$

The parameter Δq_x is equal to 0 in saturated conditions. However, in unsaturated conditions, there will be recharge of the unit volume if Δq_x is greater than zero. Inversely, if Δq_x is negative, the element will desaturate. Therefore, a variation of the water volume in the unit volume with horizontal (x) flow is equal to (Bussière, 1999):

$$\Delta q = -\left(\frac{dq}{dx}\right)\Delta x \Delta y \Delta z \qquad 2.20$$

In transient conditions, when dq⁄dx is not equal to 0 there is either recharge (wetting) or desaturation (drying) of the unit volume. This is represented with the following equation:

$$\left(\frac{d\theta}{dt}\right) = -\left(\frac{dq}{dx}\right) \qquad 2.21$$

Where θ corresponds to the volumetric water content ($\theta = V_w/V_T$, where V_w is the volume of water in a sample of total volume V_T) and t the time.

The continuity equation for the water flow through a porous material can be generalised as:

$$\left(\frac{d\theta}{dt}\right) = -\left(\frac{dq_x}{dx} + \frac{dq_y}{dy} + \frac{dq_z}{dz}\right) \qquad 2.22$$

Darcy's law (Equation 2.15) gives the specific flux in each direction with respect to the hydraulic conductivity of the material and hydraulic gradient (Todd, 1980; Hillel, 1998):

$$q = -\left(k_x \frac{dh}{dx} + k_y \frac{dh}{dy} + k_z \frac{dh}{dz}\right) \qquad 2.23$$

Richards (1931) extended Darcy's law presented in Equation 2.23 to unsaturated materials (Richards, 1931; Hillel, 1998):

$$q = -k(\psi) \cdot \nabla h \qquad 2.24$$

where $k(\psi)$ = Hydraulic conductivity with respect to suction [$L \cdot T^{-1}$];

∇h = Hydraulic head gradient (in three dimensions) [$L \cdot L^{-1}$].

Thus, Equation 2.21 can be written (Richards, 1931; Hillel, 1998):

$$\left(\frac{\delta\theta}{\delta t}\right) = -\frac{\delta}{\delta x}\left(k_x(\psi)\frac{\delta\psi}{\delta x}\right) - \frac{\delta}{\delta y}\left(k_y(\psi)\frac{\delta\psi}{\delta y}\right) - \frac{\delta}{\delta z}\left(k_z(\psi)\frac{\delta\psi}{\delta z}\right) + \frac{\delta k(\psi)}{\delta z} \qquad 2.25$$

Equation 2.25, also known as Richards' equation, defines the flow of water in unsaturated materials (and is only valid above the water table).

2.4 Unsaturated properties of porous media

The water retention curve (WRC) and the unsaturated hydraulic conductivity (k_u) are the two main parameters that are used to describe the unsaturated behaviour of a granular material. The WRC usually expresses the volumetric water content with respect to applied suction, and the k_u function represents the unsaturated hydraulic conductivity at varying suctions.

2.4.1 Water retention curve (WRC)

The WRC represents the capacity of a material to retain water at a certain negative pressure (or suction) (Fredlund and Rahardjo, 1993; Mbonimpa et al., 2000). Figure 2.8 presents the typical WRC of two types of mine wastes: mine tailings and waste rock. The shape of these curves is a function of the pore size distribution, and the pore geometry of the material. Several characteristic points are used to describe the WRC (Figure 2.8):

- The air entry value (AEV or ψ_a) represents the suction at which the material starts to desaturate (Aubertin et al., 1998), when air starts to enter the largest pores of the material (Kim and Sture, 2008). The AEV is directly related to capillary rise in homogeneous porous materials (Aubertin et al., 1998). For example, the AEV of the mine tailings in Figure 2.8 is 50 kPa.
- The water entry value (WEV) is the point where, in a wetting process (decreasing suction), water starts to infiltrate into the material (Bussière, 1999). This point is also known as the residual suction (ψ_r). The WEV of the mine tailings in Figure 2.8 is approximately 2000 kPa.

It is assumed that the volumetric water content approaches zero when the suction is very large (e.g. 1×10^5 kPa - Vanapalli et al., 2000; 1×10^6 kPa - Aubertin et al., 2003a).

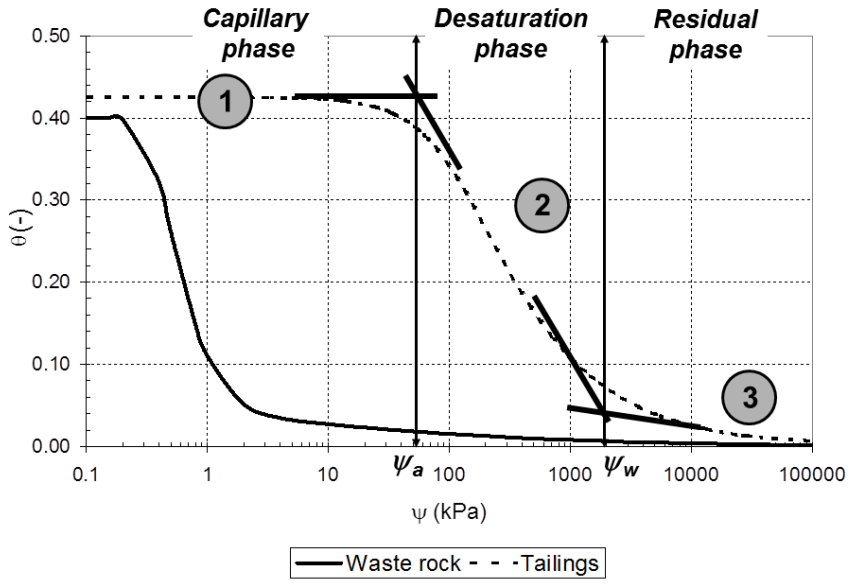

Figure 2.8: Typical water retention curves for mine tailings and waste rock (data taken from Martin et al., 2004, 2005). The tailings WRC include the three main phases of desaturation.

The pores in a finer material (such as the tailings in Figure 2.8) are smaller, and therefore desaturate at higher suctions (Aubertin et al., 1995). On Figure 2.8, the AEV of the coarse material (i.e. waste rock) is lower than the AEV of the fine material (i.e. tailings). Compressibility of the WRC at positive pressures can also estimated using an estimated or measured coefficient of volumetric compressibility (m_v) (GeoSlope, 2008; Simms et al., 2007; Fisseha et al., 2010; Daliri et al., 2016).

Measuring the WRC requires evaluation of [ψ,θ] pairs. Laboratory measurement methods include (Fredlund and Rahardjo, 1993; Ricard, 1994; Bussière, 1999; Fredlund et al., 2012): filter papers, psychrometers, drained column tests, dewpoint potentiometers, vapor sorption analyzers, Tempe cells, and pressure plate extractors. The suction (ψ) and volumetric water content (θ) can be measured using suction sensors (e.g. Thermal conductivity (HDS) sensors, or electrical conductivity such as tensiometers), and volumetric water content sensors (e.g. Time-domain reflectometry (TDR) sensors or capacitance sensors) at specified locations in the ground (Fredlund and Rahardjo, 1993; Zhan, 2000). Tempe cells and pressure plate extractors are based on the axis translation technique and were used in this research (see also Chapter 3).

The constants (or material parameters) in these models are dependent of the basic properties of the granular material such as the particle size distribution and porosity (Aubertin et al., 1998). The most commonly used models are those published by Brooks and Corey (1964), Gardner (1958), van Genuchten (1980) and Fredlund and Xing (1994).

The Fredlund and Xing (1994) model was used in this project (Fredlund and Xing, 1994) and is presented below:

$$\theta = C(\psi)\frac{\theta_{sat}}{\left\{ln\left[e+\left(\frac{\psi}{a_{fx}}\right)^{n_{fx}}\right]\right\}^{m_{fx}}} \qquad 2.26$$

where C(ψ) = Correction function: $C(\psi) = 1 - \frac{ln\left[1+\left(\frac{\psi}{\psi_r}\right)\right]}{ln\left[1+\left(\frac{10^6}{\psi_r}\right)\right]}$.

e = Napierian number.

a_{fx} = Model parameter associated with the inflection point of the WRC. It is an approximate value of ψ_a.

n_{fx} = Smoothing parameter that controls the slope of the inflection point of the WRC.

m_{fx} = Smoothing parameter of the curve linked to the residual water content and the correction function (C(ψ)).

θ_{sat} = Volumetric water content at saturation. It was assumed to be equal to the porosity (n) of the material.

ψ_r = Suction at which the volumetric water content equals its residual value (or residual suction).

The WRC predictive models base their estimations on relations between some properties of the granular materials such as the particle size distribution, the amount of organic matter, the void ratio (or porosity) and the mineralogy of the material. Many models were developed over the years, such as the model by Arya and Paris (1981). The WRC prediction model used in this project is the Modified-Kovács (MK) presented by Aubertin et al. (2003a, 2003b). This model was often used to predict the WRC of mine tailings (e.g. Bussière, 2007; Deschamps, 2009; Pabst, 2011; Saleh-Mbemba, 2016).

The MK model defines the degree of saturation (S_r) with respect to suction (ψ) using two parameters (Aubertin et al., 1998):

- The degree of saturation due to capillary suction (S_c) caused by the surface tension at the air-water interface;
- The degree of saturation caused by adhesion suction (S_a) caused by surface contacts and by the electrical attraction force.

These two parameters depend on the particle size distribution, the particle shape and the material porosity. The equations below present the MK model (Aubertin et al., 2003b):

$$S_r = S_c + \langle 1 - S_a \rangle \quad 2.27$$

$$S_c = 1 - \left(\left[\left(\frac{h_{co}}{\psi} \right)^2 + 1 \right]^{m_{MK}} \right) \times exp \left[-m_{MK} \left(\frac{h_{co}}{\psi} \right)^2 \right] \quad 2.28$$

$$S_a = a_{MK} \times C_\psi \frac{\left(\frac{h_{co}}{\psi_n} \right)}{e^{1/3} \left(\frac{\psi}{\psi_n} \right)^{1/6}} \quad 2.29$$

Table 2.1 describes the variables presented above.

Table 2.1: Parameters used in the MK model (adapted from Aubertin et al., 2003b)

Parameter	Value	Description	Units
h_{co}	$h_{co} = \frac{b}{e \times D_{10}}$	Average height of the capillary rise	cm
b	$b = \frac{0.75}{1.17 \times log(C_U) + 1}$	Pore size factor	cm^2
C_U	$C_U = \frac{D_{60}}{D_{10}}$	Uniformity coefficient	Unitless
ψ	Variable	Applied suction on the material	cm
m_{MK}	$m_{MK} = C_U^{-1}$	Shape coefficient	Unitless
a_{MK}	0.01	Smoothing coefficient	Unitless
C_ψ	$C_\psi = 1 - \frac{ln\left[1 + \left(\frac{\psi}{\psi_r}\right)\right]}{ln\left[1 + \left(\frac{\psi_0}{\psi_r}\right)\right]}$	Correction factor for dryness	Unitless
ψ_r	$\psi_r = \frac{0.42}{(e \times D_H)^{1.26}}$	Residual suction	cm
ψ_0	1×10^7	Suction at which the volumetric water content is 0	cm
D_H	$D_H = [1 + 1.17 \times log(C_u)]D_{10}$	Equivalent diameter	cm
e	Material dependent	Void ratio	Unitless
D_{10}	Material dependent	Grain diameter at which 10% of the material is smaller on the cumulative particle size distribution curve	cm
D_{60}	Material dependent	Grain diameter at which 60% of the material is smaller on the cumulative particle size distribution curve	cm

And:

$$\langle x \rangle = \frac{1}{2}(x + |x|) \qquad 2.30$$

2.4.2 Unsaturated hydraulic conductivity function

The hydraulic conductivity of a material depends on the suction (Equation 2.25). The unsaturated hydraulic conductivity (k_u) can be plotted as a function of the suction in the material (Figure 2.9). There is a correlation between the unsaturated hydraulic conductivity curve (Figure 2.9) and the water retention curve (Figure 2.8). Whereas the latter (WRC) will influence the shape of the unsaturated hydraulic conductivity function. Because coarse materials desaturate at lower suctions than fine materials (Figure 2.8), there is a certain point where the hydraulic conductivity of the fine material becomes larger than that of the coarse material (Point A in Figure 2.9). This figure shows the k_u of two materials: a coarse (waste rock) and a finer (tailings) material.

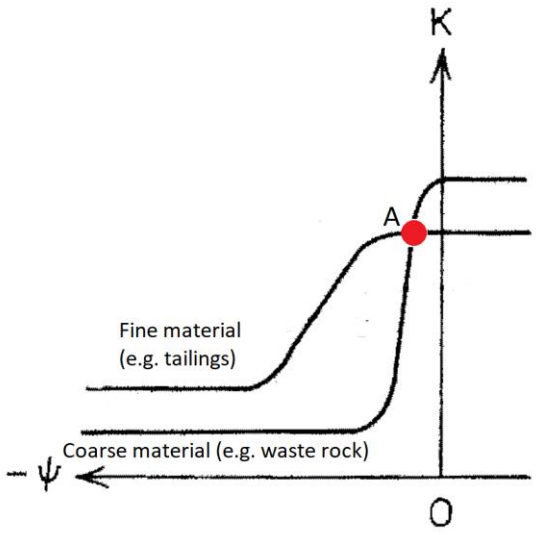

Figure 2.9: Typical unsaturated hydraulic conductivity curves for mine tailings and waste rock (adapted from Freeze and Cherry, 1979; and Aubertin et al., 1995).

The unsaturated hydraulic conductivity of granular materials is obtained through laboratory or field measurements (Fredlund and Rahardjo, 1993). However, it is quite complex to measure the

unsaturated hydraulic conductivity (k_u) in the laboratory. It is therefore usually more practical to predict the unsaturated hydraulic conductivity from the saturated hydraulic conductivity (k_s) and the WRC, using empirical, macroscopic or statistical models (Fredlund and Rahardjo, 1993; Fredlund et al., 2012).

The Fredlund et al. (1994) model was used in this project:

$$k_u = k_s \times k_{rel} = k_s \left[\frac{\int_{\ln(\psi)}^{b_{fx}} \frac{\theta(e^{y_{fx}}) - \theta(\psi)}{e^{y_{fx}}} \theta'(e^{y_{fx}}) dy_{fx}}{\int_{\ln(\psi_a)}^{b_{fx}} \frac{\theta(e^{y_{fx}}) - \theta_s}{e^{y_{fx}}} \theta'(e^{y_{fx}}) dy_{fx}} \right] \quad 2.31$$

where k_{rel} = Relative hydraulic conductivity (-);

e = Napierian number;

b_{fx} = $\ln(1 \times 10^6)$;

y_{fx} = Dummy variable standing for the natural logarithm of suction;

θ’ = Derivative of Equation 2.26.

2.4.3 Hysteresis

The WRC will usually not be the same if it is measured in a drying phase or during a wetting phase. In general, the AEV of the material will be higher in the drying phase (Haverkamp et al., 2002). Figure 2.10 shows a schematic representation of a WRC for wetting and drying cycles (Bouwer, 1969). The main drying curve (MDC) and main wetting curve (MWC) create the envelope or the extreme wetting and drying cases (Haverkamp et al., 2002).

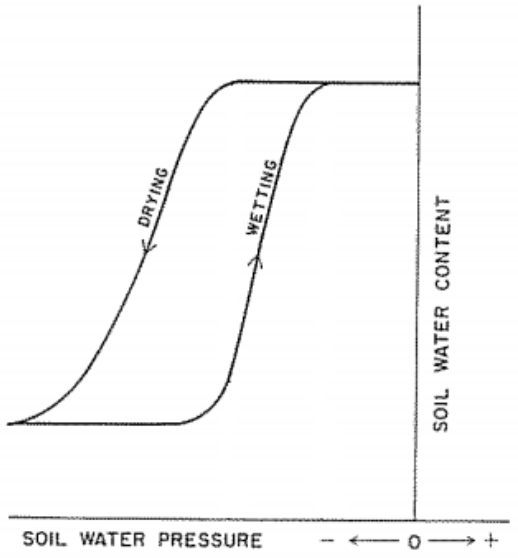

Figure 2.10: Schematic diagram of hysteresis (adapted from Bouwer, 1969).

Hysteresis of the WRC in granular materials can be attributed to several factors, including (Hillel, 1998; Delage and Cui, 2000; Maqsoud et al., 2012):

- Presence of interconnected flow paths.
- Ink bottle effect caused by the geometric non-uniformity of the individual pores.
- Contact angle effect; contact angle and radius of curvature are greater in the case of an advancing meniscus than in the case of a receding one.
- Presence of dead-end pores where water (drying curve) or air (wetting curve) could be trapped.
- Phenomena such as swelling, shrinking and aging (Mbonimpa et al., 2005, 2006) which result in differential changes of the structure of the porous material, depending on the wetting and drying history of the sample.

2.4.4 Shrinkage

The models for the WRC presented above suppose that the volume of the sample (and thus its porosity) remains constant throughout the whole suction range. However, a suction increase may induce desaturation and/or a change of volume in the case of compressible (shrinking) materials

(Alonso et al., 1990; Wheler et al., 2003; Mbonimpa et al., 2005; Saleh-Mbemba, 2010; Saleh-Mbemba et al., 2016). The shrinkage curves shown on Figure 2.11 are separated into three phases (Mbonimpa et al., 2005; Saleh-Mbemba et al., 2016):

- Phase 1: Saturated shrinkage (total volume change equals to the total volume of water lost, S_r stays constant).
- Phase 2: Residual shrinkage (total volume change is smaller than the total volume of water lost, S_r decreases).
- Phase 3: No-shrinkage (no volume change but decrease of S_r).

In Figure 2.11, we observe that the transition between phases 1 and 2 corresponds to the AEV of the material (Saleh-Mbemba, 2010). The transition between phases 2 and 3 is known as the shrinkage limit (w_{es}). Past this point, an increase in suction (or a decrease in the gravimetric water content, w) will not result in a change in the void ratio of the material. Saleh-Mbemba et al. (2016) observed that the final value of certain parameters (e.g. shrinkage limit, final void ratio, air entry value) may depend on the initial water content. This suggests that the shrinkage characteristics vary depending on the tailings type and that it is therefore important to study shrinkage of tailings with specific conditions that are representative of the *in-situ* conditions.

(a) Void ratio vs. Gravimetric water content

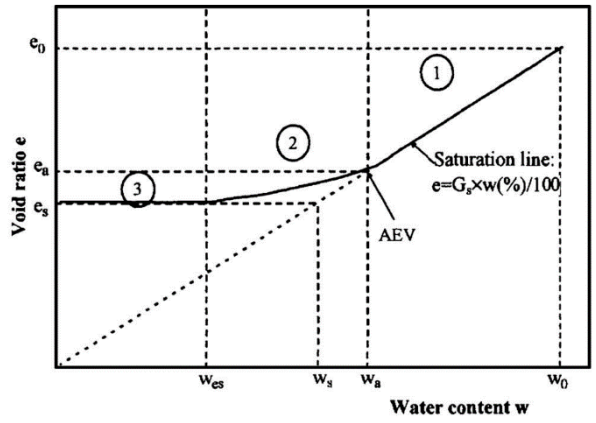

(b) Void ratio vs. Suction

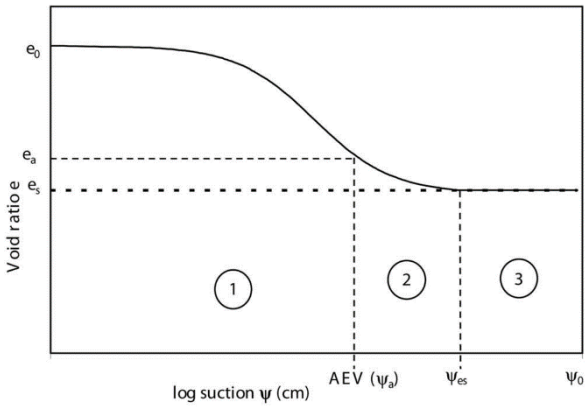

(c) Degree of saturation vs. Suction

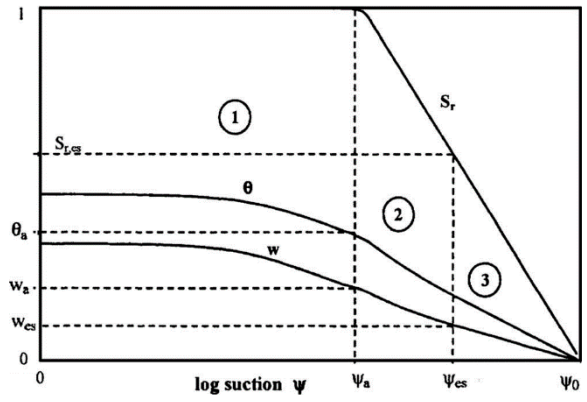

e_0 = Initial void ratio (-)

e_a = Void ratio when the suction is equal to the AEV (-);

e_s = Final void ratio (-);

w_0 = Initial gravimetric water content (% m/m);

w_a = Gravimetric water content when the suction is equal to the AEV (% m/m);

w_s = Final gravimetric water content (% m/m);

ψ_0 = Initial suction (kPa);

ψ_{es} = Suction at the shrinkage limit (kPa).

Figure 2.11: Shrinkage and desaturation phases of a compressible material, shown in various planes: a) e-w; b) e-log(ψ); c) WRC expressed as w-log(ψ), θ-log(ψ) and S_r-log(ψ) (from Mbonimpa et al., 2006).

2.5 Flow of oxygen through porous media

The oxidation reactions responsible of AMD in reactive mine wastes will increase the surface oxygen flow rate into the tailings (Equation 2.6). The oxygen flux into exposed tailings will be influenced by the oxygen diffusion coefficient (D_e) and the reactivity rate coefficient (K_r).

Molecular diffusion is the main oxygen transport mechanism in mine tailings. The diffusive flux of oxygen F(z,t) in an unsaturated porous medium can be defined using Fick's first law (e.g. Mbonimpa and Aubertin, 2003):

$$F(z,t) = -D_e \frac{\delta C(z,t)}{\delta z} = \theta_{eq} D^* \frac{\delta C(z,t)}{\delta z} \qquad 2.32$$

where C(z,t) = Concentration of oxygen at time t and depth from surface z [ML^{-3}];

D_e = Effective diffusion coefficient [L^2T^{-1}];

θ_{eq} = Equivalent (diffusion) porosity [-];

D^* = Bulk diffusion coefficient [L^2T^{-1}] defined as: $D^* = D_e/\theta_{eq}$.

In Equation 2.32, the equivalent porosity θ_{eq} considers the flux of oxygen in the air phase and in the water phase (Aubertin et al., 1999, 2000a), and is defined as:

$$\theta_{eq} = \theta_a + H \times \theta \qquad 2.33$$

where θ = Volumetric water content [-];

θ_a = Volumetric air content ($\theta_a = V_a/V_T$) [-];

H = Henry's equilibrium constant (H ≈ 0.03 at 20°C).

The effective diffusion coefficient (D_e) value is also estimated using predictive models based on basic material properties measured in the field. For example, the Aachib et al. (2004) model:

$$D_e = \frac{1}{n^2}\left[D_a^0 \theta_a^{p_a} + H D_w^0 \theta^{p_w}\right] \qquad 2.34$$

where D_a^0 = Diffusion coefficient of oxygen in air (≈ 1.8×10^{-5} m^2/s).

D_w^0 = Diffusion coefficient of oxygen in water (≈ 2.5×10^{-9} m^2/s).

p_a = Unitless exponent of the θ_a function ($p_a = 1.201\theta_a^3 - 1.515\theta_a^2 + 0.987\theta_a + 3.119$). Aachib et al. (2004) propose a value of 3.4.

p_w = Unitless exponent of the θ function ($p_w = 1.201\theta^3 - 1.515\theta^2 + 0.987\theta + 3.119$). Aachib et al. (2004) propose a value of 3.4.

Equation 2.34 is based on the Collin and Rasmuson (1988) formulation (Aachib et al., 2004).

Oxidation reactions influence oxygen flow when the tailings contain sulphides. This reaction is usually controlled by first order kinetics (Nicholson et al., 1989; Mbonimpa and Aubertin, 2003).

Thus, the oxygen consumption rate is linearly related to its concentration. The oxygen consumption is introduced into Fick's second law as follows (Mbonimpa et al., 2002a; 2002b):

$$\frac{\delta}{\delta t}\left(\theta_{eq} C\right) = \frac{\delta}{\delta z}\left(D_e \frac{\delta C}{\delta z}\right) - K_r C \qquad 2.35$$

This equation can be simplified if θ_{eq} and D_e are considered time and depth independent (Mbonimpa et al., 2002a; 2002b):

$$\frac{\delta C}{\delta t} = D^* \frac{\delta^2 C}{\delta z^2} - K_r^* C \qquad 2.36$$

Where K_r is the oxygen reactivity rate coefficient [T^{-1}], and K_r^* there is the bulk oxygen reactivity rate coefficient ($K_r^* = K_r/\theta_{eq}$).

The oxygen reactivity rate coefficient (K_r) can be estimated with the Collin (1987, 1998) model based on surface kinetics. The rate varies linearly with the sulphide content in this model. This model is written as follows (Collin, 1987):

$$K_r = K' \frac{6}{D_H}(1-n) C_p \qquad 2.37$$

where K' = Reactivity of pyrite with oxygen (K' ≈ 5×10^{-10} $m^3O_2 m^{-2}/s$);
C_p = Pyrite content over mass of dry tailings (kg/kg).

The Collin (1987) model assumes that the only sulphide is pyrite and that it is found uniformly throughout the material. Toussaint (2016) mentions that this is not always the case and that this hypothesis might result in over-estimation of the oxygen reactivity rate coefficient.

The parameter D_H represents an equivalent particle diameter that is estimated using a relationship with the particle size distribution curve (Aubertin et al., 1998; Mbonimpa et al. 2002a):

$$D_H = [1 + 1.17 \times log(C_U)] D_{10} \qquad 2.38$$

where D_{10} = Grain diameter at 10% passing (i.e. 10% of the particles in the sample have a smaller diameter than D_{10}) [L];
C_U = Coefficient of uniformity [L/L] expressed as: $C_U = D_{60}/D_{10}$;
D_{60} = Grain diameter at 60% passing (i.e. 60% of the particles in the sample have a smaller diameter than D_{60}) [L].

Once the D_e and K_r are obtained, it is possible to calculate the flux in the mine tailings. The steady-state oxygen flux (F_{O_2}) at the surface of the tailings can be calculated using this equation (Mbonimpa et al., 2003):

$$F_{O_2} = \frac{C_0 \times D_e}{L_{OT}} + 2K_r^* \left(\frac{C_0 \times D_e}{L_{OT}}\right) \sum_{j=1}^{\infty} \left(\frac{1}{\frac{j^2 \pi^2 D^*}{L_{OT}^2} + K_r^*} \right) \quad 2.39$$

Where C_0 represents the oxygen concentration in the atmosphere (20.9% or 0.28 kg/m^3 at 20°C; Mbonimpa et al., 2002b).

The parameter L_{OT} is the depth in the tailings from the surface at which the oxygen concentration becomes nil. Mbonimpa et al. (2002a) proposed the following equation to obtain L_{OT} (m):

$$L_{OT} = 4.23 \sqrt{\frac{D_e}{K_r}} \quad 2.40$$

2.6 Surface-atmosphere exchanges

The moisture exchanges between the soil (or tailings) surface and the atmosphere are mostly controlled by infiltration (entry of water in the material) and evaporation (exfiltration of water from the surface as vapour) (Wilson et al., 1994). More generally, water balance (WB) is a function of precipitation (P), evapotranspiration (ET), evaporation (E), runoff (R_{off}), interception (I_{nt}) and snowmelt (SM), recharge (R_{ech}) and change in storage (ΔST) (Blight, 1997; Wilson et al., 1997; Hillel, 1998; Morris and Stormont, 2000; Lu and Likos, 2000).

The SM parameter was not considered in this project (there was no snow at the site studied). The interception parameter (I_{nt}) represents uptake of water by plants and will be ignored thereafter since this study deals with the near-surface exchanges in an operating tailings storage facility (without any significant vegetation).

Two additional parameters are added when studying an active tailings storage facility (Blight, 1997): water from the fresh waste being deposited (W - Input), and water leaching from the waste (L - Output).

The water balance can then be represented as the difference between the input and output, plus the recharge and storage. It is defined by the following equation:

$$\left(P - R_{off}\right) + W = ET + R_{ech} + \Delta ST + L \qquad 2.41$$

This section discusses the parameters infiltration and evapotranspiration (evaporation) parameters presented in Equation 2.41.

2.6.1 Infiltration (I)

Infiltration is the general term applied to the process of water entry into a surface (Hillel, 1998). The infiltration process is a function of both the hydraulic conductivity and the hydraulic gradient at the surface of the soil or tailings (Childs, 1969). The rate of infiltration (I) into a material surface represents the water flux infiltrating into the profile per unit of surface area. The infiltrability (I_{nf}; expressed in $[L^3 \cdot L \cdot^{-2} T^{-1}]$ or $[L \cdot T^{-1}]$) is the capacity of to uptake the water at the surface (Hillel, 1998). The infiltrability is variable over time and it is also dependent on the initial water content of the material, along with the texture, structure, and uniformity (or layering) of the profile (Hillel, 1998). Any quantity of water that exceed the infiltrability of the material becomes runoff or ponding.

Infiltration tends to an equilibrium when it reaches a steady-state infiltrability (or final infiltration capacity) (Figure 2.12). Decrease in the rate of infiltration is primarily caused by the decrease of the suction gradient in the material. The steady-state rate is almost equal to the satiated (or field saturated) hydraulic conductivity (k_{fs}) of the material (Bréard-Lanoix, 2017). When the potential rate of infiltration is larger than the satiated hydraulic conductivity, surface runoff or ponding can occur, depending on the surface topography.

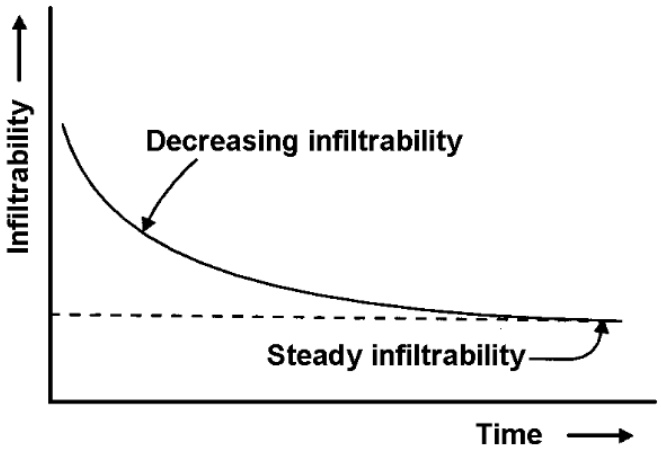

Figure 2.12: Decrease of infiltrability (a) and increase of cumulative infiltrability (b) with time (from Hillel, 1998).

Infiltrability depends on several factors including (Blight, 1997; Hillel, 1998): the initial water profile, the hydraulic conductivity of the material, the profile depth and layering, the swelling and shrinkage capacity of the material (including the presence of preferential flow paths), and the heterogeneity.

The water content profile during water infiltration in an unsaturated homogenous soil is illustrated in Figure 2.13. The top of the profile is saturated followed by a small decrease in the degree of saturation. In the transmission zone, the material is partially saturated and there is little or no change of the water content with depth. Finally, there is a sharp decrease in the water content in the wetting zone until the wetting front is reached. It consists of the boundary between the wet and the dry soil and it is characterized by a large hydraulic gradient. The soil above the wetting front is not necessarily saturated (McWorhter and Nelson, 1979).

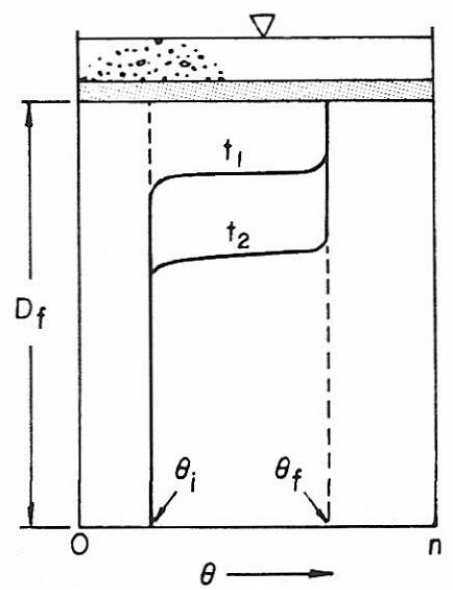

Figure 2.13: Water content profile during infiltration (McWhorther and Nelson, 1979). D_f: Depth of the wetting front; t_j: Position of the wetting front at time *j*; θ_i: Initial volumetric water content; θ_f: Final volumetric water content.

The infiltration capacity can be measured in the field using various techniques such as a single-ring, double-ring or disk (or tension) infiltrometers (Hillel, 1998; Bréard Lanoix, 2017). Infiltration can also be represented using empirical models (e.g. Kostiakov, 1932; Horton, 1940; Holtan, 1961) and mathematical models (e.g. Green and Ampt, 1911; Philip, 1957; Parlange et al., 1985) (Mollerup, 2007; Bréard-Lanoix, 2017).

The Green and Ampt (1911) model can be expressed differently depending on the boundary conditions being studied (Mein and Larson, 1973; Ali et al., 2016). For example, depending on the format of the equation, it can be used to calculate infiltration above homogeneous or layered soils, with or without ponding, and with steady-state or variable precipitations (Ravi and Williams, 1998; Bouwer, 2002). The model assumes a saturated piston flow with a uniform initial soil water content (Ali et al., 2016).

The Green and Ampt (1911) model for the infiltration rate (q_i) into a homogeneous flooded soil (Figure 2.14) is (Bouwer, 1969, 2002; Ravi and Williams, 1998):

$$q_i = \frac{dI}{dt} = k_w \frac{H_w + L_f + \psi_f}{L_f} \quad 2.42$$

$$q_i = \frac{dI}{dt} = \Delta\theta \frac{dL_f}{dt} \quad 2.43$$

where k_{fs} = Hydraulic conductivity of the wetted zone or satiated hydraulic conductivity (m/s).

H_w = Height of water above the soil (m).

L_f = Depth of the wetting front (m).

ψ_f = Suction head at the wetting front (m), can be estimated as half the AEV ($\psi_f = 0.5 \times \psi_a$) of the material (Bouwer, 1969, 2002).

I = Cumulative infiltration per surface area (m^3/m^2).

$\Delta\theta$ = Variation in the volumetric water content ($\Delta\theta = \theta_f - \theta_i$; Figure 2.13).

And the cumulative infiltration at time t is:

$$I(t) = L_f \Delta\theta \quad 2.44$$

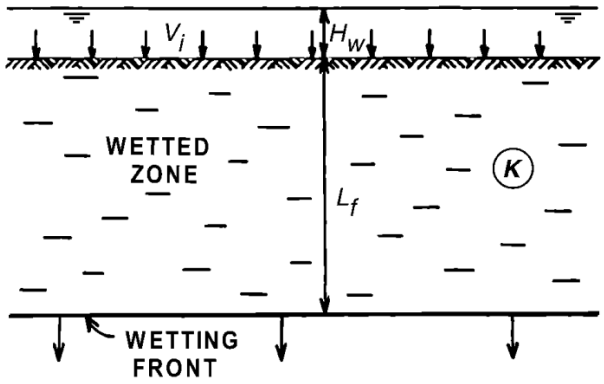

Figure 2.14: Infiltration of water into a flooded soil and parameters of the Green and Ampt (1911) model presented in Equation 2.42 (Bouwer, 2002).

Combining equations 2.42 to 2.43 yields:

$$\frac{k_{fs}}{\Delta\theta} dt = \frac{L_f}{H_w + L_f + \psi_f} dL_f \quad 2.45$$

By integrating equation 2.45 and using equation 2.44 to eliminate the parameter L_f ($L_f = I(t)/\Delta\theta$), the Green and Ampt (1911) equation for cumulative infiltration at time t is (Bouwer, 1969; Ravi and Williams, 1998; Miyazaki, 2006):

$$I(t) = k_{fs}t + \Delta\theta\left(H_w + \psi_f\right) \times \ln\left(1 + \frac{1}{\Delta\theta\left(H_w + \psi_f\right)}\right) \quad 2.46$$

The maximum hydraulic conductivity of the wetted zone (k_{fs}) is typically less than the hydraulic conductivity at saturation (k_{sat}). It is about $0.5 \times k_{sat}$ for sandy soils and $0.25 \times k_{sat}$ for clays and silts (Bouwer, 2002).

The Philip (1957) model is based on a solution of the partial differential equation of Richard's equation (Mein and Larson, 1971; Jaynes and Gifford, 1981):

$$I(t) = St^{1/2} + A't \quad 2.47$$

where S = Sorptivity (ability of the pores to absorb and release water by capillarity) ($cm/s^{1/2}$).

t = Time (s).

A' = Permeability coefficient (cm/s).

The parameter A' in Equation 2.47 is associated to the field saturated hydraulic conductivity (k_{fs} = (0.3 to 0.7) × A'). Both parameters S and A' vary depending on the initial soil moisture (Jaynes and Gifford, 1981), but are difficult to obtain (Fala, 2008).

2.6.2 Evaporation, transpiration and evapotranspiration (ET)

Evaporation is the process whereby liquid water is converted to water vapour (vaporization) and removed from the evaporating surface. The evaporation rate is a function of the vapour pressure gradient between the surface and the ambient atmosphere (Wilson et al., 1997). Transpiration is the vaporization of liquid water contained in tissues (plants) and the vapour removal to the atmosphere (Allen et al., 1998). Evapotranspiration (ET) is the combination of evaporation and transpiration. However, this project aims at studying uncovered (and non-vegetated) tailings, and so transpiration was neglected.

The potential evaporation (PE) is the quantity of water vapour that could be produced by a surface of water per unit surface area and unit time under the existing atmospheric conditions at equilibrium

(Wilson et al., 1997). Climatic conditions typically control the value of the potential evaporation (Rassam, 2002). It is expressed in [$L \cdot T^{-1}$] and is considered as the maximum rate of evaporation. The actual evaporation (AE) is the actual rate of evaporation from a surface. The AE rate is controlled by climatic conditions and material properties such as water retention curve, hydraulic conductivity and vapour diffusivity. It is also influenced by water availability (water content), material texture, and drying time (Wilson et al., 1997; Song et al., 2014). Drying curves represent the relationship between AE and PE (Figure 2.15). The ratio AE/PE begins to decrease (AE/PE < 1) as the availability of water decreases (material becomes unsaturated) (Hillel, 1980).

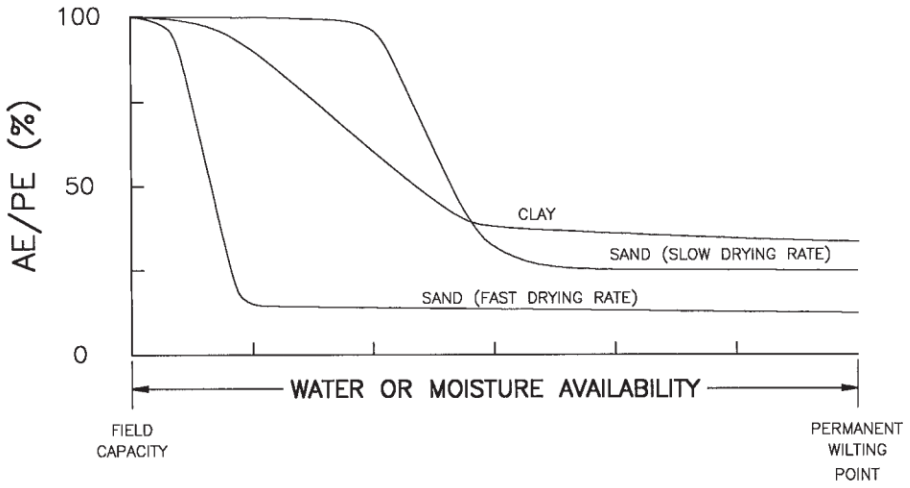

Figure 2.15: Typical drying curves for sand and clay showing AE as a percentage of PE, versus water availability (or suction) (Wilson et al., 1997).

The drying curve can be presented as a function of time (Figure 2.16). The evaporation is divided into three stages. During Stage 1, actual evaporation rate is constant and close to potential evaporation; it is solely governed by the climatic and environmental conditions (e.g. air temperature, air relative humidity, wind speed above the surface). During Stage 2, the surface starts to desaturate, and water supply is smaller than potential evaporation, the material properties (e.g. hydraulic conductivity, porosity, water retention curve) play a key role in the evaporation process. A rapid decrease of the evaporation rate characterizes Stage 2. The rate of decrease of the relative evaporation (or AE/PE ratio) is larger for coarser materials or when the PE rate is higher. Climatic

conditions also influence the evaporation rate during this stage. As drying proceeds, the evaporation rate continues to decline. At Stage 3, the water phase becomes discontinuous and water flows are predominantly through vapour diffusion. At this point, the evaporation rate is quasi-constant (Hillel, 1980; Wilson et al., 1994; Rassam and Williams, 1999a; Newson and Fahey, 2003; Bossé et al., 2015).

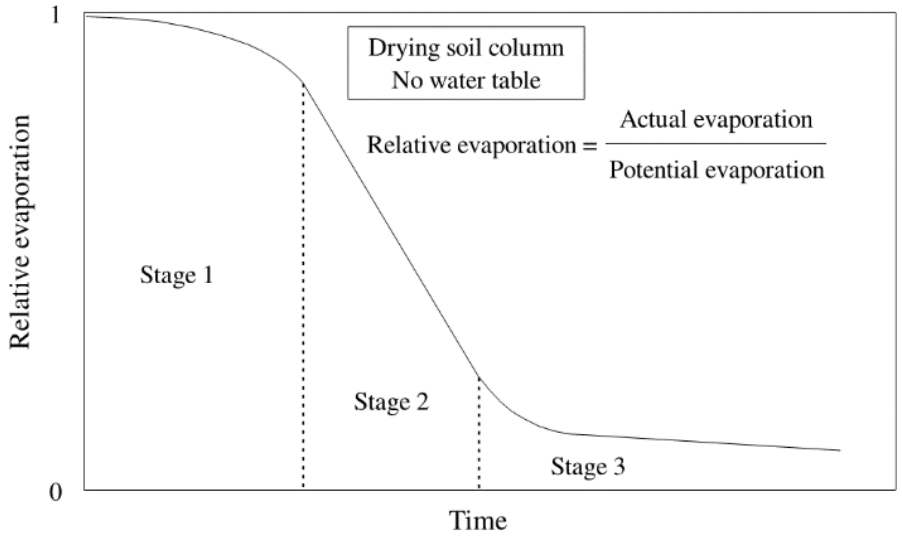

Figure 2.16: Evaporation phases from a granular material with respect to time (Rassam and Williams, 1999a).

Three main factors influence evaporation from bare surfaces are the energy at the surface, the relative humidity at the surface, and the availability of water close to the evaporative surface (Newson and Fahey, 2003; Cui and Zornberg, 2008). Evaporation is also influenced by surface osmotic suction, physical effects of salt precipitation and change in albedo (Simms et al., 2017). Evaporation is usually the largest source of water loss on a mine site in an arid or semi-arid climate (Blight, 2002), and can be the main driver for the flow of water in the active zone (Jabro, 2009). In a humid climate, when precipitation is greater than potential evaporation, the mean annual evaporation can sometimes approach potential evaporation (Zhang et al., 2004).

Relative evaporation (AE/PE) can be estimated with the following equation (Wilson et al., 1997):

$$\frac{AE}{PE} = \frac{e_{surf} - e_{va}}{e_{sa} - e_{va}} \quad 2.48$$

where e_{surf} = Vapour pressure at the surface of the material (kPa): $e_{surf} = RH_{surf} \times e_{sa}$;

RH_{surf} = Relative humidity at the surface of the material (related to suction, see Equation 2.52 below) (-);

e_{va} = Vapour pressure of the air (kPa): $e_a = RH_a \times e_{sa}$;

e_{sa} = Saturation vapour pressure at the temperature of the water (kPa);

RH_a = Relative humidity in the air (-).

The saturation vapour pressure (e_{sa} in kPa) can be estimated from the following equations (Brutsaert, 1988; cited by Song et al., 2014):

$$e_{sa} = (101.325)exp\left(13.3185t_{R_a} - 1.9760t_{R_a}^2 - 0.6445t_{R_a}^3 - 0.1299t_{R_a}^4\right) \quad 2.49$$

$$t_{R_a} = 1 - \frac{373.15}{T_a} \quad 2.50$$

where T_a = Air temperature (K).

Actual evaporation (AE) from a material surface (if the air, water and granular material temperature are the same) can also be estimated as (Campbell, 1985; cited by Rassam, 2002):

$$AE = \frac{RH_{surf} - RH_a}{1 - RH_a} \times PE \quad 2.51$$

The relative humidity at the material surface (RH_{surf}) can be expressed with the following equation (Edlefsen and Anderson, 1943; cited by Wilson et al., 1997):

$$RH_{surf} = exp\left(\frac{\psi_T \times g \times W_v}{R \times T_{surf}}\right) \quad 2.52$$

where ψ_T = Total suction in the liquid water phase expressed as equivalent matric suction (negative value) (m H_2O);

g = Gravitational acceleration (9.81 m/s^2);

W_v = Molecular weight of water (0.018 kg/mol);

R = Universal gas constant (8.3143 J/mol·K);

T_{surf} = Temperature at the surface (K).

Relative humidity at the material surface RH_{surf} with respect to suction for a given temperature using Equation 2.52. Equation 2.51 shows that the evaporation in a porous medium becomes zero when RH_{surf} is equal to the relative humidity in the ambient air RH_a.

Relative humidity in a material starts to decrease when the suction at the surface reaches around 3000 kPa. Below this suction, AE/PE = 1. This suction value (3000 kPa) is independent of time, soil water content and material texture (Wilson et al., 1997; Bossé et al., 2015).

At a certain point, water vapour flow becomes the dominant water transport mechanism when the tailings are partially saturated and depending on the void ratio (Wilson et al., 1994; Rassam and Williams, 1999a). The water vapour diffusion through a porous medium is dependent on material properties such as tortuosity. The vapour flow (f_v) in a granular material is described by Fick's first law (Campbell, 1985; cited by Rassam and Williams, 1999a; Wilson, 1994):

$$f_v = -D_v \frac{dc_{vap}}{dz} \qquad 2.53$$

where D_v = Coefficient of diffusion of vapour of the material (m^2/s);

c_{vap} = Vapour density (kg/m^3);

z = Measurement depth (m).

The coefficient of diffusion of vapour through a granular material (D_v) is less than through free air (D_a') because of the reduced cross-sectional area and increased tortuosity. Consequently, D_v in a material is defined as (Wilson, 1994; Rassam and Williams, 1999a):

$$D_v = D_a' \times \xi = \theta_a^{5/3} \left(D_{vap} \frac{W_v}{R \times T} \right) \qquad 2.54$$

where D_a' = Diffusion coefficient of water vapour in air (2.417×10^{-5} m^2/s at 20°C);

ξ = Relative diffusion coefficient (-) standing for the tortuosity of the material expressed as: $\xi = {\theta_a^2}/{n^{3/2}}$;

D_{vap} = Molecular diffusivity of water vapour in air (m^2/s):

$D_{vap} = 0.229 \times 10^{-4} \left(1 + \frac{T}{273}\right)^{1.75}$;

W_v = Molecular weight of water (0.018 kg/mol);

R = Universal gas constant (8.314 J/mol·K).

The vapour density c_{vap} is expressed as:

$$c_{vap} = RH \times c'_{vap} \quad (2.55)$$

where RH = Relative humidity at point z_i (-);

c'_{vap} = Saturation vapour density (0.017 kg/m^3 at 20°C).

The vapour flow rate (f_v) at the soil surface is equal the actual evaporation (AE) rate.

In steady-state conditions, the potential evaporation rate in a soil or tailings profile at a certain depth may be calculated from the unsaturated hydraulic conductivity function of the materials (Marshall et al., 1996):

$$z_{wt} = \int_0^{z_{wt}} dz_{wt} = -\int_0^{\psi_z} \frac{d\psi}{1 + \frac{PE}{k_u}} \quad (2.56)$$

where z_{wt} = Depth from the surface to the water table (m).

Evaporation may lead to desaturation but also, in certain cases, to desiccation of tailings (Simms et al., 2007; Fisseha et al., 2010; Daliri et al., 2016). Figure 2.17 illustrates the relationship between the variation in moisture content and the change in volume for drying freshwater tailings (Newson and Fahey, 2003). This figure is like the shrinkage curves presented in Section 2.4.4. The initial moisture content of the tailings (upon disposal) is usually higher than its liquid limit (also for paste tailings) (point A, on Figure 2.17). The material decreases in volume as the water content decreases (by drainage and evaporation). The tailings stay close to saturation until the suction reaches the AEV. The material starts to desaturate after this point, and the rate of volume change begins to decrease. Eventually, it reaches its shrinkage limit, where no further increase in density occurs, but the hydraulic conductivity continues to decrease as the degree of saturation is reduced (or suction increases) (Newson and Fahey, 2003).

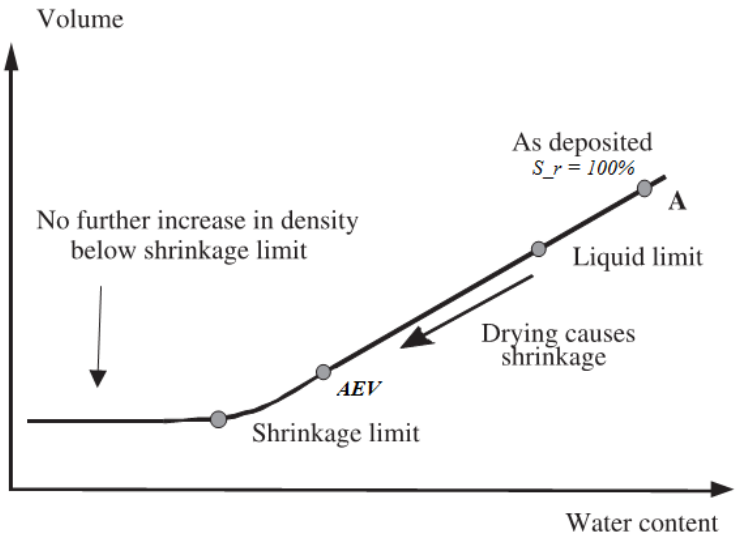

Figure 2.17: State changes in drying tailings (adapted from Newson and Fahey, 2003).

Measurement of evaporation can be done using various methods such as the evaporation pan, lysimeters, the eddy covariance method and the Bowen ratio method.

The Class A evaporation pan is a 1.22 m wide and 0.25 m deep cylindrical pan. It is placed on a level base and is filled with water. The water-level in the pan is monitored daily. Maximum and minimum daily temperatures are also recorded. Each day, water is added to refill the pan to keep the water level ±25 mm from the top (Newson and Fahey, 2003). Preliminary site potential evaporation estimates are often based on local Class A pan evaporation measurements. It offers a good reference point since it is a simple and widely used method (Newson and Fahey, 2003). Wind speed and direction may affect the measurements. The evaporation rate of sufficiently wet tailings is like the Class A pan evaporation rate (Fujiyasu et al., 2000).

A lysimeters consists in isolating a sample from the system and in determining the loss of water due to evaporation. It is typically a container filled with soil (at the same conditions as the *in-situ* surrounding soils) with system at its base to collect percolating water (Fank, 2011). Lysimeters can be weighable or non-weighable. The validity of this method depends on the boundary conditions of the lysimeters which should not influence the actual evaporation (Fujiyasu et al., 2000; Knidiri et al., 2017).

The Bowen ratio method is based on the measured energy balance. This approach requires the use of a Bowen ratio weather station equipped with a pyranometer and net radiometer to measure the net radiation (Q_{net}), humidity and temperature sensors located at 1 m and 2 m above the surface to measure the sensible heat flux (H_s), and temperature and heat flux sensors in the granular material to measure the soil heat flux (G) (Figure 2.18; Fujiyasu et al., 2000). The station is often equipped with a data logger and an independent power source, such as a solar panel. This method is preferably used for large and uniform surfaces (Qiu et al., 1998).

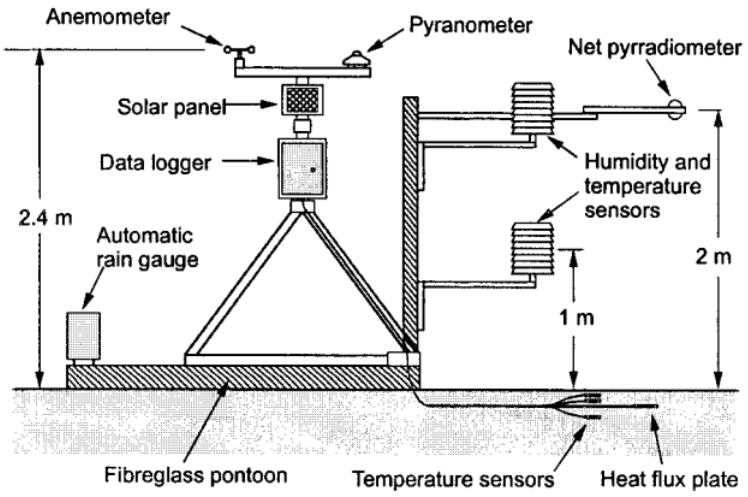

Figure 2.18: Drawing of a Bowen ratio weather station (from Fujiyasu et al., 2000).

Mathematical models can also be used to estimate the potential or actual evaporation rate (Ventura et al., 1999; Weeks and Wilson, 2003; Bossé et al., 2013). There is no consensus regarding the suitability of any model for a given climate. Each model requires local calibration before it can be used for evaporation estimations (DehghaniSanij et al., 2004).

The Penman and Modified Penman are detailed below. These models are steady state models. The Modified Penman was specifically designed for bare surfaces in semi-arid conditions.

Penman (1948) presented a relationship for the PE (in mm/d) from a soil surface (Allen, 1986; Wilson et al., 1994; Weeks and Wilson, 2006):

$$PE = \frac{\Gamma \times Q_{net} + \nu \times E_a}{\Gamma + \nu} \quad 2.57$$

where Γ = Slope of the saturation versus vapour pressure curve at the mean air temperature (kPa/°C);

Q_{net} = Net solar radiation (mm/d water equivalent – 1 mm/d = 2.45 MJ/m^{2}d; Allen, 1986; Allen et al., 1998);

ν = Psychrometric constant (kPa/°C);

E_a = Potential rate of evaporation from the Dalton-type equation $E_a = f(u)(e_{sa} - e_{air})$ (mm/d);

f(u) = Wind mixing function: $f(u) = 0.35(1 + 0.15 \times U_a)$;

e_{sa} = Saturation vapour pressure of air at mean temperature of the surface of the material T_s (kPa);

e_{air} = Vapour pressure of the air above the evaporating surface at temperature T_a (kPa);

U_a = Wind speed (in km/h for the f(u) function).

The main advantage of this method is that it requires simple climatic parameters such as wind speed, temperature and relative humidity. However, its main disadvantage is that it provides an estimate of PE that assumes that water is freely available throughout the measurement period and thus overestimates evaporation from unsaturated surfaces (Wilson, 1990; Wilson et al., 1997). Most evaporation models from a soil surface (with or without crops) are based on the PE model.

The Modified Penman (MPe) model was developed by Wilson (1990) to estimate actual evaporation AE from bare unsaturated surfaces, and is represented in the following form (Wilson, 1990; Weeks and Wilson, 2006):

$$AE = \frac{\Gamma \times Q_{net} + \nu \times E_a'}{\Gamma + \nu} \quad 2.58$$

where E_a' = $f(u)e_{air}(B_{RH} - A_{RH})$;

B_{RH} = Inverse of the air relative humidity (-): $B_{RH} = RH_{air}^{-1}$;

A_{RH} = Inverse of the relative humidity at the material surface (-): $A_{RH} = RH_{surf}^{-1}$.

This equation gives a more accurate estimate of the AE from bare surfaces of unsaturated materials (Wilson, 1990; Wilson et al., 1994; Weeks and Wilson, 2003).

In certain conditions, precipitation of salts on the tailings surfaces during evaporation leads to the development of thin salt crusts that can reduce the rate of evaporation by increasing the albedo of the material and the resistance to moisture transfer, and by decreasing the saturation vapour pressure of the pore fluid (Fujiyasu and Fahey, 2000; Newson and Fahey, 2003; Dunmola and Simms, 2010; Dunmola, 2012a). In addition, the actual rate of evaporation will decrease as the salt concentration increases. In these conditions, the actual evaporation is significantly reduced and the only effective mechanism of moisture transfer from the surface to the air is by diffusion in the vapour phase.

Shrinkage can cause cracking of the surface of materials (Section 2.4.4), and evaporation can occur from the vertical surfaces of these cracks. The total exposed surface area of cracked tailings may therefore be as large as four times the original crack-free surface area (Fujiyasu et al., 2004). In a study by Fujiyasu et al. (2000), desiccation cracks contributed up to 90% of the total evaporation from a tailings facility. The following equation was proposed to estimate the total actual evaporation (E_{total}) from a tailings facility with desiccation cracks (Fujiyasu et al., 2000):

$$E_{total} = E_{intact}\frac{A_{intact}}{A_{total}} + E_{crack}\frac{A_{crack}}{A_{total}} \quad 2.59$$

where E_{total} = Total evaporation from the tailings facility [L/T];
E_{intact} = Evaporation from the intact tailings [L/T];
E_{crack} = Evaporation from the desiccation cracks [L/T];
A_{total} = Total area of the tailings facility [L^2];
A_{intact} = Surface area of the intact tailings [L^2];
A_{cracks} = Horizontal surface area of the cracks (not to the total exposed surface area in the cracks) [L^2].

Fujiyasu et al. (2000) proposed that the PE measured with a Class A pan was like E_{crack} in the equation above. A_{crack} can be estimated with these equations:

$$A_{total} = A_{intact} + A_{crack} \quad 2.60$$

$$\frac{A_{intact}}{A_{total}} = \left(\frac{1+e_t}{1+e_{in}}\right)^{\frac{2}{3}} \quad 2.61$$

where e_t = Surface void ratio of the intact area (-);
e_{in} = Surface void ratio at crack initiation, where $e_i \geq e_t$.

In a highly desiccated area, it might be important to consider desiccation cracks to obtain the total evaporation.

2.6.3 Zero-flux plane (ZFP)

The water budget (evaporation vs. recharge) in an unsaturated soil profile can be understood using the zero-flux plane (ZFP) concept. The zero-flux plane (ZFP) is defined as the border plane where the hydraulic gradient (i = dh/dz) is 0 (i.e. where there is a reversal in the direction of the unsaturated hydraulic gradient – Richards et al., 1956; Arya et al., 1975; Scanlon et al., 2002; Miyazaki, 2006; Healy, 2010) (Figure 2.19). The gradient is oriented upwards above the ZFP and downwards below (Dreiss and Anderson, 1985). The objective of determining the ZFP is to approximate the contribution of both evaporation and percolation to the overall water budget (assuming precipitation and runoff are known) (Arya et al., 1975; Cooper et al., 1990; Healy, 2010).

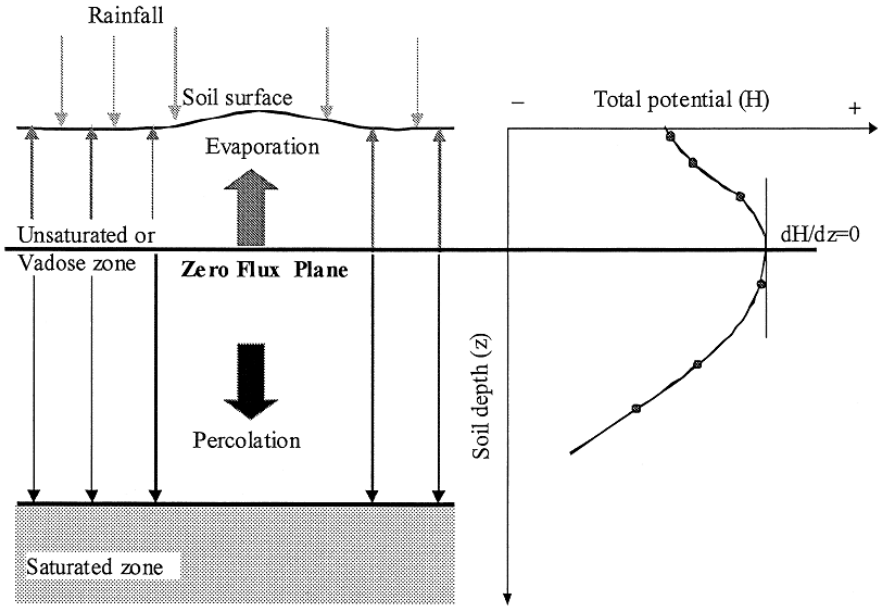

Figure 2.19: Zero-flux plane concept (from Khalil et al., 2003).

Knowledge of the WRC of the material is required to evaluate the position of the ZFP in a profile (Cooper, 1980). Moreover, it is necessary to know either the volumetric water content or the suction

(ideally both) at various time intervals throughout the soil profile (Dreiss and Anderson, 1985; Sharma et al., 1991; Evett et al., 2012).

One of the main assumptions of the ZFP is that the water moves vertically through the unsaturated zone as periodic and distinct pulses that can be monitored over time (Healy, 2010). It is therefore more or less realistic depending on the climate and the season. Figure 2.20 presents four hypothetical flow profiles that can be observed in the unsaturated zone:

a) Profile A presents a downward flux (with no ZFP). This would occur if the potential evaporation was very low (e.g. snowmelt or at the end of a rainy season).

b) Profile B shows an upwards flux (with no ZFP). This represents cases where the potential evaporation is very high, for example at the end of the summer or dry season.

c) Profile C is a "typical" ZFP. The change in the slope (dh/dz) from positive to negative indicates that the water at the top of the soil is evaporating whereas the water below the ZFP is percolating downwards. This would be the case in situations at the beginning of a dry period following a wet (rainy) period.

d) Profile D is a mixed case where a wetting pulse is on surface, above an evaporative gradient. In this example, the topmost ZFP will migrate towards the bottom until a fully percolating profile develops (Profile A). With time (and assuming no additional precipitation), a profile like Profile C will reappear (Khalil et al., 2003). This type of situation could occur at the beginning of a wet season following a dry period.

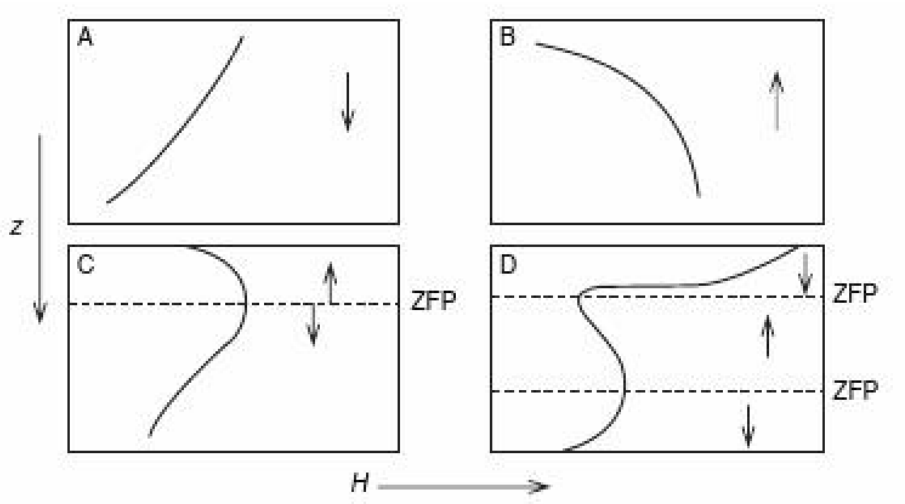

Figure 2.20: Hypothetical vertical profiles of total head within the unsaturated zone indicating: (a) downward flux (no ZFP); (b) upward flux due to evaporation (no ZFP); (c) a single ZFP; (d) two ZFP (could be present after a storm occurring following a dry spell, for example) (from Healy, 2010).

The position of the ZFP in the soil profile is not constant through time. As a soil dries, it moves downwards in the soil profile (Figure 2.21a) and a progressively greater depth of profile contributes to evaporation (Copper et al., 1990). Figure 2.21b presents an example of the hydraulic potential with respect to depth below the surface of a field. The inflexion of the curve (where the slope $d\psi/dz = 0$) indicates the position of the ZFP. As the summer progresses (low precipitation/high potential evapotranspiration), the suction throughout the soil profile increases and the depth of the ZFP increases. The displacement rate of the ZFP decreases as time of drying increases. The depth of the ZFP can decrease rapidly in response to large rainfall at any time of the year, even if the soil is very dry (Healy, 2010).

(a) (b)

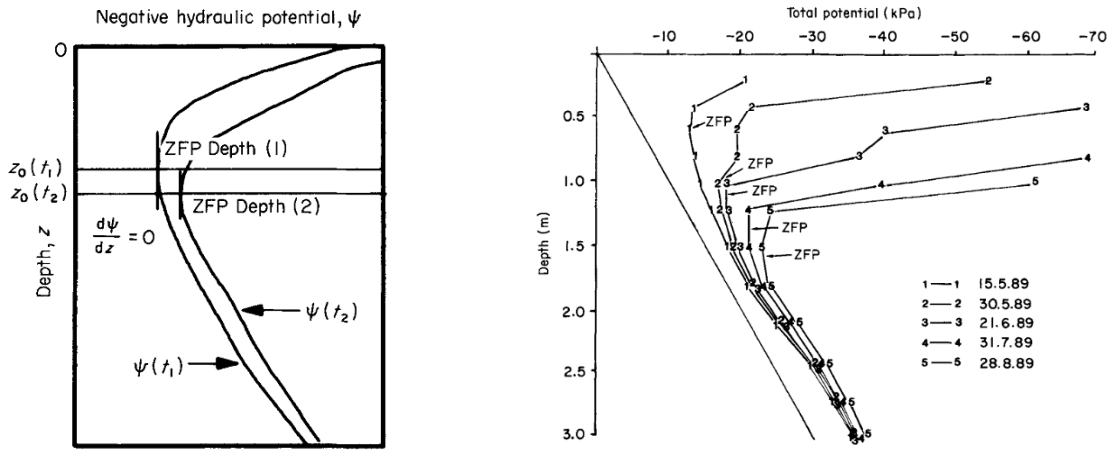

Figure 2.21: (a) Variation of hypothetical suction profiles (between times t_1 and t_2) in the ZFP method (Cooper et al., 1990). (b) Example of the variation of the ZFP with time (Cooper et al., 1990).

A limitation of the zero-flux plane method is that it can only be used under conditions where a ZFP exists (Cooper et al., 1990). It is best applied in regions that display a wide range of soil-water contents throughout the year (Healy, 2010). Moreover, it ignores the potential for horizontal flow above and below the ZFP. All flow is assumed vertical (Healy, 2010). Furthermore, the ZFP method is sensitive to soil water content (or suction) measurements (McGowan and Williams, 1980), and it ignores hysteresis (Khalil et al., 2003).

2.7 Numerical simulations

The software Vadose/W from the GeoStudio was used to complete the hydrogeological numerical simulations in this project. It is a saturated/unsaturated finite element hydrogeological simulation software. It is based on the software Seep/W also from GeoStudio for the hydrogeological calculations. The software Seep/W has been used in saturated/unsaturated transient conditions to simulate the behaviour of mine tailings (Aubertin et al., 1996; Bussière, 1999; Bussière et al., 2007; Cissokho, 2008)

Vadose/W also integrates measured daily climatic conditions (e.g. precipitation, maximum and minimum temperature, maximum and minimum relative humidity, wind speed, radiation) to allow the simulation of sol-atmosphere processes (i.e. evaporation, transpiration, freeze-thaw cycles). The potential evaporation is estimated using the modified Penman equation (Equation 2.58; Wilson, 1990), and computation of the diffusion and consumption of oxygen is also possible with this software (Pabst, 2011). Others have validated the software, for example: Barbour et al. (2005), Shackelford and Benson (2006), Gosselin (2007), Demers (2008), Demers et al. (2010), Pabst (2011), Vanapalli and Adem (2013), and Saleh-Mbemba (2010, 2016). Table 2.2 summarizes the numerical properties of the software Vadose/W (adapted from Pabst, 2011).

Table 2.2: Numerical properties of the software Vadose/W (GeoSlope, 2007, 2016).

Properties	**Vadose/W**
Resolution method	Residual vector norm
Elements	Quadrilateral or triangular
Interpolation function	Linear or quadratic
Numerical integration	Gauss quadrature scheme
Temporal integration	Adaptive time stepping using finite difference approximation scheme
Matrix resolution	Gaussian numerical integration
Convergence	Tolerance on the vector norm

Vadose/W requires the input of the WRC and unsaturated hydraulic conductivity curves, and of the thermal conductivity and volumetric heat capacity of the material. In addition, pressure or flow boundary conditions can be applied to the model. Climatic conditions (placed at the surface of the model) can be entered by the user. The PE is either entered manually, calculated using the climatic conditions, or estimated using the latitude of the site and time of year. The model is sensitive to the shape of the WRC. The software does not also account for hysteresis and preferential flow paths (Adu-Wuzu et al., 2007; Pabst, 2011).

CHAPTER 3 EXPERIMENTAL METHODOLOGY

3.1 Field work

A two-week field campaign was conducted in October 2004 at the Bulyanhulu mine tailings storage facility. The main objectives of this campaign were to observe surface deposition of paste tailings, conduct modified oxygen consumption (MOC) tests, gather information from the Bulyanhulu mine, and collect samples of Bulyanhulu paste tailings.

3.1.1 The Bulyanhulu tailings disposal site

The Bulyanhulu mine is in Northern Tanzania, roughly 50 kilometres south of Lake Victoria (Figure 3.1). It is now operated by Acacia Mining but was initially operated by Barrick Gold Corporation. It is an underground mining operation hoisting around 3000 tonnes (0.3 oz/tonne) of ore per day. It has produced more than 3 million ounces of gold since the beginning of production in March 2001 (Acacia Mining, 2018).

Figure 3.1: Location of the Bulyanhulu mine site (source: Google maps).

Deposition of paste tailings on the surface at Bulyanhulu lasted for about 15 years before the mine moved to a traditional (slurry) tailings deposition (with reprocessing of the old paste tailings tailings). During surface paste tailings disposal, thickeners and disc filters dewatered tailings from

the mill. The filter cake (gravimetric water content, w = 23%; Shuttleworth et al., 2005) was placed in a paste conditioner where water was added to attain the desired paste consistency with a gravimetric pulp density (P_m) of around 74% (or w = 35%). Two positive displacement pumps transported the pulp to the tailings storage facility (TSF). Deposition was cycled through 10 deposition towers to create a uniform rate of rise for the entire facility (Figure 3.2). The size of the paste tailings storage facility was approximately 500 m × 800 m with a maximum elevation of 12 m. The typical deposition thickness of a paste layer varied between 0.3 m and 1 m (upstream), and the deposition slope was approximately 1:12 (V:H) (Shuttleworth et al., 2005). The paste was left to consolidate and desaturate through evaporation and drainage, until a new layer was deposited on top.

Figure 3.2: Paste tailings disposal towers located in the Bulyanhulu Mine tailings storage facility in October 2004 (picture taken by the Author).

The surface of the tailings shrinked and cracked as they desaturated (also observed by Saleh-Mbemba, 2010). Figure 3.3 presents pictures of tailings from the Bulyanhulu mine at various stages after deposition. Fractures appeared within a few hours after deposition. Fairly rapid shrinkage can

be expected in paste tailings since these contain less water than typical tailings (P_m = 74% for these paste tailings compared to $P_m \approx$ 30% to 45% for conventional tailings).

(a) During deposition (fractures from previous layer filled with fresh tailings).

(b) During deposition.

(c) 4 hours after disposal, drying patterns start to appear.

(d) Four days after disposal.

(e) Two weeks after disposal.

Figure 3.3: Bulyanhulu paste tailings at various stages following deposition in the tailings storage facility (pictures taken by the Author in October 2004).

3.1.2 Sampling of Bulyanhulu paste tailings

Paste tailings samples were collected at the Bulyanhulu mine and characterized in the laboratory at Polytechnique Montréal. Tailings were sampled from the paste mixer before pumping to the tailings storage facility. A total of six 5-gallon (20 L) buckets were collected (Buly-04-01 to Buly-04-06) in 2004. Additional samples (six 5-gallon buckets) were also sampled from the paste mixer and sent to Polytechnique Montréal in the summer of 2007 (Buly-07-01 to 06). The reactive tailings were saturated and kept under water in the buckets, to limit oxygen ingress and acid mine drainage (AMD) generation, until they were characterized in the laboratory.

3.2 Characterization of tailings

3.2.1 Storage and preparation of tailings samples and specimens

Upon reception in the laboratory, the tailings had consolidated in the buckets, leaving a free water cover above the tailings surface. The (clear) surface water was removed and all the buckets were emptied in a mixing drum (45 gallons). Demineralized water was added, and the tailings were mixed thoroughly until a smooth tailings slurry was obtained. The homogenized tailings slurry was then transferred into buckets.

A mini-slump test was used to estimate the pulp consistency and density of the paste during laboratory experiments (Figure 3.4). It consisted of a small cylinder (diameter $\approx$ 5 cm; height $\approx$ 12 cm), based on the work of Pashias et al. (1996). Crowder (2004) also used a similar equipment to prepare paste tailings specimens. The relationship between the slump height (after removal of the cylinder) and gravimetric pulp density (P_m) was established in the laboratory for both Buly-04 and Buly-07 tailings (Figure 3.5).

Figure 3.4: Example of slump test used to evaluate the appropriate paste consistency.

The desired pulp density (P_m) for these experiments was 74% (based on the pulp density of the tailings at the Bulyanhulu mine; Golder, 2005), which corresponded to a slump height of 7.8 cm (Figure 3.5). Tailings specimens were prepared at a paste-like pulp density (by adding demineralised water) before being used in the laboratory. This relation is valid only for the Bulyanhulu mine tailings and the slump cylinder used in this project. A specific characteristic curve, such as the one shown in Figure 3.5, would be required for other tailings and/or equipment.

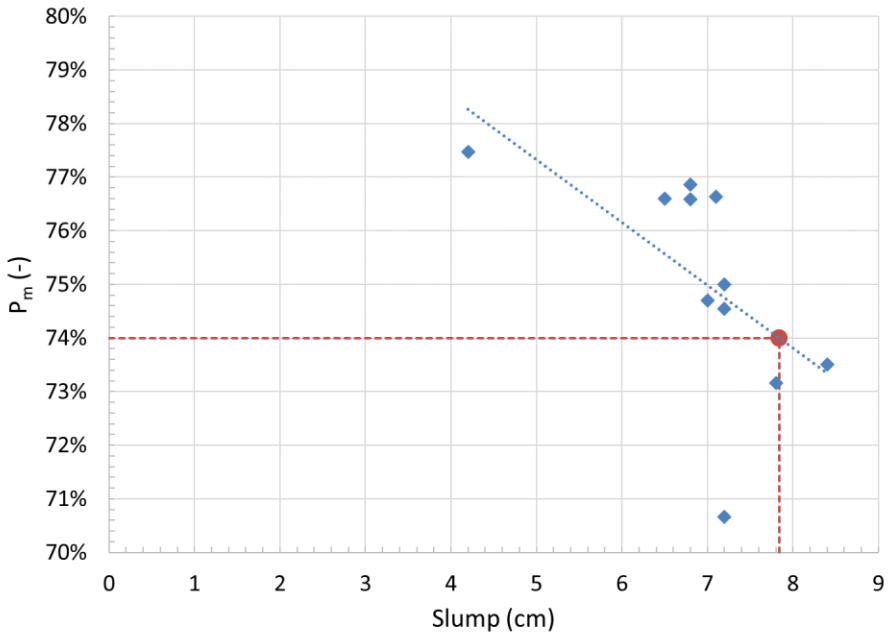

Figure 3.5: Relationship between the slump height and the gravimetric water content for Bulyanhulu tailings and the slump cylinder used in this project.

3.2.2 Particle size distribution

The particle size distribution curves were obtained using sieving (particle diameter > 0.08 mm) and sedimentation analysis (particle diameter < 0.08 mm) (ASTM D422). The mesh sizes of the sieves used were 2.5 mm, 1.25 mm, 0.63 mm, 0.32 mm, 0.16 mm and 0.08 mm. Tests were carried out on ten samples of Buly-04 tailings and three samples of Buly-07 tailings.

The particle size distribution of the Buly-04 tailings (6 specimens) was also determined using a laser diffraction particle size analyzer (Malvern Mastersizer) at the Université du Québec en Abitbi-Témiscamingue (UQAT).

Results from these tests (and other described below) are presented in Chapter 4.

3.2.3 Relative density of the solid particle (Specific gravity)

The relative particle density (D_r) was obtained by the water pycnometer method (ASTM D854). Six specimens of Buly-04 tailings and six specimens of Buly-07 tailings were characterized.

3.2.4 Atterberg limits

Tests to determine Atterberg limits (liquid and plastic limits) were performed using the method described in ASTM D4318. The liquid limit (w_l) is obtained using a brass cup (Casagrande cup). The plastic limit (w_p) is measured by rolling a thread on a flat surface. The measurement of the Atterberg limits was attempted for both the Buly-04 and Buly-07 tailings.

3.2.5 Mineralogy

The mineralogy of the tailings was evaluated by X-ray diffraction (Bruker A.X.S. Advance D8) at UQAT (Villeneuve, 2005). The objective was to identify the minerals present in the Bulyanhulu tailings. Six finely ground samples (at the UQAT laboratory) of Buly-04 samples were analysed.

3.2.6 Saturated hydraulic conductivity

The saturated hydraulic conductivity (k_s) of the tailings was determined using flexible wall permeameters (ASTM D5084). A backpressure of 650 kPa was used to ensure saturation of the specimens. The degree of saturation was assessed for each sample upon dismantling. Seven variable head tests were carried out (Table 3.1).

Table 3.1: Properties of the specimens for the measurement of the saturated hydraulic conductivity of the Bulyanhulu tailings in flexible wall permeameters.

Test #	Material	n (-)	e (-)	Height (cm)	Diameter (cm)	S_r (-)
1	Buly-04	0.42	0.73	9.5	7.2	93.0%(1)
2	Buly-04	0.41	0.71	8.2	7.2	93.2%(1)
3	Buly-04	0.44	0.79	8.4	7.2	96.8%(1)
4	Buly-04	0.42	0.73	8.6	7.2	93.2%(1)
5	Buly-04	0.41	0.71	11.3	7.2	91.4%(1)
6	Buly-07	0.39	0.64	10.8	7.2	100%(2)
7	Buly-07	0.40	0.66	9.6	7.2	100%(2)

(1) Specimen was not completely saturated, so saturated hydraulic conductivity (k_s) could be underestimated (Chapuis, 2004).

(2) Calculated degree of saturation exceeded 100%. Specimens were assumed to be saturated.

3.2.7 Water retention curves

The water retention curve (WRC) of Bulyanhulu tailings (Buly-04 and Buly-07) was measured using the modified Tempe cells and the pressure plate extractor (PPE). Both methods have been used extensively in the past to determine the water retention curve of mine tailings (Aubertin et al., 1998, 2003a, 2003b; Saleh-Mbemba, 2010, 2016; Pabst, 2011). The methodology used in this project was based on standards ASTM D3152-72 and ASTM D6836.

Nine Tempe cells tests were carried out to determine the WRC of the Bulyanhulu tailings (five tests with Buly-04 samples, and four tests with Buly-07 samples). Initial sample conditions are presented in Table 3.2.

Table 3.2: Initial conditions of the Tempe cell tests. e: void ratio; w: gravimetric water content; P_m: gravimetric pulp density; θ_i: initial volumetric water content.

Tailings	Sample	e (-)	w (-)	P_m (-)	θ_i (-)
Buly-04	Buly-04-T1	0.71	24.2%	80.5%	0.42
	Buly-04-T2	0.63	21.6%	82.2%	0.43
	Buly-04-T3	0.74	25.1%	79.9%	0.41
	Buly-04-T4	0.66	22.5%	81.6%	0.42
	Buly-04-T5	0.73	25.0%	80.0%	0.39
Buly-07	Buly-07-T1	0.68	23.0%	81.3%	0.38
	Buly-07-T2	0.72	24.5%	80.3%	0.38
	Buly-07-T3	0.72	24.5%	80.3%	0.39
	Buly-07-T4	0.70	23.8%	80.8%	0.38

Samples for the Tempe cell tests were compacted and saturated using a flexible wall permeameter (ASTM D5084-03).

The pressure plate extractor consists of a pressurised sealed chamber that can contain up to a dozen specimens (instead of one for the Tempe cell). The procedure used here is based on ASTM standards D3152-72 and ASTM D6836, but has been slightly modified to fit the objectives of the project.

Saturated specimens (of known volume) were prepared to the desired pulp density (Section 3.2.1) and placed on a saturated cellulose membrane. The chamber was then sealed, and gas pressure was applied. Water can freely flow from the bottom of the apparatus. The pressure plate extractor was opened regularly, every 48 h or so, once the samples were at equilibrium at each pressure level (no more water flowing from the outlet at the base). One of the specimens was collected, weighed, measured and dried in an oven to obtain the gravimetric water content (w). The pressure plate was then sealed again, and a higher pressure was applied. The procedure was repeated for 8 - 10

incremental pressure steps. The maximum pressure that can be applied for a cellulose membrane in a PPE is about 14 MPa (2000 psi; Richards, 1947; Langfelder, 1964; Soilmoisture, 2000).

Shrinkage, cracking and oxidation were assessed during testing. Most of the increments were below the air-entry value of the material. It was observed that little or no volume change due to drainage and suction occurred past the AEV (see also Saleh-Mbemba, 2010; Fisseha et al., 2010; Saleh-Mbemba et al., 2016). Image analysis using the software ImageJ was used to measure sample diameter (Figure 3.6b). This method was, for example, used by Benzaazoua et al. (2004) to assess crack development in paste tailings (which was not observed in the PPE tests) (Deschamps, 2009).

(a) (b)

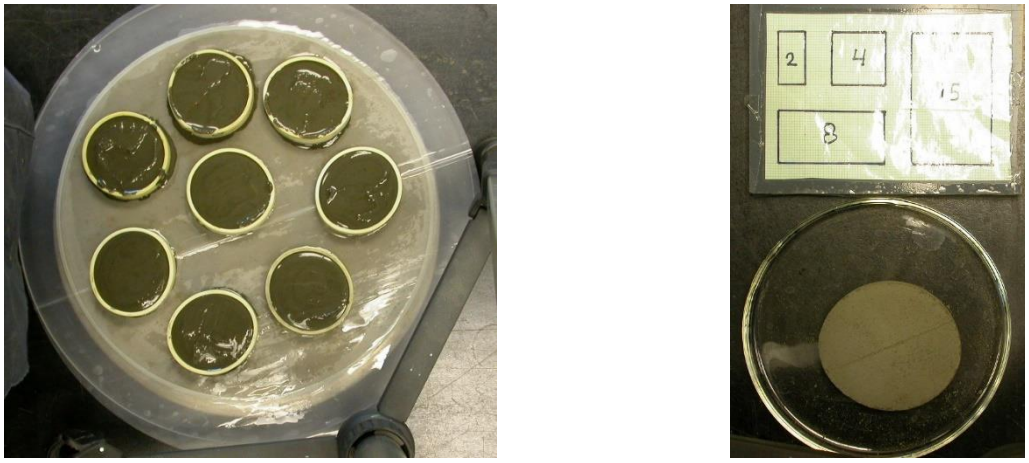

Figure 3.6: (a) Bulyanhulu tailings specimens at $P_m \approx 74\%$ ($w \approx 35\%$) prepared for pressure plate extractor testing on a cellulose membrane; (b) Specimen removed from the pressure plate extractor, next to a measurement scale (in cm^2) for analysis with ImageJ.

The void ratio (e) and volumetric water content (θ) for a given suction (ψ, which corresponds to the applied gas pressure) were calculated from the gravimetric water content and volume measured at each pressure step.

Four PPE tests were completed to determine the WRC of the Bulyanhulu tailings (two tests with Buly-04 and two tests with Buly-07 tailings) (conditions given in Table 3.3).

Table 3.3: Initial specimen conditions for pressure plate extractor tests. e_i: initial void ratio; w_i: initial gravimetric water content; P_m: gravimetric pulp density; θ_i: initial volumetric water content.

Test	e_i (-)	w_i (-)	P_m (-)	θ_i (-)
Buly-04-PPE1	0.72	24.6%	80.3%	0.42
Buly-04-PPE2	1.06	36.0%	73.5%	0.51
Buly-07-PPE1	0.98	33.6%	74.8%	0.50
Buly-07-PPE2	0.85	29.1%	72.4%	0.47

The Fredlund and Xing (1994) curve fitting equation (Equation 2.26) was used to describe the WRC; it was fitted (i.e. adjusted parameters a_{fx}, m_{fx}, n_{fx}, ψ_a, ψ_r) using the data points measured in the laboratory. This model has been used by others in the past to describe the WRC of mine tailings (e.g. Qiu and Sego, 2001; Milczarek et al., 2006; Bussière, 2007; Pabst, 2011; Saleh-Mbemba, 2016).

3.2.8 Consolidation

One-dimensional consolidation tests were carried out on Buly-04 tailings using previously calibrated fixed ring oedometers (ASTM D2435). The specimens were initially saturated in a flexible wall permeameter with an initial gravimetric water content (w) of 24.7% (P_m = 80.2%; n = 0.42). Table 3.4 gives the properties of the two specimens at the beginning of the consolidation tests. The test characteristics (applied loads and duration of loading and unloading cycles) are presented in Table 3.5. The tests were completed with a 11:1 loading ratio (the mass via a lever increased the force on the specimen by 11 times).

Table 3.4: Properties of the two oedometer cells prepared for consolidation tests. $M_{initial}$: initial mass of the specimen; h_i: initial thickness of the specimen; d: diameter of the specimen; e_i: initial void ratio of the specimen.

Identification	$M_{initial}$ (g)	h_i (cm)	d (cm)	e_i (-)
C1	134.3	2.02	6.33	0.71
C2	141.1	2.04	6.34	0.66

Table 3.5: Loads applied and duration of loading and unloading cycles (loading ratio: 11:1). M: mass added in the oedometer (applied mass on the specimen ×11); Duration: duration of the loading increment.

	M (kg)	Duration (h)
Loading	0.1	23.0
	0.5	24.1
	1	24.0
	2	72.3
	4	20.6
	8	28.6
	16	21.3
	32	97.2
	64	48.3

	M (kg)	Duration (h)
Unloading	16	22.9
	4	24.2
	1	71.4
	0	48.9

3.3 In-situ modified oxygen consumption tests

A total of seven modified oxygen consumption (MOC) tests were conducted on paste tailings at the Bulyanhulu tailings storage facility in October 2004. The objective of the tests was to assess the oxygen diffusion (D_e) and reactivity rate (K_r) coefficients, and to calculate the steady-state oxygen flux in the exposed tailings (F_{O_2}) (Mbonimpa et al., 2002b, 2003). The test consisted of inserting a cylinder (d = 15 cm) into the mine tailings, with a 2 to 5 cm headspace left at the top to

create an air (oxygen) chamber (see Figure 3.7). The cylinder was then sealed hermetically with a cap and oxygen concentration in the reservoir was monitored over time. A variation in the oxygen concentration in the reservoir of at least 3% to 5% needed to be recorded during the tests to obtain relevant results.

A control oxygen sensor was placed in the isolated box next to cylinder to correct measurements for fluctuations caused by external factors like ambient temperature and atmospheric pressure variations (Tibble, 1997; Bussière et al., 2002; Mbonimpa et al., 2002b, 2011; Dagenais, 2005).

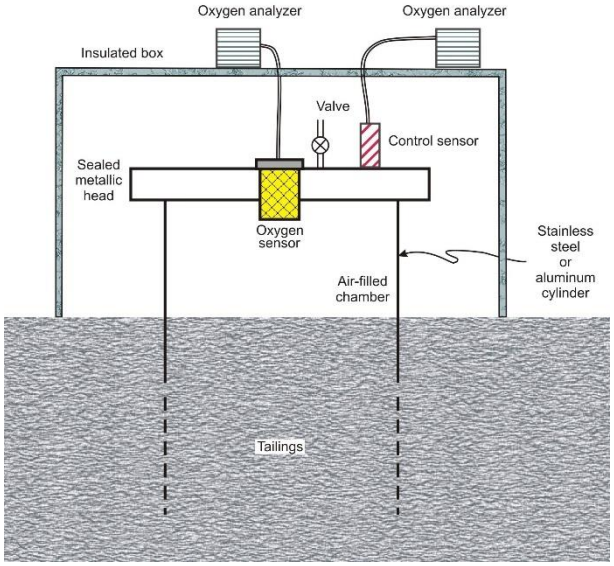

Figure 3.7: Modified oxygen consumption test in exposed tailings (adapted from Bussière et al., 2002).

These tests were interpreted with the software Vadose/W (GeoSlope, 2007, 2016; Pabst, 2011).

The tests were carried out in the south-east area of the tailings storage facility (Figure 3.8).

Figure 3.8: Location of the 2004 MOC tests on Bulyanhulu TSF (Photo: Barrick Gold Corporation, 2008).

Tailings samples were collected after the diffusion tests to evaluate the *in-situ* volumetric water content and porosity of the tailings using a ring and the volume replacement method (Table 3.6).

Table 3.6: Characteristics of the tailings at the MOC tests locations. T_a: air temperature; $h_{reservoir}$: height of the reservoir (between the tailings surface and the cover); n: porosity; S_r: degree of saturation at the beginning of the test; ρ_d: dry density.

Site	**T_a (°C)**	**Duration of test (min)**	**$h_{reservoir}$ (cm)**	**n (-)**	**S_r (-)**	**ρ_d (kg/m^3)**
B-1	32.8	86	2.9	0.44	69%	1653
B-2	33.2	60	3.8	0.40	82%	1607
B-3	29.9	185	3.6	0.34	98%	1746
B-4	34.0	28	4.1	0.39	60%	1630
B-5	32.6	66	3.5	0.41	68%	1560
B-7	33.2	59	3.3	0.43	82%	1677
B-10	31.4	129	3.7	0.40	92%	1746

The air temperature (T_a) for all tests was at or above 30°C. Tests were stopped after a significant decrease of the oxygen concentration in the cylinder (about 5%) was recorded. The MOC tests

lasted in general approximately 60 minutes but could be longer (see Table 3.6) when the oxygen diffusion coefficient was small (e.g. Test B-3, which lasted 185 minutes for S_r = 98%).

The porosity (n) of the tailings at the testing locations was between 0.34 to 0.44, with an average of 0.40. The tailings were thus partially consolidated; it was possible to walk on the surface in this area. The degree of saturation (S_r) of the tailings varied from 60% to 98%. The *in-situ* dry density (ρ_d) of the tailings was comprised between 1560 kg⁄m^3 and 1676 kg⁄m^3.

3.4 Physical models

3.4.1 Single-layer (SL) column tests

Four columns with an internal diameter of 29 cm and filled with Bulyanhulu tailings were prepared in the laboratory to investigate the impact of layer thickness and pulp density on the hydrogeotechnical response of the tailings. Three columns were filled with tailings at a paste-like gravimetric pulp density ($P_m \approx 74\%$; $w \approx 35\%$). The last column contained a tailings slurry of lower density ($P_m \approx 66\%$, $w \approx 51\%$). A fifth column was filled with distilled water to measure potential evaporation in the laboratory. Table 3.7 presents characteristics of each SL column test.

Table 3.7: Single-layer column (SL) tests characteristics used to investigate the impact of layer thickness (h_L) and gravimetric pulp density on the response of Bulyanhulu tailings. M_{pulp}: mass of tailings (solids and water); P_m: gravimetric pulp density; w_i: initial gravimetric water content; RD_p: relative pulp density; n: pulp porosity; h_i: initial thickness.

Identification	**M_{pulp} (kg)**	**P_m (-)**	**w_i (-)**	**RD_p (-)**	**n (-)**	**h_i (cm)**
SL-01	10.3	71.7%	39.4%	1.90	0.54	10.2
SL-02	22.0	71.8%	39.1%	1.90	0.53	19.8
SL-03	33.3	71.2%	40.4%	1.88	0.54	30.0
SL-04	29.0	66.1%	51.2%	1.77	0.60	27.7

The columns were left open to the atmosphere and water could drain through the bottom; water draining from the base was collected. The weight of the columns (with tailings) was measured hourly the first day of the test and daily afterwards. A Watermark suction sensor (Irrometer Company, Inc.) was installed approximately 5 cm above the base of the tailings to monitor suction near the base of the column. These sensors have a range of 1-199 kPa, and a resolution of 1 kPa. Suctions were recorded everyday. Laboratory temperature and relative humidity were measured daily. The elevation of the tailings surface was regularly recorded to monitor settlement. Figure 3.9 shows the setup of the Bulyanhulu column tests and a view of the surface of SL-01 and SL-04 at the beginning of the test.

(a) (b)

(c) (d)

Figure 3.9: (a) Testing setup for single-layer (SL) column tests (in plastic buckets) filled with Bulyanhulu tailings (SL-02 and SL-04). (b) Placement of the Watermark sensor in SL-01. (c) Top view of a single-layer column filled with lower water content (w = 39.4%) tailings (SL-01) (d) Top view of the higher water content (w = 51.2%) tailings (SL-04).

Several pictures of the surface of the single-layer columns were taken during the tests to follow the development of cracks at the surface of the tailings. The surface area and density of fractures were assessed using the software ImageJ.

The results from these tests are presented in Chapter 5.

Figure 3.10: Examples of cracks in SL-01, ten days after deposition.

3.4.2 Multilayer (ML) instrumented column tests

Four instrumented columns were used to study paste tailings surface disposal scenarios. The Plexiglas columns had an inside diameter of 29.5 cm and a height of 45 cm. Between 2 and 4 layers of paste tailings were deposited at regular intervals to investigate the interaction between fresh and dried paste tailings layers. The tailings were placed at a pulp density close to the *in-situ* design density ($P_m \approx 74\%$, $w \approx 35\%$). Table 3.8 presents the characteristics of the instrumented column tests carried out in this project.

Table 3.8: Characteristics of the instrumented column tests. h_L: initial design thickness layer.

Identification	Material	h_L [(1)] (cm)	# layers
Col-01	Buly-04 tailings	10	3
Col-02	Buly-07 tailings	10	4
Col-03	Buly-07 tailings	20	2
Col-04	Buly-07 tailings	20	2

(1) Design value.

The column tests are identified by the column name (Col-01 to Col-04; e.g. Col-01 corresponds to the first column test) and the layer number (L1 to 4; the first layer of column Col-01 is identified as Col-01-L1).

Figure 3.11a shows a sketch of the multilayer (ML) instrumented column with the position of the instruments and sensors during the tests. Figure 3.11b is a picture of Col-04 after the deposition of Layer 2. Results from the instrumented column tests are presented in Chapter 6. Table 3.9 presents a summary of the initial characteristics of the paste tailings placed in the instrumented columns. The initial water content of each layer could slightly vary depending on the manipulation and preparation of the samples (using the mini-slump test, Section 3.2.1).

(a) (b)

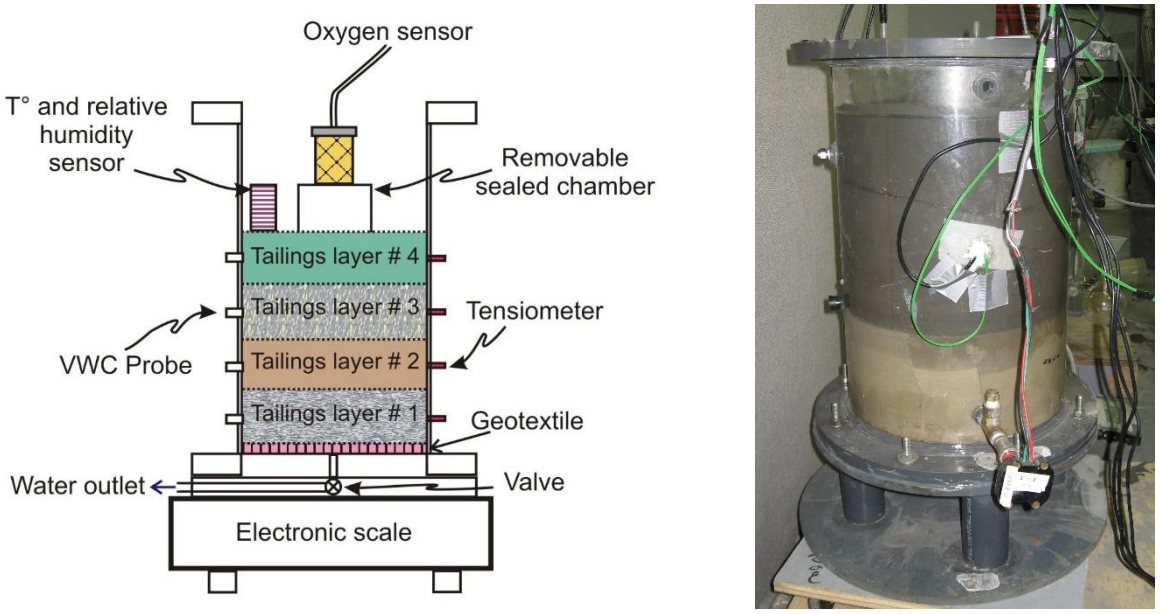

Figure 3.11: (a) Column test configuration (not to scale) and sensor locations. (b) Instrumented column Col-04 filled with two 20 cm layers of Bulyanhulu tailings.

Table 3.9: Characteristics of the instrumented columns tests. M_{pulp}: mass of tailings (solids and water); h_L: initial thickness of the layer; w_i: initial gravimetric water content; P_m: initial gravimetric pulp density; n: initial porosity.

Column #	Identification	M_{pulp} (kg)	h_L (cm)	w_i (-)	P_m (-)	n (-)	Duration of test (days)
1	Col-01-L1	13.8	10.9	33.2%	75.1%	0.49	18.9
	Col-01-L2	14.9	11.0	36.0%	73.5%	0.51	13.9
	Col-01-L3	16.2	12.1	30.5%	76.6%	0.47	14.8
2	Col-02-L1	13.8	10.6	34.1%	74.6%	0.50	32.8
	Col-02-L2	13.1	10.5	41.5%	70.7%	0.55	20.0
	Col-02-L3	14.0	10.0	33.9%	74.7%	0.50	18.8
	Col-02-L4	13.9	10.3	33.3%	75.0%	0.49	12.7
3	Col-03-L1	25.2	19.2	30.6%	76.7%	0.47	189.0
	Col-03-L2	32.6	24.4	33.4%	75.0%	0.49	111.0
4	Col-04-L1	22.8	18.2	30.5%	76.6%	0.47	189.0
	Col-04-L2	26.2	19.2	33.3%	75.5%	0.49	111.0

The following information was available when (or immediately after) a fresh layer of tailings was placed in the column: the particle relative density (D_r), the gravimetric water content of the tailings pulp in the layer (w_{Lj}), the height of the fresh tailings layer (h_{Lj}), the mass of the tailings pulp deposited in the column ($M_{Tailings}$), and the cross-sectional area of the column (A_{col}). The parameters D_r and A_{col} were invariable. The water content (w_{Lj}), height of the fresh tailings layer (h_{Lj}), and mass of the pulp could vary with time (depending on the amount of water loss through evaporation and drainage, and the settlement).

Each column was weighed daily during the tests to monitor mass variation and assess the effect of drainage from the bottom of the column and evaporation. The underflow of the column was also collected in a graduated cylinder to measure drainage flow rate. The mass of tailings and water was measured with a precision of ±2 g. Mass variations of the columns were assumed to be due only to

change in water content. A loss of mass that did not correspond to the water collected at the base of the column was therefore assumed to be due to evaporation.

For this project, the flow (Q) was normalized with respect to the cross-section area of the columns (A = 660.5 cm^2) to obtain the specific flow (q):

$$q = \frac{Q}{A} \tag{3.1}$$

This simplified comparison between drainage and evaporation for the various tests.

Coated TDR probes (Soilmoisture Corp.) were placed in the middle (mid height) of each layer to measure the variation of volumetric water content (VWC or θ). Coated probes are less sensitive to salinity than traditional TDR probes (Jones et al., 2002). The coated TDR probes were replaced with EC-5 capacitance probes (Decagon Devices, Inc.; 0.001 m^3/m^3 resolution with ±0.02 m^3/m^3 accuracy) in columns Col-03 and Col-04. Both types of VWC probes (TDR and EC-5) were calibrated specifically for the Bulyanhulu paste tailings. VWC measurements were taken at 1-hour intervals in all columns.

The pore water pressure was measured with several types of sensors, installed in the middle of each tailings layer. PX240 sensors (Omega) were coupled with 1 bar ceramic cups to measure both positive and negative pore water pressures (±100 kPa) in columns Col-01 and Col-02. The ceramic cups tend to desaturate at high suctions (above about 80 kPa) and needed to be resaturated regularly. For column tests Col-02, Col-03 and Col-04, Watermark probes (suction range 1-199 kPa, resolution 1 kPa) were used to monitor suction in the tailings. An MPS-1 suction probe (Decagon) was also placed 5 cm from the bottom of Col-03-L1. This probe measures suctions between 10 and 500 kPa (±5 kPa from 10 to 50 kPa and ±20% from 50 to 500 kPa). Pore water pressures were measured at 1-hour intervals. The Watermark probes have frequently been used to measure suction in mine tailings in the field and in the laboratory (e.g. Bussière, 1999; Bussière et al., 2003; Dagenais, 2005; Kalonji Kabambi et al., 2017; Éthier, 2017).

The columns were also instrumented at the surface of the tailings layers (Figure 3.12). Two 0243 LVDT (Trans-Tek Inc., range 12.7 mm) were used to monitor tailings displacement (settlement). Automated measurements were taken at 1-hour intervals. The LVDT sensors were installed on the fresh tailings layers once there was no more free water at the surface. The tailings settlement and

the thickness of free water were also measured manually every 1 to 2 hours during 48 hours after placement of a fresh layers and once a day afterwards. It was assumed that, once a fresh layer of tailings is deposited on a former consolidated layer, the thickness of the underlying layer remained constant (i.e. additional consolidation occurs only in the fresh layer).

A T5 tensiometer (Meter Group) was inserted 1 cm below the surface of column tests Col-01 and Col-02 to measure suction. The sensor tip had a diameter of 5 mm. It measured suctions near the surface of the tailings to values up to 80 kPa with an accuracy of 0.5 kPa every hour.

A camera was also installed at the top of the instrumented columns Col-01 and Col-02 (Figure 3.12b).

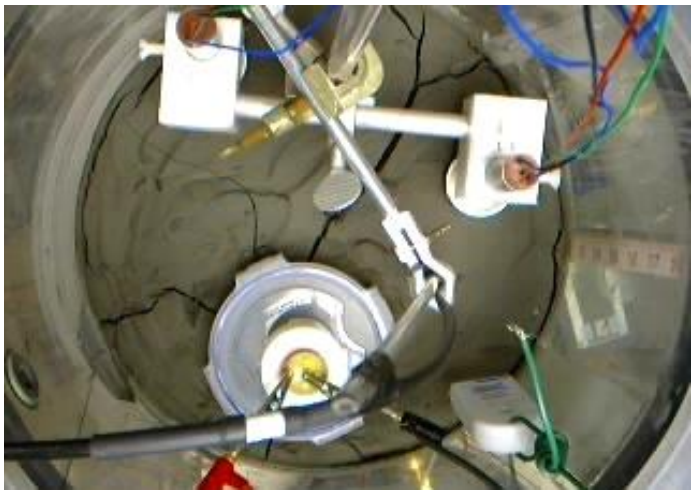

Figure 3.12: Top view of the instruments installed in ML column Col-02-L3.

A plastic cylinder with an inside diameter of 5 cm was also inserted in the surface layer of column Col-02 (Figure 3.12). This cylinder was sealed with a cover fitted with an oxygen sensor (Apogee Instruments SO-121; 2.6 mV at 21% O_2) to perform small-scale oxygen consumption tests on the tailings (see Section 3.3 for the procedure). The lid with the oxygen sensor was removed after the MOC tests but the plastic cylinder in the tailings remained in place for the duration of the test. No shrinkage of the tailings around the cylinder for the MOC tests was observed.

Table 3.10 presents a summary of the position of the instruments placed in the multilayer instrumented columns.

A sensor (Omega OM-62) was placed next to the tailings surface to take hourly recordings of the ambient air temperature (0.05°C resolution at ± 0.5°C accuracy) and relative humidity (0.05% resolution at ± 2% accuracy) during the tests. A column with the same diameter than the multilayer column was filled with distilled water to measure potential evaporation rate in the laboratory.

Table 3.10: Position of the instruments in the multilayer instrumented columns (the base of the tailings is at elevation y = 0 cm).

Instrumented columns Col-01 and Col-02					
Column	**Layer**				**Surface**
	1 (y = 5 cm)	**2 (y = 15 cm)**	**3 (y = 25 cm)**	**4 (y = 35 cm)**	
Col-01	Coated TDR PX-240 sensor	Coated TDR PX-240 sensor	Coated TDR PX-240 sensor	Coated TDR PX-240 sensor	LVDT (×2) Camera Temp/RH
Col-02	Coated TDR PX-240 sensor Watermark	Coated TDR PX-240 sensor Watermark	Coated TDR PX-240 sensor Watermark	Coated TDR PX-240 sensor Watermark	LVDT (×2) T-5 sensor O_2 sensor Camera Temp/RH
Instrumented columns Col-03 and Col-04					
	Layer				**Surface**
	1 (y =10 cm)		**2 (y = 30 cm)**		
Col-03	MPS-1 **y =**5 cm EC-5 Watermark		EC-5 Watermark		LVDT (×2) Temp/RH
Col-04	EC-5 Watermark		EC-5 Watermark		
Note: Distances (in cm) are given with reference to the base of the tailings (y = 0 cm).					

The porosity (n) and the void ratio (e) during the test for each of the deposited layer were estimated from the initial pulp porosity and adjusted as the tailings settled and changed volume.

The volume of a fresh layer (V_L) deposited in the column was measured using the thickness of the layer (h_L) and area of the cylindrical column (A). The volume cracks in the (old) layer (below the fresh tailings layer) could be estimated:

$$V_{cracks} = V_{tailings} - h_f \times A \quad 3.2$$

Where $V_{tailings}$ is the total volume of tailings poured in the column. It was assumed (and confirmed when dismantling the columns) that the fresh tailings would fill the cracks of the underlying layer. The volume of tailings of each layer was corrected for the cracks present in the underlying layer.

The CIF of the tailings in the ML columns could not be determined using image analysis because the instruments installed at the surface of the columns (e.g. LVDT probes, cylinder for MOC test, T5 tensiometer) obstructed the pictures used to determine the cracked area. It was estimated from the tailings volume (V_{cracks}), and by assuming that the cracks were triangular with a depth equal to the thickness of the tailings layer.

Interlayer flow represents the water exchanges between two layers and was used to calculate the water balance in each of the tailings layers. It can be negative (downwards flow) or positive (upwards flow). The interlayer flow gives an estimate of how much water is lost through drainage or evaporation, and to determine how water flows in the variably saturated tailings column. The interlayer flow was estimated in each layer at each stage of the column test. It was calculated from laboratory measurements and simulated in Vadose/W (Section 7.1.4). Figure 3.13 presents a conceptual model of the multilayer columns with a definition of the parameters used to calculate the interlayer flow and change in storage in the tailings layers of the instrumented laboratory columns.

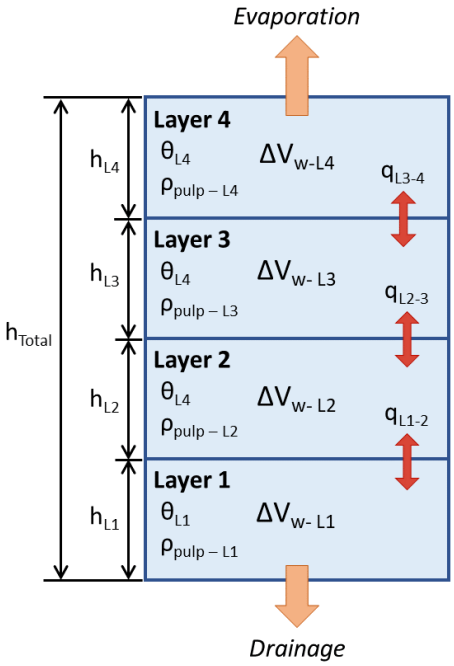

Note:

- Evaporation is always positive.
- Drainage is always negative.
- If q_{Lj} is positive, the flow is upwards.
- If q_{Lj} is negative, the flow is downwards.
- If $\Delta V_{w\text{-}Lj}$ is positive, there is recharge in the layer.
- If $\Delta V_{w\text{-}Lj}$ is negative, there is desaturation in the layer.

Figure 3.13: Interlayer flow and changes in storage in each tailings layer of the multilayer laboratory columns. θ_L: VWC of the layer; ρ_{pulp}: pulp density when the layer was poured (g/cm^3); $\Delta V_{w\text{-}L}$: change in the water volume in the layer (cm^3); q_L: unit flux (cm/s) at the interface between two layers.

The suffix "L*j*" referred to the number of the layer considered. The specific volume of water in the columns was expressed in cm (or cm^3⁄cm^2). For a given layer, a negative volume indicated loss of water. A positive sign therefore indicated an increase in the water content of the layer. Flow of water was in cm/s. Loss of water by drainage (downward) was negative, and by evaporation was positive.

The following hypotheses were adopted for the calculation of the interlayer fluxes:

- The characteristics (e.g. particle size distribution, relative density) of the tailings were homogeneous and constant for each layer.
- The cracks at the surface of older layers were filled with fresh tailings when a new layer was deposited.

- Desiccated (old) layers were incompressible, and the height, total volume, and porosity in these layers were assumed constant. In other words, consolidation after deposition was assumed to happen only in the new fresh layer.
- The water content was uniform in each layer.
- The change of mass in the column was due exclusively to loss of water by drainage or evaporation.

3.5 Numerical simulations

Numerical simulations were carried out with Vadose/W (Geo-Slope International, version 7.21). This finite element software can simulate saturated and unsaturated groundwater flow and exchanges with the atmosphere considering climatic conditions at the surface of the model, in one or two dimensions (but not axisymmetric).

The numerical simulations were compared to the laboratory results and observations from single-layer (Chapter 5) and multilayer column tests (Chapter 6). Additional 1D numerical simulations were carried out to assess the hydrogeological behaviour of paste tailings disposed under field conditions (Chapter 7). These simulations also included a parametric study to evaluate the influence of certain properties (layer thickness, cycle time, position of the water table, tailings hydrogeological properties, climatic conditions) on the behaviour of a surface paste tailings storage facility.

The single-layer and multilayer column tests were modeled in 1D (see Figure 3.14). Evaporation, infiltration, and outflow were normalized for the area of the column and are presented either in L^3/L^2 (mm^3/mm^2, cm^3/cm^2 or m^3/m^2).

(a) Single-layer columns (b) Multilayer columns

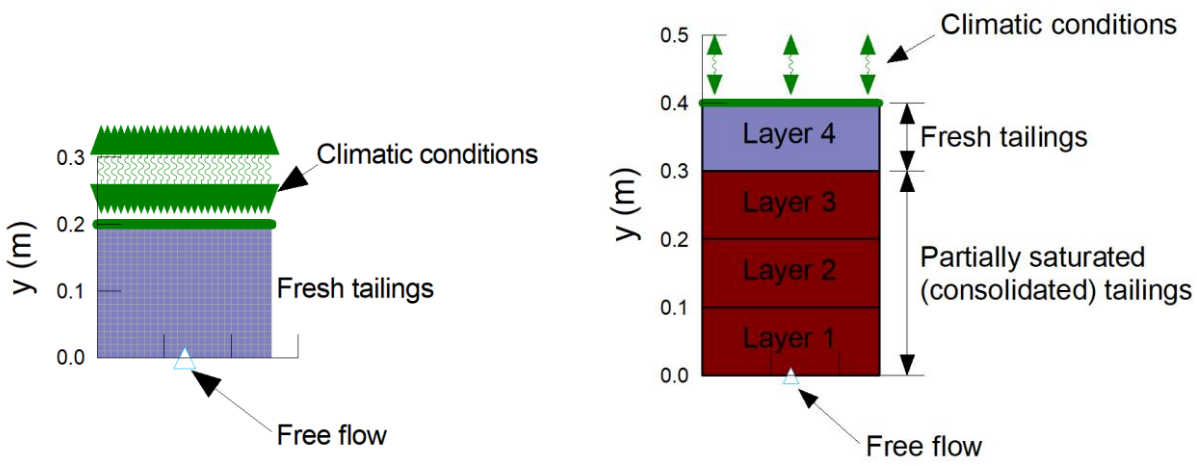

Figure 3.14: Geometry of the models used to simulate the single layer (a) and multilayer (b) laboratory column tests. Boundary conditions and mesh (1 cm × 1 cm) are shown.

Two materials were defined in the multilayer column test simulations (Figure 3.14). The first (purple – on the surface) represented fresh and unconsolidated paste tailings, whereas the second (brown) material was partially saturated and consolidated tailings (previous layers). These two materials were used to represent the evolution in the properties of the paste tailings, properties for fresh tailings were replaced by the properties of consolidated tailings once a new layer was added. The WRC of the fresh paste tailings was obtained from the PPE and the WRC of the partially saturated (consolidated) tailings was obtained from the Tempe cell tests. Only fresh paste tailings were considered in the simulations of the SL column tests. Compressibility of the fresh paste tailings was therefore not directly simulated in the numerical models but indirectly accounted for by modifying the water retention curve of the materials. This approach could have influenced the calculation of drainage (Simms et al., 2007; Fisseha et al., 2010; Daliri et al., 2016; also see discussion and recommendations in Chapter 8 for more details).

The SL columns that were run in parallel were modelled for 71 days. The simulations for the ML columns, were conducted in a series of cycles. Each cycle began with the deposition of a layer of fresh tailings (either alone or above a partially desaturated and consolidated layer). Figure 3.15 illustrates the steps for a four-layer column test simulation. Each layer had a specific porosity which

impacted slightly the hydrogeological properties (i.e. water retention curve and hydraulic conductivity).

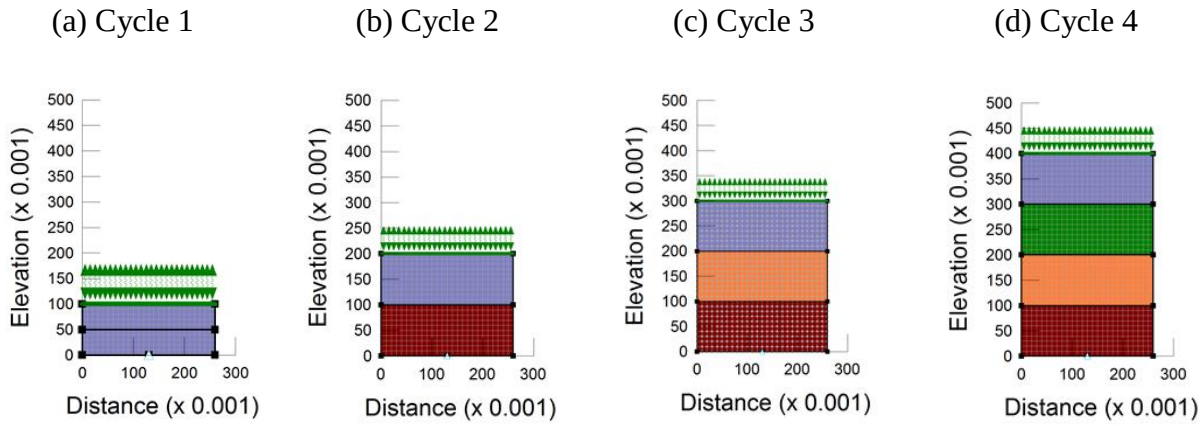

Figure 3.15: Sketch of the simulated deposition cycle of a four-layer ML column using Vadose/W (mesh/element size: 1 cm × 1 cm).

The thermal conductivity (α_T) and the volumetric heat capacity (C_T) of the materials were assumed constant in the numerical simulations. The thermal conductivity and volumetric heat capacity used in the simulations were 150 kJ/d·m°C and 2300 kJ/m^3°C respectively (GeoSlope, 2008). These values were considered the same for both fresh and consolidated tailings.

A free flow boundary condition (BC) was applied at the bottom of the tailings to simulate the center drain in the column where water could flow freely (Figure 3.14).

A climatic boundary (temperature, relative humidity, wind speed and precipitation intensity) was imposed at the top of the column test models. The maximum and minimum daily temperature and relative humidity measured in the laboratory during the column experiments were applied in the simulations (Figure 3.16).

(a) SL Columns

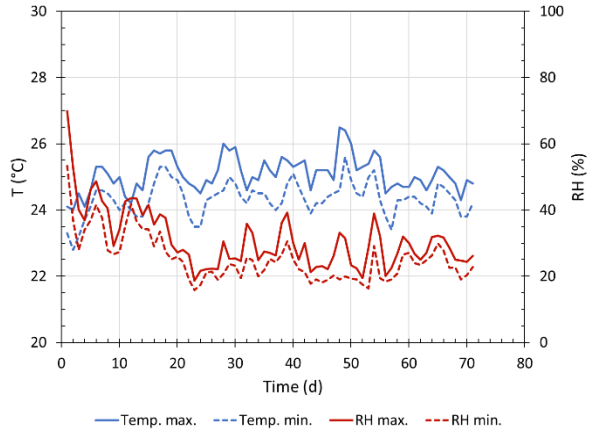

(b) Col-01

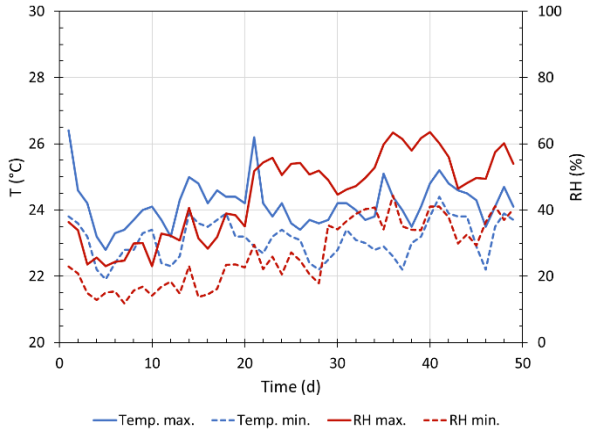

(c) Col-02

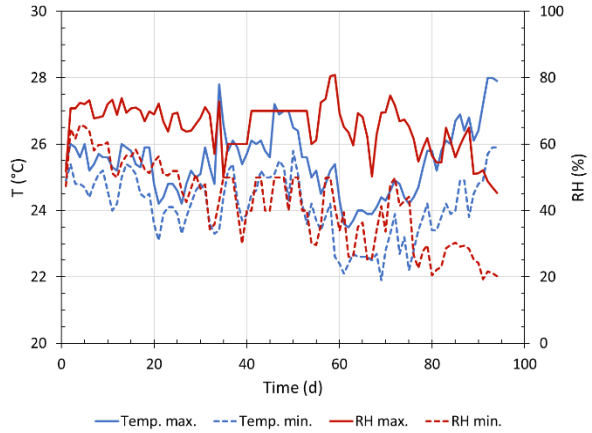

(d) Col-03 and Col-04

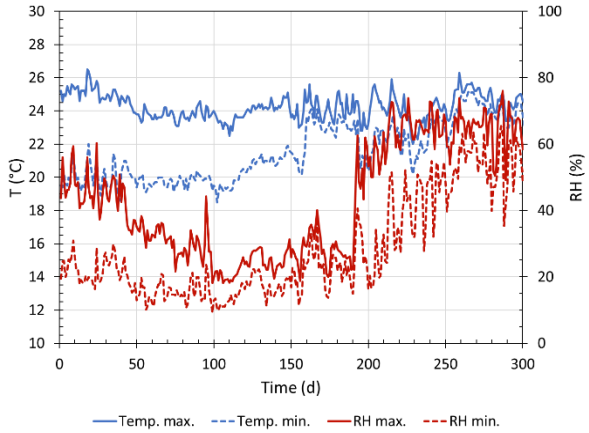

Figure 3.16: Measured temperature and relative humidity in the laboratory during the SL and ML column tests.

The potential evaporation (PE) measured in the laboratory was used as the reference PE in Vadose/W. In the multilayer columns, the potential evaporation was fixed for each modeled layer based on the measured value (which varied depending on the column and the layer).

The initial conditions for the simulation of each cycle was defined using a pressure head spatial function. The pressure head at the base of a fresh (saturated) tailings layer corresponded to the weight (thickness) of the layer, while it was zero at its surface. The initial pressure head profiles in

the consolidated layers were obtained from the numerical simulations of the previous cycle and applied as an initial condition to the following simulated cycle.

The largest rate of change in the material hydrogeological characteristics (e.g. suction and volumetric water content) occurred in the hours following placement of a fresh tailings layer in the column tests. The time steps in the numerical simulations were defined accordingly:

- 0 - 1 hour after the addition of the fresh layer: 2-minute time steps.
- 1 - 24 hours after the addition of the fresh layer: 7.5-minute time steps.
- More than 1 day after the addition of the fresh layer: 6-hour time steps.

The convergence and time stepping parameters are presented in Table 3.11. Adaptive time stepping was used to improve convergence.

Table 3.11: Convergence parameters used for the numerical simulations of the laboratory columns with Vadose/W.

	Parameter	**Value**
Convergence parameters	Max. number of iterations	50
	Min. pressure head difference (m H_2O)	0.005
	Initial rate of change	1
	Minimum rate of change	0.1
	Rate reduction factor	0.65
	Rate reduction frequency (iterations)	10
	Number of reviews	10
Adaptive time stepping	Calculate from vector norm	
	Minimum time step (s)	0.1
	Maximum time step (s)	1800

CHAPTER 4 RESULTS FROM LABORATORY CHARACTERIZATION AND FIELD WORK

This chapter presents the results of the laboratory and field experimental program. Section 4.1 focuses on tailings hydrogeotechnical properties while Section 4.2 presents and discusses the results of the modified oxygen consumption (MOC) tests conducted in the field in October 2004.

4.1 Laboratory characterization

Laboratory tests were conducted to characterize Bulyanhulu tailings, including their particle size distribution, relative grain density (specific gravity), and Atterberg limits. The mineralogy, saturated hydraulic conductivity, water retention curves, and consolidation properties were also determined.

4.1.1 Particle size distribution

Bulyanhulu tailings are a well-graded non-plastic silt (ML) according to the USCS (ASTM D2487) (Figure 4.1). There is no significant difference between the tailings sampled in 2004 and in 2007. The average curve will be used afterwards for the definition of some material characteristics for the numerical modeling. The D_{10} and D_{60} are 3 μm and 38 μm respectively (uniformity coefficient, C_U = 13). On the average curve, 75% of the particles are smaller than 75 μm and 8% of the particles are smaller than 2 μm. This is slightly finer than hard rock tailings studied by Aubertin et al. (1996) (70% of the particles smaller than 75 μm) and Qiu and Sego (2001), but somewhat coarser than other local tailings characterized more recently (e.g. L.-Bolduc, 2012; Essayad, 2015; Saleh Mbemba, 2016).

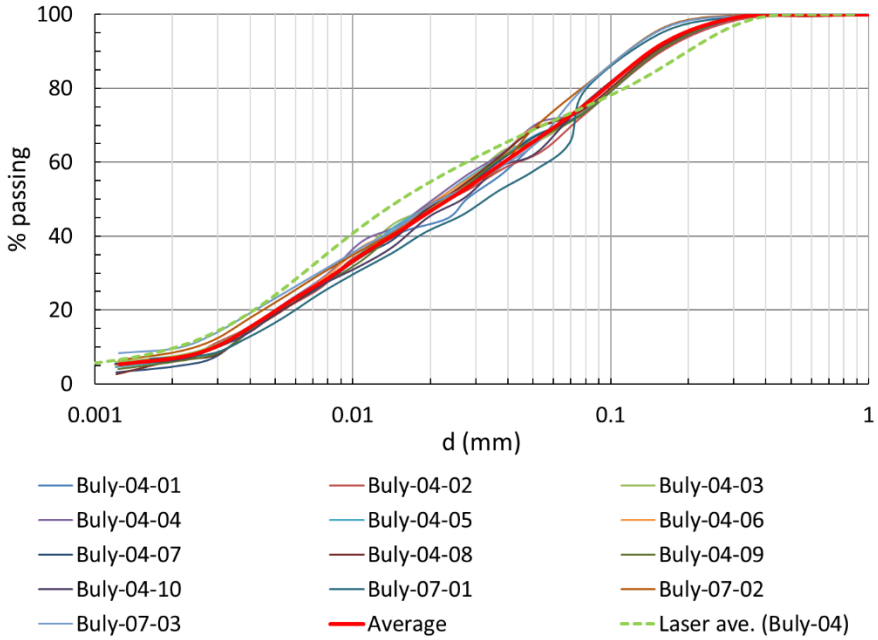

Figure 4.1: Particle size distribution curves of the Bulyanhulu tailings.

4.1.2 Relative density (Specific gravity)

The average relative density of the grains (D_r; also called specific gravity, G_s) for Buly-04 and Buly-07 tailings are respectively 2.929 and 2.921 (Table 4.1). Comparable results (D_r = 2.9) were obtained by Bryan et al. (2010) and Daliri et al. (2014, 2016) for tailings from the Bulyanhulu mine. This value of D_r is in the typical range for hard rock mine tailings (e.g. Aubertin et al., 1996, 2002; Qiu and Sego, 2001; Gawu and Fourie, 2004; Bussière, 2007). A value of D_r higher than that of natural soils (2.6 to 2.7) may indicate the presence of metals (particularly iron sulfides).

Table 4.1: Relative density (D_r) of the Bulyanhulu tailings measured using a water pycnometer.

Specimen	Buly-04	Buly-07
1	2.928	2.906
2	2.929	2.928
3	2.936	2.923
4	2.926	2.927
5	***(1)	2.937
6	2.928	2.907

(1) Standard deviation between three tests was too high and did not meet ASTM D854 standard.

4.1.3 Atterberg limits

The liquid (w_l) and plastic (w_p) limits were too close to distinguish using ASTM standard D4318. Both the liquid and plastic limits were in the 20% - 22% range and the difference was too small ($\leq$ 2%) too interpret. Haigh (2012) mentions that standard deviations of the measured water content for the liquid limit of 3% can be expected (and are acceptable). The liquid limit of tailings (when measurable) is typically less than 40%, and the plastic limit is comprised between 0% and 15% (Bussière, 2007).

Alternative methods (e.g. Swedish cone) were not used because they are only valid if Atterberg limits can also be obtained (validated) with the original techniques outlined in ASTM standard D4318 (Leroueil and Le Bihan, 1996; Haigh, 2012). Table 4.2 presents the Atterberg limits of Bulyanhulu tailings measured by others. Grabinsky (Personal communication, February 25, 2005) reported that Crowder et al. (2002) used a modified Casagrande cup that was coated with epoxy and fine sand to prevent slipping.

Table 4.2: Plastic limit (w_p) and liquid limit (w_l) of the Bulyanhulu tailings published by others.

Author	w_p (-)	w_l (-)	Method
Crowder et al. (2002)	20.4	21.2	Modified Casagrande cup (Grabinsky, 2005)
Simms et al. (2007)	20	23	Swedish cone

4.1.4 Mineralogy

The mineralogy of Buly-04 tailings was obtained by X-Ray diffraction tests carried out at the Université du Québec en Abitibi-Témiscamingue (UQAT) (Table 4.3). Buly-04 tailings contain almost 50% quartz, and 12% pyrite (sulfide). Neutralising minerals, like calcite (4.5%) and dolomite (4%), were also detected. These results include a somewhat similar proportion of neutralising minerals (calcite, ankerite) compared to the Bulyanhulu tailings tested by Simms et al. (2007) (Silicates - 80%; Pyrite - 6%; Calcite - 5%; Ankerite - 4%), but the pyrite content in the present study is significantly higher. The Bulyanhulu mine was extracting ore from two different areas at the time these samples were collected. These sectors produced two different types of tailings (called scavenger and rough tailings, respectively; Golder, 2005), which could explain the difference in the mineralogy. However, the Bulyanhulu tailings studied by Bryan et al. (2010) had a comparable pyrite content (C_p = 11%).

Table 4.3: Mineralogical composition of Buly-04 tailings (DRX testing at UQAT).

Mineral	Average value (% w/w)
Quartz	49.7%
Pyrite	11.8%
Muscovite	23.0%
Albite	2.2%
Chlorite	4.8%
Dolomite	4.0%
Calcite	4.5%

4.1.5 Saturated hydraulic conductivity

The saturated hydraulic conductivity (k_s or k_{sat}) was obtained from falling head tests in flexible-wall permeameters (ASTM D 5084, Section 3.2.6). Laboratory test results were compared to values given by the Kozeny-Carman (KC – Equation 2.16; Chapuis and Aubertin, 2003) and the modified Kozeny-Carmen (KCM – Equation 2.18; Mbonimpa et al., 2002a) predictive models (Figure 4.2).

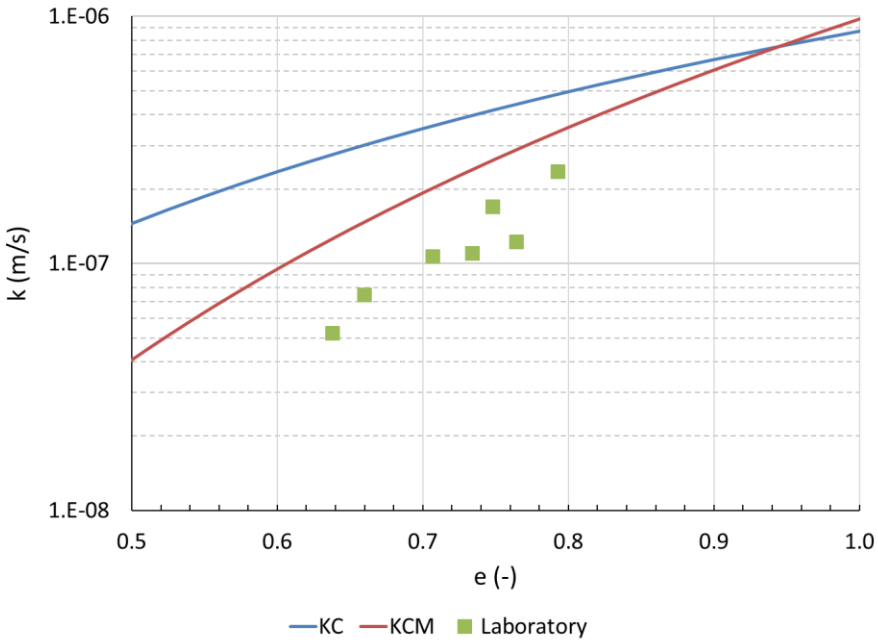

Figure 4.2: Measured and predicted saturated hydraulic conductivity for the Bulyanhulu tailings.

Measured saturated hydraulic conductivities are comprised between 5×10^{-8} m/s (e = 0.64) and 2×10^{-7} m/s (e = 0.79). Predictive models tend to overestimate the saturated hydraulic conductivity, with a difference up to half an order of magnitude (and more). Most results are within the expected range of variation for saturated hydraulic conductivity (Chapuis and Aubertin, 2003). The measured hydraulic conductivities are in the low range of tailings from hard rock mines compare to other reported values (e.g. Aubertin et al., 1996; Bussière, 2007; Saleh-Mbemba, 2016).

4.1.6 Water retention curve

Tempe cell (TC) and pressure plate extractor (PPE) tests were used to determine Bulyanhulu tailings water retention curve (see Section 3.2.2).

Nine specimens (5 × Buly-04 and 4 × Buly-07) were tested to determine the water retention curve (WRC) using the TC (Table 4.4), and four PPE tests were carried out on the same tailings (the initial and final PPE test conditions are presented in Table 4.5). The specimens for the Tempe cell tests were compacted and saturated in a flexible membrane permeameter. The specimens for the PPE tests were prepared at an initial water content (pulp density) like paste tailings deposited at the Bulyanhulu mine and were not compacted.

Table 4.4: Initial and final conditions for the Tempe cell tests. e_i: initial void ratio; θ_i: initial volumetric water content; θ_f: final volumetric water content.

Tailings	Sample	e_i (-)	θ_i (-)	θ_f (-)
Buly-04	Buly-04-T1	0.71	0.42	0.09
	Buly-04-T2	0.63	0.43	0.08
	Buly-04-T3	0.74	0.41	0.04
	Buly-04-T4	0.66	0.42	0.03
	Buly-04-T5	0.73	0.39	0.09
Buly-07	Buly-07-T1	0.68	0.38	0.20
	Buly-07-T2	0.72	0.38	0.11
	Buly-07-T3	0.72	0.39	0.16
	Buly-07-T4	0.70	0.38	0.27

Table 4.5: Initial and final conditions for the pressure plate extractor tests. e_i: initial void ratio; θ_i: initial volumetric water content, e_f: final void ratio; θ_f: final volumetric water content.

	e_i (-)	θ_i (-)	e_f (-)	θ_f (-)
Buly-04-PPE1	0.72	0.42	0.62	0.09
Buly-04-PPE2	1.06	0.51	0.66	0.01
Buly-07-PPE1	0.98	0.50	0.68	0.04
Buly-07-PPE2	0.85	0.47	0.62	0.17

The tailings were placed in the PPE at a paste like consistency (higher θ), compared to the TC tests, and shrunk during the test (decrease in e).

The results from the TC and PPE tests are similar, with a desaturation that begins at a suction between 50 kPa and 70 kPa (i.e. the Air Entry Value, AEV). The residual suction (sometimes called the water entry value, WEV) is not apparent in the Tempe cell tests but appears to be between 1000 kPa and 1500 kPa in the PPE. Results from PPE tests completed by Saleh-Mbemba (2010) on tailings samples from the Bulyanhulu mine are also presented (Figure 4.3b).

(a) Tempe cells (b) PPE

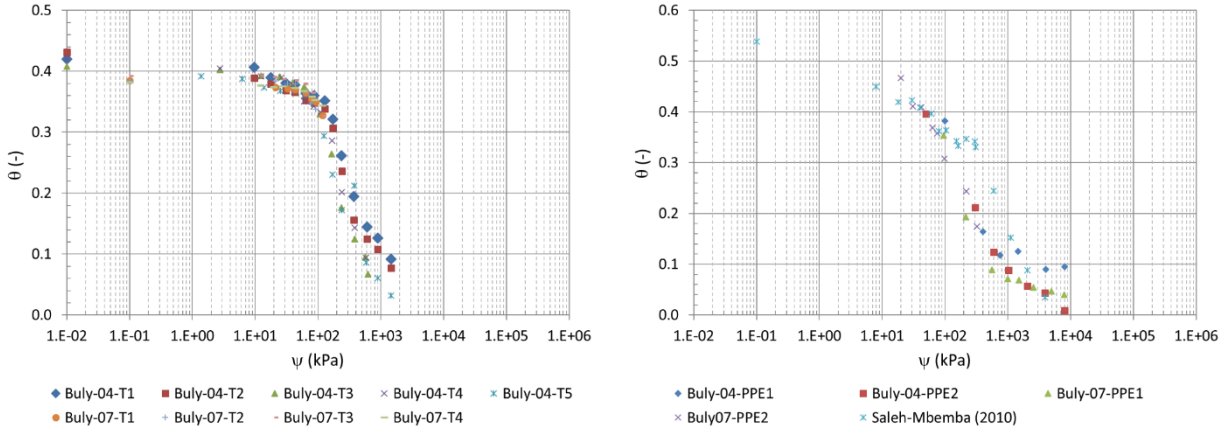

Figure 4.3: Volumetric water content at different suctions for Bulyanhulu tailings specimens tested in (a) Tempe cells and the (b) pressure plate extractor. Suctions < 0.01 kPa correspond to initial (saturated) conditions.

The results from both the Tempe cells (TC) and PPE were used to obtain fitted WRCs using the Fredlund and Xing (1994) model (Equation 2.26). Table 4.6 presents the fitted FX parameters obtained.

Table 4.6: Fredlund and Xing (1994) model (Equation 2.26) parameters for the water retention curve of the Bulyanhulu tailings.

	Parameter	Tempe cell tests	Pressure plate extractor tests
Fredlund and Xing (1994)	a_{fx} (kPa)	211.83	247.87
	n_{fx} (-)	1.35	0.84
	m_{fx} (-)	1.87	2.67
ψ_r (kPa)		1116	1669
ψ_a or AEV (kPa)		58	24
θ_s (-)		0.41	0.49

Figure 4.4 presents the two water retention curves for these tailings. The first WRC (PP – FX) was obtained using the pressure plate extractor results and the second WRC (PP – TC) was obtained from the Tempe cell results.

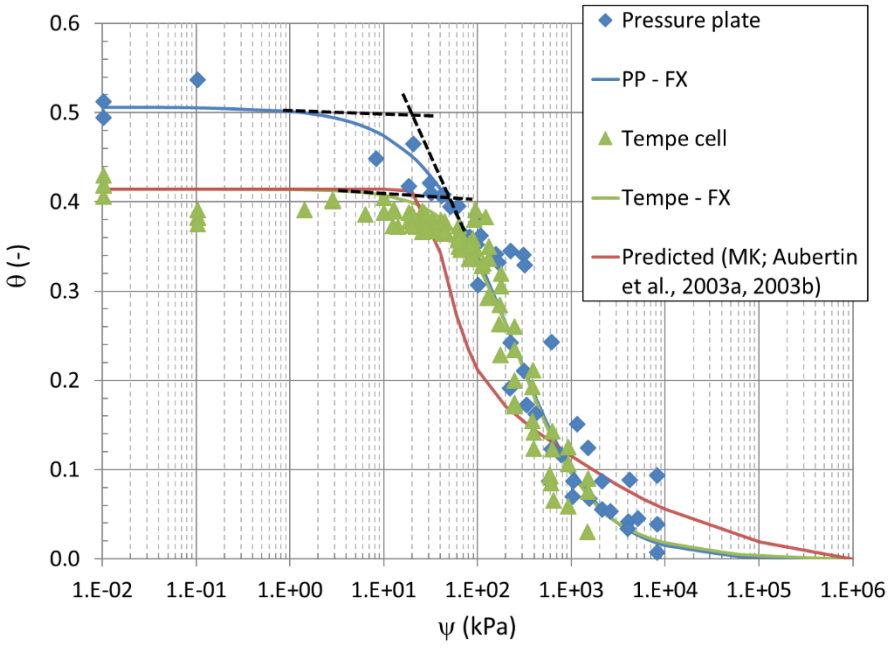

Figure 4.4: Water retention curves of the Bulyanhulu tailings fitted to the FX equation.

Results from PPE and Tempe cells tests yield comparable results once the suction is greater than about 100 kPa. There is a difference in the void ratio of the tailings specimens for the two experimental methods at suctions lower than ≈ 100 kPa. The specimens in the PPE have a higher initial void ratio (between 0.98 and 1.07) and therefore a higher volumetric water content (θ). The initial void ratio of the specimens in the Tempe cells is around 0.70 (and remains constant during the tests). In the PPE tests, the void ratio decreases due to desiccation and shrinkage of the tailings as suction increases (e.g. Mbonimpa et al., 2006; Saleh-Mbemba, 2010). The AEV of these tailings obtained by the tangent method from the Tempe cell tests is around 58 kPa. Predicted WRC (with MK; Aubertin et al., 2003a; 2003b) was relatively similar to values measured with the Tempe cells, AEV = 20 kPa in the MK model.

The decrease in the VWC for the lower suctions in the PPE tests can be associated with a decrease in void ratio (porosity, n); therefore, the degree of saturation (S_r) can remain at 100% even when the VWC is reduced. It was possible to evaluate the change in the void ratio (or porosity) at each suction step during the PPE test (see Section 3.2.7) (Figure 4.5). This shrinkage behaviour was also observed by Saleh-Mbemba (2010) and Saleh-Mbemba et al. (2016). The initial loss of water can then be correlated with a decrease in the void ratio of the material. The degree of saturation remains around 100% during the initial drainage of the specimen in the PPE (loss of water is correlated to a decrease in the void ratio). Once the suction exceeds the air-entry value ($\psi_a \approx 58$ kPa), the void ratio becomes almost constant and loss of water is associated to a desaturation of the specimen (Figure 4.5). Comparable results were obtained with Bulyanhulu tailings by Mizani et al. (2013).

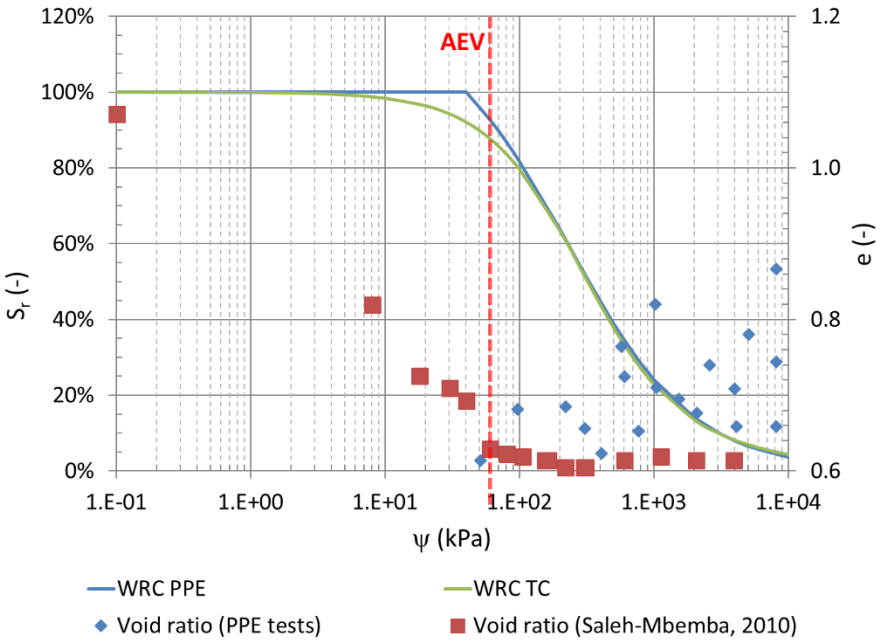

Figure 4.5: Relationship between the suction and degree of saturation or void ratio for Bulyanhulu tailings.

4.1.7 Consolidation

One-dimensional consolidation tests were conducted in a fixed ring oedometer (ASTM D 2435; Section 3.2.8). The change in void ratio (e) with respect to the effective stress (σ') is presented in Figure 4.6 (a - Arithmetic; b - Semi-log).

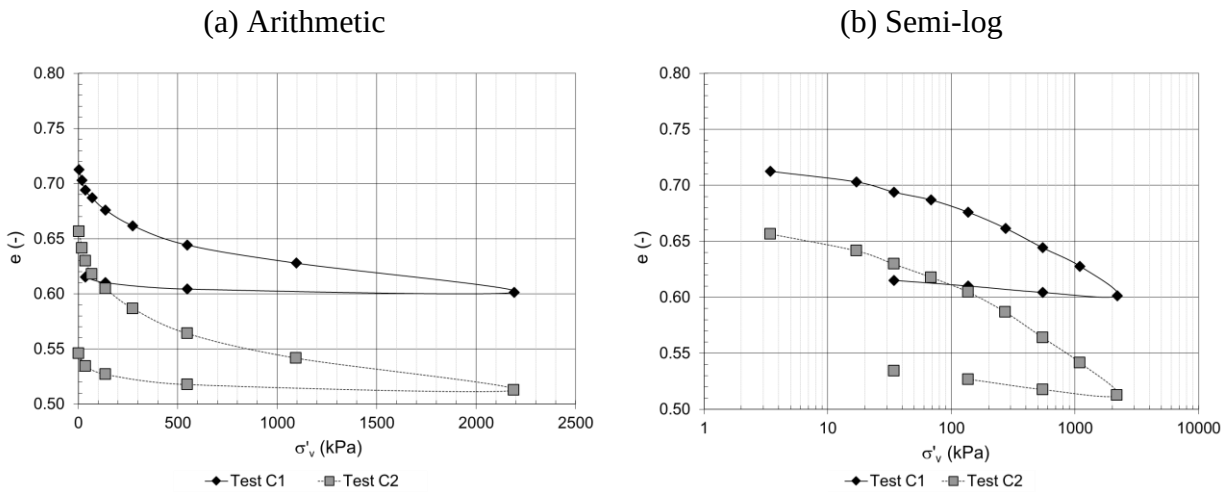

Figure 4.6: Void ratio (e) as a function of effective vertical stress (σ'_v) for the oedometer tests conducted on the Buly-04 tailings (a - arithmetic; b - semi-log).

The initial void ratio (e_i) for the specimens in tests C1 and C2 was respectively 0.71 and 0.66. The specimens were initially densified and saturated in a flexible wall permeameter. The final void ratio (e_f) at a final effective vertical stress of approximately 2190 kPa was 0.60 (C1) and 0.51 (C2). These results suggest that there is a relationship between the initial and final void ratio for the same σ'_v (Essayad, 2015).

The compression coefficients (Bowles, 1984) can be determined from the plots in Figure 4.6. The compression index $\left(C_c = \Delta e/\left(log(\sigma'_2/\sigma'_1)\right)\right)$ is 6.5×10^{-2} for both specimens. The coefficient of compressibility $(a_v = \Delta e/\Delta\sigma';\ \Delta\sigma' = \sigma'_2 - \sigma'_1)$ defined in the same stress range as C_c is 7.9×10^{-5} kPa^{-1} for test C1 and 9.5×10^{-5} kPa^{-1} for test C2 (Figure 4.6a). The coefficients of volumetric compressibility ($m_v = a_v/(1 + e_1)$ – where e_1 is the initial void ratio in the determined interval) are 4.6×10^{-5} kPa^{-1} and 5.7×10^{-5} kPa^{-1} for tests C1 and C2, respectively. This parameter (m_v) is used to define the volumetric compressibility (on the WRC) in the numerical simulations presented in Chapters 5, 6 and 7. The results from these tests compared to other tailings from hard rock mines (e.g. Aubertin et al., 1996; Bussière, 2007; Saleh-Mbemba, 2016).

4.2 Field tests

There was an almost linear decrease of the oxygen concentration ([O_2]) during the modified oxygen consumption (MOC) tests (Figure 4.7). The concentration measured in two tests (B-3 and B-10) remained greater than 20% for the duration of the tests (variation of about 1%), and it decreased to 13%-17% for the other five tests.

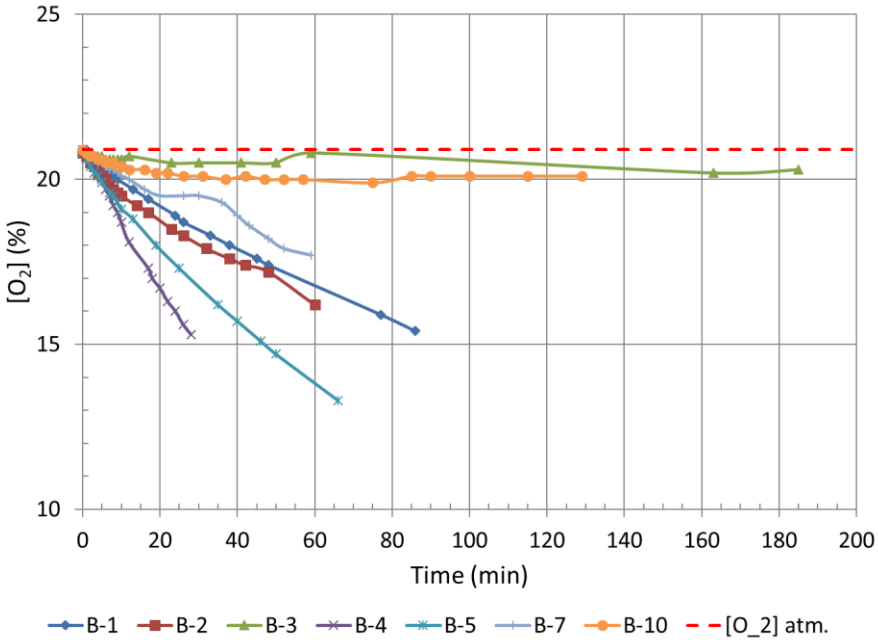

Figure 4.7: Oxygen concentration of oxygen over time during the MOC tests conducted *in-situ* on the Bulyanhulu tailings (October 2004).

Using the results from Figure 4.7, the effective diffusion coefficient (D_e - Figure 4.8) and oxygen reaction rate coefficient (K_r - Figure 4.9) were assessed using the software Vadose/W and the procedure described in Section 3.3. The measured effective diffusion coefficients are comprised between 3×10^{-6} m^2/d (3.5×10^{-11} m^2/s) and 2×10^{-2} m^2/d (2.6×10^{-7} m^2/s). The effective diffusion coefficient is also compared with predicted values obtained with Equation 2.34 (Aachib et al., 2002, 2004). Field results are close to the predicted values. The results are well correlated with the degree of saturation of the material.

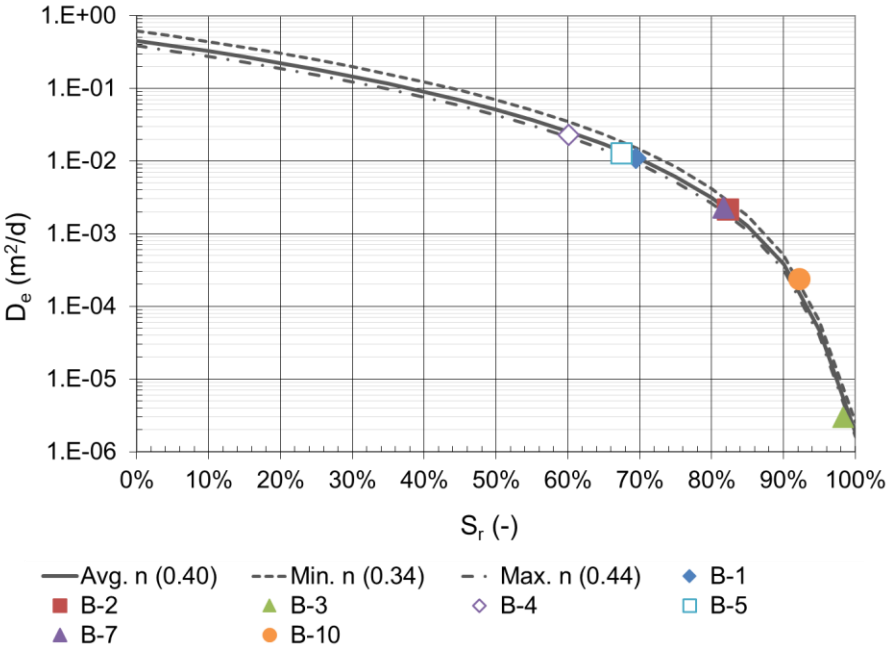

Figure 4.8: Effective diffusion coefficient (D_e) measured *in-situ* as a function of the degree of saturation (S_r) and compared to the Aachib et al. (2004) (Equation 2.34) model (for different porosities, n).

The value of the oxygen reaction rate coefficient (K_r; in the modified 2nd Fick's law, Equation 2.35) obtained from the tests (interpreted with Vadose/W) is presented as a function of the degree of saturation (S_r) for the test sites in Figure 4.9. The oxygen reaction rate coefficient results are comprised between 2.7×10^{-3} d^{-1} and 2.1 d^{-1}. The predicted value with the Collin (1987) model (Equation 2.37) is 2.7 d^{-1} (for the average in-situ porosity value of 0.40). These values of the are typical of reactive tailings (Dagenais, 2005; Gosselin, 2007; Pabst, 2011; Mbonimpa et al., 2011, 2012). Oxygen reaction rate coefficient (K_r) measurement are relatively imprecise for high degree of saturation (S_r > 85%) because of a high sensitivity to the diffusion coefficient (Toussaint, 2016).

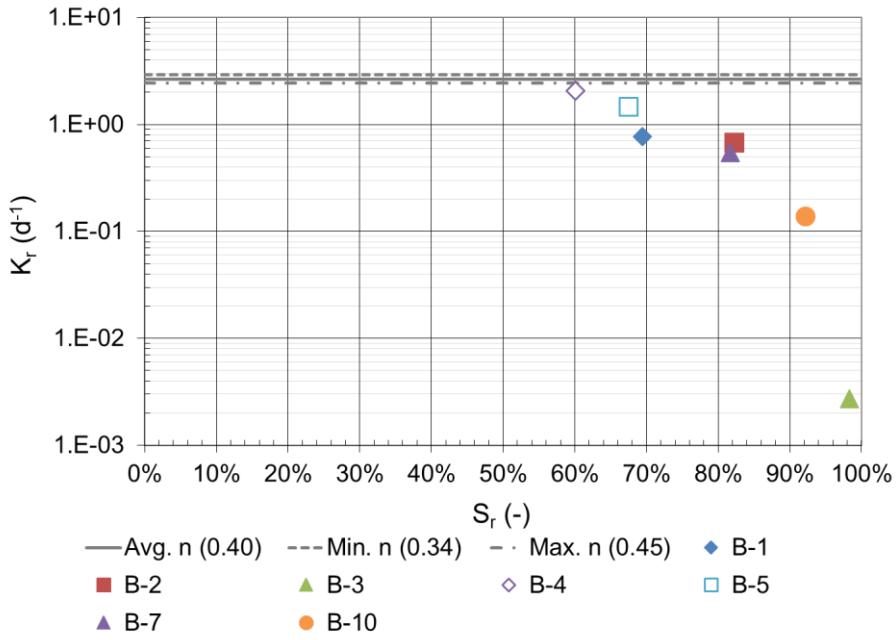

Figure 4.9: Oxygen reaction rate coefficient (K_r) (in the modified 2nd Fick's law, Equation 2.35) as a function of degree of saturation (S_r).

The measured oxygen flux (F_{O_2}) is presented as a function of the degree of saturation (Figure 4.10). It varies between 2 g/m^{2}d and 162 g/m^{2}d. The oxygen flux tends to decrease when the degree of saturation is higher. The calculated steady-state oxygen flux (with the predicted values of D_e and K_r and using Equation 2.39) is also presented on this figure. The fluxes obtained from these tests are fairly like other tests conducted on exposed reactive tailings from other mine sites with similar pyrite content (e.g. Pabst, 2011). The oxygen flux obtained from these *in-situ* tests varies between 2 g/m^{2}d (Test B-3, S_r = 98%) and 162 g/m^{2}s (Test B-4, S_r = 60%). There is a good correlation between the experimental (*in-situ*, with a MOC test) and calculated (using the predicted D_e and K_r, and Equation 2.39) steady-state oxygen fluxes.

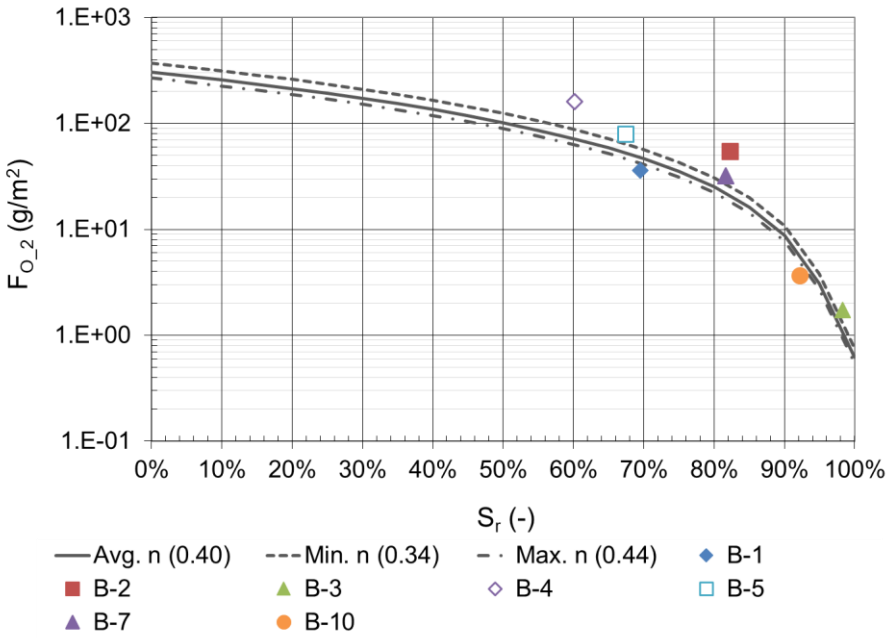

Figure 4.10: Measured and calculated (with Equation 2.39) oxygen flux (F_{O_2}) with respect to degree of saturation measured in the Bulyanhulu tailings.

4.3 Tailings properties for numerical simulations of the laboratory column tests

Two set of tailings characteristics were defined for the numerical simulations with Vadose/W (Table 4.7):

- Fresh tailings correspond to paste tailings (saturated) at an initial gravimetric pulp density (P_m) of approximately 73% (design value).
- Consolidated (partially saturated) tailings correspond to the tailings that have desiccated and shrunk and that have a constant porosity (n_{consol}) around 0.40.

The properties of fresh tailings were applied to the layer closest to the surface in the models (Figure 3.14b). The consolidated tailings properties were applied to the other layers below. Each of the simulated tailings layer of the SL and ML tests had a specific porosity, with a specified PE rate (measured in the laboratory, Table 4.7). The effect of surface cracks was neglected in the numerical simulations.

The duration of the numerical simulations was the same as the laboratory tests.

Table 4.7: Numerical model characteristics adopted for simulating the single-layer and multilayer column tests on tailings. n_{fresh}: porosity of the fresh tailings when placed in the column (corresponds to n_p); n_{consol}: porosity of the consolidated tailing; PE: potential evaporation rate.

Column Type	Column test	P_m (-)	n_{fresh} (-)	n_{consol} (-)	PE (mm/d)	Duration (days)
Single-layer columns	SL-01	71.4%	0.54	N/A	1.4	71
	SL-02	72.2%	0.53	N/A	1.3	71
	SL-03	72.2%	0.53	N/A	2.8	71
	SL-04	66.1%	0.60	N/A	2.0	71
Multilayer columns	Col-01-L1	75.3%	0.49	0.42	1.6	20
	Col-01-L2	73.8%	0.51	0.44	2.0	14
	Col-01-L3	76.8%	0.47	N/A	1.9	15
	Col-02-L1	74.5%	0.50	0.39	1.4	33
	Col-02-L2	70.6%	0.55	0.49	1.6	21
	Col-02-L3	74.5%	0.50	0.45	1.1	19
	Col-02-L4	75.3%	0.49	N/A	1.5	19
	Col-03-L1	76.8%	0.47	0.38	1.1	191
	Col-03-L2	75.3%	0.49	N/A	1.2	109
	Col-04-L1	76.8%	0.47	0.38	1.1	191
	Col-04-L2	75.3%	0.49	N/A	1.2	109

The Fredlund and Xing (1994; Section 2.4.1) model was used in Vadose/W to define the water retention curve of each material. Results from the pressure plate extractor tests were used to define the water retention curve of the fresh (paste) tailings (Section 4.1.6), while Tempe cell results (with densified tailings) were used to simulate the consolidated tailings (Section 4.1.6). Water retention curves were adjusted with the Fredlund and Xing (1994) equation (Equation 2.26) for each model

for the porosity measured during the test (Figure 4.11). The saturated volumetric water content (θ_s) on the WRC tends to vary with the initial porosity of the layer, and it was adjusted in the model.

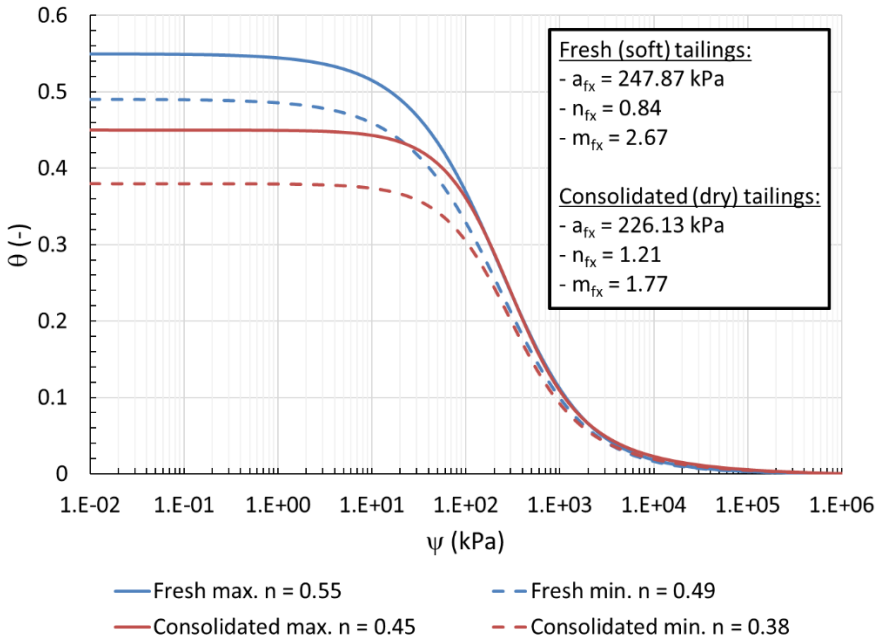

Figure 4.11: Water retention curve of the fresh and consolidated tailings used in the numerical simulations of the laboratory SL and ML column tests.

The consolidated tailings in the simulations have a saturated hydraulic conductivity of 1×10^{-7} m/s which is the geometric average from the tests carried out in the laboratory (Section 3.2.6). The hydraulic conductivity of the fresh tailings ($k_{sat} = 5\times10^{-7}$ m/s) was estimated using the Kozeny-Carman Modified model (KCM, Mbonimpa et al., 2002; Section 2.3.2). The unsaturated hydraulic conductivity function was defined in Vadose/W using the Fredlund et al. (1994) predictive model (Section 2.4.2, Figure 4.12). Two different unsaturated hydraulic conductivity curves were used for the fresh tailings (higher hydraulic conductivity because of a higher porosity) and the consolidated tailings (with a lower hydraulic conductivity). A minimum hydraulic conductivity of 1×10^{-14} m/s was imposed in the simulations (as suggested by Fredlund, 2006).

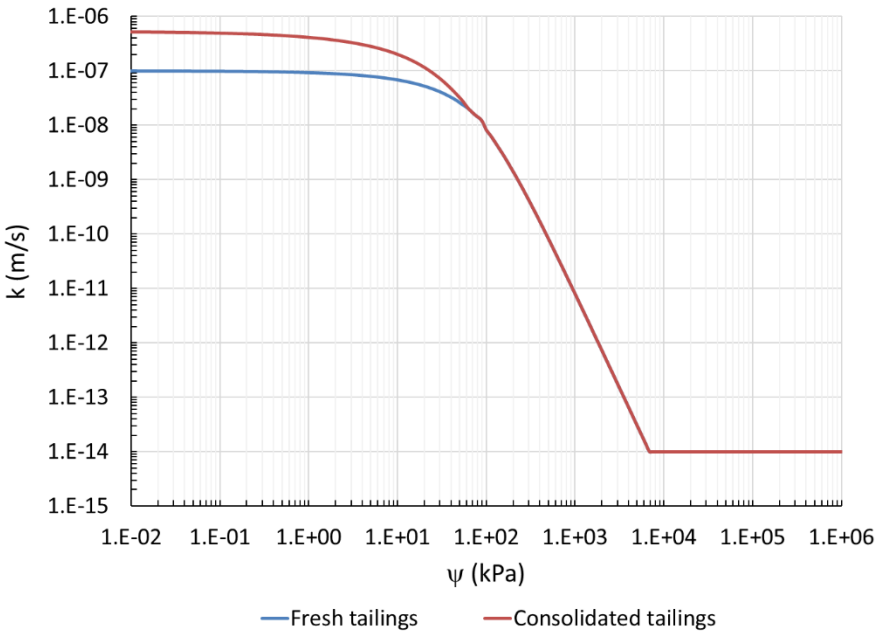

Figure 4.12: Unsaturated hydraulic conductivity (k_u) functions of the fresh and consolidated tailings used in the numerical simulations obtained with the Fredlund et al. (1994) model (using the WRCs).

It was observed in preliminary simulations that a large contrast between a dry surface (low pore water pressure) and a fresh tailings layer could generate convergence issues. The initial hydraulic gradient at the interface between the fresh and the consolidated tailings was therefore slightly reduced to limit this problem. The suction below the interface (in the consolidated tailings) was slightly decreased for this purpose and fixed at twice the residual suction (i.e. 1116 kPa or 341 m, Figure 4.4). The volumetric water content (θ) in the consolidated tailings at a suction of 340 m is 0.04 ($\theta_r \approx 0.06$, Figure 4.4).

Results from the numerical simulations are presented in Sections 5.6, 6.1.6, 6.2.6 and 6.3.6, and in Chapter 7.

CHAPTER 5 RESULTS FROM SINGLE-LAYER LABORATORY COLUMN TESTS

Single-layer (SL) column tests were performed in the laboratory to characterize the hydrogeotechnical response of freshly deposited paste tailings. The effect of layer thickness and pulp density on the hydrogeological behaviour of tailings after deposition on the surface was more specifically assessed.

Three SL column tests were carried out with various tailings thicknesses (SL-01: 10.2 cm, SL-02: 19.8 cm and SL-03: 30.0 cm). The tailings had a higher initial water content in column test SL-04 but the same thickness (27.7 cm) as column SL-03 (SL-03: $w \approx 40\%$; SL-04: $w \approx 50\%$). Tailings in SL columns were left to desaturate by drainage and evaporation for 62 days in column tests SL-01, SL-02 and SL-03, and 70 days for column test SL-04.

This chapter presents the evolution of the mass, thickness and volume, pore water pressure, and water content of the tailings with time during these tests. Cracking at the surface of the SL columns is also addressed. Numerical simulations complement the experimental results (see Section 5.6).

5.1 Evolution of the mass

The tailings specimens initial total mass was comprised between 10 kg for test SL-01 and 33 kg for test SL-03 (Section 3.4.1). Loss of mass during the tests occurred through loss of water (Section 3.4).

A rapid loss of mass was observed in the first two days following the beginning of the tests (Figure 5.1a). For example, SL-04 lost 2.5 kg of water in the first two days, which corresponded to 26% of the total initial mass of water. The rate of change of the mass then gradually decreased with the drainage rate (see below) and then remained constant (i.e. constant slope in Figure 5.1a) for over 30 days. The total mass of the specimens in the columns became quasi-constant after approximately 40 to 50 days, depending on the tailings thickness (39 days for SL-01, 47 days for SL-02 and 43 days for SL-03). This time was slightly longer ($\approx$ 60 days) for column test SL-04 (slurry tailings), which had a higher initial water content.

The total loss of mass in test SL-04 was greater than in test SL-03 (+ 1.0 kg; Figure 5.1b). However, the initial water loss (around 2 kg) and the subsequent rate of change of the mass (approximately -

0.2 kg/d) in column tests SL-03 and SL-04 are similar (Figure 5.1b and c), which may indicate that layer thickness has a more significant effect on the tailings response than the initial water content for the tested conditions.

The rate of change of the total mass in columns SL-01 and SL-02 was also similar (-0.1 kg/d) but tailings in SL-01 appeared to have lost more water and more rapidly then column SL-02 in terms of relative masses (Figure 5.1c). The relative change of total mass (change in mass divided by the initial mass of the tailings) in column SL-03 (which is 2 and 1.5 times thicker than SL-01 and SL-02 respectively), showed a similar behaviour than SL-01 during the first 20 days, but became similar to column SL-02 by the end of the test (after day 50; Figure 5.1c).

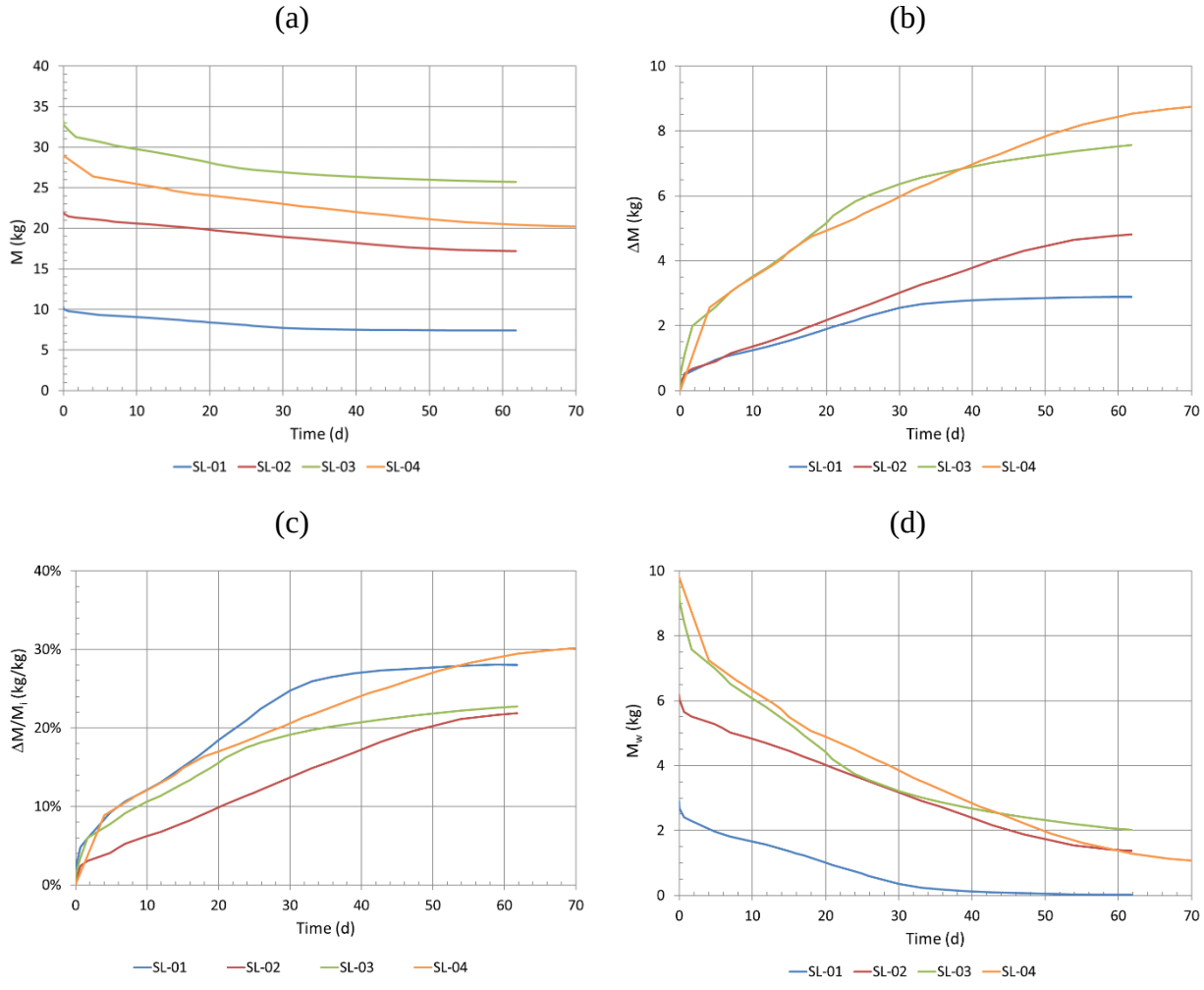

Figure 5.1: (a) Total mass, (b) change in mass, (c) relative change of total mass, and (d) mass of water during the SL column tests.

The thicker tailings layers tended to retain a greater proportion of water than thinner layers (at least for the duration of these tests). For example, tailings in SL-01 (10.2 cm thick) lost 28.0% of its mass during the test, while tailings in SL-02 (19.8 cm thick) and SL-03 (30.0 cm) lost respectively 21.9% and 22.7% of their mass; the difference between column tests SL-02 and SL-03 was small). Tailings in SL-01 were almost dry after 40 days, while the remaining water mass in columns SL-02, SL-03 and SL-04 after 60 days was between 1.5 and 2 kg (Figure 5.1d). The water mass and water content after 60 days were smaller in the tailings in column SL-04 (slurry tailings) than in column SL-03 (paste tailings), even though the former had a greater initial water content.

Drainage at the base of column SL-01, which contained the thinner tailings layer, lasted only one day (Figure 5.3). Drainage for the thicker tailings layers in columns SL-02 and SL-03 lasted 10 days, with 25% of the water draining out during the first two days. The drainage period for column test SL-04 was twice as long as for SL-03: total drainage lasted approximately 20 days with the former, with 90% of the drained water lost during the first 4 days of the test.

The maximum actual evaporation (AE) rate measured in from the laboratory columns was comprised between 1.4 mm/d and 2.6 mm/d. The average PE rate measured in the laboratory was also 1.9 mm/d (Figure 5.2) but varied with the distance of the water surface to the top of the column. The initial (maximum) AE rate was estimated and adjusted for each SL column test depending on the distance between the tailings surface and the top of the column (Table 5.1).

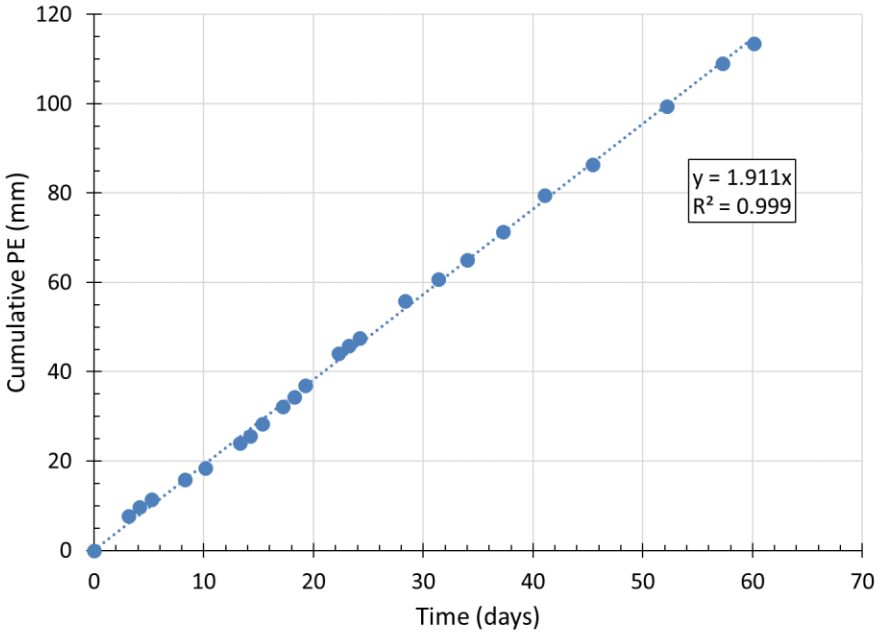

Figure 5.2: Measured cumulative potential evaporation (PE) in a water column during the SL tests. Average daily PE rate corresponds to the slope of the curve.

Table 5.1: Actual evaporation rate (AE) and time at which the maximum evaporation rate decreases.

Test	AE (mm/d)	Time (days)
SL-01	1.4	31
SL-02	1.3	50
SL-03	2.6	29
SL-04	2.0	52

The actual evaporation (AE) rate was calculated by subtracting the mass of water drained at the base of each column from the total mass loss (Section 3.4). The results indicate that the AE rate was almost constant at the beginning of the SL column tests (and approximately equal to PE rate), for approximately 25 to 55 days, depending on the tailings thickness and initial water content (Figure 5.3b).

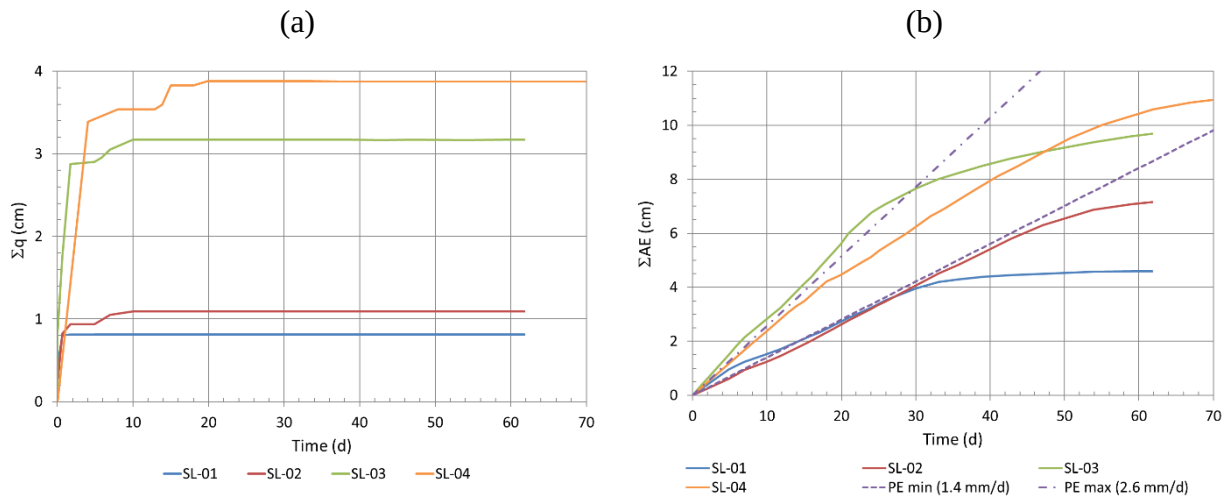

Figure 5.3: (a) Total measured drainage and (b) actual evaporation (AE) during the SL column tests.

Column tests SL-01 and SL-02 showed a similar AE rate of around 1.4 mm/d. The AE rate for column tests SL-03 and SL-04 was also similar but greater than in the other columns (SL-03: 2.6 mm/d, SL-04: 2.0 mm/d). The AE rate in column test SL-03 (paste tailings) began to decrease after 25 days, while it remained constant for over 50 days in SL-04 (slurry tailings).

The initial value of the (gravimetric) water content (w) was obtained from oven drying of a sample taken before placement of the tailings in the SL columns. The water content w at various times was calculated by considering that a change of mass (ΔM) during the test was due to a loss of water (with a fixed mass of solid and assuming a homogeneous distribution of water in the tailings). Early drainage from the columns caused the initial rate of change of the water content to be more rapid (Figure 5.4).

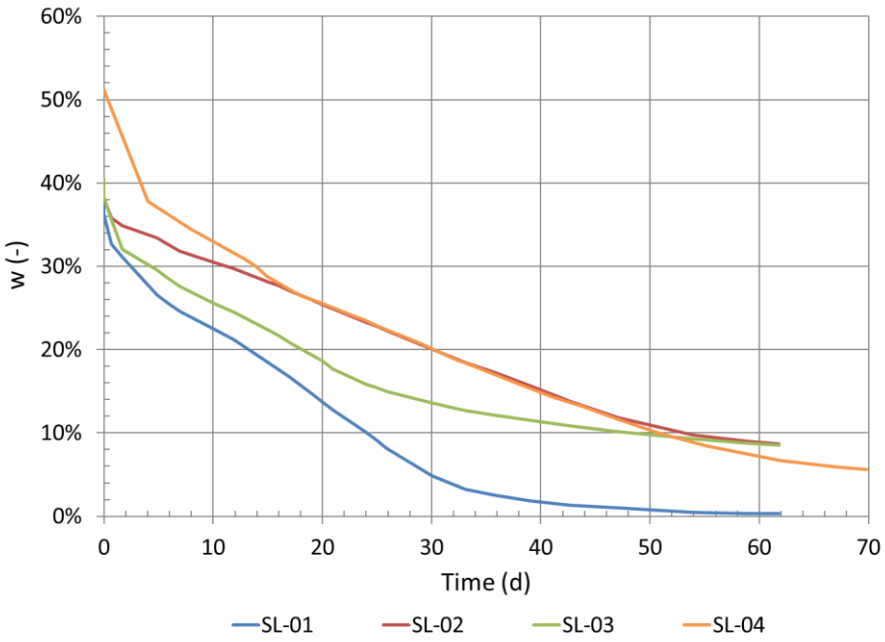

Figure 5.4: Variation of the gravimetric water content (w) for the tailings in the SL columns.

The column with the thinnest tailings layers (SL-01) became almost completely dry at the end of the test (w = 0.3%); the water content with the thicker tailings layers (column tests SL-02 and SL-03) was higher at the end of the testing period (SL-02: w = 8.7%; SL-03: w = 8.5%).

The impact of the higher initial water content for the tailings in column test SL-04 ($w_{initial}$ = 51.2%) was limited after 60 days (SL-04: w = 5.6%) compared to the water content of SL-03 ($w_{initial}$ = 40.4%).

5.2 Thickness

The thickness of the tailings layers in the SL column tests was monitored to assess the settlement rate.

The highest rate of settlement of the tailings was observed in the early part of the tests (Figure 5.5a). The total change of thickness for the tailings in columns SL-01 and SL-02 was respectively 1.8 cm and 2.3 cm during the first 10 days (Figure 5.5b). The rate of change of the thickness in column SL-03 was almost three times greater than the other paste tailings columns (SL-01 and SL-02), and it lasted approximately 15 days for a total change in the thickness of around 5 cm. The

rate of change in column SL-04 (slurry tailings) was lower than for SL-03 (paste tailings), but consolidation continued for twice as long (total displacement around 7 cm after ≈ 30 days for SL-04, and ≈ 5 cm for SL-03). The thickness of the tailings in the columns became constant after 10 days for column test SL-01, and up to 15 days for column test SL-03; both were still losing water afterwards (mostly through evaporation).

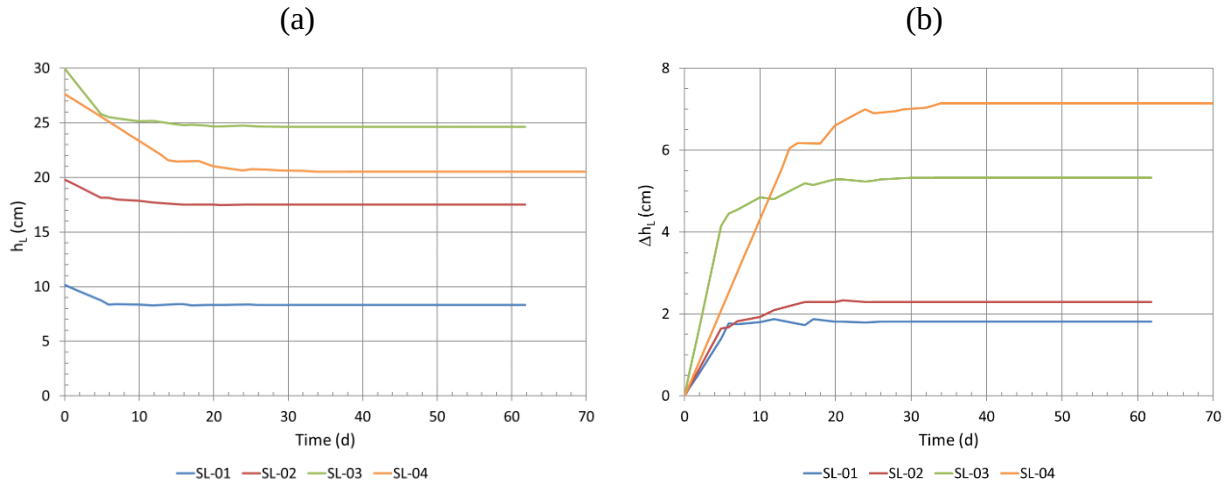

Figure 5.5: Total thickness (a) and change in total thickness (b) for the tailings in SL column tests.

The thickness of the tailings layers place in the columns tends to affect the total change in thickness during the tests (Figure 5.5b), and the rate of change (Figure 5.4a). The thicker the tailings layers, the greater the settlement and the faster the rate. For example, the total settlement in tests SL-01, SL-02 and SL-03 was respectively 1.8 cm, 2.3 cm and 5.3 cm; the average settlement rate was 0.2 cm/d for SL-01 and SL-02, and 0.4 cm/d for SL-03. There was also a correlation between the rate of change of the thickness and the PE rate (Figure 5.3b). A higher PE rate during the SL column tests was associated with a greater settlement (Δh_L) rate (independently from the initial water content and thickness) (Figure 5.6b).

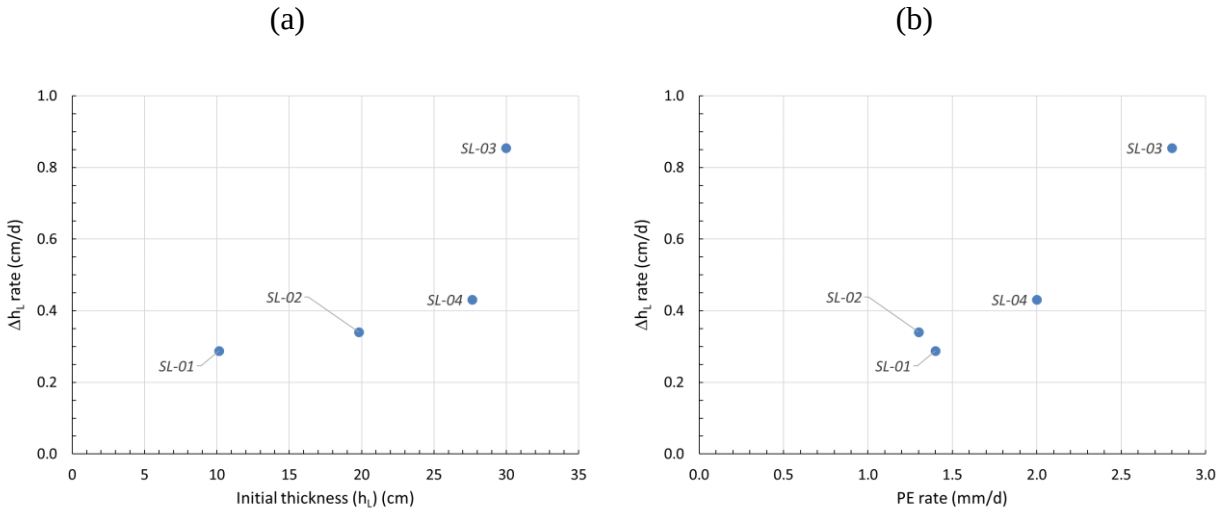

Figure 5.6: Rate of change of the thickness (Δh_L rate) of the tailings during the SL column tests as a function of (a) the initial thickness and (b) the PE rate.

5.3 Pore water pressure

The suction (ψ) was measured in the tailings during the SL column tests using Watermark sensors (Section 3.4.1) placed 5 cm above the base of each layer (Figure 5.7). The suction range of the sensors was 1 – 200 kPa. The suction increased more rapidly in the thinner layers for column SL-01 (Day 7) than in SL-02 (Day 15) and SL-03 (Day 10). The rate of change of the suction in all four column tests decreased once ψ reached the AEV of the tailings ($\psi_a \approx 58$ kPa). The rates tended to increase later, after a time of 5 to 20 days.

Suction in the paste tailings (SL-03) initially increased more rapidly compared to tailings with a higher water content (SL-04). However, the suction measured during test SL-04 continued to increase and eventually became larger than the suction in test SL-03. This appears to correlate with the tendencies observed in columns SL-04 and SL-03.for the change in mass (Figure 5.1b), drainage (Figure 5.3a) and AE rate (Figure 5.3b)

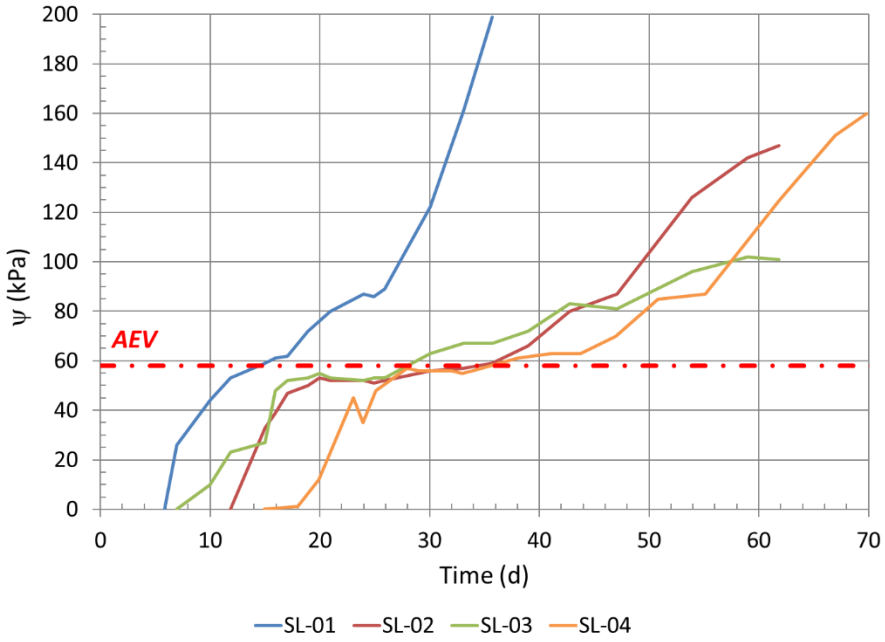

Figure 5.7: Evolution of the suction measured with the Watermark sensors in the tailings for SL column tests (Note: Watermark sensors have a range of 0 to 199 kPa).

5.4 Surface cracking

The cracked surface area was assessed on the surface of each tailings specimen in the columns using image analysis (Section 3.4.1). The crack intensity factor was calculated for each column ($CIF = A_{cracks}/A_{col}$, where A_{cracks} is the surface crack area and A_{col} is the total area of the SL column; Miller et al. 1998, Deschamps, 2009; Saleh-Mbemba, 2010) (Figure 5.8). The CIF tended to increase with the tailings layer thickness in the column tests SL-01 to 03. The final CIF from tests SL-01, SL-02 and SL-03 was respectively 2.5%, 4.2% and 9.6% (Figure 5.8). Wetter (slurry) tailings (in test SL-04) began cracking later (10-11 days) than dryer (paste) tailings in test SL-03 (5-6 days), for a similar initial layer thickness. The final CIF of column SL-04 was 8.5%. The fractured area remained stable for the four column tests after about 33 days.

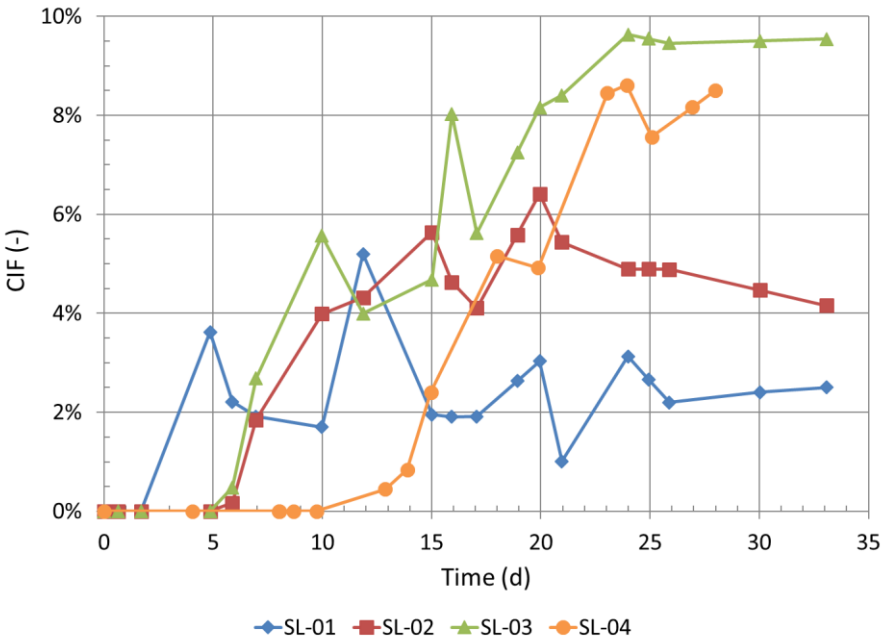

Figure 5.8: Crack intensity factor (CIF) determined for the tailings the SL column tests.

Crack initiation began at a gravimetric water content between 29% and 32% (Figure 5.9). Others (Qiu and Sego, 2001; Saleh-Mbemba et al., 2016; Simms et al., 2017) also observed crack initiation at a gravimetric water content around 30%. This range of value was not significantly affected by the layer thickness or the initial water content.

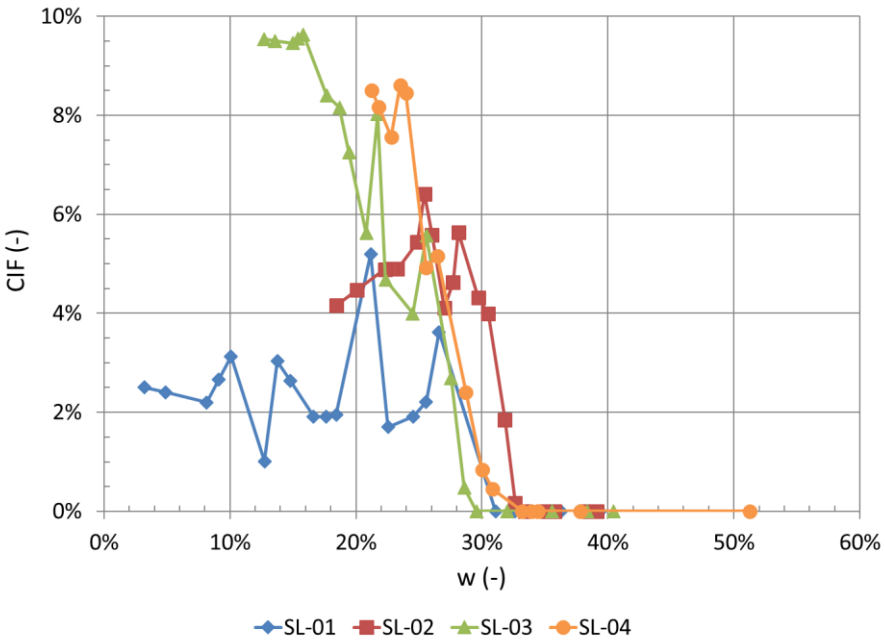

Figure 5.9: Crack intensity factor (CIF) as a function of gravimetric water content (w) for the tailings placed in the SL columns.

The CIF also seems to correlate with to the measured PE rate in the columns (Figure 5.10); the higher PE rate tend to produce a higher CIF. An elevated PE rate generates a higher suction gradient near the surface and this may increase shrinkage (and cracking) of the tailings. Cracking may also lead to a temporary increase of the actual evaporation, sometimes to a value greater than the potential evaporation rate (Simms et al., 2017).

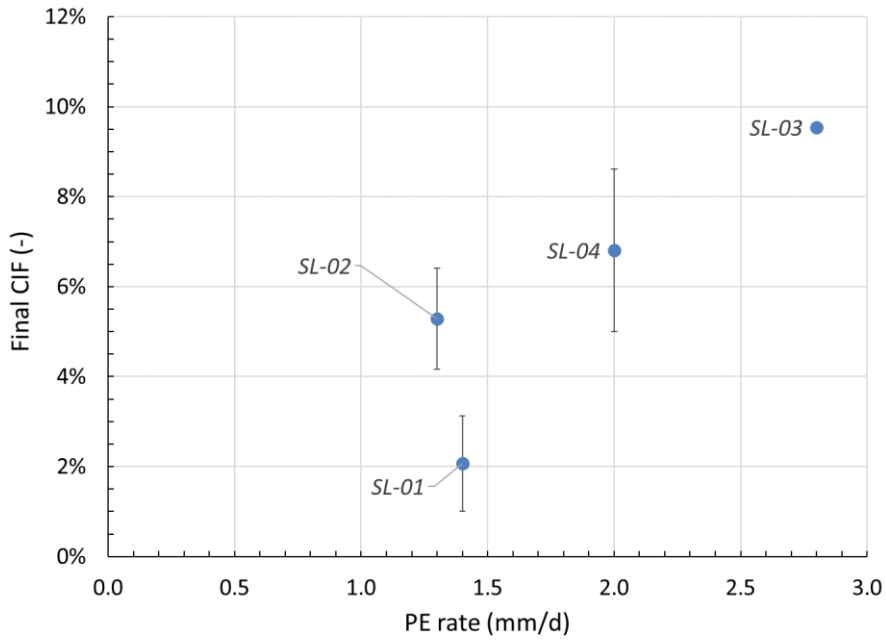

Figure 5.10: Final CIF at the surface of the tailings in SL columns as a function of the PE rate during the SL column tests.

The void ratio ($e = V_v/V_s$; Figure 5.11) of the tailings was estimated for each SL column test using the procedure and hypotheses presented in Section 3.4.

Tailings with a lower initial water content tend to reach a constant void ratio more quickly than tailings with a larger water content (Figure 5.11a). The void ratio became constant after approximately 20 days for the tailings in column SL-03 and 25 days for those in column SL-04.The void ratio in the tailings layer became almost constant after around 10-20 days (i.e. SL-01: ≈ 10 days; SL-02: ≈ 15 days; SL-03: ≈ 20 days) (Figure 5.11b). Evolution of the cracks stopped when the tailings void ratio became constant.

(a) (b)

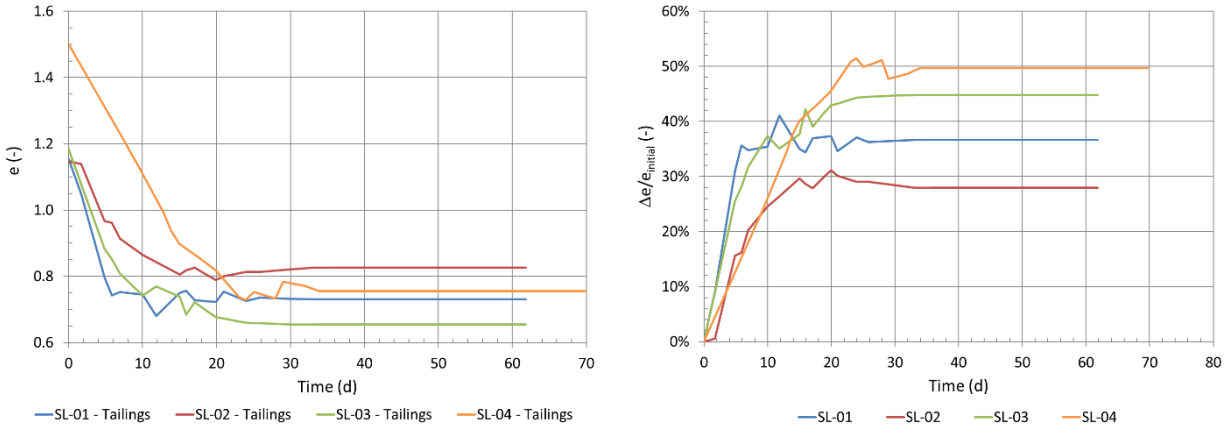

Figure 5.11: Void ratio of the tailings (a) and relative change in the void ratio (b) during the SL column tests.

The void ratio (e) of the tailings varied more significantly at the beginning of the drying cycle. It then became (almost) constant when the gravimetric water content reached 25% to 30% (Figure 5.12), regardless of the initial water content of the tailings. Qiu et Sego (2001) and Saleh-Mbemba et al. (2016) also observed that shrinkage of mine tailings tends to stop at similar gravimetric water content values, and that the final void ratio of the tailings is correlated to the initial void ratio.

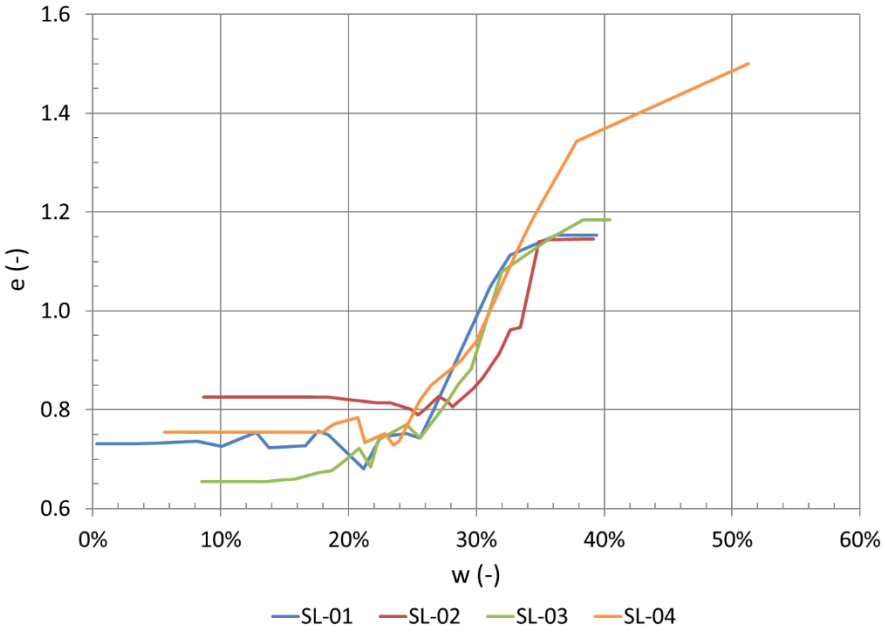

Figure 5.12: Void ratio (a) and relative change in the void ratio (b) as a function of the tailings water content (w) during the SL column tests.

The final void ratio also appeared to be correlated to the AE rate (Figure 5.13). The higher desaturation rate at the surface lead to a lower void ratio. The tailings void ratio at the end of test SL-03 (highest actual evaporation rate) was 0.66. Tailings in column SL-02 (lowest actual evaporation rate) had a final tailings void ratio of 0.83. Tailings in column SL-01 (AE rate between SL-03 and SL-02) had a final tailings void ratio of 0.73.

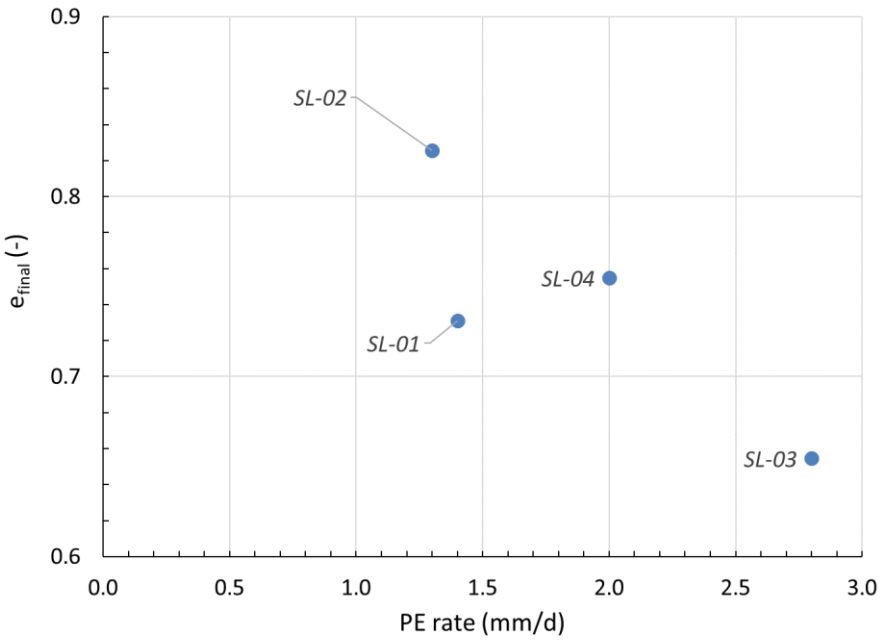

Figure 5.13: Final void ratio at the surface of the tailings at the end of SL column tests as a function of the PE rate

5.5 Volumetric water content

It is possible to calculate the volumetric water (θ) content in the tailings for SL column tests using their void ratio and gravimetric water content (Section 5.4) (Figure 5.14). Tailings in columns SL-01 and SL-03 showed a similar rate of change for θ, but the final value of θ was higher for column SL-03 at 0.12 (vs. 0.01 for SL-01).

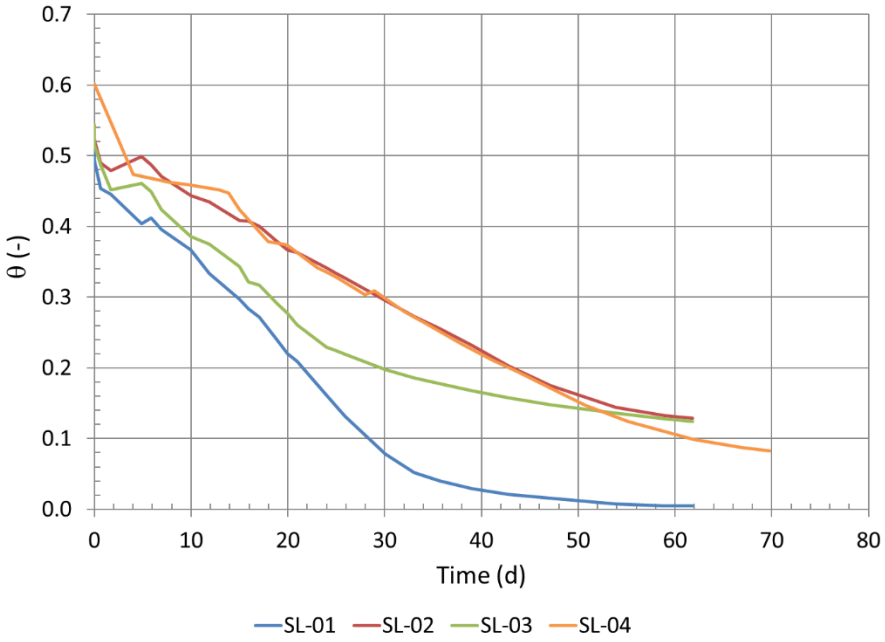

Figure 5.14: Variation of the volumetric water content (θ) in the tailings during the SL column tests (SL-01 to SL-04).

Suction (ψ) and volumetric water content (θ) (adjusted for the void ratio) values obtained from the column tests can be compared with the water retention curves of the Bulyanhulu tailings measured in the laboratory (presented in Figure 4.4). Tailings in all four SL column tests had a similar behaviour in terms of the WRC, regardless of the layer thickness or initial water content (Figure 5.15). The value of the VWC and of the degree of saturation for the tailings placed in the columns was lower than those in the tests to determine the water retention curves (WRC), for a given suction (ψ). Nonetheless, the onset of tailings desaturation for the four column tests occurred around the experimentally determined AEV ($\psi_a \approx 58$ kPa). Saleh-Mbemba (2010) also obtained a WRC that was similar to the WRC measured with the Tempe cells and PPE in this project.

(a) (b)

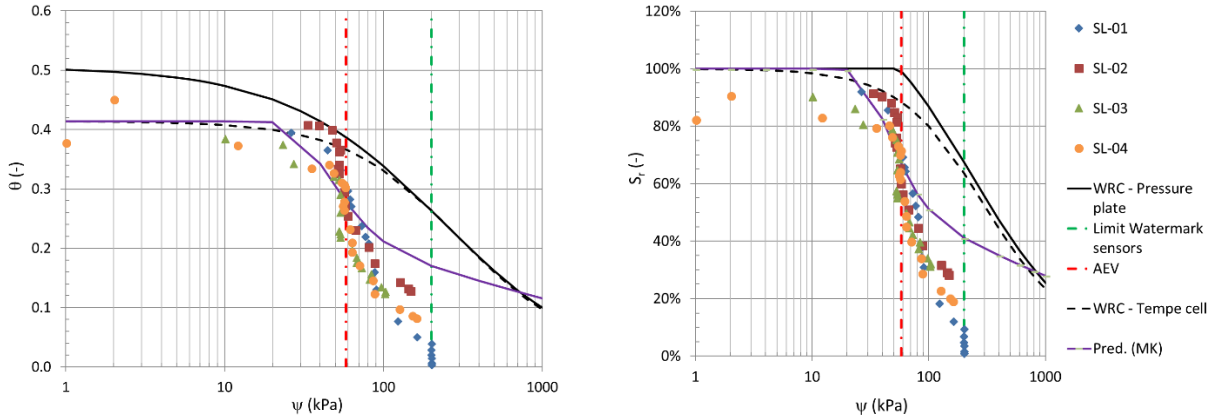

Figure 5.15: (a) Volumetric water content and (b) degree of saturation as a function of suction determined from the SL column tests and from the Pressure plate tests.

Cracking of the tailings surface occurred at a VWC (θ) between 0.45 and 0.49 (Figure 5.16). The layer thickness or initial water content did not appear to influence the value of the volumetric water content at which cracking begins.

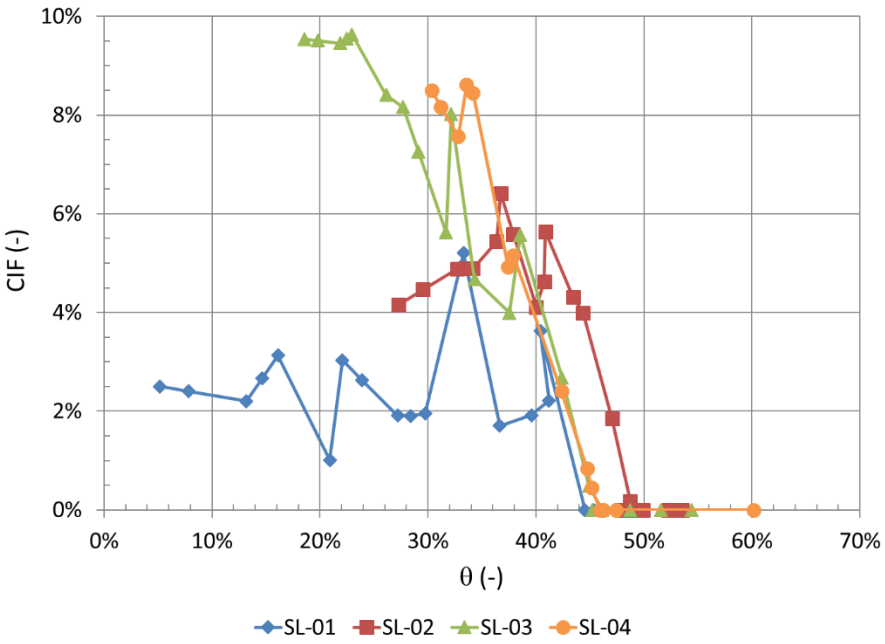

Figure 5.16: Crack intensity factor (CIF) as a function of the volumetric water content (θ) in the SL columns.

5.6 Numerical simulations

Numerical simulations of the SL column tests on tailings were carried out with Vadose/W (Section 3.5). Typical simulation results are shown in Figure 5.17, in terms of outflow (q: bottom; AE: surface). The simulated amount of water drained at the base of each column (SL-01: 0.02 cm, SL-02: 0.08 cm; SL-03: 0.1 cm; SL-04: 0.2 cm; Figure 5.17a) is much smaller than the measured drainage. The PE is well reproduced in the first phase of the simulations, but the AE tends to be overestimated; the decrease in the evaporation rate occurred more rapidly in the laboratory column tests than in the simulations (Figure 5.17b).

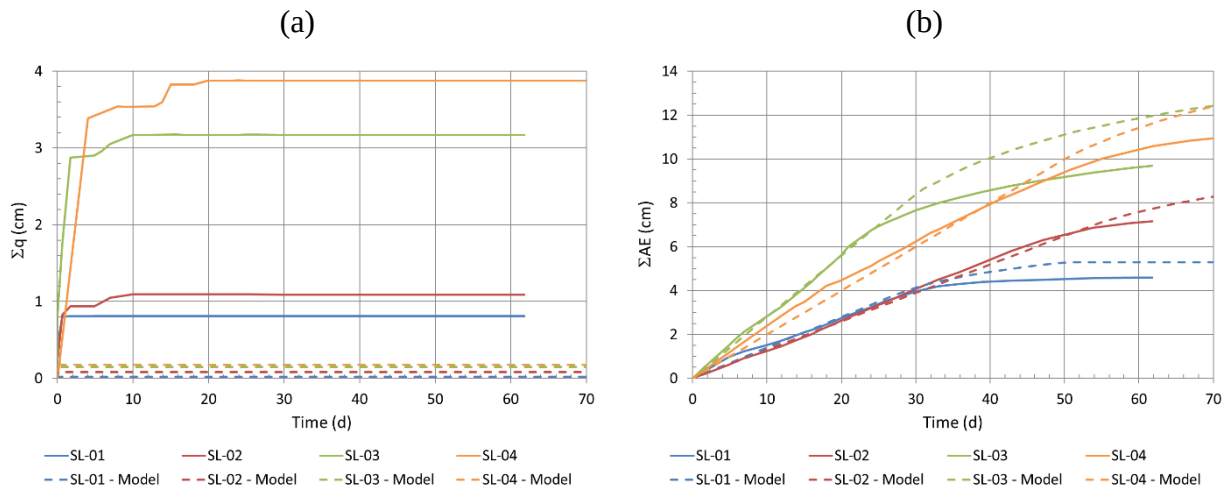

Figure 5.17: Total measured and simulated drainage (a) and actual evaporation (b) in the tailings during the SL column tests. Both the cumulative flow (q) and the actual evaporation (AE) were normalized by the column surface area.

The simulated VWC is slightly higher than the actual value obtained from the measurements, but the overall shapes of the curves showing the evolution of the VWC are similar (Figure 5.18). There is always more water in the simulated tailings since the simulated amount of drainage is significantly lower than the actual drainage from the column tests. This difference could be explained by the initial self-weight consolidation of the tailings before suction develops. The initial drop of the VWC due to drainage is not replicated well with the numerical simulations (e.g. SL-04), but the slope of the desaturation curve is close for both the laboratory and simulated results.

(a) (b)

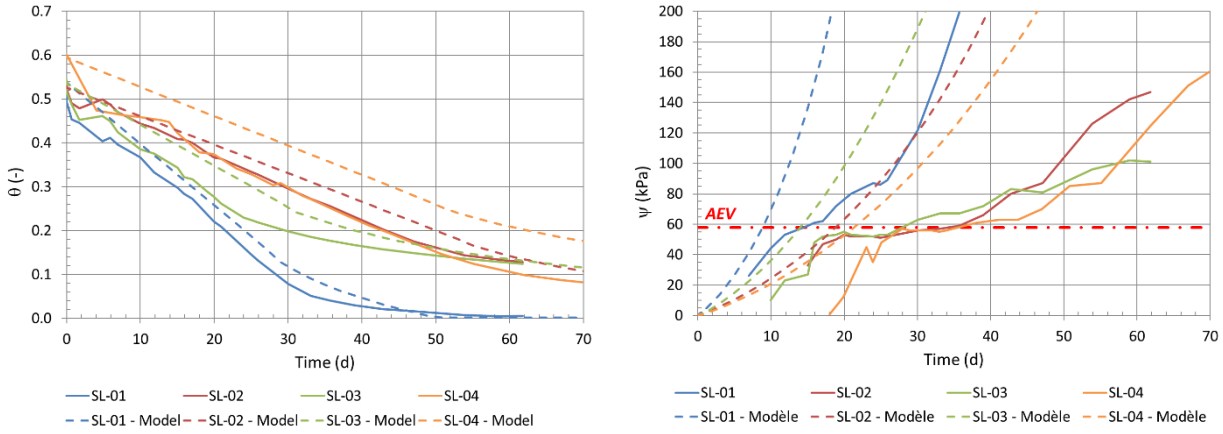

Figure 5.18: Simulated and experimental variation of the (a) volumetric water content and (b) suction in the tailings during the SL column tests (SL-01 to SL-04).

The SL column tests allowed to evaluate the influence of the layer thickness (10 cm, 20 cm and 30 cm) and tailings initial water content on the water movement and desaturation behaviour of tailings. In the following chapter, the influence of multiple tailings layers in a column will be examined.

CHAPTER 6 RESULTS FROM MULTILAYER LABORATORY COLUMN TESTS

The single-layer (SL) column tests helped identified how specific factors (layer thickness and initial pulp density) influence the behaviour of tailings. Multilayer (ML) column tests were also completed to help understand how variably saturated paste tailings layers interact.

The experimental results from ML column test are presented and briefly discussed in Sections 6.1 (Col-01), 6.2 (Col-02) and 6.3 (Col-03 and Col-04). This is followed by a presentation of the small-scale oxygen consumption tests carried out in Col-02 (Section 6.4). The evolution of the volume of tailings in the ML columns is addressed in Section 6.5.

6.1 Multilayer column (ML) test Col-01

The instrumented multilayer column test Col-01 comprised three 10 cm layers (with w = 30.5% to 36.0%) of Buly-04 tailings. The characteristics of the layers is presented in Section 3.4.2. The cycle time (deposition intervals) for layers 1, 2 and 3 was respectively 20 days, 14 days, and 15 days, for a total of 49 days.

6.1.1 Mass

The mass of the tailings in the column was measured at regular intervals (from 0.5 to 24 hours). Water was lost by both drainage (from the base of the column) and evaporation (from the surface). The rate of change of the mass (i.e. the slope of the change of mass as a function of time curves in Figure 6.1a) in all three layers was similar (around 120 g/d or 2 mm/d; Figure 6.1a), except during the first day of the test (Figure 6.2). Water loss the first day was mostly due to drainage, with 333 ml in 21 hours collected at the bottom drain of the column (80% of total mass loss during this period). No drainage was measured afterwards (Figure 6.2) so the rate of change of the mass was then equal to the actual evaporation (AE) rate. Some water remained in the pores at the end of each cycle, when the following layer was deposited (Figure 6.1b).

(a) (b)

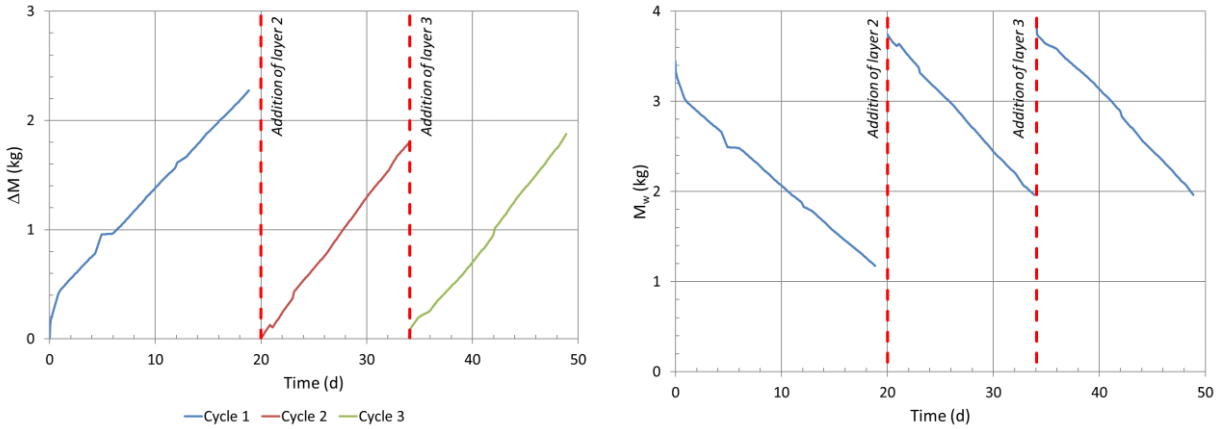

Figure 6.1: (a) Change of mass (ΔM) and (b) mass of water remaining in the column (M_w) for the three cycles of test Col-01.

The average rate of water loss through combined drainage and evaporation was almost four times more rapid than through evaporation alone (Table 6.1). Total drainage and evaporation respectively accounted for 0.5 cm and 0.1 cm during the first day of the test. For layers Col-01-L2 and Col-01-L3, the evaporation rate was respectively 2.0 mm/d and 1.9 mm/d, which is close to the average PE rate recorded in the laboratory (≈ 1.9 mm/d).

Table 6.1: Rate of mass change (in g⁄d and mm-H_2O⁄d) in the three layers of column test Col-01.

Layer	**Rate of change (g⁄d)**	**Rate of change (mm⁄d)**	**Cause**
Col-01-L1	376.27	5.7	Drainage (primary) and evaporation (secondary)
Col-01-L1 (after drainage)	101.66	1.5	Evaporation
Col-01-L2	129.25	2.0	Evaporation
Col-01-L3	123.25	1.9	Evaporation

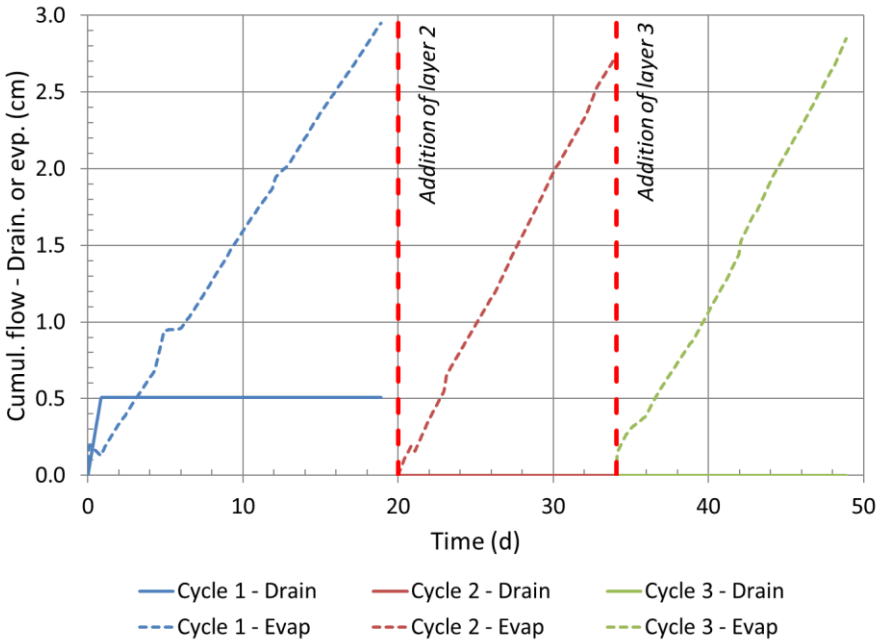

Figure 6.2: Cumulative drainage and actual evaporation (normalized by the area, in cm^2) in the layers of column test Col-01.

6.1.2 Geometric characteristics

The thickness of the surface layers of column Col-01 was monitored during the test. The thickness of the layers became almost constant (±1 mm) about 4 days after the deposition of the fresh tailings in the column (Figure 6.3). A change of tailings thickness in the columns was associated only to a change of thickness in the fresh tailings layer at the surface.

The settlement rate increased as the number of layers increased (Figure 6.3b). The paste tailings deposited on a partially saturated layer settled more rapidly than the first layer poured at the bottom of the column. The time required to observe a 1 cm thickness variation in the layers was 2.7 days for layer 1, 1.5 days for layer 2 and 0.3 days for layer 3. The total displacement was comprised between 1.0 cm and 1.4 cm and seemed independent of the layer number.

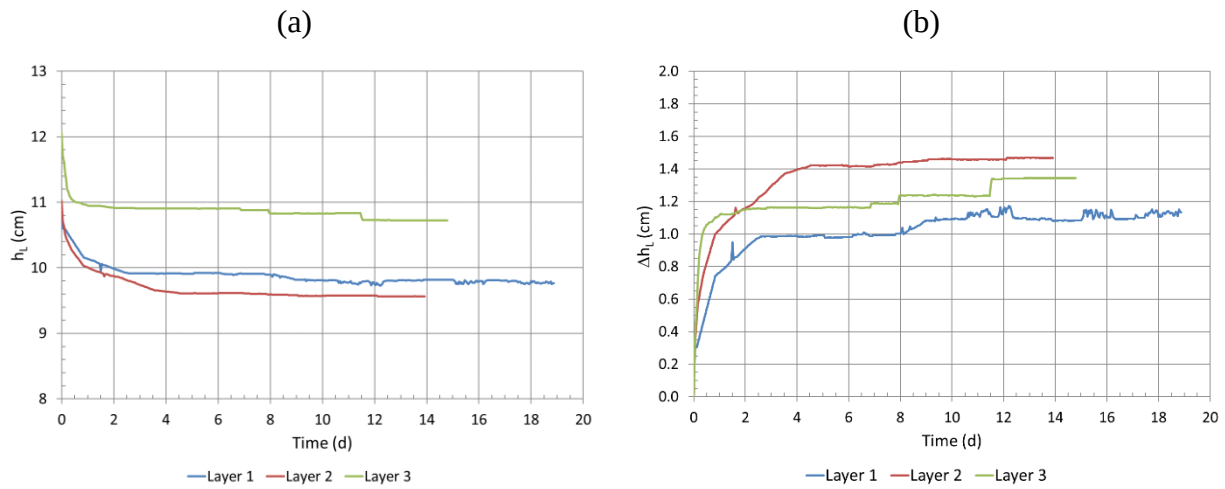

Figure 6.3: (a) Total thickness and (b) change in thickness for the three tailings layers during column test Col-01.

A camera was placed above the surface of the column to take pictures at regular intervals and monitor the evolution of cracks developing at the surface of the tailings during the test. Cracking of the surface started 8.6 days after deposition of layer 1, 4.0 days after deposition of layer 2 and 2.3 days after deposition of layer 3. Figure 6.4 shows pictures of the surface of column Col-01-L2 taken at 2-day intervals. Cracking appeared after 4 days but continued to develop until day 10; no more change was observed afterwards. The visible fractures were typically curved in shape, with a maximum opening width of approximately 5 mm.

(a) 0 days (b) 2 days (c) 4 days

(d) 6 days (e) 8 days (f) 10 days

(g) 12 days (h) 14 days

Figure 6.4: Evolution of the fractures on the tailings surface during column test Col-01 (layer L2).

6.1.3 Pore water pressures

An Omega PX240 sensor measured pore water pressure (PWP) in the middle (mid-height) of each tailings layer during the test. An additional T-5 transducer (UMS) was placed ≈ 5 mm from the surface of each new tailings layer (labelled “Surface” in Figure 6.5). The PWP in the middle and

at the surface of each layer of fresh tailings was the same during the first ten days following placement of tailings layers 1 and 2 in the column (Fig. 6.5).

The capacity of the pressure transducers to record negative water pressures was, however, limited by the desaturation of the porous ceramic sensors (at -20 kPa for layer 1, -40 kPa for layer 2, and -10 kPa for layer 3), and this observation could not be confirmed for higher suctions. Larger suctions are, however, expected to develop closer to the surface (e.g. Wilson et al., 1994, 1997). It was not possible to resaturate the ceramics since they were at the end of a capillary tube in the middle of the layer, which limited their operating range and period.

Suction increased (i.e. pressure decreased) more rapidly in layer 2 than in layer 1. The AEV (about 58 kPa) was reached respectively 12 days in layer 1 and 7 days in layer 2 after the placement of the fresh tailings layer. The presence of a partially desaturated layer below a fresh layer increased the desaturation rate of the upstream layer. Suction was recorded for 4 days in layer 3.

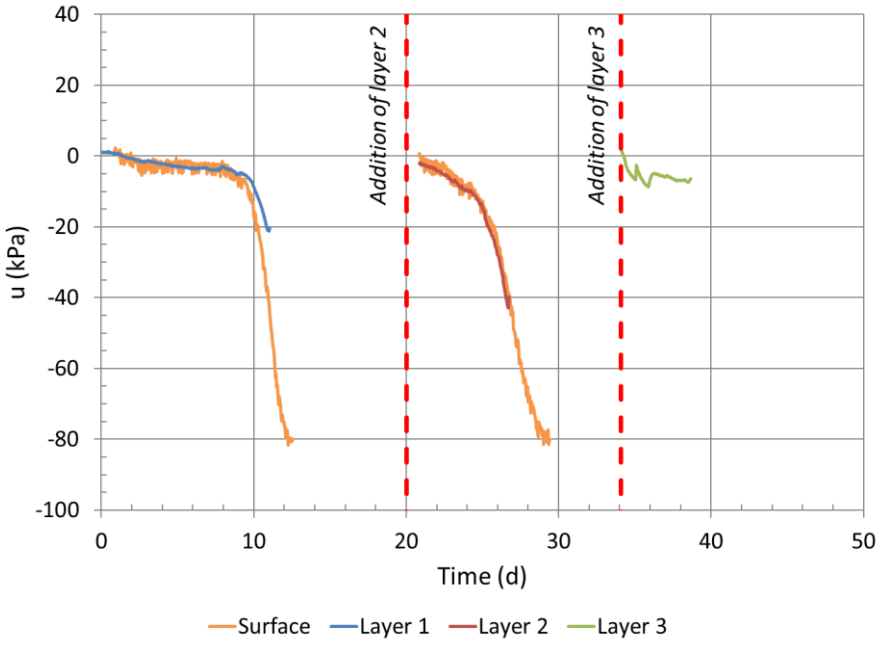

Figure 6.5: Evolution of the pore water pressures in the tailings during column test Col-01. Surface: T-5 tensiometer; Layers 1 to 3: PX240 tensiometers.

6.1.4 Volumetric water content

The volumetric water content (VWC; θ) was measured in each layer during test Col-01 using coated TDR probes (Section 3.4.2). The addition of a fresh layer of tailings at the surface increased the volumetric water content in the underlying layers (Figure 6.6). The water in the fresh layer of tailings drained in the layers below causing a rapid increase in the VWC of the partially saturated layer underneath (e.g. the VWC increased from 0.12 to 0.30 in layer 1 after the deposition of layer 2). The drainage rate was influenced by the downwards hydraulic gradient due to the difference in suction (and water content) between the partially saturated and fresh tailings layers (see Section 6.1.6 below for more details). Filling of the cracks with fresh tailings also contributed to the overall water content increase in the underlying layer; this allowed water from the fresh tailings to penetrate deeper and faster in the unsaturated tailings.

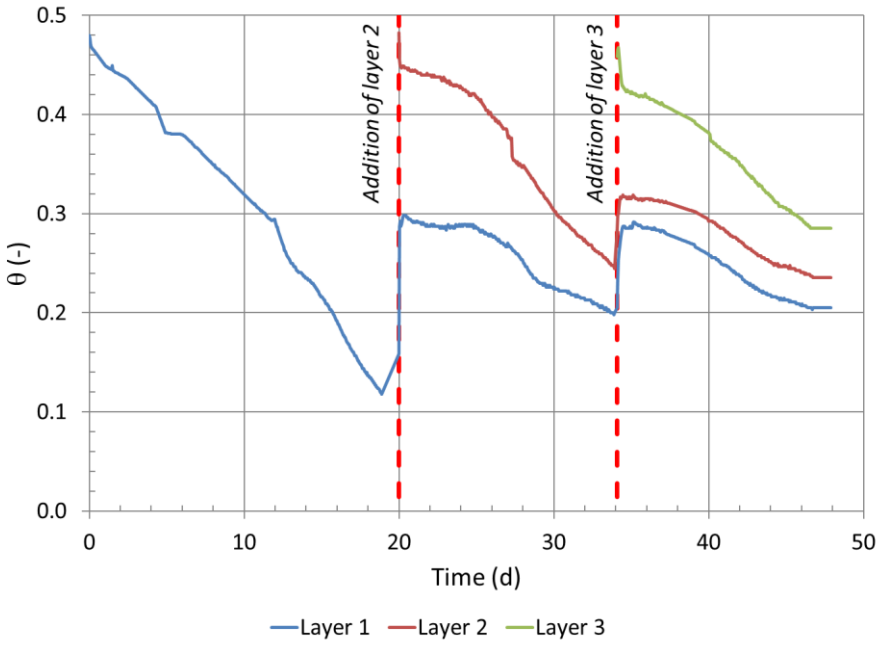

Figure 6.6: Evolution of the volumetric water content (θ) in the different tailings layers during column test Col-01.

The measured VWC was compared with the tailings WRC determined from the pressure plate and Tempe cell tests (Figure 6.7a). The suction was measured by the surface sensor (T-5) for layers 1

and 2, and it was assumed that suction was similar in the middle of the layer, as suggested by results shown in Figure 6.5. The VWC was measured with the TDR probe in the top (fresh) layer during the corresponding cycle (layer 1 for cycle 1, layer 2 for cycle 2). The corresponding data on the WRC tend to agree with values obtained from layer 2, with an AEV of approximately 40-50 kPa (58 kPa on the WRC). The VWC recorded in layer 2 was higher than for layer 1 (≈ 0.02–0.10) for a similar suction. This might be caused by issues with the TDR waveguide in layer 1 (e.g. signal interference, poor contact between the waveguides and the surrounding material). The initial porosities (n) of layers 1 and 2 were respectively 0.49 and 0.51. The degree of saturation (Sr) of the layers was also slightly lower than the one given by the WRC (Figure 6.7b), possibly because of uncertainties related to TDR measurements (even though the probes were calibrated).

(a) (b)

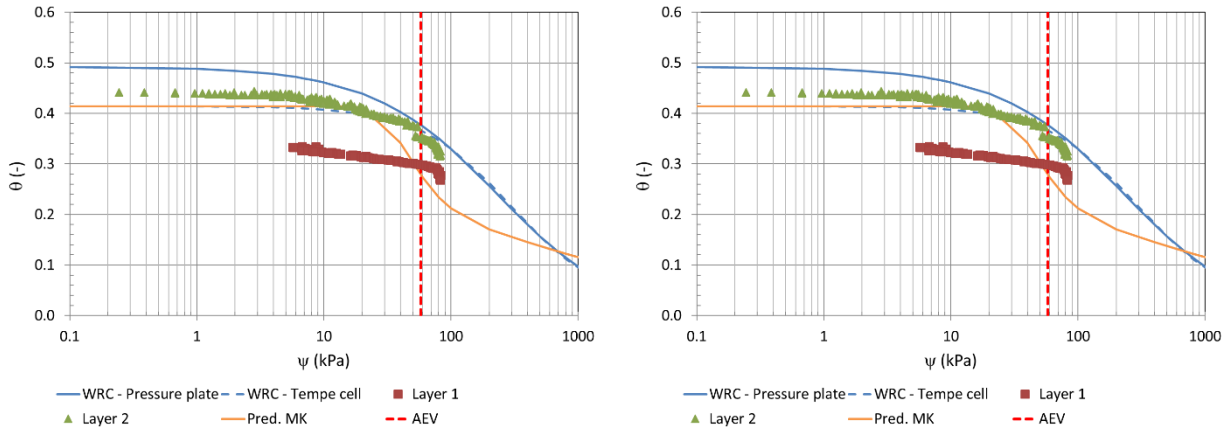

Figure 6.7: (a) Volumetric water content (θ) and (b) degree of saturation (S_r) as a function of suction (ψ) measured in the tailings during test Col-01 compared with the water retention curve of the tailings (see Section 3.2.7).

6.1.5 Interlayer fluxes

The interlayer water fluxes were evaluated using the measured VWC in the tailings layers for test Col-01 (layers 2 and 3) and the procedure presented in Section 3.4.2. As a reminder, upwards flow (normalized by the area) due to evaporation is considered positive and downwards flow

(normalized) due to water drainage is considered negative. For example, Figure 6.8 shows the total (normalized) flow between layers 1 and 2 (interface 1-2); there is -1.4 cm of water that moves from the fresh layer (layer 2) into the partially saturated layer (layer 1) in the first 12 hours following deposition. Around day 21, the slope of the curve (Figure 6.8) became positive, which indicates that water was moving up by evaporation from layer 1 back into layer 2.

Water flow out of the column from the bottom was only measured during cycle 1 (for layer 1). The fresh tailings layers desaturated in the hours following deposition in the column for cycles 2 and 3 (Figure 6.8). This outflow of water from the surface layer resulted from an inflow of water into the older tailings layers below at the interfaces between layers 1 and 2 (Int. 1-2), and layers 2 and 3 (Int. 2-3) (Figure 6.8). The fractures filled with fresh (high water content) tailings, and the suction gradient between the fresh and the old tailings layers, which favored downwards flow into the desaturated layers, both contributed to the resaturation of the downstream layers. The water flow from the fresh to the desaturated tailings lasted for less than one day. There was no water outflow at the bottom of the column. The hydraulic gradient changed after about 1 day in the older tailings layers as they started desaturating by evaporation later (illustrated by a positive slope in Figure 6.8).

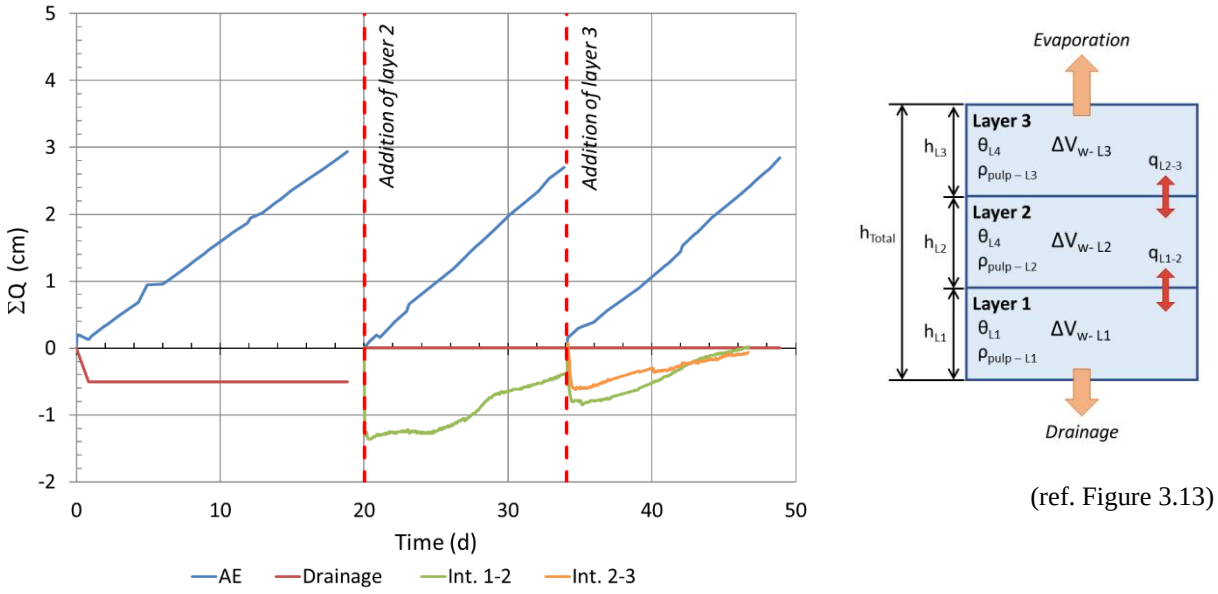

(ref. Figure 3.13)

Figure 6.8: Calculated normalized interlayer flow in column Col-01.

6.1.6 Numerical simulations

Col-01 test was simulated using Vadose/W (Sections 3.5 and 4.3). Water flow (evaporation and drainage) is normalized by the area of the column and expressed in unit of length ([L] or [L T^{-1}]) to facilitate comparison between numerical results and laboratory measurements.

The total water flow from the surface and the bottom of the column, and the total interlayer flow (between layers) were simulated (Figure 6.9). The applied PE rate in the models was equal to the measurements (Table 6.1); the AE rate was well simulated with the numerical models (Figure 6.9). The AE was equal to the PE for the simulated period in the three cycles (only PE was imposed in the model, AE was calculated).

Simulated total drainage at the base of the model is 0.1 cm (Figure 6.8). It is underestimated for test Col-01 with Vadose/W; this was also observed for the SL column tests (see Figure 5.17a). The simulated flow at the interface between layers 1 and 2 is like the one calculated from the VWC values; the simulated flow is overestimated (by about 1 cm) at the interface between layers 2 and 3 (compared with experimental values).

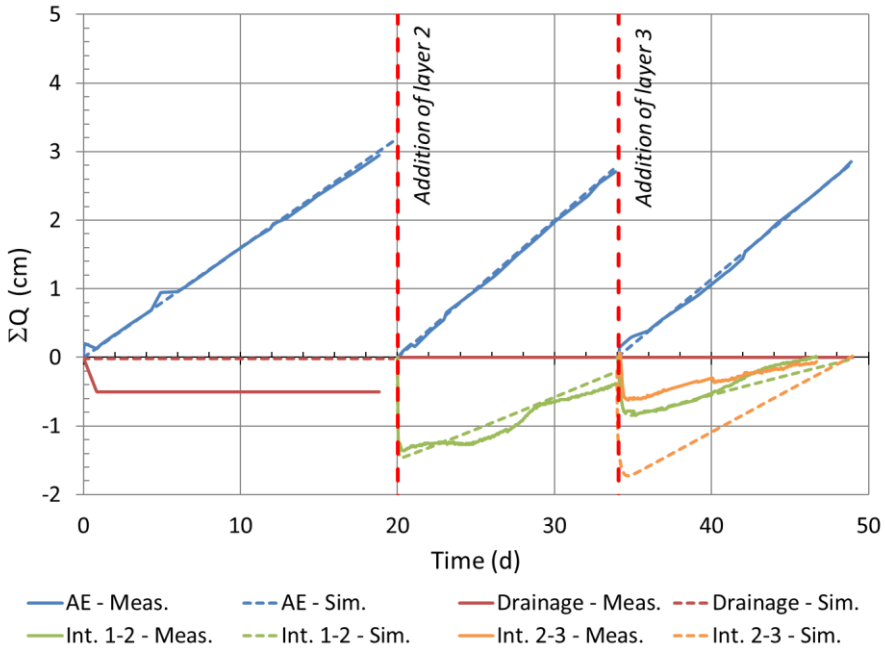

Figure 6.9: Measured and simulated normalized flow in Col-01.

The total outflow (evaporation and drainage) are comparable between the laboratory tests and numerical simulations for the three cycles of column test Col-01 (Figure 6.10). The total outflow during cycle 1 was higher in the laboratory test, mainly due to the drainage water collected in the laboratory (greater than the simulated drainage). The simulated outflow is higher for cycles 2 and 3. The inter-layer flow is simulated accurately (e.g. interface between layers 1 and 2) (Figure 6.9).

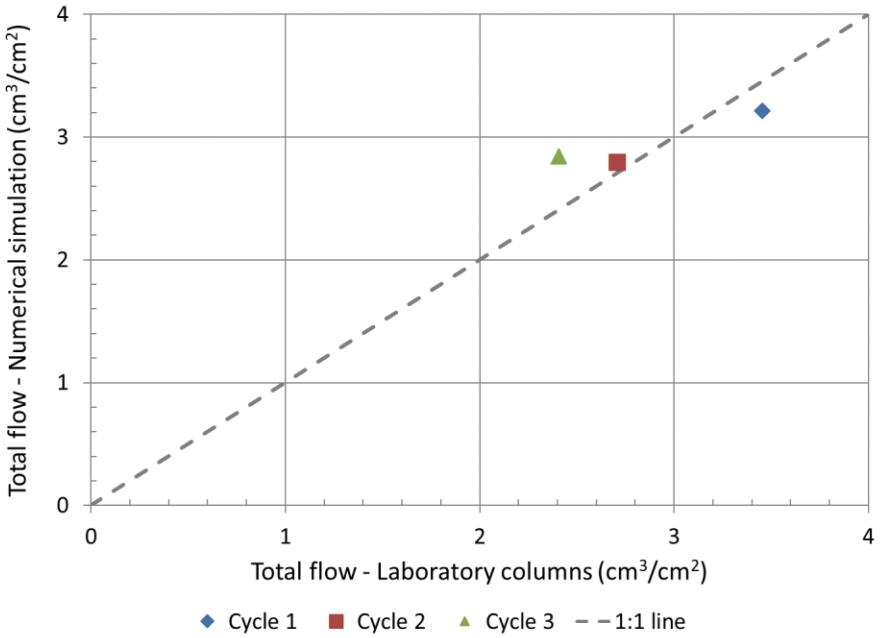

Figure 6.10: Total flow out of the multilayer laboratory column Col-01 and numerical simulation for the three cycles.

The simulated water content is like the water content measured in the laboratory test (Figure 6.11). The measured and simulated volumetric water contents in cycle 1 (layer 1) decreased at a similar rate (-0.0152 d^{-1} for the lab vs. -0.0159 d^{-1} for the numerical simulation). The desaturation of the fresh layer in cycles 2 and 3 is more pronounced with the numerical simulation compared to the laboratory measurements. There is a 0.1 difference between the measured and the simulated volumetric water contents in the fresh layers at the beginning of the cycles; this difference decreases during the cycles (it is around 0.02 at the end of cycle 2). During cycle 3, the VWC in layers 1 and 2 is well represented (Figure 6.11)

The variation of the volumetric water content in the laboratory test was more gradual than in the simulation. The fresh tailings layer in the numerical simulation initially desaturated at a higher rate than in the laboratory. The behavior of the layer below was modeled more accurately. This could be associated with a volume change of the fresh tailings layer that was not directly accounted for in the simulations. The simulated values of the volumetric water content progressively approached the laboratory values. Differences in the prediction of the interlayer flow can also be associated to inaccuracies in the VWC measurement using the probes. The volumetric water content in the

deeper layers is reproduced well by the numerical simulations. For example, in cycle 3, the difference between the average measured and simulated VWC is 0.03 for both layers 1 and 2 (which is comparable to the precision of the VWC sensors used in the column tests).

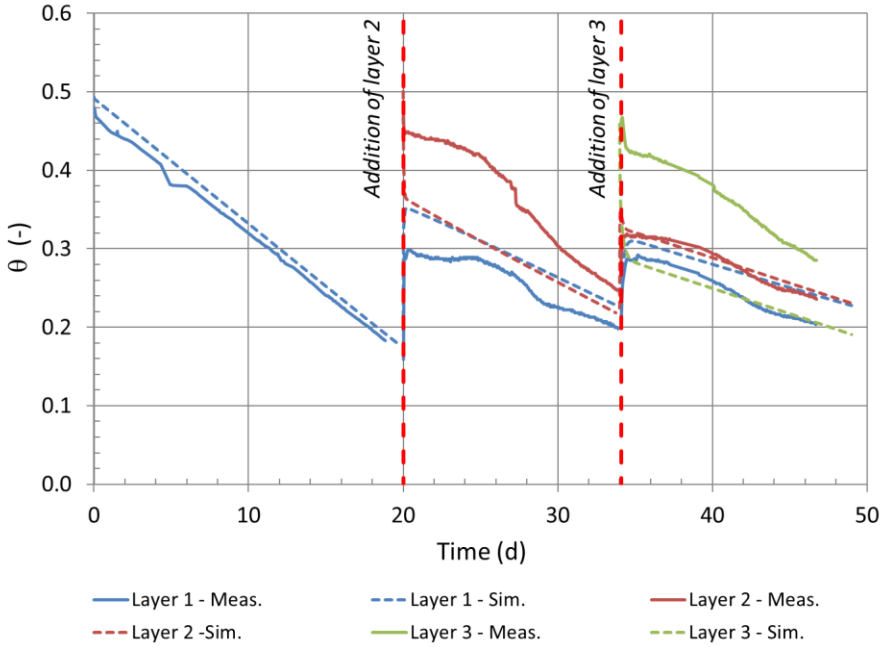

Figure 6.11: Measured and simulated volumetric water content (a) and suction (b) in column test Col-01.

The simulated rate of change of the volumetric water content is more stable than in the laboratory model. The former can be divided in two phases. The first simulated phase, early in the cycle, consist of a rapid desaturation of the fresh layer from drainage into the underlying layers. simulates a more gradual desaturation of the layers by evaporation. The simulated reduction of volumetric water content by drainage from the top layer is approximately 0.15 m^3/m^3 in the day after the placement of the fresh layer (cycles 2 and 3).

6.2 Multilayer (ML) column test Col-02

Column test Col-02 comprised the placement of four 10 cm layers of Buly-07 tailings. The characteristics of each layer (following deposition in the columns) are presented in Section 3.4.2. The cycle time was 33 days for layer 1, 20 days for layer 2, 19 days for layer 3, and 13 days for layer 4; the total test duration was 84 days.

6.2.1 Mass

The change of mass observed in test Col-02, shown in Figure 6.12, was like the one in test Col-01 (see Figure 6.1). There was a rapid loss of mass from drainage after deposition of layer 1 Afterwards, the rate of loss of mass of the column corresponded to the AE rate. Drainage occurred in the first day following deposition of the first tailings layer and 459 ml were collected at the base of the column. There was also drainage during the first three hours of cycle 2 where 7.4 ml were recovered. The fractures on the surface of the tailings and from the shrinkage on the sides of the column prior to the pouring of layer 2 (Figure 6.13) favored preferential flow to the bottom of the column.

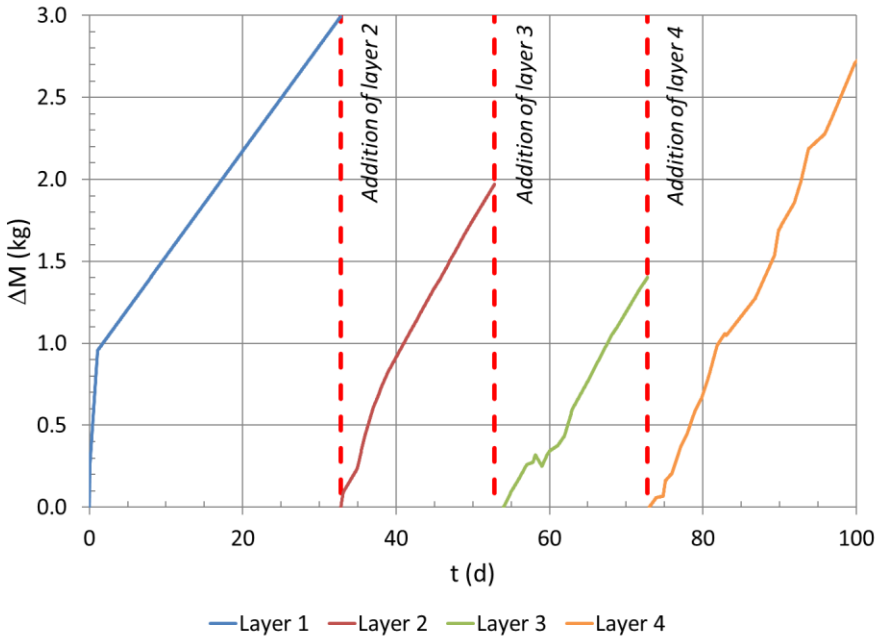

Figure 6.12: Evolution of the mass for column test Col-02.

Figure 6.13: Surface of Col-02 four days prior to deposition of layer 2.

The rate of change of the mass for the different cycles of column test Col-02 is in Table 6.2. The rate of change for layer 1 is divided into two periods: drainage and evaporation.

Table 6.2: Rate of change of the mass in the four cycles of column test Col-02.

Layer	**Rate of change (g/d)**	**Rate of change (mm/d)**	**Cause**
Col-02-L1	736.05	11.1	Drainage (primary) and evaporation (secondary)
Col-02-L1 (after drainage)	64.30	1.0	Evaporation
Col-02-L2	94.30	1.4	Evaporation
Col-02-L3	75.58	1.1	Evaporation
Col-02-L4	108.33	1.6	Evaporation

Flow from the bottom of the column occurred during the first 26 hours of cycle 1 and the first 3 hours of cycle 2 (Figure 6.14). Otherwise, all loss of water was evaporated from the top of the

column. The actual evaporation (AE) rate (slope of the curves in Figure 6.14) during the four cycles remained constant.

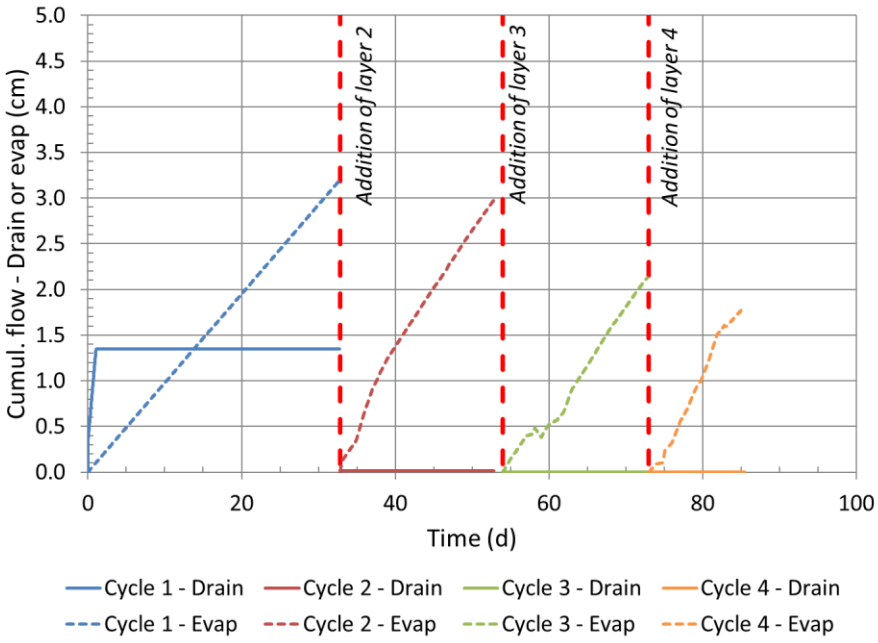

Figure 6.14: Cumulative drainage and actual evaporation in the layers of column Col-02.

6.2.2 Geometric characteristics

The thickness of the surface layer was monitored during column test Col-02 (Figure 6.15). The decrease of thickness in layer 1 was about double that of the other three layers in Col-02 (1.9 cm vs. ≈ 1 cm; see Figure 6.15b). The rapid drainage recorded for layer 1 accelerated its settlement at the beginning of cycle 1.

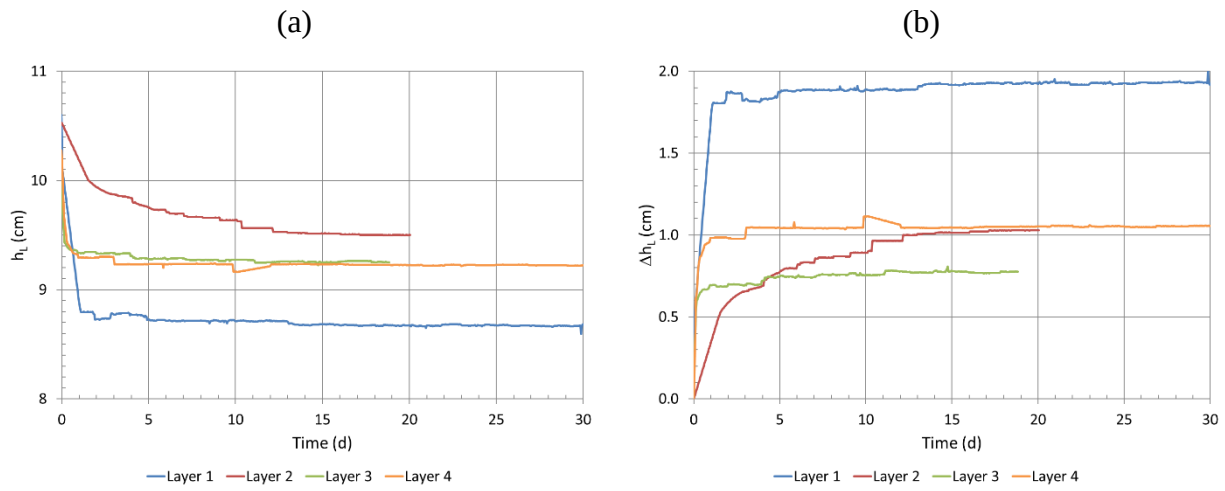

Figure 6.15: Total thickness (a) and change in thickness (b) for the three layers of column Col-02.

The thickness of the layers became constant (± 1 mm) after less than 2 days for layers 1 (1.9 days), 3 (0.9 days) and 4 (0.8 days). The thickness of layer 2 was constant after 10.4 days. Layer 2 had a lower pulp density (P_m = 70.7%) than the other three layers (layer 1: P_m = 74.6%; layer 3: P_m = 74.7%; layer 4: P_m = 75.0%), and it appears that a lower pulp density increased the settling time of the tailings (Figure 6.16). This was also observed in the SL columns where the consolidation time of column SL-04 (P_m = 66.1%) was larger than column SL-03 (P_m = 71.2%) (Section 5.2).

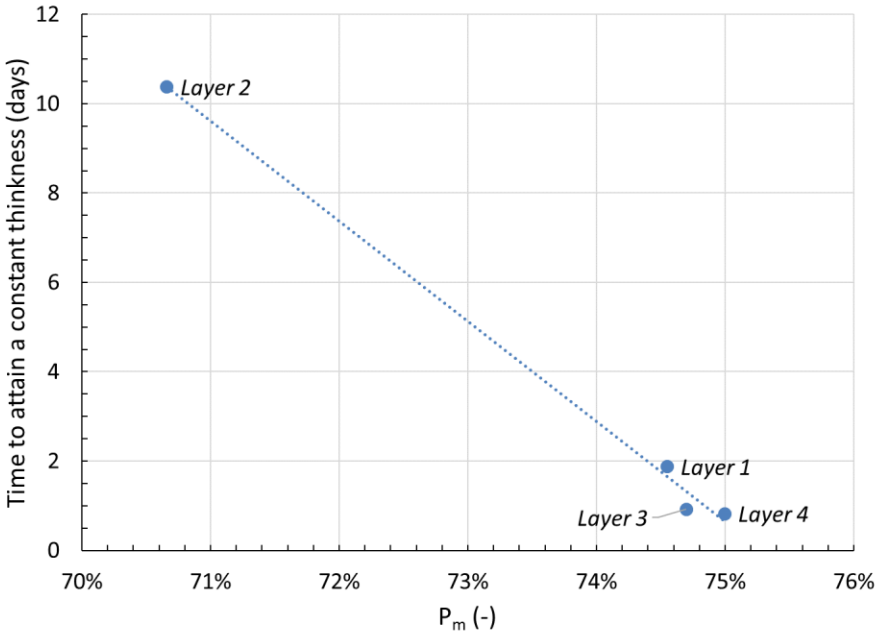

Figure 6.16: Time required for the thickness of the tailings layers to become constant (±1 mm) in column test Col-02 (line added for indication only).

Cracks also developed at the surface of the column during the desaturation process. The time following deposition before the appearance of fractures was 2.9 days for layer 1, 1.1 days for layer 2, 0.8 days for layer 3, and 0.05 days for layer 4. The presence of semi-saturated layers downstream increased the desaturation rate and decreased the time before cracks appeared (similar observations were made in Col-01 and by Benzaazoua et al., 2004).

6.2.3 Pore water pressure

The pore water pressure and suction were monitored using three types of sensors in column test Col-02 (Figure 6.17). The four pressure transducers did not work correctly throughout the test (Figure 6.17a). The T-5 probe placed on surface gave reliable results to a pressure between -70 and -80 kPa. The suction from the Watermark sensors reached a plateau at a value between 30 kPa and 55 kPa (although the theoretical measurement range is 199 kPa).

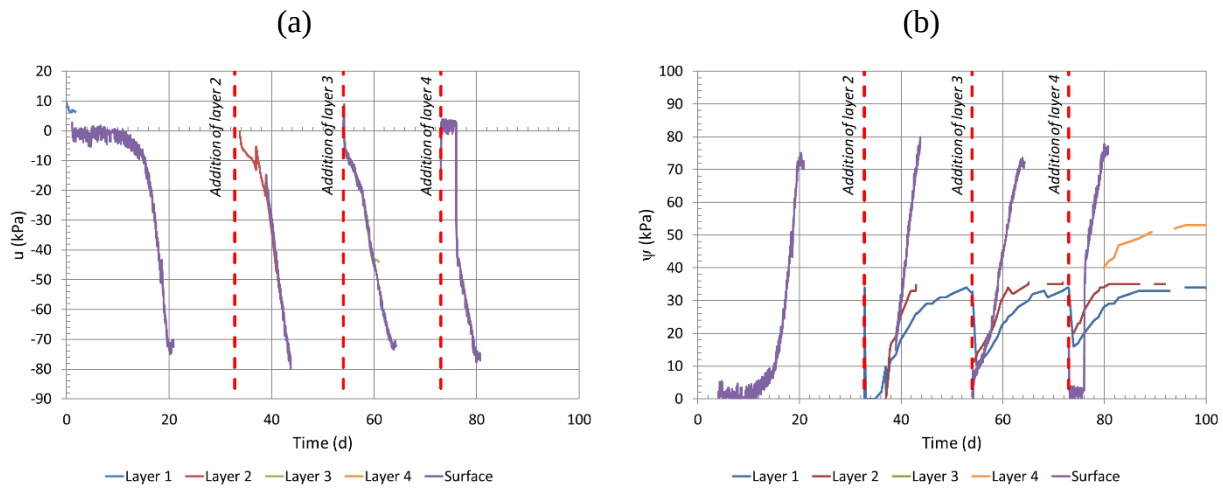

Figure 6.17: Pore water pressure (a) and suction (b) with respect to time for Col-02.

The time to attain the air entry value of the tailings (58 kPa) with the T-5 sensor for each layer in column test Col-02 decreased as the number of layers increased (Layer 1: 18.9 days; Layer 2: 9.2 days; Layer 3: 7.5 days; Layer 4: 4.8 days). This was also observed in Col-01 and is explained by an increase in the drainage rate of water from the fresh tailings layer to the partially saturated layers below. This is also illustrated with the calculation of the interlayer flow (see Section 6.2.5 below).

6.2.4 Volumetric water content

The volumetric water content (VWC) was also measured using coated TDR probes placed in the middle of the paste tailings layer. Figure 6.18 presents the evolution of the VWC measurements for the four cycles of column test Col-02.

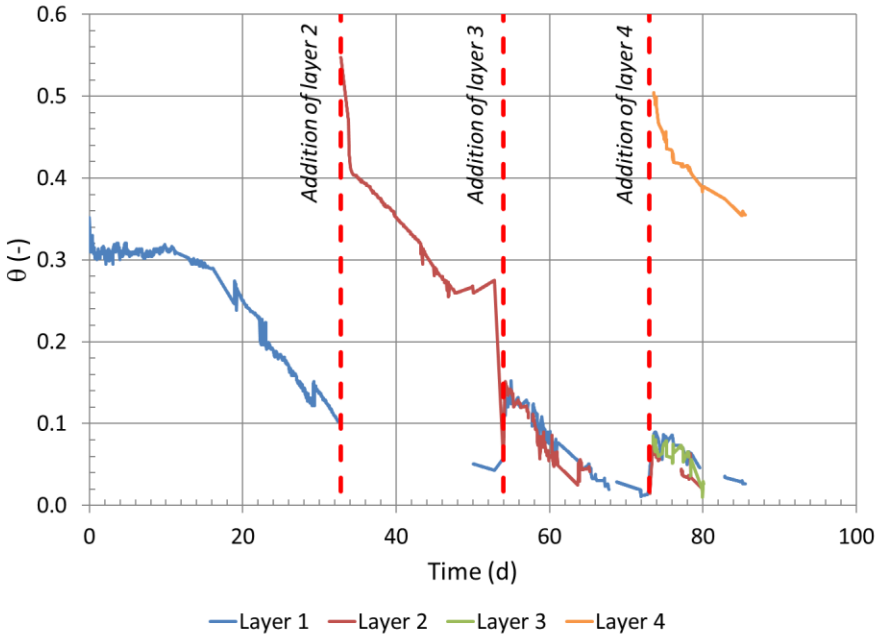

Figure 6.18: Volumetric water content in the layers of column test Col-02.

The data from TDR sensors in this test became erratic (Figure 6.18). Exposure to an oxidative environment in the tailings caused failure of the probes.

The laboratory measurements were compared to the actual WRC (θ vs. ψ and S_r vs. ψ) obtained using the Fredlund and Xing (1994) (Table 4.6; a_{fx} = 247.87 kPa; n_{fx} = 0.84; m_{fx} = 2.67) (Figure 6.19). The VWC and degree of saturation measured in the columns with the TDR probes was always lower than the value from the WRC of the tailings. However, the curves have a similar shape with an inflexion point close to the measure AEV of the tailings.

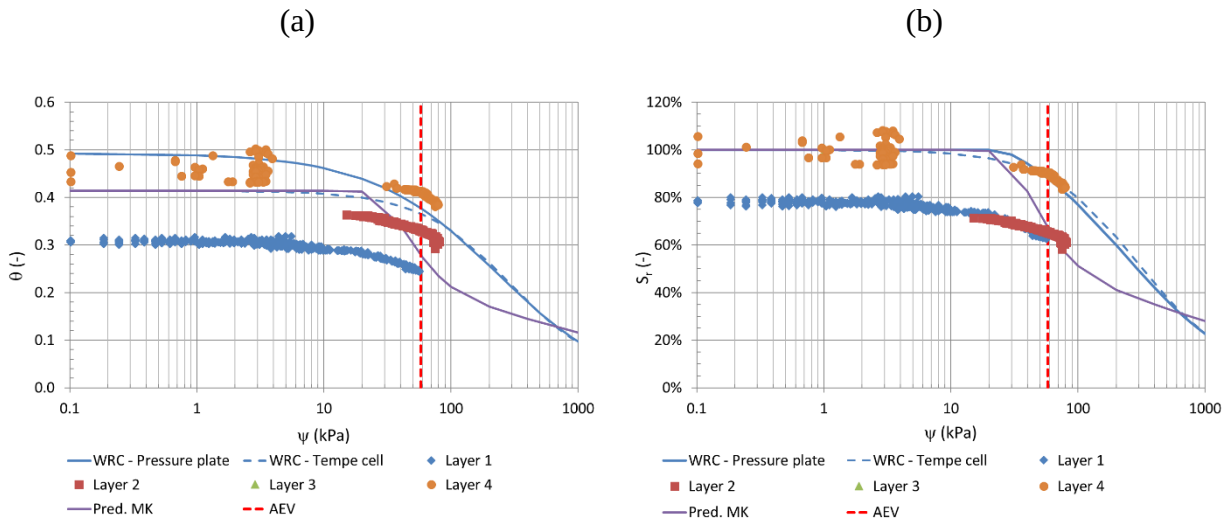

Figure 6.19: (a) Volumetric water content (θ) and (b) degree of saturation (S_r) as a function of surface suction (ψ, measured with T-5 sensors – Decagon Inc.) in Col-02 compared with the water retention curve of the tailings.

6.2.5 Interlayer flow

The presence of a partially desaturated layer below a fresh tailings layer accelerated the tailings desaturation rate after placement of a fresh tailings layer (as observed in Col-01) (Figure 6.21). For example, there was a rapid outflow from the fresh tailings into layer 1 following their placement of layer 2 (Figure 6.21). The inter-layer flows in cycles 2 to 4 in Figure 6.21 are more erratic. The TDR probes used to measure the volumetric water content in each layer (and to extrapolate the flow) stopped working consistently during column test Col-02 (Section 6.2.4). It is not possible to calculate the inter-layer flow without valid volumetric water content measurements.

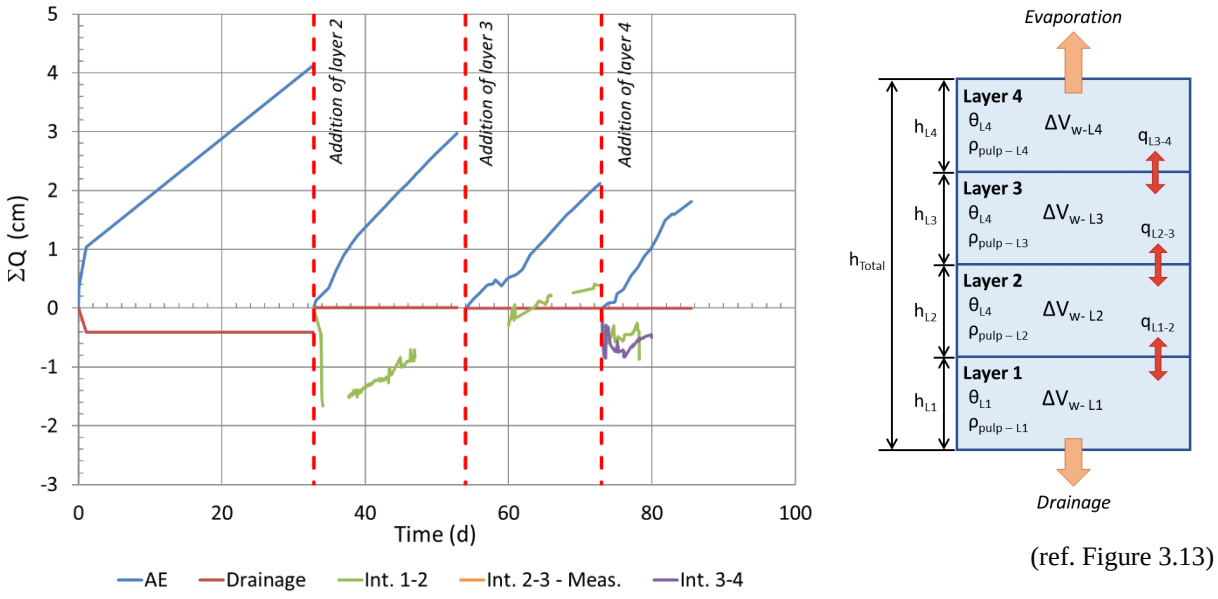

Figure 6.20: Calculated normalized interlayer flow in column Col-02.

6.2.6 Numerical simulations

The simulated and experimental column test Col-02 lasted 85 days. Cycle 1 (layer 1) was left exposed to the atmosphere for 33 days, and cycle 2 (layer 2) was exposed to the atmosphere for 20 days. Cycles (layers) 3 and 4 were exposed to the atmosphere for 19 and 13 days respectively.

Figure 6.21 below presents the flow calculated in the laboratory column, and the flow calculated in the numerical simulation. The overall behaviour of the numerical simulation represents the behaviour of the laboratory column. The evaporation rates are similar since the simulated potential evaporation corresponds to the measured evaporation in the laboratory. The drainage from the laboratory column was larger than from the numerical simulation (0.41 cm vs. 0.017 cm). There was also infiltration from a fresh layer to the partially saturated layer below in the hours after deposition for layers 2, 3 and 4 (negative slope in the curves in Figure 6.21). For example, approximately 2 cm of water flowed at the interface between the fresh (layer 2) and partially saturated (layer 1) tailings at the beginning of cycle 2. This was observed both in the laboratory model and in the numerical simulations. However, there was no more infiltration in the older layers 1 to 2 days after deposition of the fresh layer, and desaturation was only through evaporation.

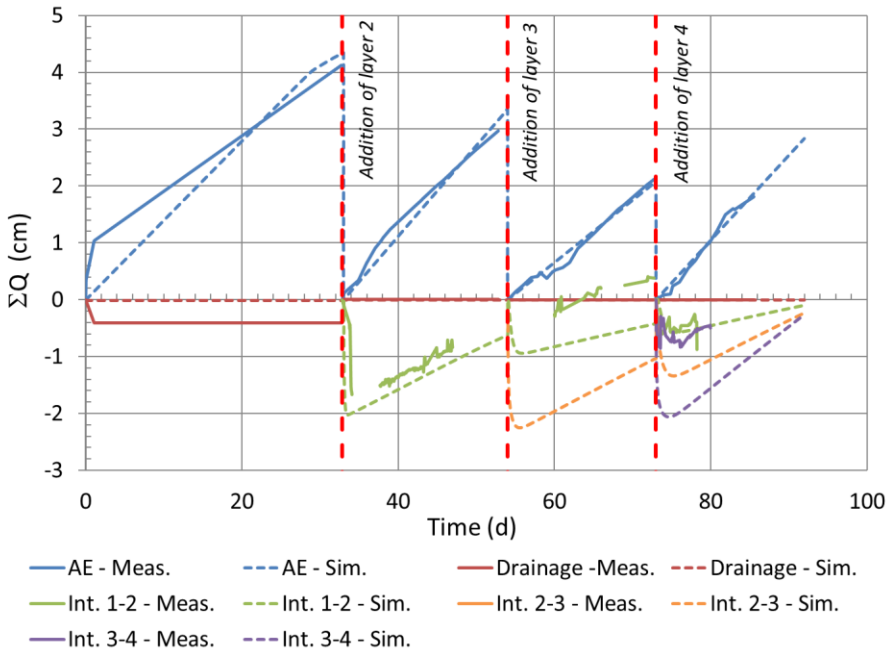

Figure 6.21: Measured and simulated normalized flow in column test Col-02.

The difference between the measured and simulated total outflow from the column was rather small (Figure 6.22). There is a decrease in the total flow as the number of layer increases. This is most probably associated with the decrease in the cycle time (e.g. layer 1 – 33 days, layer 2 – 20 days, layer 3 – 19 days, layer 4 – 13 days).

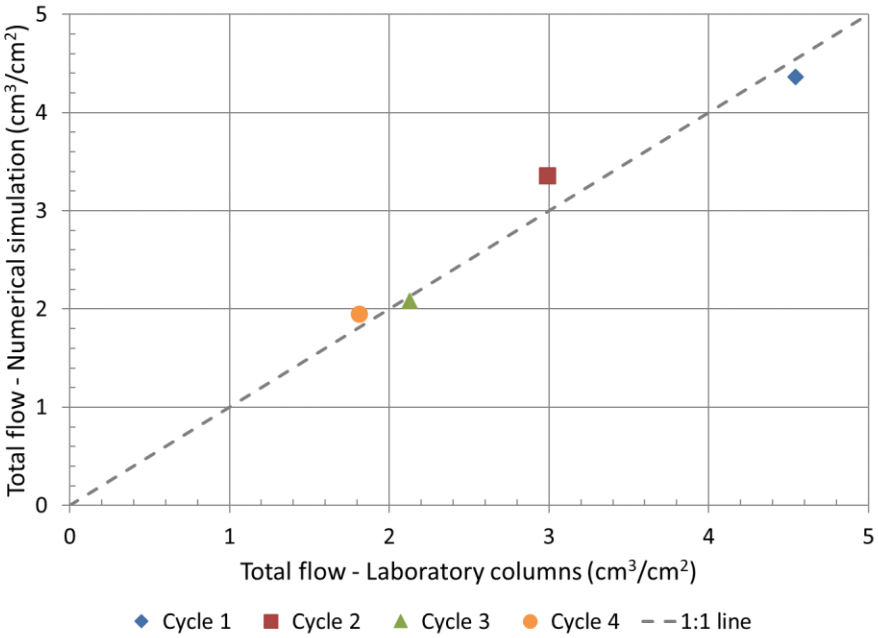

Figure 6.22: Total flow out of the laboratory column and numerical simulation for the four cycles.

Figure 6.23 presents the VWC in the middle of each layer for both the laboratory model and numerical simulation. The overall VWC trends are similar for the laboratory column and the numerical simulation, especially for the first 50 days of column test Col-02. The measured VWC in the surface layers (for cycles 1, 2 and 4; the laboratory results from cycle 3 could not be interpreted) is typically higher than in the simulated VWC. The VWC in layer 1 was similar for both the laboratory model and numerical simulation during cycle 2 (days 34 to 54). The volumetric water content in layer 2 from days 66 to 73 (during cycle 3) was also similar between the two models.

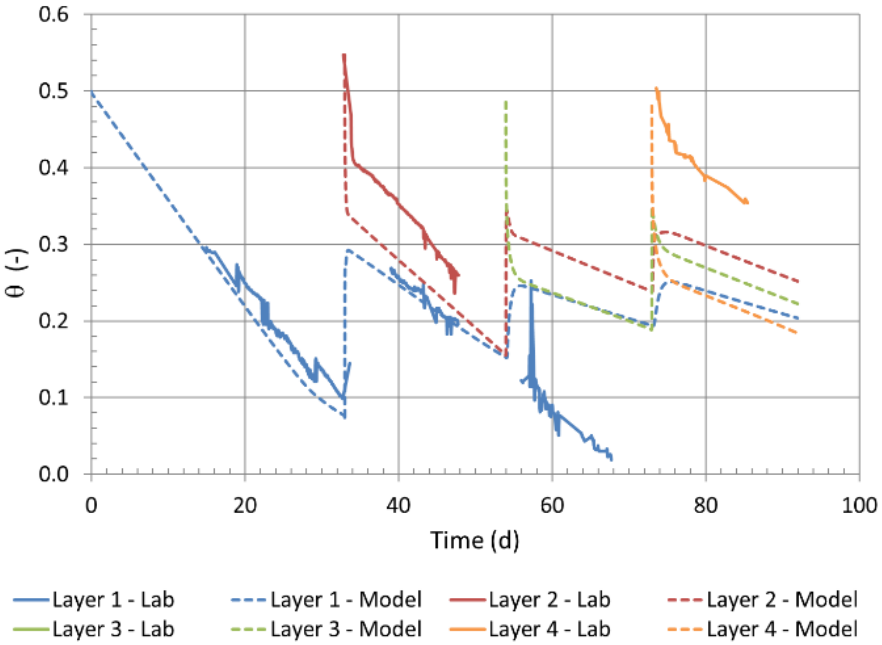

Figure 6.23: Measured and simulated volumetric water content (a) and suction (b) in column test Col-02.

The quick desaturation following the deposition of a fresh layer and rapid saturation of the layers below was observed both in the laboratory and in the numerical simulations. Furthermore, the variations in the volumetric water content become less noticeable in the deeper layers, as the number of layers increase in the column.

6.3 Multilayer (ML) column tests Col-03 and Col-04

Column tests Col-03 and Col-04 were composed of two 20 cm layers of Buly-07 tailings. The properties of the layers are presented in Section 3.4.2. The exposure time was 190 days for layer 1, and 108 days for layer 2.

6.3.1 Mass

The rate of change of the mass was similar for both columns (Figure 6.24). The longer duration of the cycles allowed to observe the decrease in the AE rate at the surface of the columns, especially during the second cycle, where a change in the AE rate was observed 40 days after placement of

the fresh layer (Figure 6.25b). The mass from the columns had to be extrapolated from days 35 to 160.

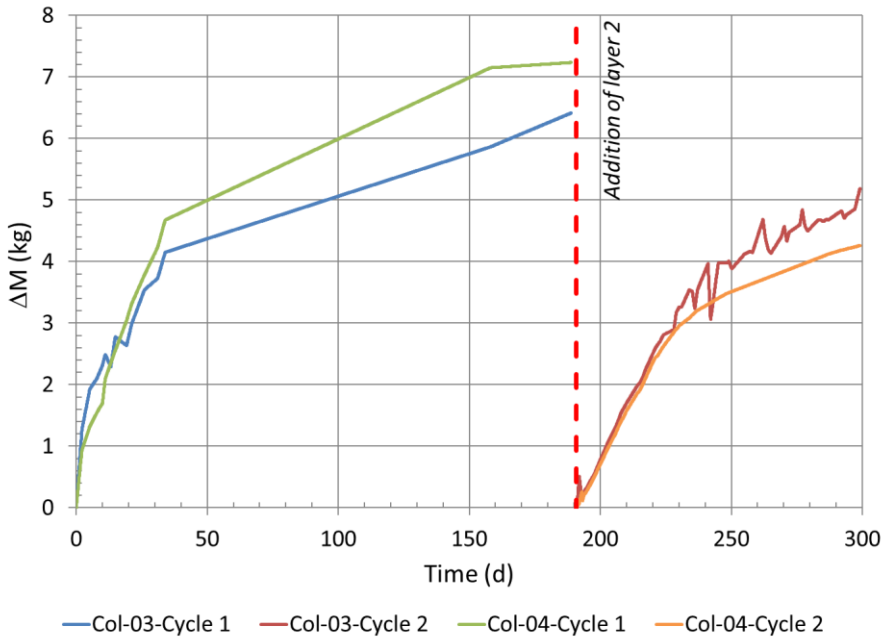

Figure 6.24: Evolution of the mass the column tests Col-03 and Col-04.

The total amount of water drainage for Col-03-L1 and Col-04-L1 was respectively 1.6 L and 1.4 L (Figure 6.25a). This is between 1.5 and 4.0 times more drainage than for the columns with thinner layers (Col-01 and Col-02).

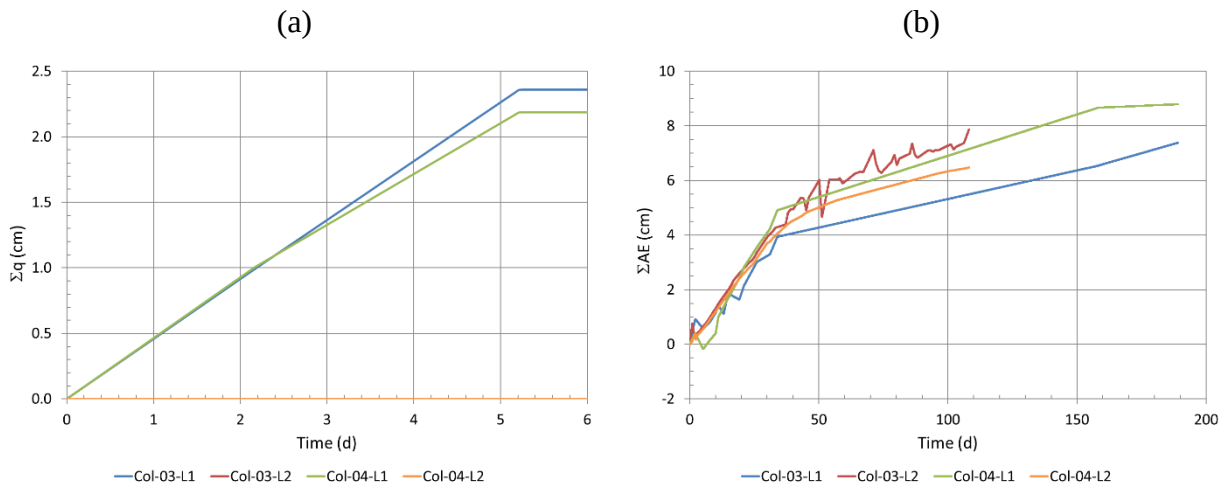

Figure 6.25: Total drainage (a) and actual evaporation (b) for columns Col-03 and Col-04.

Table 6.3 presents the rate of change of mass (through evaporation and/or drainage) for three stages during the column tests Col-03 and Col-04. During Stage 1, the loss of mass was mainly through drainage. This stage lasted 5.2 days for Col-03-L1 and 5.3 days for Col-04-L2. There was no drainage for Col-03-L2 and Col-04-L2. In Stage 2, loss of mass was only through evaporation and the rate varied between 1 mm/d and 2 mm/d (between 66 ml/d and 132 ml/d). These rates compare to the AE rate observed in Col-01 and Col-02. Finally, in the last stage, which happened roughly 40 days after the start of the tests, the evaporation rate decreased, and varied between 0.2 mm/d and 0.4 mm/d (13 ml/d and 26 ml/d). Stage 3 was observed when the degree of saturation (S_r) in the surface layer had decreased to a value of about 60%.

Table 6.3: Drainage and evaporation rate of the layers in Col-03 and Col-04.

Layer	Rate of change (g/d)	Rate of change (mm/d)	Cause
Col-03-L1	354.66	5.4	Drainage (primary) and evaporation (secondary)
Col-03-L1 (after drainage to day 35)	74.4	1.1	Evaporation
Col-03-L1 (residual)	14.23	0.2	Evaporation
Col-03-L2 (first 30 days)	83.79	1.3	Evaporation
Col-03-L2 (residual)	26.76	0.4	Evaporation
Col-04-L1	240.81	3.7	Drainage (primary) and evaporation (secondary)
Col-04-L1 (after drainage to day 35)	115.77	1.8	Evaporation
Col-04-L1 (residual)	18.12	0.3	Evaporation
Col-04-L2 (first 30 days)	81.54	1.2	Evaporation
Col-04-L2 (residual)	20.49	0.3	Evaporation

6.3.2 Geometric characteristics

Figure 6.26 presents the thickness (a) and change of thickness (b) in Col-03 and Col-04. The change in thickness was gradual for layer 1 and it became constant after approximately 12 days in both Col-03 and Col-04 (Figure 6.26). The presence of the partially dry tailings layer below accelerated the rate of change in thickness when the second layer was placed in Col-03 and Col-04.

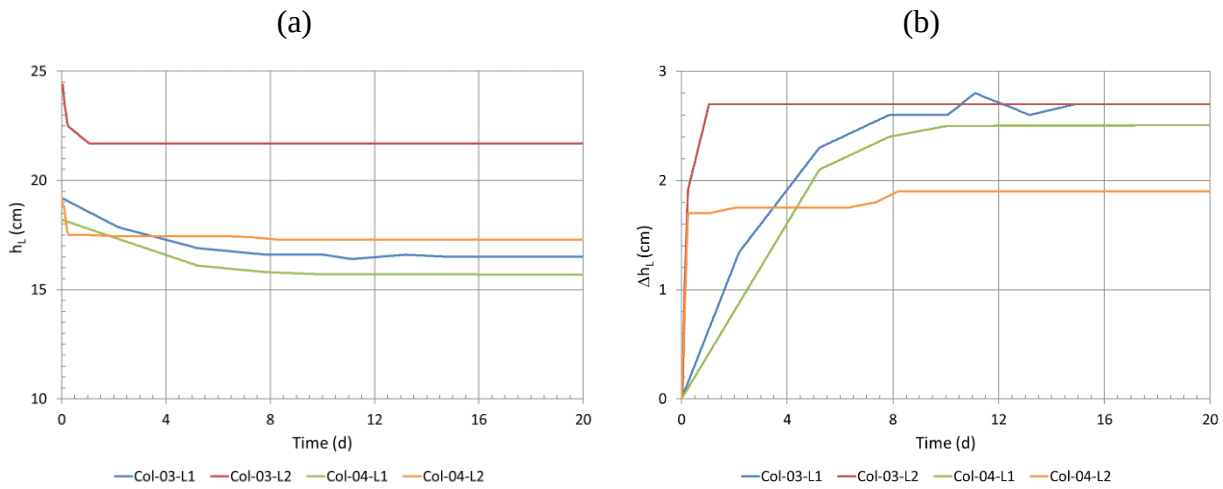

Figure 6.26: Total thickness (a) and change in thickness (b) for column tests Col-03 and Col-04.

6.3.3 Pore water pressure

Watermark suction sensors (Irrometer) were installed in the middle of the layers and one MPS-1 suction sensor by Decagon was also placed 5 cm above the bottom of Col-03. This sensor has a suction measurement range of 10 to 500 kPa, while the Watermark sensors have a range of 1 to 199 kPa.

The suction recorded with the MPS-1 sensor was much higher than for the other sensors (Figure 6.27). The Watermark sensors behaved similarly as was observed in ML column Col-02 and in the SL columns and did not record suction values greater than 50-60 kPa. The measured suction in the MPS-1 probe levelled at around 450 kPa as it was approaching the upper range of the sensor (500 kPa).

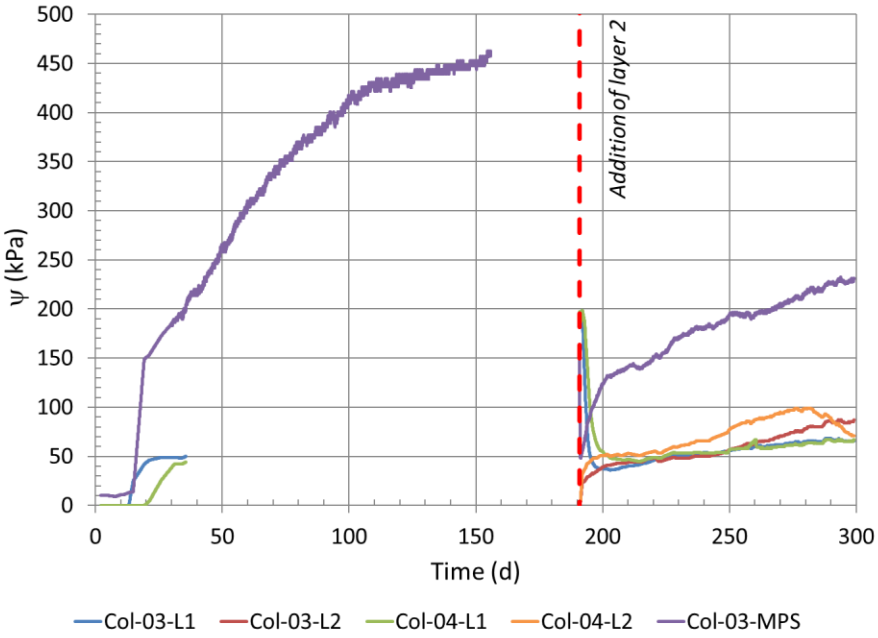

Figure 6.27: Suction with respect to time for the layers of columns Col-03 and Col-04.

Upon deposition of the second layer, the suction from the MPS-1 sensor decreased to roughly 50 kPa (quick infiltration of water into layer 1 following placement of layer 2) during cycle 2. It then increased to 130 kPa over a 10-day period. Subsequently, the curve leveled off. After 110 days of recording (data logger was removed), the suction at this point was 231 kPa (versus approximately 425 kPa after 110 days during cycle 1). The presence of layer 2 in the second cycle limited desaturation by evaporation from layer 1. The Watermark sensors in cycle 2 showed that within 30 days, the value from the sensors in the top and bottom layers converged to values located around 50 kPa (in both multilayer column tests, Col-03 and Col-04).

6.3.4 Volumetric water content

The volumetric water content in column tests Col-03 and Col-04 was measured with EC-5 sensors (Decagon). Sensors were calibrated specifically for Bulyanhulu tailings before the beginning of the tests. The sensors were placed horizontally in the middle of the fresh tailings layers. There was a decrease in the volumetric water content (and degree of saturation) starting at day 10 (Figure 6.28). This was also recorded (through an increase in suction) by the MPS-1 sensor in Col-03-L1 (Figure 6.27). For cycle 2, there was a resaturation of the bottom layer after deposition of the fresh tailings,

and the values decreased and tended to converge. The final VWC was between 0.21 and 0.24 (except Col-04-L1 which had a value of 0.15) at the end of cycle 2. Afterwards, the suction in the columns increased through drying by evaporation.

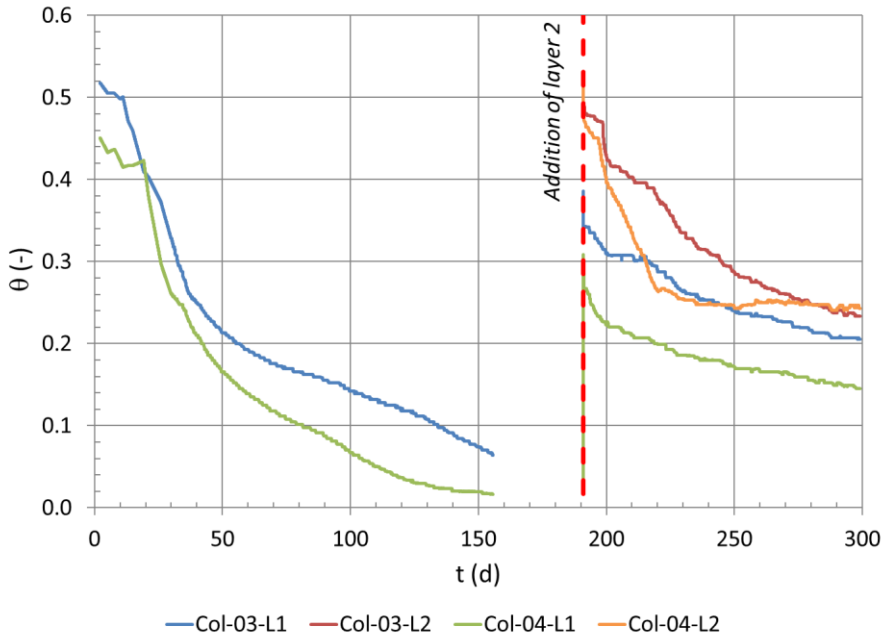

Figure 6.28: Volumetric water content of the layers of column tests Col-03 and Col-04.

The higher actual evaporation rate in Col-04-L1 (1.8 mm/d) compared to Col-03-L1 (1.1 mm/d) explained the lower volumetric water content in the former column test. The decrease in the rate of desaturation (in Col-03-L1 and Col-04-L1) that was observed around day 40 (Figure 6.28) was also associated with a decrease in the actual evaporation rate (Figure 6.25b and Table 6.3).

The two WRC of the tailings obtained with the Fredlund and Xing (1994) parameters (Table 4.6; a_{fx} = 247.87 kPa; n_{fx} = 0.84; m_{fx} = 2.67) were compared with the measured ψ vs. θ and ψ vs. S_r values (Figure 6.29). The air-entry value measured in the column with the MPS-1 was higher (145 kPa) than for the other curves (58 kPa). However, there is a similarity between the measured and theoretical curves. Some hysteresis is apparent between the first and second cycles of Col-03-L1. In addition, the values obtained with the Watermark sensors seem to show the AEV.

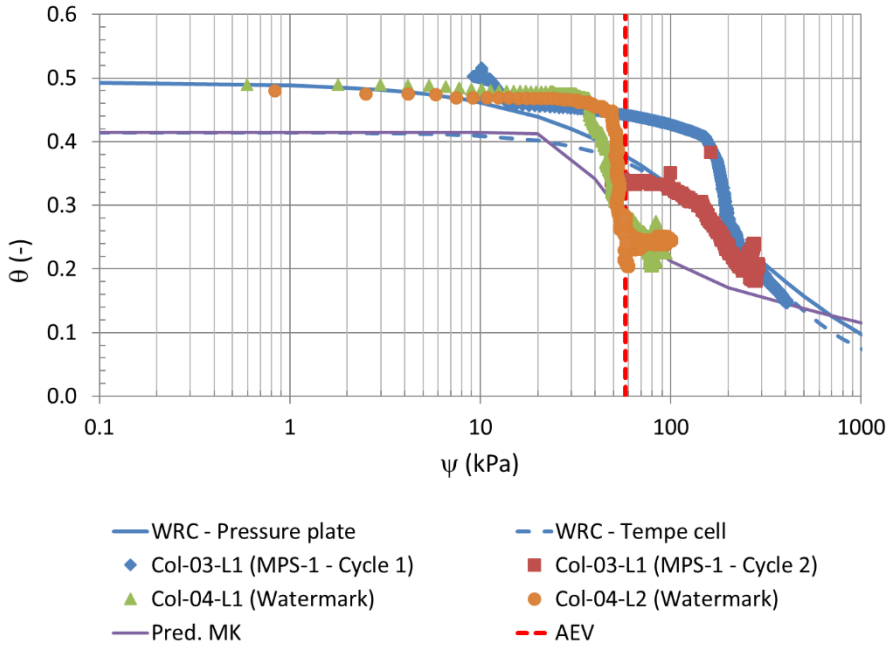

Figure 6.29: Measured VWC as a function of suction in columns Col-03 and Col-04 compared to the actual WRCs (obtained from the pressure plate extractor and Tempe cells) of the material.

6.3.5 Interlayer flow

The calculated interlayer flow for both columns indicate that about there was about 2 cm of water that infiltrated into layer 1 after the deposition of layer 2 (Figure 6.30). However, there was no water that drained from the bottom of the column: all the water that infiltrated from layer 2 remained in layer 1. After 12 (Col-03) or 22 (Col-04) days, there was a reversal of the gradient and the water in layer 1 was transported by evaporation into layer 2. Eventually, all the water from the fresh tailings layer was evaporated back into layer 2.

The total calculated inter-layer flow in column tests Col-03 and Col-04 also demonstrate that the presence of a desaturated layer would increase the drainage rate in a fresh paste tailings layer (Figure 6.30). Drainage from the bottom of the columns (Col-03 and Col-04) stopped 6 days after deposition of layer 1. The evaporation rate decreased in cycle 2 30 to 40 days after disposal of the paste tailings in the column.

(a) Col-03 (b) Col-04

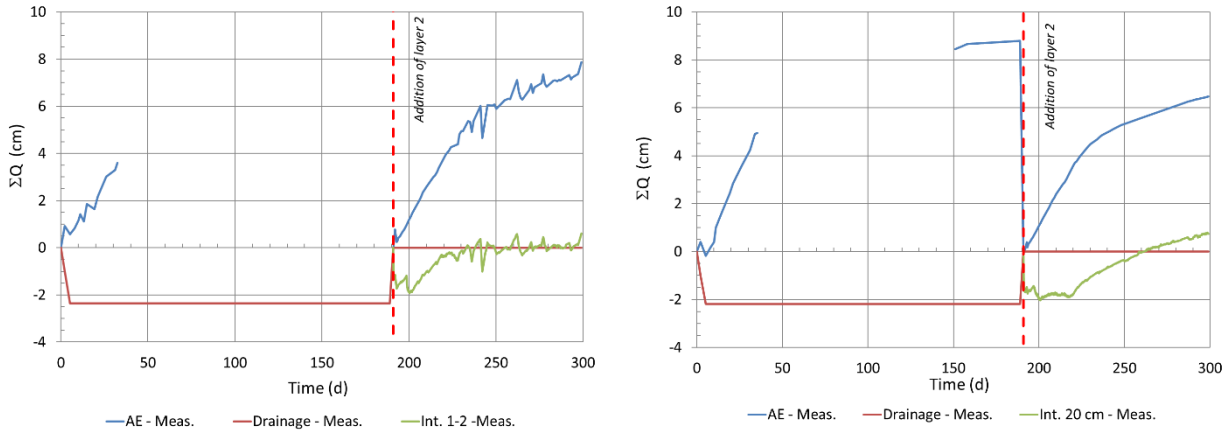

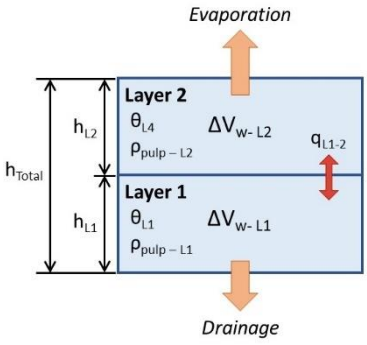

(ref. Figure 3.13)

Figure 6.30: Calculated interlayer flow in columns (a) Col-03 and (b) Col-04.

6.3.6 Numerical simulations of tests Col-03 and Col-04

Column test Col-03 and Col-04 were composed of two 20 cm layers. The first cycle was 190 days and the second lasted 110 days.

The simulated drainage was smaller than the measured drainage. It was 0.07 cm in the numerical simulation vs. 2.4 cm measured in the laboratory for Col-03, and 2.19 cm in the laboratory vs. 0.07 cm in the numerical simulation for Col-04 (Figure 6.31). The actual evaporation rate was reproduced accurately in the numerical simulations, especially in cycle 2 of the simulation of Col-03. The PE evaporation was fixed at 1.3 mm/d (Col-03) and 1.2 mm/d (Col-04) in the numerical simulations for the duration of the cycles, and the AE was calculated with the software. The

measured and simulated total flow for the two cycles of column tests Col-03 and Col-04 are similar (Figure 6.32).

(a) Col-03 (b) Col-04

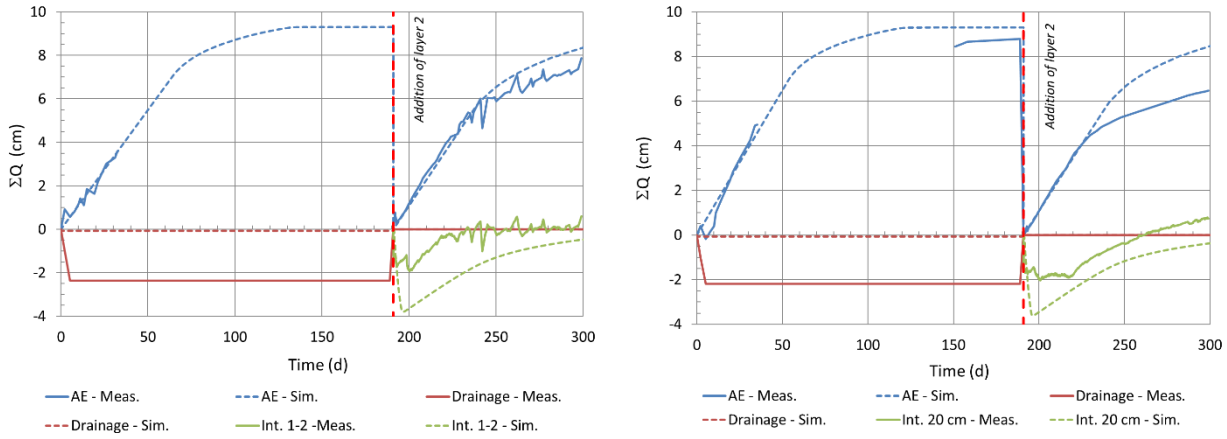

Figure 6.31: Total outflow measured from the laboratory columns (a – Col-03; b – Col-04) and given by numerical simulations for the two cycles.

(a) Col-03 (b) Col-04

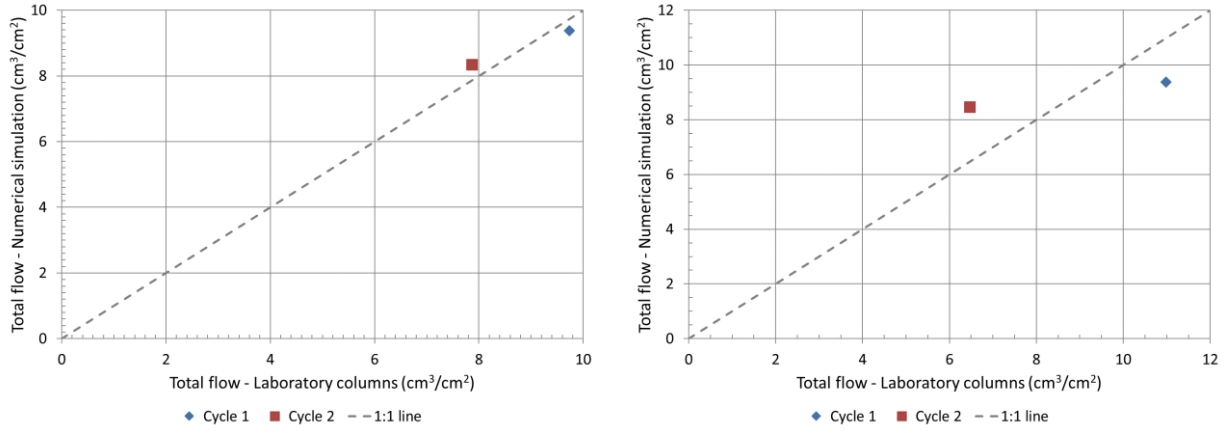

Figure 6.32: Measured and simulated flow in columns Col-03 (a) and Col-04 (b).

The comparison between the measured and simulated volumetric water content and suction is presented in Figure 6.33. The laboratory results present values measured at 10 cm (layer 1) and 30 cm (layer 2) form the bottom of the laboratory model. The behaviour observed in Figure 6.33 is similar to the comparison between the measured and simulated VWC for columns Col-01 and Col-02: the behaviour of the first cycle is well simulated but the simulated desaturation in the second cycle is much faster than the laboratory measurements. The initial suction at the interface between the fresh and the desaturated layers at the beginning of the second cycle was around 3500 kPa. This simulated a strong downwards gradient at the beginning of cycle 2 ($i \approx -1 \times 10^4$).

(a) Col-03 (b) Col-04

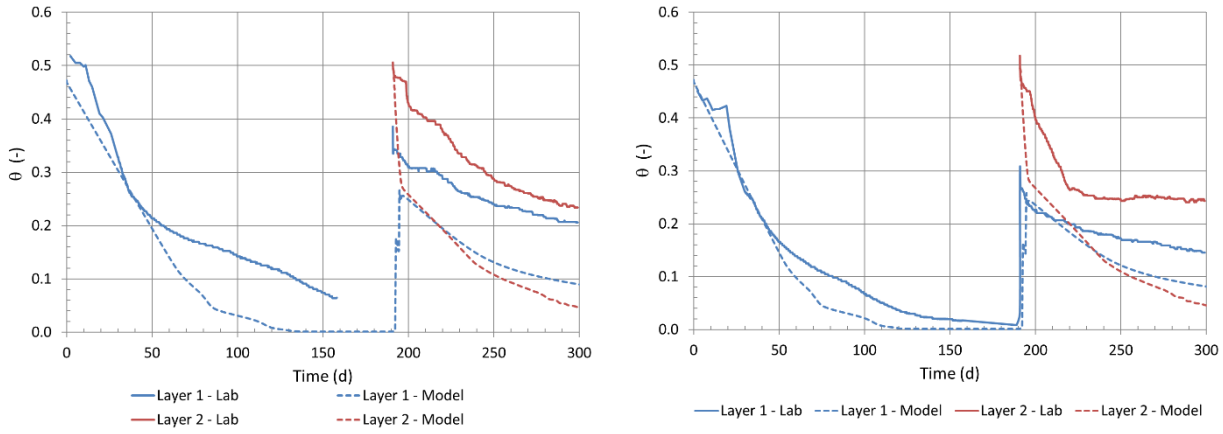

Figure 6.33: Measured and simulated volumetric water content in columns Col-03 (a) and Col-04 (b).

The measured volumetric water content was higher, and the measured suction was lower than the simulated values, but the overall behaviour of the columns could be reproduced using numerical simulations with Vadose/W. This is consistent with the observations made in the other columns (Column-01 – Section 6.1 and Column-02 – Section 6.2).

6.4 Oxygen consumption and diffusion in columns

The oxygen diffusion coefficient (D_e) and reaction rate coefficient (K_r), included in the modified Fick's 2nd law (Equation 2.35; Mbonimpa et al., 2003, 2011), were assessed during column test Col-02. The experimental procedure was fairly similar to that of the modified oxygen consumption (MOC) tests carried out in the field (Section 3.3), but on a smaller scale.

The laboratory tests were performed at various times (and degrees of saturation) following the deposition of each fresh tailings layer in the column for test Col-02, in part to assess the influence of the degree of saturation (S_r) on the oxygen flux and related diffusion and reaction rate coefficients (D_e and K_r). The main conditions for these tests are given in Table 6.4.

The oxygen consumption test cell was initially closed and sealed. The evaporation from the tested section was significantly reduced, but it was assumed that the degree of saturation in the surface layer of the column remained constant during the MOC test, which lasted less than 2 hours. The degree of saturation varied from 100% to about 25% between the seventeen MOC tests carried out on the four tailings layers during testCol-02.

Table 6.4: Degree of saturation (S_r) of the tailings at the beginning of each modified oxygen consumption (MOC) tests in Col-02.

Test #	Layer 1		Layer 2		Layer 3		Layer 4	
	S_r (-)	Time (min)	S_r (-)	Time (min)	S_r (-)	Time (min)	S_r (-)	Time (min)
1	99.6%	63	92.0%	178	85.4%	299	88.4%	438
2	25.3%	136	80.4%	35	73.9%	403	80.0%	360
3			56.1%	106	63.7%	343	76.0%	369
4			53.6%	56			73.6%	379
5							64.4%	208
6							57.5%	259
7							46.0%	232
8							41.4%	218

The variation of the oxygen concentration during the test period was sometimes too small to obtain a relevant value for D_e and K_r; this was especially the case when the degree of saturation $S_r > 80\%$ (theoretical value $D_e < 10^{-3}$ m^2/d, Aachib et al., 2004). The variation of oxygen concentration should be at least 2 to 3% to determine D_e and K_r (Mbonimpa et al., 2011; Dagenais et al., 2012).

(a) Col-02-L1

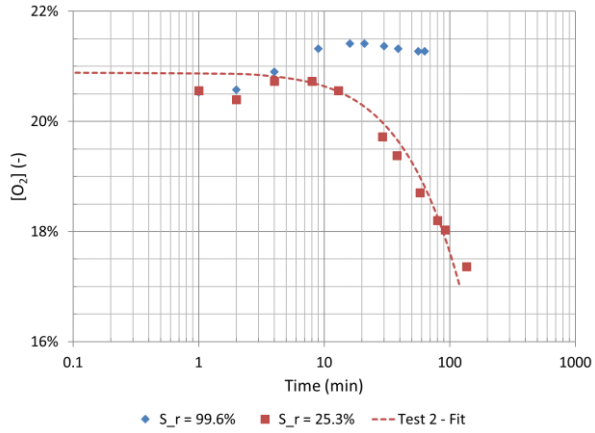

(b) Col-02-L2

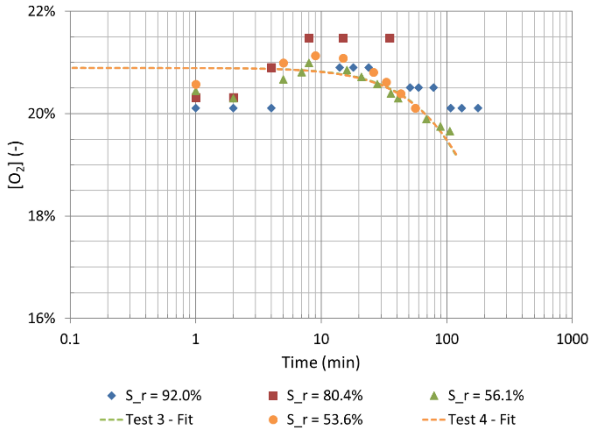

(c) Col-02-L3

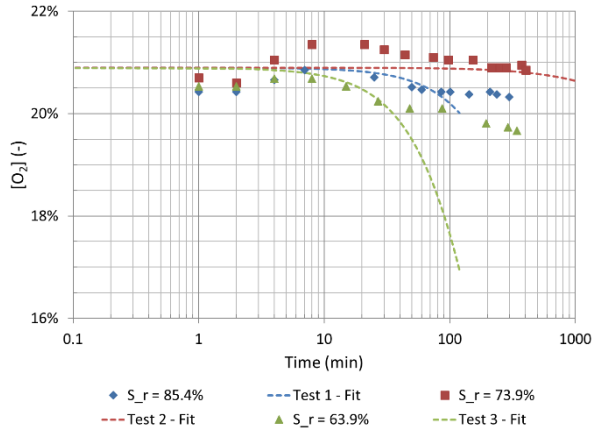

(d) Col-02-L4 (Tests 1 to 4)

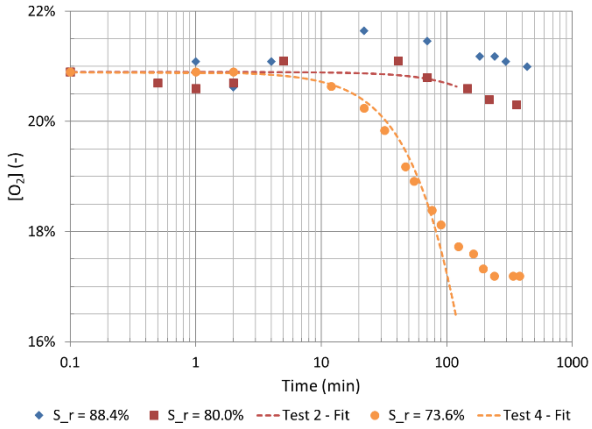

(e) Col-02-L4 (Tests 5 to 8)

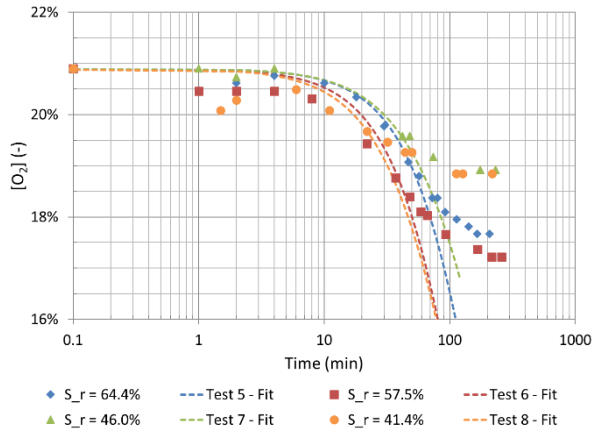

Figure 6.34: Oxygen concentration measured during the modified oxygen consumption (MOC) tests on the exposed tailings during column test Col-02.

The oxygen diffusion coefficient (D_e) estimated from the MOC tests (and using Vadose/W) can be compared to the predicted value calculated with Aachib et al. (2004) model (Equation 2.34) (Figure 6.35). The results indicate that the value of D_e increases as the value of S_r decreases.

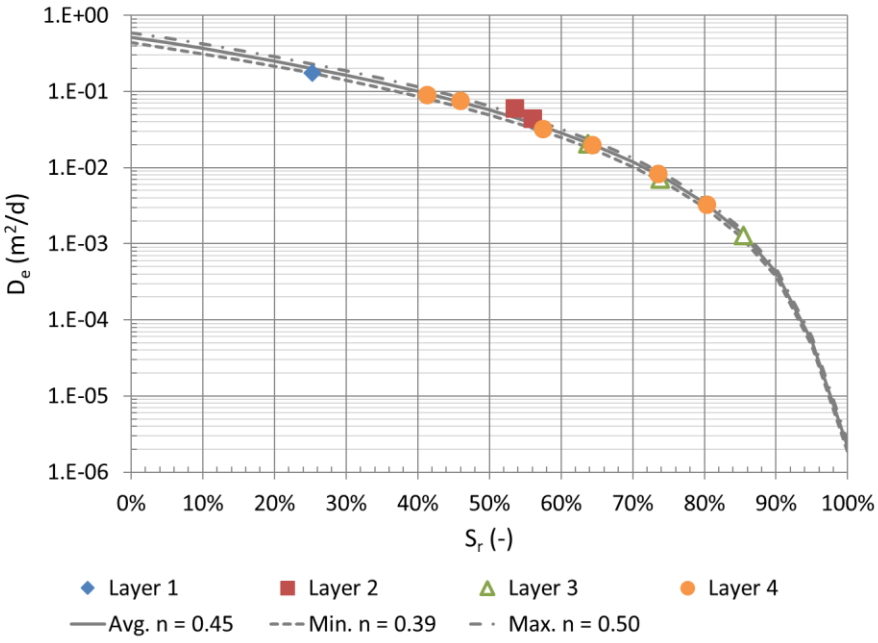

Figure 6.35: Oxygen diffusion coefficient (D_e), as a function of degree of saturation (S_r), obtained from the numerical interpretation of the modified oxygen consumption tests on tailings during column test Col-02; the relationship given by the Aachib et al. (2004) model is also shown (lines).

The oxygen reaction rate coefficient (K_r) as a function of the degree of saturation (S_r) obtained from the simulations with Vadose/W is also compared with the Collin (1987) model (Equation 2.37; $K_r = 2.5\ d^{-1} = 899\ y^{-1}$) (Figure 6.36). For most tests, K_r is about 500 y^{-1} (1.4 d^{-1}). The test results with the highest degree of saturation (S_r = 80.4%) analysed with Vadose/W (tailings Layer 2, Test 2) gives a value K_r equal to 10 y^{-1} (0.03 d^{-1}). It is fairly common for the Collin (1987) model to overestimate the K_r (Gosselin, 2007; Pabst et al., 2014; Toussaint, 2016), when the value of K' (in Equation 2.37) is set as a constant (which may not be the case in practice).

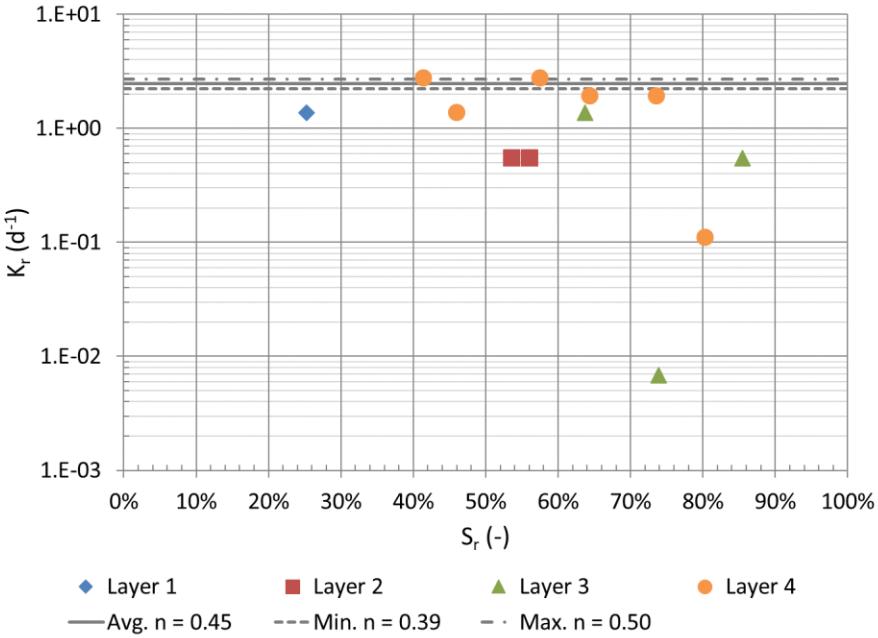

Figure 6.36: Oxygen reaction rate coefficient (K_r) as a function of degree of saturation (S_r) for the modified oxygen consumption tests in column test Col-02.

The MOC tests completed during column test Col-02 indicate that the oxygen diffusion coefficient (D_e) increases as the S_r of the tailings layer decreased. The oxygen flux (F_{O_2}) obtained from the measurements during the MOC tests, as a function of the degree of saturation (column test Col-02) can be compared with the flux calculated with Equation 2.39 (Figure 6.37). The latter ("theoretical" or predicted) flux varies between 0.3 g⁄m^{2}d and 136 g⁄m^{2}d.

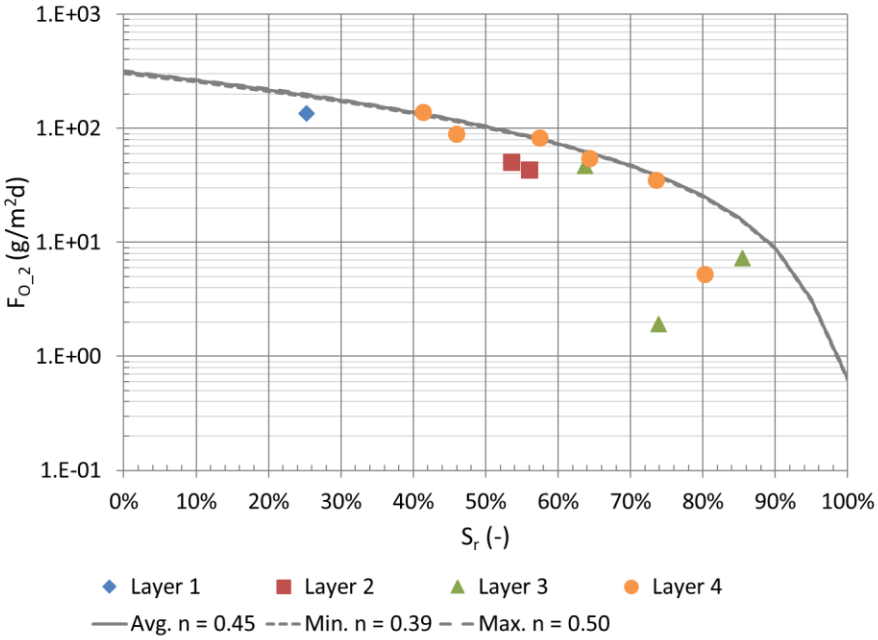

Figure 6.37: Calculated and predicted (Equation 2.39) steady-state oxygen flux (F_{O_2}) as a function of degree of saturation (S_r) for the modified oxygen consumption tests in multilayer (ML) column test Col-02.

6.5 Evolution of the volume of paste tailings

The void ratio at the beginning of each column test ($e = V_v/V_s$) was estimated by measuring the diameter, the thickness, total mass, and the water content of each layer. A change in volume (settlement due to drainage or shrinkage) during the test can directly be associated with a decrease in the void ratio of the tailings (for each layer):

$$e_T = e_{T-1} - \frac{\Delta V_v}{V_s} \tag{6.1}$$

where e_T = Void ratio at time t (-);

e_{T-1} = Void ratio at the previous time t-1 (-);

ΔV_v = Change in void volume between times t-1 and t [L^3]. It corresponds to the change in the volume of the layer during the period studied.

V_s = Volume of solids (calculated at the beginning of the column tests with $V_s = M_s/(D_r \times \rho_w)$).

The void ratio (e) was also calculated for each layer for the ML column tests using the volumetric equations (Section 3.4.2). The initial void ratio ($e_{initial}$) corresponds to the value calculated using the gravimetric water content obtained by oven drying (Table 3.9). The final void ratio (e_{final}) of each layer in ML column tests was evaluated by measuring the dimensions of the drying tailings layer and using Equation 6.1. The final void ratio (e_{final}) was compared with the initial void ratio ($e_{initial}$) of the layers placed in the four tailings columns (Figure 6.38). The initial void ratio (determined by oven drying) was between 0.9-1.2 and the final void ratio was between 0.5-1.0. The results obtained from the ML column tests shown in Figure 6.38 indicate that a higher initial void ratio (or water content) typically leads to a higher final void ratio of the material (also observed by Saleh-Mbemba, 2010).

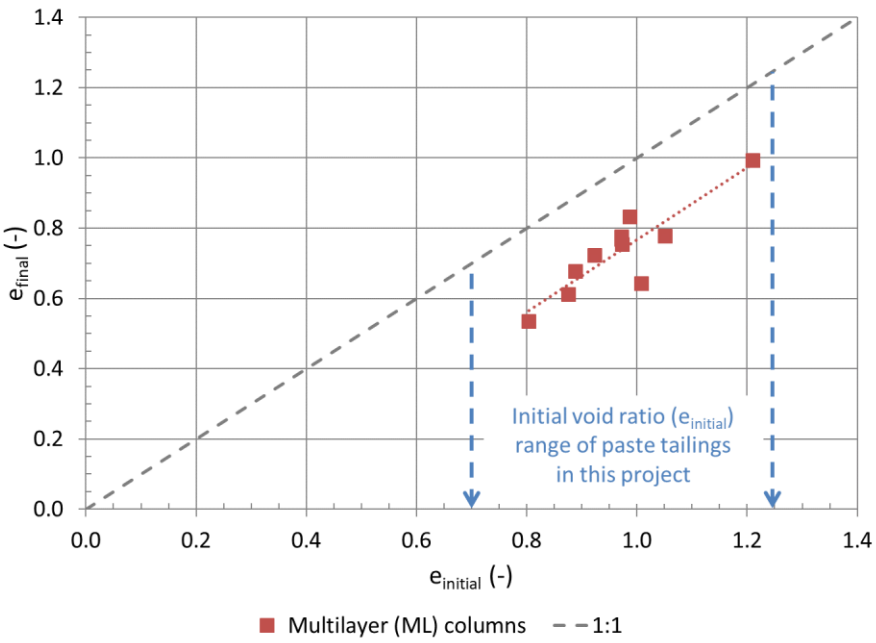

Figure 6.38: Final void ratio with respect to initial void ratio in each layer of the columns.

Figure 6.39 presents the relationship between the actual evaporation (AE) rate on the relative change in the void ratio ($\Delta e/e_{initial}$) for the layers placed in columns for the SL and ML laboratory tests. It appears that a greater AE rate may yield a larger change in the void ratio for the tailings

layer placed in the multilayer columns (tests Col-01 to Col-04) (i.e. a higher drying rate tends to produce a smaller void ratio).

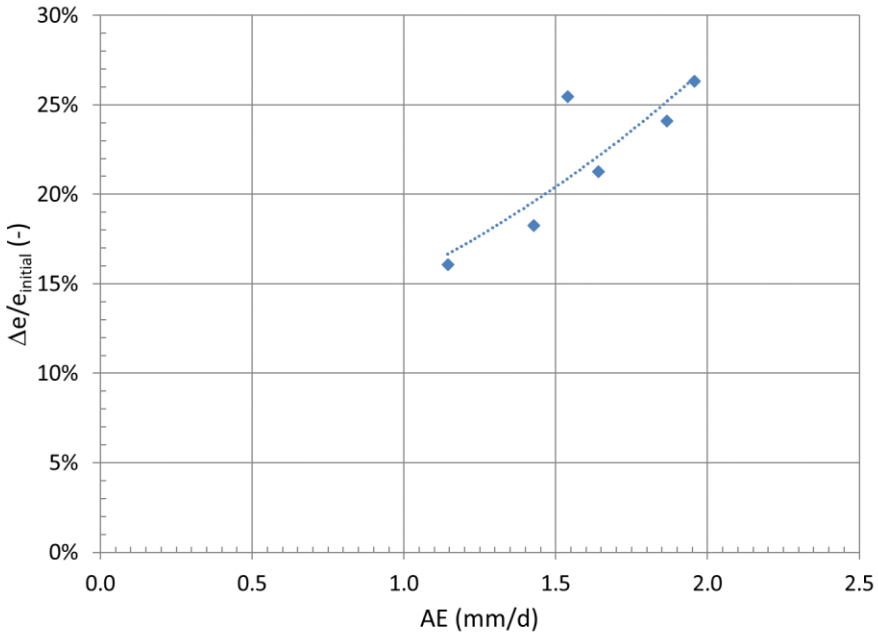

Figure 6.39: Relationship between the relative change in void ratio ($\Delta e/e_{initial}$) and actual evaporation rate (AE) for the surface tailings layers during the column tests.

The laboratory results of the multilayer columns helped understand the movement of water in a 1D tailings column with multiple layers of varying water contents. Vadose/W was used to represent these columns and to offer more insight on their hydrogeological behaviour. In the upcoming chapter, the numerical simulations are extrapolated to 1D field numerical simulations that will be done to evaluate the impact of certain parameters (e.g. layer thickness, climate, tailings hydrogeological properties) on the water movement in a paste tailings stack.

CHAPTER 7 SIMULATIONS OF FIELD CONDITIONS

The numerical simulations of the column tests (Chapters 5 and 6) represent well the behaviour of tailings during the column tests at a laboratory scale. This preliminary validation suggest that numerical models can be used to evaluate how various characteristics would influence the hydrogeological behaviour of (paste) tailings in the field (for different conditions). The effect of layer thickness, deposition rate, tailings hydrogeological properties, subsoil properties, water table position and climatic conditions are specifically assessed in the series of simulations presented below (see Section 7.2 and Table 7.1). The main aspects considered can be summarized as follows:

- Deposition characteristics:
    - Deposition rate and layer thickness: between 0.5 m and 12 m (baseline model: 2 m). The final thickness of the tailings stack is 12 m in every model, with a total deposition time of 360 days.
    - Time between the deposition of two fresh layers: between 30 and 120 days (baseline model: 60 days).
- Material hydrogeological properties:
    - Tailings properties (e.g. porosity, water retention curve and hydraulic conductivity) can vary with the actual field conditions and characteristics of the mining operation. Tailings from the Bulyanhulu mine (Section 4.3) and from two mines located in the province of Quebec are considered here: Osisko tailings from the Canadian Malartic mine (Narvaez, 2013, Bolduc and Aubertin, 2014) are slightly finer than Bulyanhulu tailings; Goldex tailings (Pabst, 2011) are somewhat coarser.
    - The hydrogeological properties of the subsoil can influence drainage from the tailings stack. A sandy subsoil is used in the base case and the effect of a clayey subsoil is assessed (Beit Netofa clay – van Genuchten, 1980, with a saturated hydraulic conductivity of 1×10^{-8} m/s).
- The position of the water table can also influence the hydrogeological properties and pressure distribution in the underlying soil (i.e. a deeper water table results in a higher suction at the surface at equilibrium). Water table depths between 0 m and 12 m (from the subsoil surface) are simulated (baseline model: 12 m).

- Climatic conditions, which may have a major impact of the system response:
    - Five fixed potential evaporation (PE) rates are considered: 0.5 mm/d, 1 mm/d, 2 mm/d, 5 mm/d and 10 mm/d.
    - Four sets of climatic conditions (defined using the Köppen classification system – Oliver, 2005) are simulated and compared to Bulyanhulu monthly average climatic conditions:
        - Goldstrike (Eureka County, Nevada, USA): Cold arid steppe climate (BSk) (Zhan, 2003).
        - Kalgoorlie (Western Australia): Hot arid steppe climate (BSh) (Australian Bureau of Meteorology http://www.bom.gov.au/).
        - Porgera (Enga Province, Papua New Guinea): Tropical rainforest climate (Af) (Weather Base http://www.weatherbase.com/).
        - Val-d'Or (Quebec, Canada): Continental humid climate (Dfi) (Environment Canada).

The objective of the parametric study was to evaluate the effect of these various factors and assess how these could influence planning and optimisation of paste tailings deposition on the surface . Since paste tailings contain less pore water than traditional slurry tailings, they may become unsaturated more rapidly. If the tailings can generate contaminated mine drainage (AMD or CND; Section 2.1), a sufficiently high degree of saturation must be maintained to limit the generation of contaminated drainage (e.g. S_r > 85%-90%); otherwise, drainage of potentially contaminated pore water from the tailings must be controlled.

Numerical models are used to simulate a tailings storage facility consisting of successive layers of fresh (paste) tailings deposited at regular time intervals. The same approach is used for all the simulations presented in this chapter. The first layer of paste tailings is deposited directly on the surface of a homogeneous subsoil. It is then left to dry through drainage and evaporation. The water table (u = 0 kPa boundary conditions) is usually a located 12 m below the soil surface (Figure 7.1). The subsequent fresh layers of tailings are deposited on the previous ones, which may be partially saturated. The thickness and exposure time for each layer varies with the model. The final thickness of the tailings is always 12 meters in the simulations, which corresponded to the final design height

of the Bulyanhulu mine paste TSF (Golder, 2005). Climatic conditions are applied at the surface of the models.

Long-term simulations are carried out in 1D, which is deemed to be representative of paste tailings deposited on the surface with a small slope (< 5%). The model is 1 m wide and 1 m deep (out-of-plane direction), and its height (thickness) increased with deposition. The finite elements in the 1D model are rectangular (5 cm × 50 cm) (Figure 7.1). Excess water at the surface of the models can runoff (no ponding allowed in the 1D Vadose/W simulation).

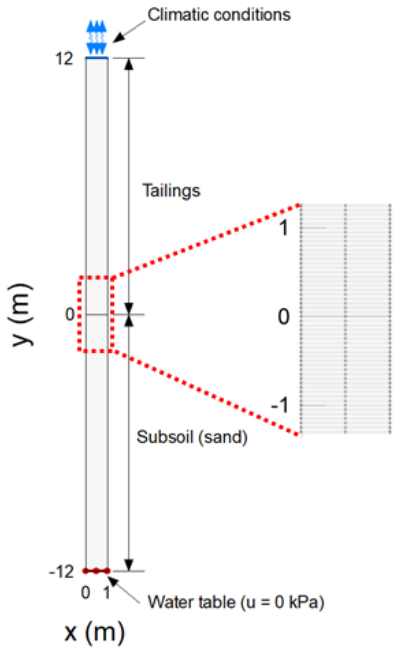

Figure 7.1: Sketch of the 1D model to simulate field conditions; mesh, and surface and bottom boundary conditions are shown.

Convergence parameters in the simulations were presented in Section 3.11. Adaptive time-stepping was used to improve convergence. Water balance is calculated at each time step to confirm that the models converged (Section 7.1).

A total of twenty-eight numerical simulations were carried out for this part of the study (Table 7.1). A typical simulation would require between 2 and 3 days of computing time.

Table 7.1: Numerical simulations conduct to assess the effect of various influence factors related to field conditions. Variations from baseline (reference) model are shown in grey.

#	Identification	Layer thickness (m)	Time between layers (days)	Type of tailings	Subsoil	Water table position (m)	Climatic conditions	Initial pore pressure conditions
1	Annual (Baseline)	2	60	Buly. (Fresh and consol.)	Sand	-12 m	Buly. annual	Hydrostatic
2	Monthly	2	60	Buly. (Fresh and consol.)	Sand	-12 m	Buly. monthly	Hydrostatic
3	Daily	2	60	Buly. (Fresh and consol.)	Sand	-12 m	Buly. daily data (2000 – 2005)	Hydrostatic
4	50 cm	0.5	15	Buly. (Fresh and consol.)	Sand	-12 m	Buly. annual	Hydrostatic
5	1 m	1	30	Buly. (Fresh and consol.)	Sand	-12 m	Buly. annual	Hydrostatic
6	1.5 m	1.5	45	Buly. (Fresh and consol.)	Sand	-12 m	Buly. annual	Hydrostatic

Table 7.1 (continued): Numerical simulations conduct to assess the effect of various influence factors related to field conditions. Variations from baseline (reference) model are shown in grey.

#	Identification	Layer thickness (m)	Time between layers (days)	Type of tailings	Subsoil	Water table position (m)	Climatic conditions	Initial pore pressure conditions
7	6 m	6	180	Buly. (Fresh and consol.)	Sand	-12 m	Buly. annual	Hydrostatic
8	12 m	12	360	Buly. (Fresh and consol.)	Sand	-12 m	Buly. annual	Hydrostatic
9	30 days (Half time)	2	30	Buly. (Fresh and consol.)	Sand	-12 m	Buly. annual	Hydrostatic
10	120 days (Double time)	2	120	Buly. (Fresh and consol.)	Sand	-12 m	Buly. annual	Hydrostatic
11	Consolidated	2	60	Buly. consol. tailings	Sand	-12 m	Buly. annual	Hydrostatic
12	Osisko	2	60	Osisko (Canadian Malartic)	Sand	-12 m	Buly. annual	Hydrostatic

Table 7.1 (continued): Numerical simulations conduct to assess the effect of various influence factors related to field conditions. Variations from baseline (reference) model are shown in grey.

#	Identification	Layer thickness (m)	Time between layers (days)	Type of tailings	Subsoil	Water table position (m)	Climatic conditions	Initial pore pressure conditions
13	Goldex	2	60	Goldex	Sand	-12 m	Buly. annual	Hydrostatic
14	Clay	2	60	Buly. (Fresh and consol.)	Beit Netofa clay	-12 m	Buly. annual	Hydrostatic
15	WT @ -6 m	2	60	Buly. (Fresh and consol.)	Sand	-6 m	Buly. annual	Hydrostatic
16	WT @ -3 m	2	60	Buly. (Fresh and consol.)	Sand	-3 m	Buly. annual	Hydrostatic
17	WT @ -2 m	2	60	Buly. (Fresh and consol.)	Sand	-2 m	Buly. annual	Hydrostatic
18	WT @ -1 m	2	60	Buly. (Fresh and consol.)	Sand	-1 m	Buly. annual	Hydrostatic

Table 7.1 (continued): Numerical simulations conduct to assess the effect of various influence factors related to field conditions. Variations from baseline (reference) model are shown in grey.

#	Identification	Layer thickness (m)	Time between layers (days)	Type of tailings	Subsoil	Water table position (m)	Climatic conditions	Initial pore pressure conditions
19	WT @ 0 m	2	60	Buly. (Fresh and consol.)	Sand	0 m	Buly. annual	Hydrostatic
20	PE = 0.5 mm/d	2	60	Buly. (Fresh and consol.)	Sand	-12 m	Buly. Annual (PE = 0.5 mm/d)	Hydrostatic
21	PE = 1 mm/d	2	60	Buly. (Fresh and consol.)	Sand	-12 m	Buly. Annual (PE = 1 mm/d)	Hydrostatic
22	PE = 2 mm/d	2	60	Buly. (Fresh and consol.)	Sand	-12 m	Buly. Annual (PE = 2 mm/d)	Hydrostatic
23	PE = 5 mm/d	2	60	Buly. (Fresh and consol.)	Sand	-12 m	Buly. Annual (PE = 5 mm/d)	Hydrostatic
24	PE = 10 mm/d	2	60	Buly. (Fresh and consol.)	Sand	-12 m	Buly. Annual (PE = 10 mm/d)	Hydrostatic

Table 7.1 (continued): Numerical simulations conduct to assess the effect of various influence factors related to field conditions. Variations from baseline (reference) model are shown in grey.

#	Identification	Layer thickness (m)	Time between layers (days)	Type of tailings	Subsoil	Water table position (m)	Climatic conditions	Initial pore pressure conditions
25	Goldstrike	2	60	Buly. (Fresh and consol.)	Sand	-12 m	Goldstrike monthly	Hydrostatic
26	Kalgoorlie	2	60	Buly. (Fresh and consol.)	Sand	-12 m	Kalgoorlie monthly	Hydrostatic
27	Porgera	2	60	Buly. (Fresh and consol.)	Sand	-12 m	Porgera monthly	Hydrostatic
28	Val-d'Or	2	60	Buly. (Fresh and consol.)	Sand	-12 m	Val-d'Or monthly	Hydrostatic

7.1 Baseline model

The objective of the baseline model is to simulate the hydrogeological behaviour of Bulyanhulu TSF under representative field conditions. Drainage from the tailings to the underlying soil and water table, which could be critical in the case of AMD or CND generating tailings, is also assessed.

7.1.1 Model geometry and characteristics

The baseline model consists of six successive 2-m thick layers of tailings (Figure 7.2). Each layer is deposited instantaneously in the simulations and left to rest (with drainage and evaporation) for 60 days before adding the next layer. Settlement is not accounted for in the simulations in unsaturated conditions conducted with Vadose/W. After the final layer was disposed of, the hydrogeological behaviour of the stack is simulated for 5 additional years (1825 days) using climatic conditions representative of the site.

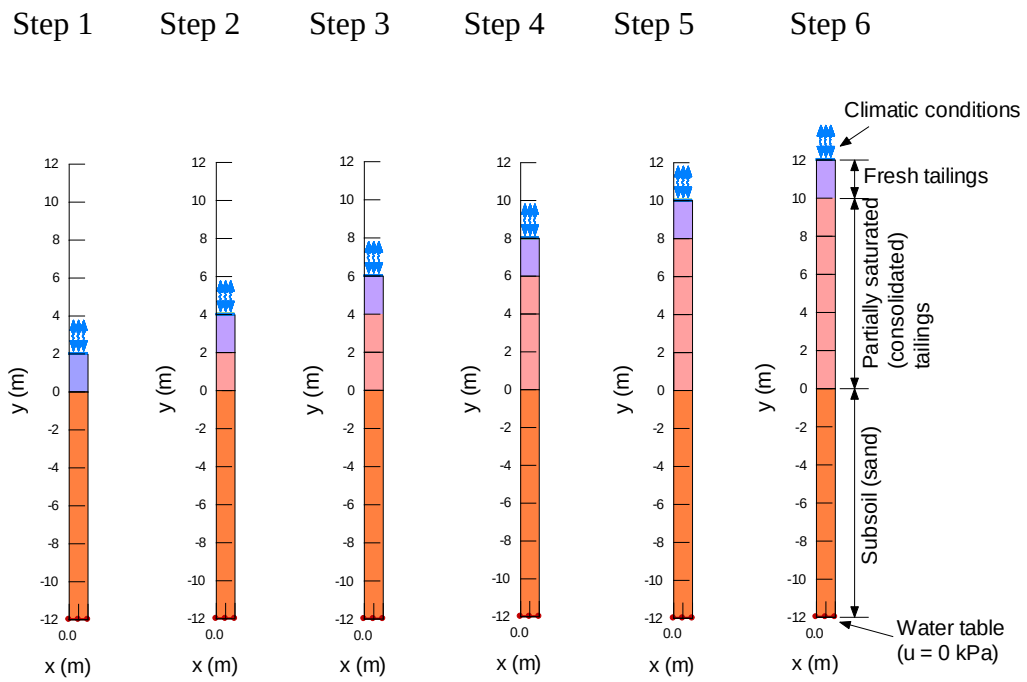

Figure 7.2: Numerical models for each addition of a 2-m thick fresh tailings layer of the baseline simulation conducted with Vadose.

The WRC of the fresh tailings was defined from pressure plate extractor tests (Section 4.1.6) and the WRC of the consolidated tailings was obtained from Tempe cell tests (Section 4.1.6); both curves are described using the Fredlund and Xing (1994) model (Figure 7.3a). The initial VWC (equal to porosity) of the fresh and the consolidation tailings was 0.49 and 0.41, respectively.

The saturated hydraulic conductivity of the fresh tailings (k_{sat} = 5×10^{-7} m⁄s) was estimated using the Modified-Kozeny-Carman model (Mbonimpa et al., 2002; Section 2.3.2). The saturated hydraulic conductivity of the consolidated tailings (k_{sat} = 1×10^{-7} m⁄s) is given by the average from laboratory tests (Section 4.1.5). The permeability functions of both fresh and consolidated tailings were determined using Fredlund et al. (1994) predictive model (Section 2.4.2 and Figure 7.3b).

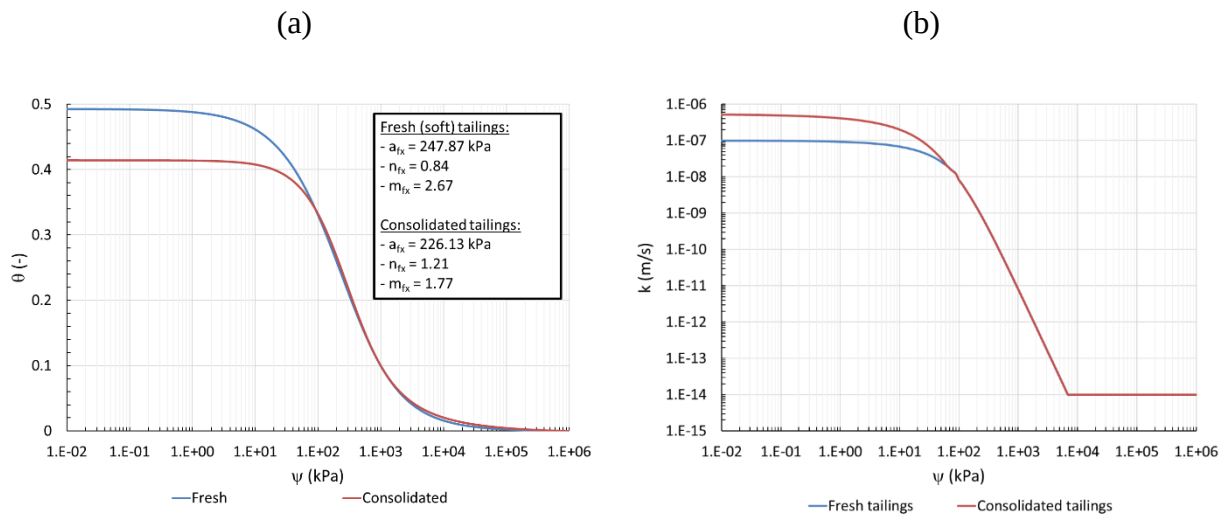

Figure 7.3: (a) Water retention curves and (b) permeability functions of fresh and consolidated tailings used in the baseline simulations.

Paste tailings were deposited on a sandy underlying (foundation) soil at the site (Figure 7.2; no lining at the bottom of the TSF). The water retention curve of the sand was estimated with the Modified Kovàcs model (MK; Aubertin et al., 2003a, 2003b) using the grain size distribution curve (D_{10} = 0.08 mm; C_U = 6.3) and porosity (n = 0.40) reported by Golder (1998). The saturated hydraulic conductivity (k_{sat} = 1×10^{-5} m⁄s) was obtained from site investigations (Kilborn, 1998).

The permeability function of the sand was also defined using Fredlund et al. (1994) predictive model (Figure 7.4b).

(a) (b)

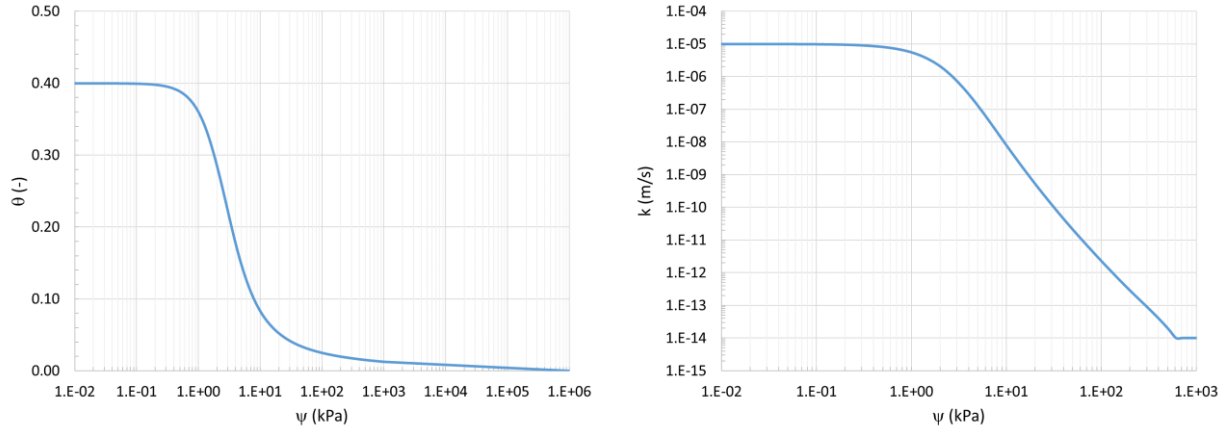

Figure 7.4: (a) Water retention curve and (b) permeability function of the underlying (foundation) sandy soil in the baseline simulation.

The climatic boundary conditions applied at the surface of the baseline model (in Vadose/W) were determined from average annual conditions measured at the Shinyanga weather station located approximately 100 km south-east of the Bulyanhulu mine (SRK, 2002) (Table 7.2).

Table 7.2: Yearly average climatic conditions measured at the Shinyanga weather station close to the Bulyanhulu mine (SRK, 2002) and used as boundary conditions in the baseline model. T_{min}: minimum temperature; T_{max}: maximum temperature; T_{avg}: average temperature; RH: relative humidity; v_w: average wind speed; Precip.: precipitation.

Parameter	Average	Measurement period
T_{min} (ºC)	18.1	1987/01-1996/12
T_{max} (ºC)	30.2	1987/01-1996/12
T_{avg} (ºC)	24.2	1987/01-1996/12
RH (-)	58%	N/A
v_w (m/s)	7.1	1985/01-1994/12
Precip. (mm/d)	2.3	1987/10-1996/10

The depth of the water table at the site was comprised between 5 and 20 m on average (but depths between were 1.5 m and 90 m were also measured; Golder, 2000; SRK, 2002; Wegs, 2002); this depth it is fixed at -12 m in most simulations. The effect of the water table position is investigated in Section 7.2.6.

Initial pressure conditions in the simulations were defined using a spatial function, where the starting pressure distribution in the subsoil corresponded to hydrostatic conditions (as shown in Figure 7.5). The initial pore water pressure at the base of each saturated fresh tailings layer correspond to the overburden stress due to its thickness (e.g. 2 m × 9.8 kPa/m= 19.6 kPa for a 2-m thick layer). The initial pore water pressure at the surface of each fresh tailings layer is 0 kPa (tailings are initially saturated upon deposition).

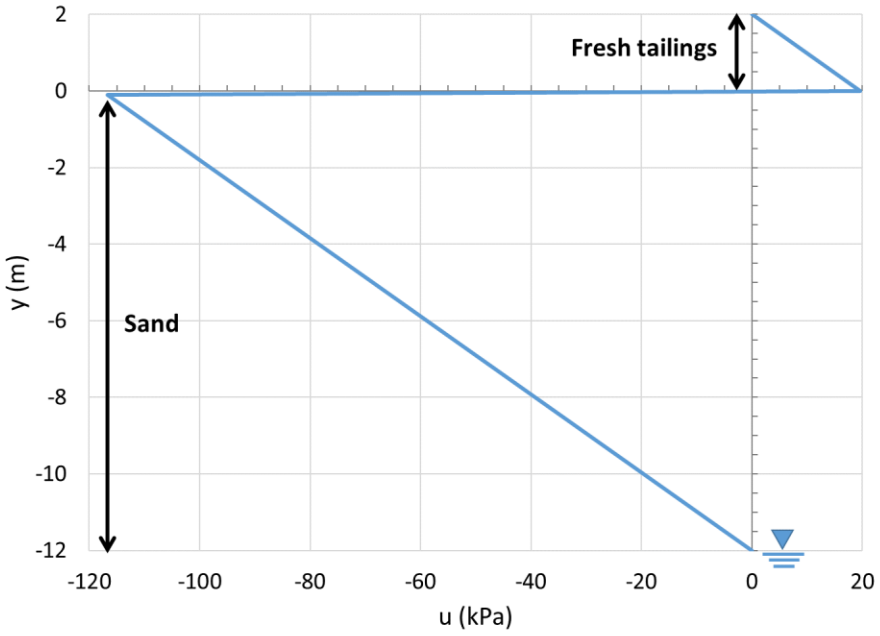

Figure 7.5: Initial pore pressure distribution for the deposition of the first paste tailings layer in the baseline simulation.

Vadose/W was also used to simulate the oxygen flux in the reactive tailings, and to assess the effect of tailings and site properties on surface oxygen flow rate. Ideally, the oxygen fluxes in the tailings should be minimised to control tailings oxidation and limit the risk for contaminated drainage generation.

The surface oxygen flux was calculated by Vadose/W by solving Fick's second law (Equation 2.35) (Mbonimpa and Aubertin, 2003; Mbonimpa et al., 2003; GeoSlope, 2007, 2016). The effective diffusion coefficient (D_e) was estimated in Vadose/W using the Collin and Rasmuson (1988) model (which generally gives very similar results to Aachib et al. (2004) model). The reaction rate coefficient (K_r) was estimated from the modified oxygen consumption tests carried out *in-situ* (Section 4.2). Reaction rate coefficients obtained from field measurements were mostly comprised between 0.27 d^{-1} (100 y^{-1}) and 2.7 d^{-1} (1000 y^{-1}); the latter value of $K_r \approx 2.7$ d^{-1} is used in the simulations.

The convergence of the numerical simulations was assessed by manually calculating the water balance error at the end of the simulation (WB_{error}):

$$WB_{error} = \frac{\sum WB}{V_v} \quad 7.1$$

where ΣWB = Cumulative water balance for the modelling period calculated by the software Vadose/W (m^3);

V_v = Volume of the voids in the model (m^3).

The value of WB_{error} was less than 0.01%. for every layer of the 27 simulations presented in this chapter.

7.1.2 Volumetric water content

The variation of volumetric water content (VWC, θ) and suction (ψ) was assessed in the middle of each of the tailings layers. The VWC in the freshly deposited tailings layers is initially high and equal to the porosity (saturated tailings, θ = n = 0.49; Figure 7.6), but rapidly decreases after deposition. VWC decreased, for each new layer, from 0.49 to approximately 0.32 within 50 days. VWC then became constant until a new tailings layer was added. The placement of a fresh tailings layer caused an increase of the VWC in the underlying tailings (Figure 7.6a). The increase was relatively rapid (< 5 days) and could exceed +0.08. The VWC then decreased slowly until a new tailings layer was added. The rate of decrease varied depending on the distance to the surface and was more rapid when tailings were closer to the surface. The final VWC (after 60 days) was always higher than the initial value, but it tended to become constant with time and deposition. The VWC after one year of deposition appeared to be higher in the deeper layers ($\theta(y = 1\ m) > \theta(y = 3\ m) > \ldots > \theta(y = 11\ m)$ at $t = 365$ days) because of infiltration of precipitation and a limited effect of evaporation in the deeper layers of the model.

The effect of the deposition of a new layer on the VWC decreased with depth (and the distance to the new layer). For example, the deposition of layer 6 (y = 11 m) resulted in an increase of VWC of 0.08 in layer 5 (y = 9 m) but of only 0.01 in layer 1 (y = 1 m). Deposition of layers 5 and 6 had almost no effect on the VWC of layer 1 at the bottom of the stack.

The deposition of a new layer of fresh and saturated tailings added a large amount of water (equivalent to 986 mm for each layer, every 60 days), and it had much more effect on the VWC of tailings than precipitations. Long-term simulations of climatic conditions (after the end of deposition) showed that despite 876 mm of annual rain, the water balance was mostly negative and

the VWC decreased in the whole tailings stack (Figure 7.6b). The decrease of VWC was slightly more rapid (after day 300) in the top layer (y = 11 m) but very similar in the underlying tailings (y = 1 to 9 m). The VWC in the stack five years after the deposition of the last fresh tailings layer was comprised between 0.22 at the surface and 0.35 at the base of the model. There was little indication of a significant desaturation slowdown (Figure 7.6b), and evaporation was expected to cause a decrease of VWC.

(a) Days 0 to 500 (b) Days 0 to 2185

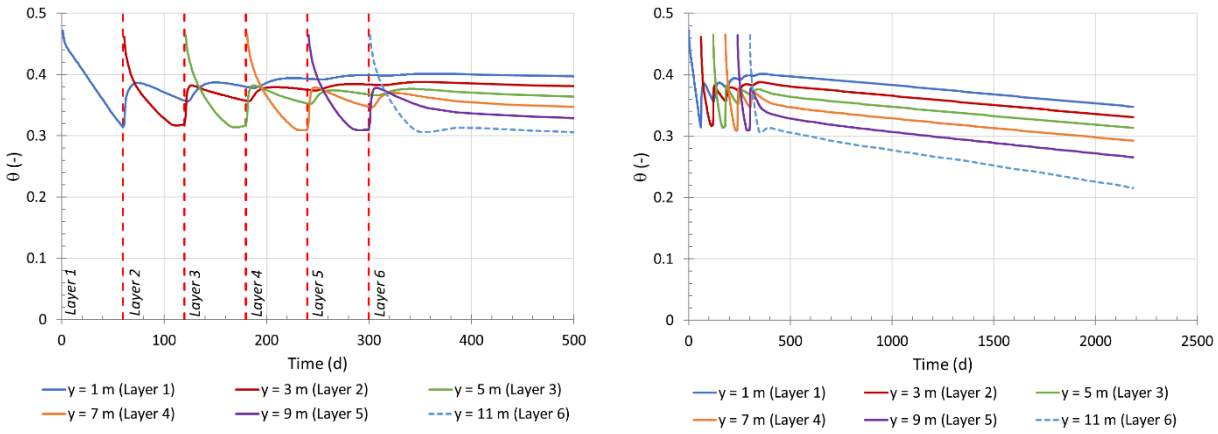

Figure 7.6: Volumetric water content (θ) in the baseline simulation (a) from day 0 to day 500 and (b) from day 0 to day 2185 (deposition + 5 years) at various depth (y = 1 to 11 m above the base of the TSF).

The degree of saturation remained higher than 75% in the tailings during the first 500 days of the simulation, and it was generally above 85% (in the middle of the layers) after the deposition of one or two additional layers (Figure 7.7a). At the end of the deposition of the 6 layers (total thickness = 12 m), the degree of saturation near the bottom of the stack (y = 1 m) was above 95% until day 500. A similar behaviour was observed in the ML columns (Chapter 6), although at a different scale.

The degree of saturation after day 300 (after the end of the deposition) decreased uniformly by approximately 15% in five years (final degree of saturation between 55% and 85% in the middle

of the tailings layers; Figure 7.8b). The decrease was slightly more rapid closer to the surface (y = 11 m) but uniform throughout the tailings stack.

(a) Days 0 to 500 (b) Days 0 to 2185

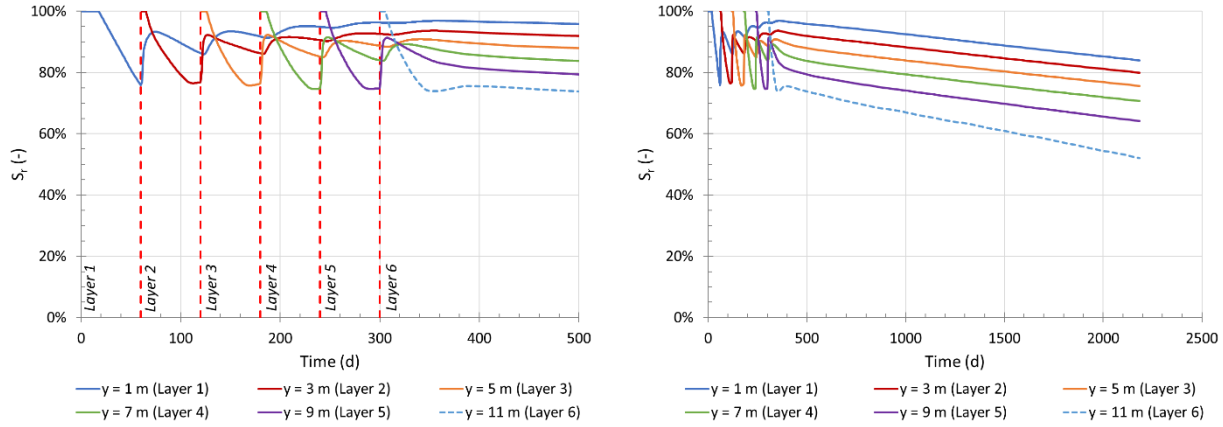

Figure 7.7: Degree of saturation (S_r) in the baseline simulation (a) from day 0 to day 500 and (b) from day 0 to day 2185 (deposition + 5 years) at various depth (y = 1 to 11 m above the base of the TSF).

The deposition of a new layer of paste tailings (for example layer 6, y = 10 to 12 m) mostly affected the degree of saturation of the top 4 m of the underlying tailings (y = 6 to 10 m; Figure 7.8a), i.e. the portion of the tailings stack which initially had a lower degree of saturation (S_r < 90%). The fresh tailings started to desaturate right after deposition while downward drainage continued to increase the degree of saturation of the underlying layer at the same time. For example, ten days after placement of layer 6, the degree of saturation at y = 8 m had increased from 80% (day 300) to 90% (day 310), while the degree of saturation at y = 11.5 m (in the top layer) had decreased from 100% to 92%. The effect of the new layer on the degree of saturation continued up to 50 days after the deposition, almost to the bottom of the stack. A similar behaviour was observed in the previous layer depositions (results not shown here).

A general desaturation of the tailings stack by drainage and evaporation was observed after the deposition of the last paste tailings layer. Without any new significant addition of water, the degree

of saturation started to decrease uniformly throughout the stack (Figure 7.8b). The desaturation was slightly more pronounced in the top 2 to 3 m of the stack (y = 9 to 12 m). Evaporation was particularly intense very close to the surface and contributed to a reduction of the degree of saturation in the top 10 cm to almost 0%.

(a) Days 300 to 360 (b) Days 360 to 2000

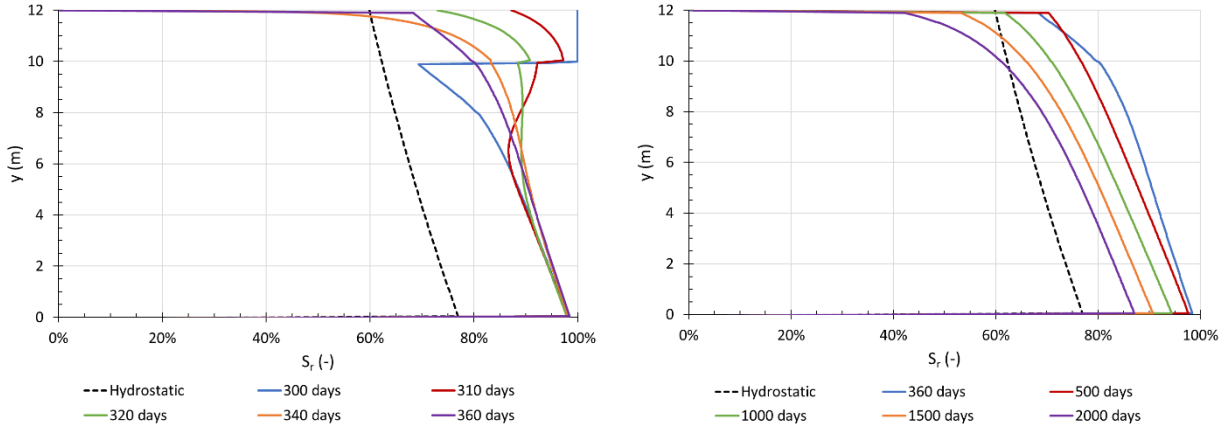

Figure 7.8: Degree of saturation in the tailings (baseline simulation) for (a) days 300 to 360 (following deposition of layer 6) and (b) days 360 to 2000 (at the end of the deposition period). Hydrostatic condition is for a constant water table (u = 0 kPa) at y = -12 m.

The degree of saturation should ideally remain above about 85% to prevent oxidation of reactive tailings (Aubertin et al., 2002). This general criterion is only an approximation, and the actual requirements may vary depending on the properties of the tailings (e.g. mineralogy, particle size distribution, pre-oxidation; Ouangrawa, 2007; Pabst, 2011). The risk of contaminated drainage generation by paste tailings was assessed by estimating the time required for the degree of saturation to decrease below 85% (t_{85}) in the middle (mid-height) of each tailings layer. The time between the placement of two paste tailings layers should be smaller than t_{85} to limit the risk of oxidation

The parameter t_{85} for the baseline model was in general around 24 days except for layer 1 (43 days; Table 7.3). In other words, tailings would maintain a degree of saturation below 85% during

approximately 36 days (for the 60 days cycle) before a new saturated layer is deposited at the surface. The degree of saturation would then increase with the deposition of a new layer and remain above 85% for some time, as shown in Figure 7.7. This does not apply to the top layer 6, directly exposed to atmospheric conditions, which would then remain prone to desaturation, oxidation and contaminated water generation.

Table 7.3: Time to attain a degree of saturation (S_r) of 85% (t_{85}) after the deposition of each new layer, 1 m below the surface, in the baseline simulation.

Layer	y (m)	t_{85} (d)
1	1	43.1
2	3	26.2
3	5	24.1
4	7	25.4
5	9	23.1
6	11	23.0

7.1.3 Pore water pressure and suction

The suction (ψ) in the middle of the tailings layers is presented in Figure 7.9. It decreased quickly after deposition of each new paste layer and then increased again, more slowly. The decrease of suction was mostly due to the downwards drainage of water from the new saturated paste layer, as indicated also by the increase of VWC in the layer underneath (Figure 7.6); this effect was more significant closer to the interface with the new layer. For example, the suction in layer 1 decreased from 120 kPa to almost 0 kPa (-120 kPa) after the deposition of layer 2; it decreased from 30 kPa to 15 kPa (-15 kPa) after the deposition of layer 6 (y = 11 m). The decrease in suction was also somewhat quicker closer to the surface.

After this initial decrease, suction then tends to increase because of drainage and evaporation. The suction increase was interrupted by the addition of new tailings layers. Simulated suction could exceed 100 kPa in tailings directly exposed to the atmospheric conditions (in the 60 days after their deposition, before the placement of a fresh tailings layer above); suction did not remain below

80 kPa after subsequent layers were deposited. Simulated suction was below tailings air entry value (ψ < AEV = 58 kPa) at elevations $y \leq 5$ m between days 300 and 500 (Figure 7.9a), which is consistent with the higher degree of saturation (S_r > 85%) observed during the same period (Figure 7.7a).

The simulated suction continued to increase progressively after the deposition of the sixth (last) layer of paste tailings (day 300; Figure 7.9b). The increase was more pronounced at first (days 300-350), due to the combined effect of drainage and evaporation. The behaviour during this early period was similar than observed with the previously deposited layers. The suction increase then slowed down and the rate became relatively constant (approximately 10 kPa/100 days) for the rest of the simulation(s). The suction increased somewhat faster in the surface layer (mid-layer at y = 11 m) than in the underlying tailings layers; the simulated suction increase tended to accelerate with time near the surface.

(a) Days 0 to 500

(b) Days 0 to 2185

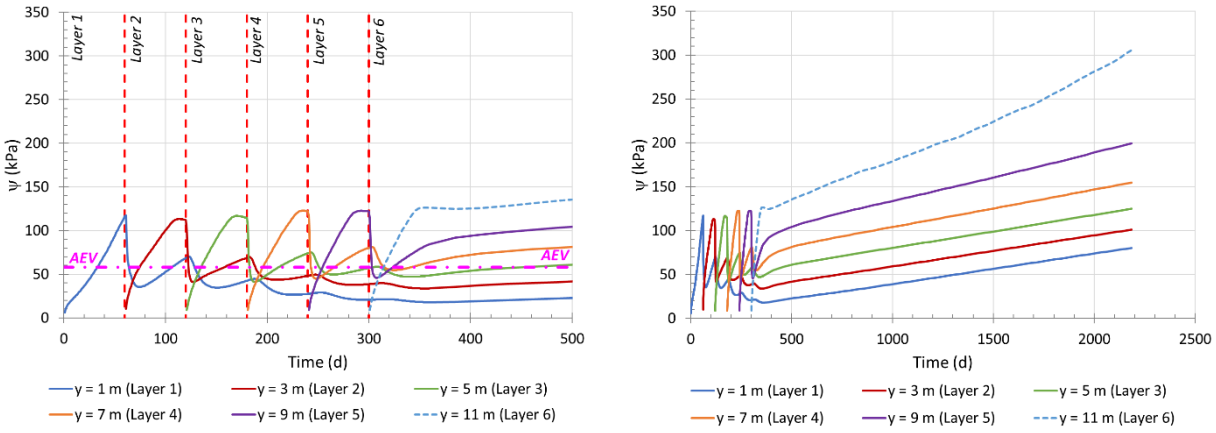

Figure 7.9: Suction (ψ) in the baseline simulation (a) from day 0 to day 500 and (b) from day 0 to day 2185 (deposition + 5 years) at various depth (y = 1 to 11 m above the base of the TSF).

The deposition of a fresh layer of tailings influences the suction profile up to several meters below the surface (Figure 7.10a). For example, the suction significantly decreased over 6 m after the deposition of the sixth paste tailings layer (about -100 kPa at the interface, y = 10 m, 10 days after

the deposition). The effect of the additional layer on the suction profile is visible up to 60 days after deposition. A similar behaviour was observed for each new deposited layer (layers 1 to 6).

In the long-term, the value of suction progressively increased throughout the tailings stack (Figure 7.11b). The effect of evaporation near the surface of the tailings tended to increase with time.

(a) Days 300 to 360 (b) Days 360 to 2000

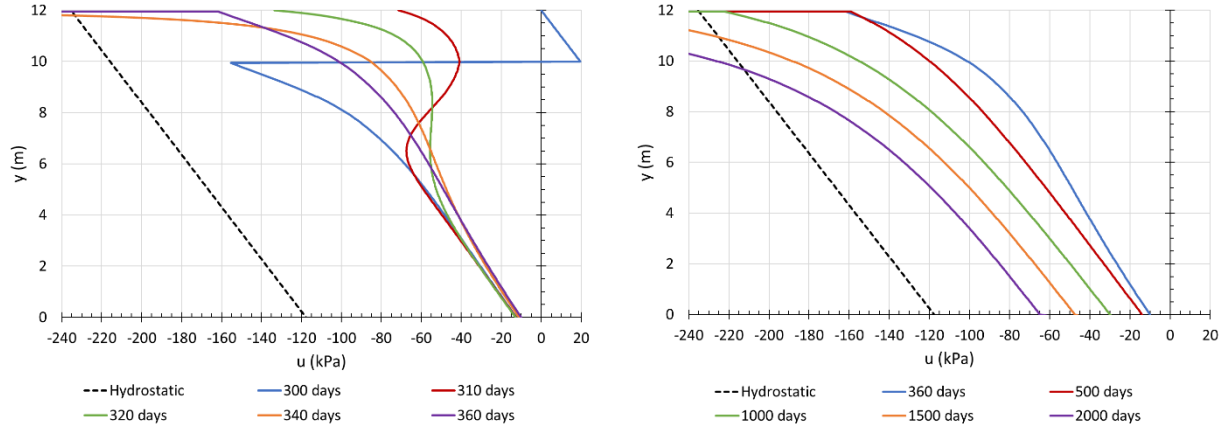

Figure 7.10: Pore water pressure profiles in the tailings (baseline simulation) for (a) days 300 to 360 (following deposition of layer 6) and (b) days 360 to 2000 (at the end of the deposition period).

7.1.4 Hydraulic gradient and water fluxes

A simulated negative hydraulic gradient ($i = \Delta h/\Delta z$) indicates drainage (i.e. dominated by downwards flow), while a positive gradient is associated with evaporation (moisture moving upward, toward the surface). The gradient in the freshly deposited tailings is typically negative (drainage) for approximately 9 days after the deposition, before it becomes positive and continues to increase to values up to +5 (similar value for all new layers; Figure 7.11a). Drainage from the fresh layer to the underlying layers lasted for approximately 9 days for layers 2 to 6 (4 days for layer 1). The gradient was also negative in the underlying tailings following the deposition of a

new paste tailings layer. The duration of the drainage period in the deeper layers increased as the number of layers increased. For example, the drainage-dominated period in layer 1 increased from 9 days after the placement of layer 2, to over 30 days after the placement of layer 6. The hydraulic gradient continued to increase during the next five years following the end of the deposition (Figure 7.11b).

The deposition time in the numerical simulations was six 60-day periods followed by 5 years with no deposition. The gradient increase is significantly more pronounced in the surface layer, which is more influenced by the climatic conditions. The gradient is positive throughout the entire profile (y = 0 to 12 m) after day 500 (200 days after the end of the deposition), and the influence of evaporation tends to manifest deeper with time (Figure 7.12b).

The gradient at the surface of the simulated column was generally negative (downwards flow) after the deposition of a fresh tailings layer (e.g. Day 300 - Figure 7.12a). The presence of partially saturated tailings below contributed to accelerate the desaturation of the fresh layer in the days following its deposition. However, after a certain time (for example after day 320 in Figure 7.12a), the gradient became positive (upwards flow) indicating that most of the water loss was through evaporation. It was even possible to observe an upward flow of water from the underlying layers. A similar behaviour was observed in laboratory and numerical simulations carried out by Daliri et al. (2016) for comparable conditions.

(a) Days 0 to 500

(b) Days 0 to 2185

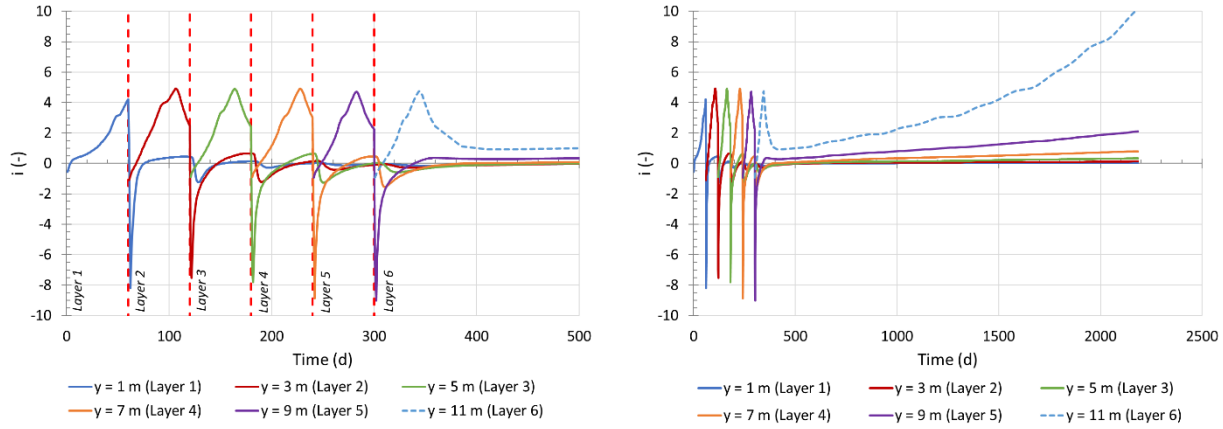

Figure 7.11: Hydraulic gradient (i) in the baseline simulation (a) from day 0 to day 500 and (b) from day 0 to day 2185 (deposition + 5 years) at various depth (y = 1 to 11 m above the base of the TSF).

(a) Days 300 to 360

(b) Days 360 to 2000

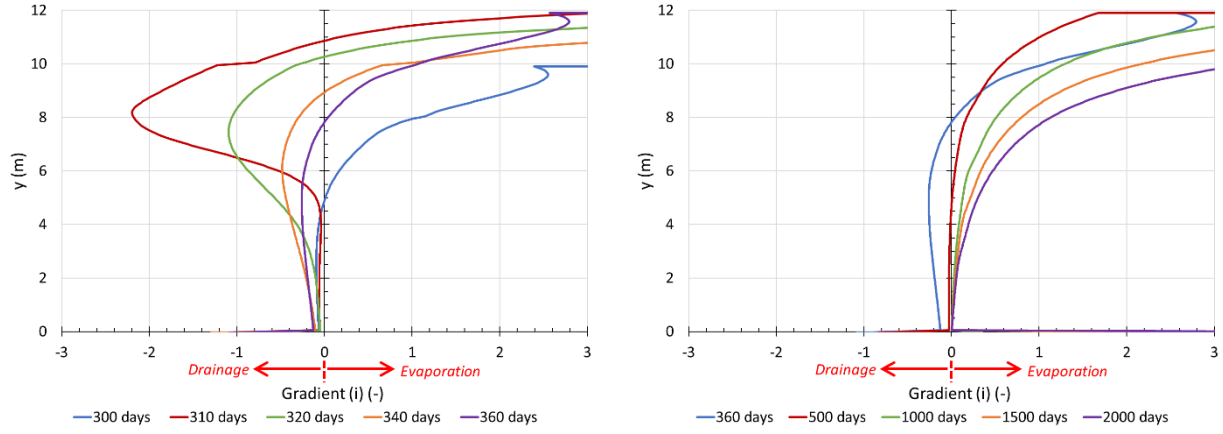

Figure 7.12: Hydraulic gradient profile in the tailings (baseline simulation) for (a) days 300 to 360 (following deposition of layer 6) and (b) days 360 to 2000 (at the end of the deposition period).

The zero-flux plane (ZFP, Section 2.6.3), defined as the position where the hydraulic gradient is nil, is a useful indicator to asses how water moves in the tailings layers stack. The hydraulic gradient is positive above the ZFP (flow dominated by evaporation), and negative below (dominated by downward drainage). The ZFP reflects the depth of influence of evaporation in the simulations. The position of this ZFP is not static and may vary with time. Rewetting at the surface tends to raise its position. Inversely, the ZFP moves deeper when the water balance remains negative. Furthermore, several ZFP planes can sometimes develop during the active (deposition) period or following large precipitation (Figure 2.20). In the following analyses, the ZFP is taken as the deepest point influenced by infiltration or evaporation.

The ZFP is typically located close to (or at) the surface of the tailings after the deposition of a fresh paste tailings layer (Figure 7.13a) and then moves downwards in the stack with time. Its position fluctuates between the tailings and the underlying sand layer until the deposition of layer 4. The ZFP remained more stable once it was in the sand (coarse grained materials like sand are typically effective evaporation barriers, e.g. Dagenais et al., 2006). The influence of evaporation on the desaturation of the tailings increased after the active (deposition) period (> day 300). The elevation of the ZFP progressively decreased until it reached the underlying sand subsoil at day 898 (Figure 7.13b). Evaporation becomes the main mechanisms for water transport in the tailings after this date. Consequently, potentially contaminated pore water from the tailings (assuming the tailings were reactive) could have drained into the underlying soil for almost 900 days (for this simulated case). The depth of influence (position of the ZFP), which was approximately 7 m after 500 days, exceeded 12 m after 2000 days (total duration of the simulation: 2185 days).

(a) Days 0 to 500 (b) Days 0 to 2185

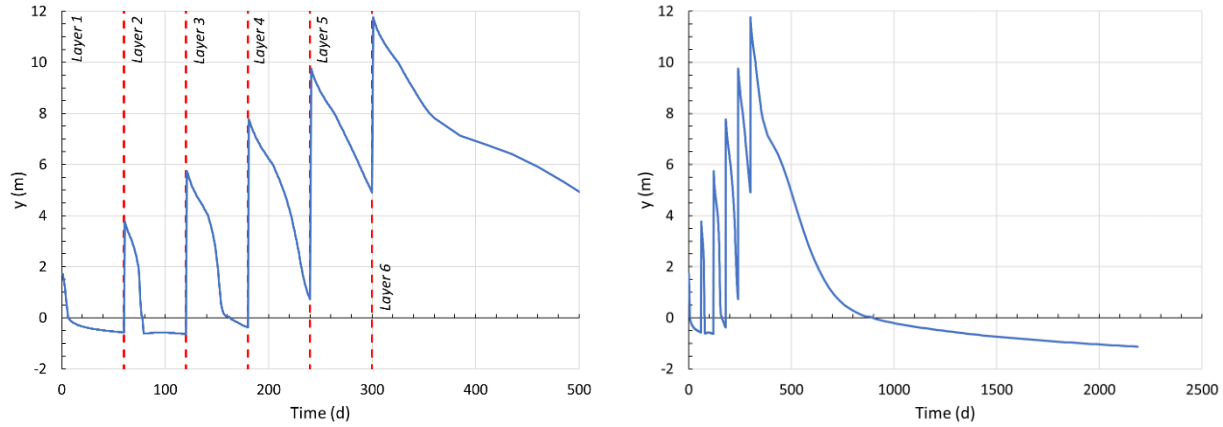

Figure 7.13: Position of the zero-flux plane (ZFP) in the baseline simulation (a) from day 0 to day 500 and (b) from day 0 to day 2185 (deposition + 5 years).

Water flow rate at the bottom of the tailings layers (y = 0 m), at the interfaces between the various layers (y = 2 m, 4 m, …, 10 m) and at the surface was also assessed with the simulations to evaluate the relative influence of drainage and evaporation on the hydrogeological behaviour of paste tailings (Figure 7.14).

The deposition of a fresh tailings layer always result in the water flowing into the underlying, partially saturated, tailings layers (as observed in the ML columns Chapter 6).There was thus percolation following the placement of a fresh layer into the underlying layer below (Figure 7.14) (e.g. -160 mm of water at y = 2 m in the first 15 days following the deposition of layer 2). The volume and direction of flow is correlated with the hydraulic gradient, as discussed above. A positive slope (cumulative flow vs. time) in Figure 7.14 indicates a positive hydraulic gradient (i), with water flowing upwards (due to evaporation) at the interface. A negative slope means that there is a negative hydraulic gradient (i) and that water movement is downwards (i.e. percolation) at the interface.

There was -70 mm of infiltration at the tailings/sand interface 7 days after the deposition of layer 1. Afterwards, there was almost no infiltration in the sand until the deposition of layer 6, and -100 mm of water drained into the underlying soil after the placement of layer 6 from day 300 to day 500.

This is somewhat similar to the trend observed in the simulations of the interlayer flow in the ML laboratory columns (although the drainage period was shorter because the layers in the laboratory models were thinner). The hydraulic gradient was mostly negative in the baseline numerical simulation during the active (deposition) period, when water was added due to the fresh tailings layers. After the initial flow of water from the fresh tailings layers, the direction was reversed, with water moving upwards back to the surface layer (e.g. at the interface between layer 2 and layer 3 after from days 121 to 180).

(a) Days 0 to 500 (b) Days 0 to 2185

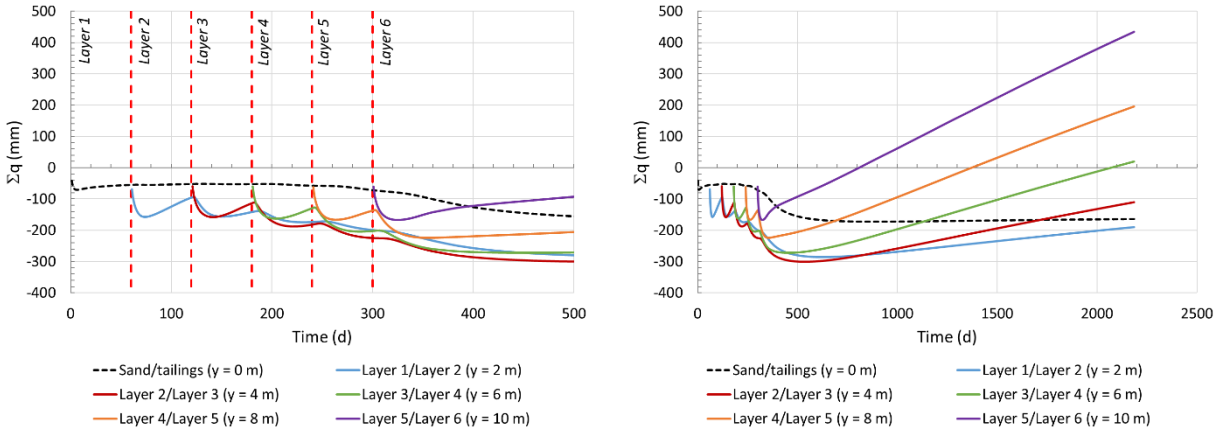

Figure 7.14: Simulated cumulative interlayer flow in the baseline simulation (a) from day 0 to day 500 (deposition of tailings from day 0 to day 300) and (b) from day 0 to day 2185 (deposition + 5 years).

The cumulative (actual) evaporation (ΣAE) at the end of the simulation period (2185 days) was 7607 mm (cumulative PE of 1.7×10^4 mm) (Figure 7.15b). The AE rate became smaller than the PE rate approximately 105 days after the beginning of the simulation (Figure 7.15a). The deposition of a fresh tailings layer tends to increase the evaporation ratio (AE/PE) back to around 1.0. But, it would drop to 0.36 – 0.38 within 40 to 45 days (Figure 7.16b). The evaporation ratio was around 0.36 from day 340 until the end of the simulation (2185 days).

(a) Days 0 to 500 (b) Days 0 to 2185

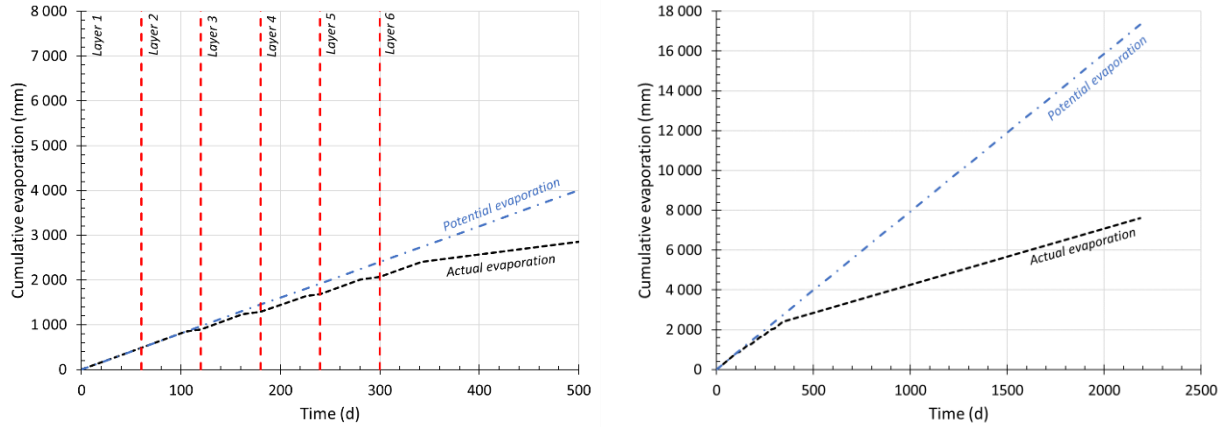

Figure 7.15: Simulated actual evaporation in the baseline simulation (a) from day 0 to day 500 (deposition of tailings from day 0 to day 300) and (b) from day 0 to day 2185 (deposition + 5 years).

(a) Days 0 to 500 (b) Days 0 to 2185

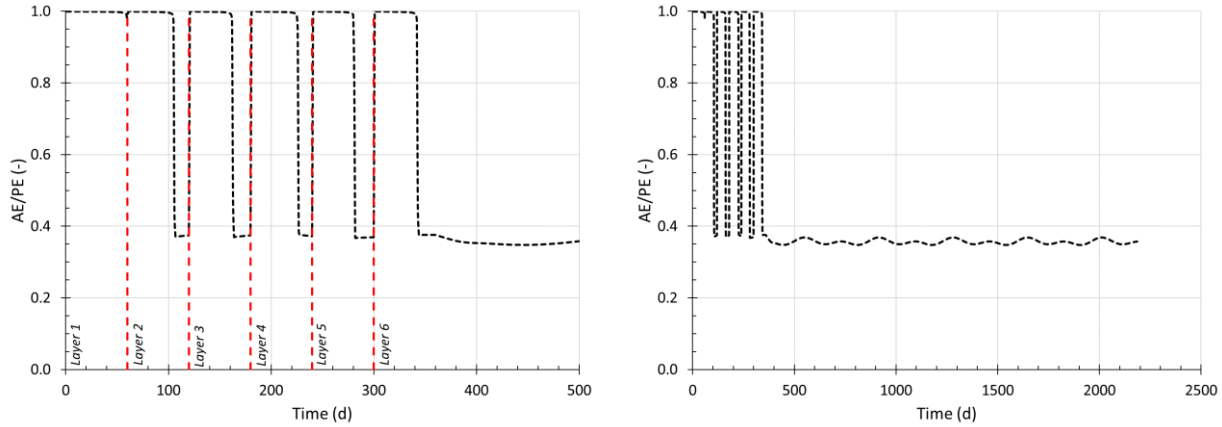

Figure 7.16: Simulated evaporation ratio (AE/PE) in the baseline simulation (a) from day 0 to day 500 (deposition of tailings from day 0 to day 300) and (b) from day 0 to day 2185 (deposition + 5 years).

7.1.5 Oxygen flux

The simulated cumulative oxygen flux at the surface of the tailings (baseline simulation, with K_r = 1000 y^{-1} or 2.7 d^{-1}) after 500 days is 24 kg/m^2 (Figure 7.17a) or 15 kg/m^2/y; this value is well above the target of about 40 g/m^2/y (0.11 g/m^2/d) sometimes recommended to control AMD generation (e.g. Aubertin et al., 1999; Dagenais, 2005). The estimation of K_r, based on field MOC tests (Section 4.2), is however relatively high and imprecise, so lower values were also simulated (representing less reactive tailings). The simulated oxygen flux is then significantly reduced (5 kg/m^2 and 1.2 kg/m^2 after 500 days for K_r = 0.27 d^{-1} (100 y^{-1}) and 0.027 d^{-1} (10 y^{-1}) respectively), but it remains well above the target maximum flux. The deposition of fresh tailings layers does not appear to influence the oxygen flux in the tailings, which is relatively constant throughout the simulation period (the tailings were highly reactive). The oxygen flux kept increasing after day 500 (Figure 7.16b), as the degree of saturation continuously decreased in the tailings stack (Figure 7.7).

As will be shown below, the simulated oxygen flux may also be influenced by other parameters, including the tailings deposition rate and layer thickness (Section 7.2.2), the time between the deposition of two layers (Section 7.2.3) and the potential evaporation rate (Section 7.2.7).

(a) Days 0 to 500 (b) Days 0 to 2185

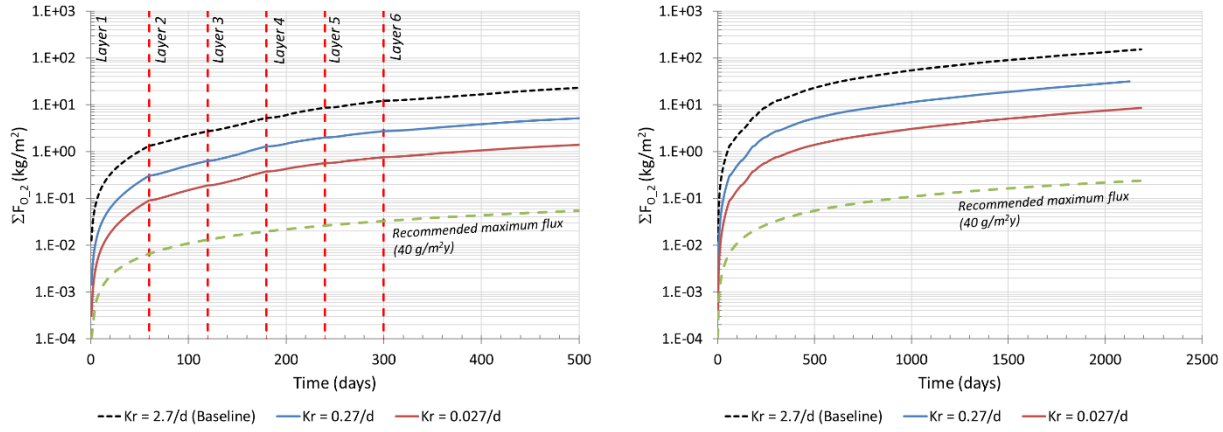

Figure 7.17: Cumulative oxygen flux at the surface of the tailings for three oxygen reaction rate coefficients (K_r) in the baseline simulation (a) from day 0 to day 500 and (b) from day 0 to day 2185 (deposition + 5 years).

7.2 Parametric study

The effect of the main factors of influence, identified above, are assessed through a series of simulations. The main characteristics and results are presented in the follows.

7.2.1 Field climatic data resolution

The effect of the local climate resolution (yearly, monthly or daily data) is evaluated in below. Availability and quality of climate data for remote mine sites can vary significantly from site to site. Various climate resolutions (annual average, monthly average and daily measurements) were therefore considered in the simulations to assess the effect of input data on results. Daily climatic data was recorded at the Bulyanhulu mine for five years (from January 2000 to August 2005, Figure 7.18a). Monthly average conditions were obtained from a design report (SRK, 2002; see Table 7.4 and Figure 7.18b). Annual conditions were calculated from average monthly conditions in Table 7.4 (Figure 7.18b). The climate at the Bulyanhulu mine corresponds to a tropical savanna (Aw') according to the Köppen Classification System (Oliver, 2005). It experiences a relatively dry winter, and a wet spring and summer (Figure 7.18b).

Table 7.4: Monthly climatic characteristics at the Bulyanhulu mine (SRK, 2002). T_{min}: minimum daily temperature; T_{max}: maximum daily temperature; T_{avg}: average daily temperature; RH: average daily relative humidity; v_w: average daily wind speed; Precip: cumulative monthly precipitation.

	T_{min} (ºC)	**T_{max} (ºC)**	**T_{avg} (ºC)**	**RH (-)**	**v_w (m/s)**	**Precip (mm)**
January	18.6	28.9	23.7	70%	5.2	117.4
February	18.4	29.2	23.8	71%	5.3	108.1
March	18.4	29.9	24.2	72%	6.0	130.6
April	18.5	29.6	24.1	69%	6.4	118.7
May	17.6	29.6	23.6	61%	7.4	33.0
June	16.1	30.0	23.1	54%	8.2	3.1
July	14.9	29.8	22.4	49%	8.8	0.0
August	16.5	30.7	23.6	46%	9.1	0.5
September	18.7	32.2	25.4	43%	8.5	6.5
October	20.0	32.5	26.2	42%	7.9	51.7
November	19.9	31.1	25.5	51%	6.9	114.2
December	19.4	30.3	24.9	67%	5.9	168.1
Annual	**18.1**	**30.3**	**24.2**	**58%**	**7.1**	**851.9**

(a) Daily values (b) Monthly and annual average values

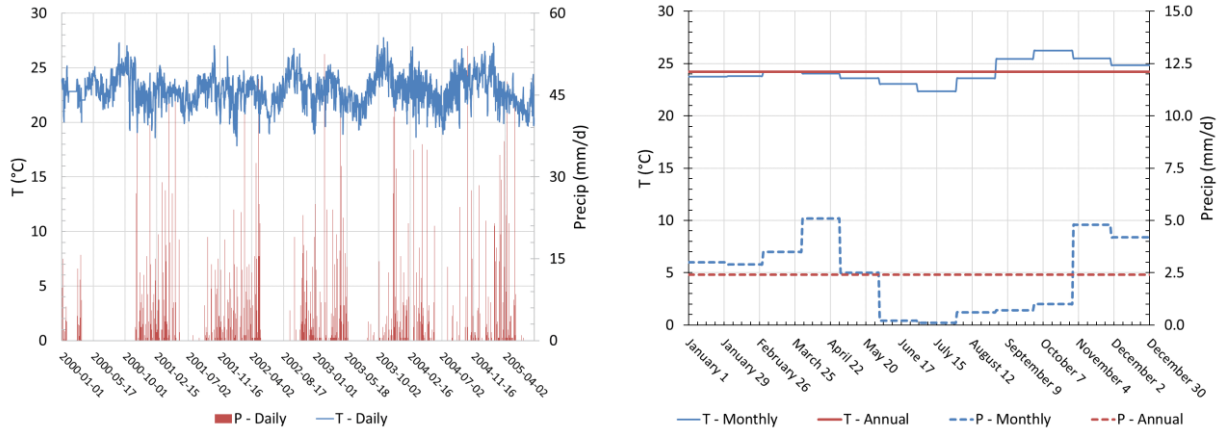

Figure 7.18: Bulyanhulu climate data (a) Daily measurements (data from the Bulyanhulu mine) (b) Monthly and annual averages(SRK, 2002).

The total precipitation in the daily, monthly, and annual (Baseline) simulations is 3730 mm, 5179 mm, and 5244 mm, respectively, for the 6 years that were simulated. The total precipitation in the daily simulation is approximately 30% lower than the annual and monthly simulations, because it corresponds to five years that were drier than the average values. The months of June, July, August and September at the Bulyanhulu mine are typically dry with almost no precipitation during this (winter) period (Table 7.4).

The climatic conditions were applied in Vadose/W using a daily average value (constant average condition), where the software applied all climate parameters as constant or averaged values through the day. The values would step to a new constant or average value on the following day.

The daily potential evaporation (PE) was estimated by the software using the Penman (1948) model based on maximum and minimum daily temperatures and relative humidity, wind speed, and latitude (Figure 7.19). The annual and monthly average calculated PE rates were 7.9±0.2 mm⁄d and 8.1±1.7 mm⁄d, respectively. The average daily PE rate was 5.4±1.0 mm⁄d. The PE rate calculated for the simulations with daily and monthly climate resolutions are highly variable. Seasonal trends are also more marked using monthly data. The actual evaporation (AE) was calculated using the modified Penman method (Wilson, 1990; Equation 2.58).

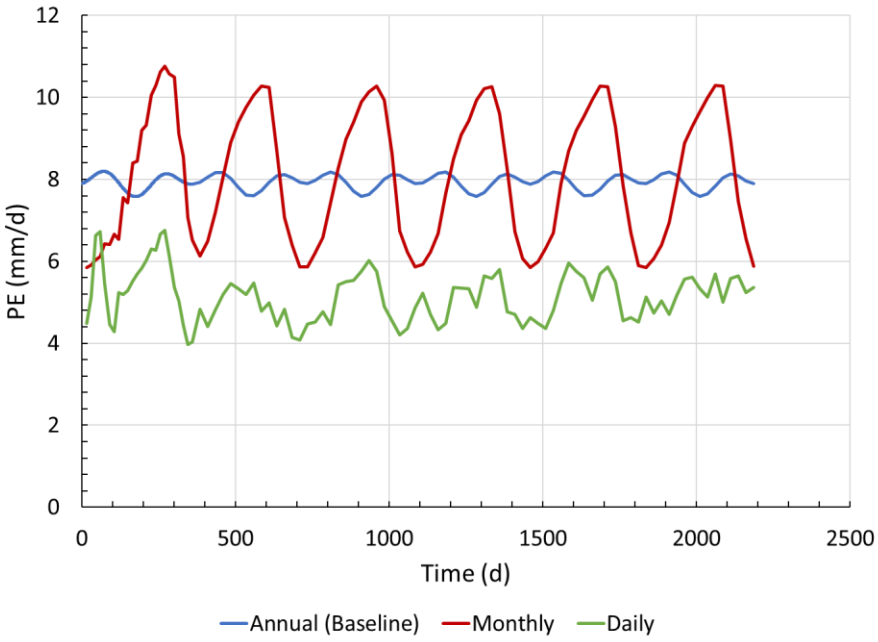

Figure 7.19: Simulated potential evaporation rate (PE) for the three climate data resolutions (daily, monthly, annually) (Simulations #1, #2, and #3 - Table 7.1).

The VWC simulated in the tailings for the three climate data resolutions are very similar. For example, the difference between the VWC simulated in the center (mid-height) of the models (y = 5 m) never exceeded 0.02 during the active (deposition) period, independently of the resolution of climatic data (Figure 7.20). Results at other locations in the model are similar (Appendix D).

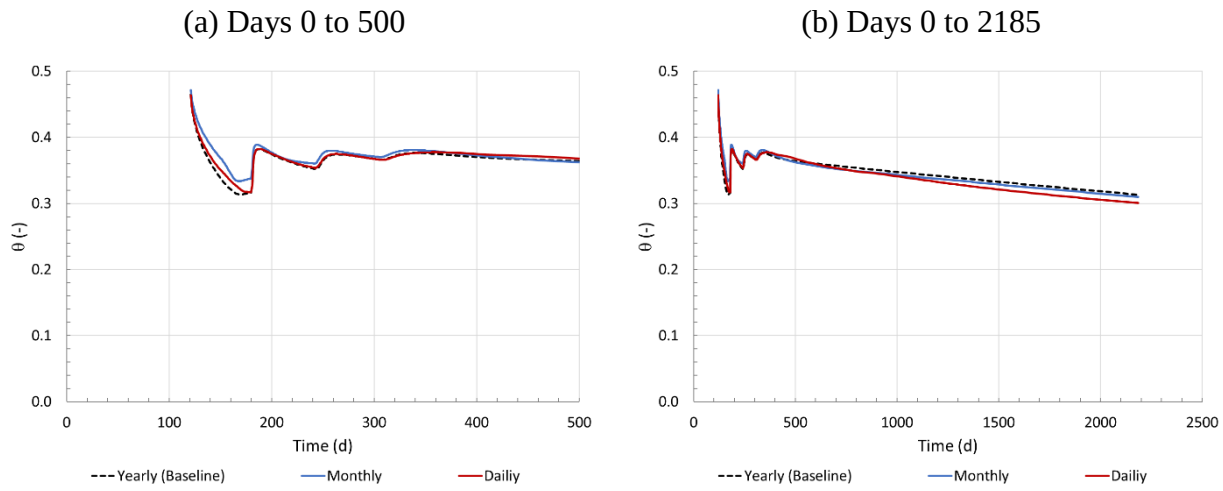

Figure 7.20: Volumetric water content at y = 5 m for varying climate resolutions (yearly, monthly and daily) (a) from day 0 to day 500 and (b) from day 0 to day 2185 (deposition + 5 years) (Simulations #1, #2, and #3 - Table 7.1).

The hydrogeological response of the tailings near the surface is typically more affected by climatic conditions (than at depth). Numerical results indicate that the effect of climate resolution on the VWC 1 m below the surface is very limited (Figure 7.20). The final VWC 1 m below the surface using daily climate data is only slightly lower (0.18 versus 0.21) than with monthly or yearly data. This may be explained by the lower precipitation during the simulated period.

Suction results showed similar trends (Appendix E) and confirmed that the resolution of climatic data had little effect on the simulated hydrogeological behaviour in the tailings stack.

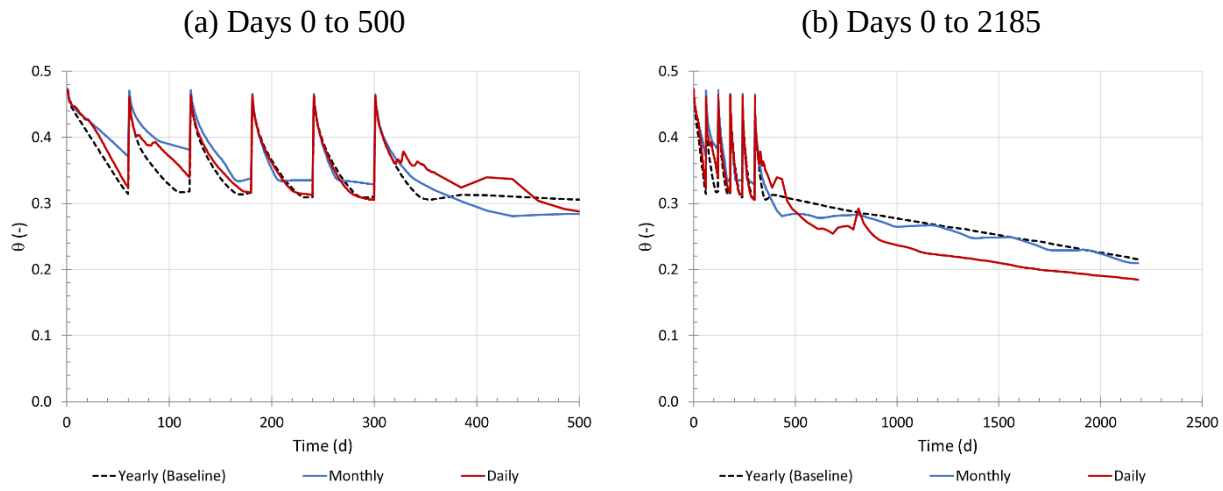

Figure 7.21: Volumetric water content for varying climate resolutions (yearly, monthly and daily), 1 m below the surface of the tailings (a) from day 0 to day 500 and (b) from day 0 to day 2185 (deposition + 5 years) (Simulations #1, #2, and #3 - Table 7.1).

The total outflow into the sand layer ($\Sigma q_{y = 0\ m}$) simulated at y = 0 m (base of the TSF) during the 6 years of the simulation was -164 mm, -327 mm, and -225 mm with the yearly, monthly and daily data, respectively (Figure 7.23a,b), for total precipitations of 5244 mm (yearly), 5179 mm (monthly), and 3730 mm (daily). The simulated total actual evaporation (ΣAE) was 7607 mm for the yearly climate conditions, 7358 mm for the monthly climate conditions and 4304 mm for the daily climate conditions (Figure 7.22c,d). It may have been expected that the simulation with the daily climate data would produce the least infiltration since it corresponds to the lowest total precipitation.

There was more variability in the outflow and actual evaporation using the monthly climate data than with yearly data, because precipitation events are mostly concentrated during the wet season (70% of yearly precipitation; Kilborn, 1998). Constant precipitations of lower intensity in the annual (Baseline) model resulted in a lower infiltration into the underlying subsoil. It seems that extremes conditions (e.g. wet/dry seasons, storms, droughts) tend to cause the most significant impact on the outflow from the tailings.

(a) Days 0 to 500

(b) Days 0 to 2185

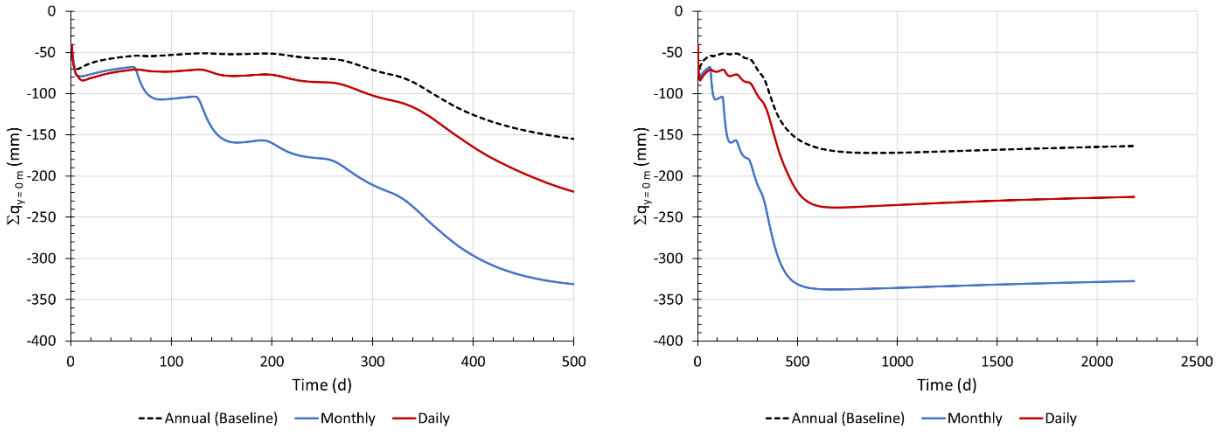

(c) Days 0 to 500

(d) Days 0 to 2185

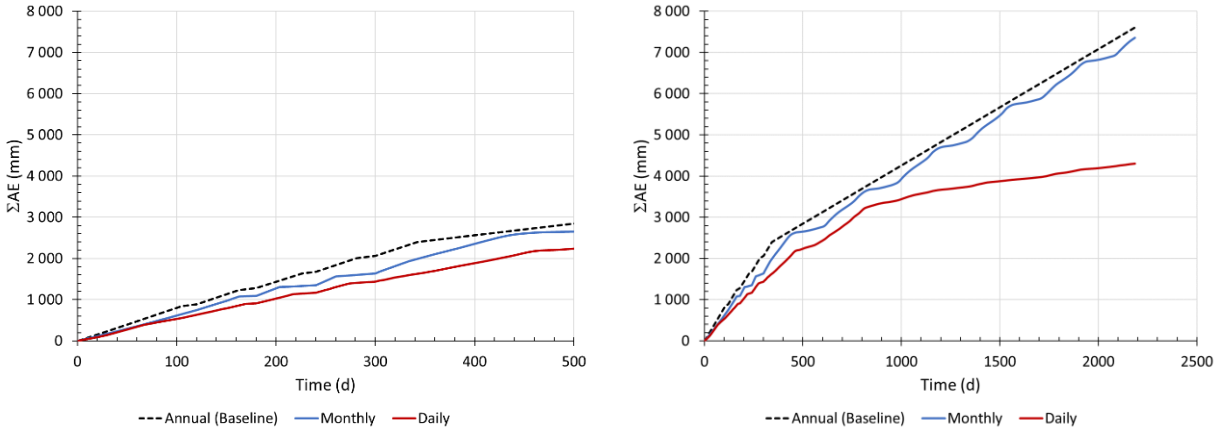

Figure 7.22: (a, b) Total flow and (c, d) total actual evaporation for varying climate resolutions (yearly, monthly and daily) (Simulations #1, #2, and #3 - Table 7.1).

The position of the zero-flux plane (ZFP) is very similar for the three climatic conditions; it tends to migrate within the sand, 1 m below the base of the tailings interface, after 2185 days (Figure 7.23).

(a) Days 0 to 500 (b) Days 0 to 2185

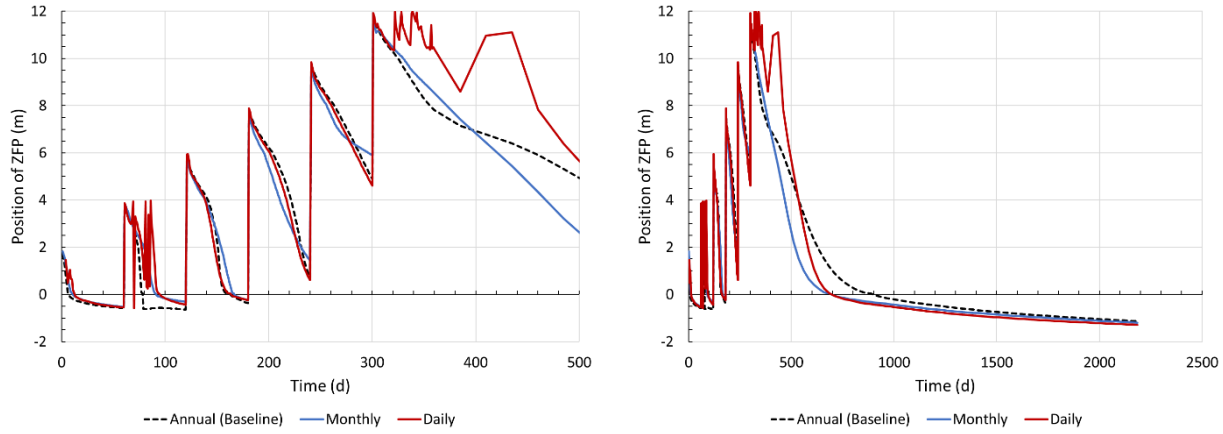

Figure 7.23: Position of the ZFP for varying climate resolutions (yearly, monthly and daily) (a) from day 0 to day 500 and (b) from day 0 to day 2185 (deposition + 5 years) (Simulations #1, #2, and #3 - Table 7.1).

As indicated above, parameter t_{85} represents the time required (after tailings deposition) to attain a degree of saturation of 85% in the middle (mid-height) of the tailings layers (at y = 1 m for layer 1, y =3 m for layer 2, y = 5 m for layer 3, etc.). The value of t_{85} was less than 50 days for all 6 layers using the yearly climate resolution (Table 7.5). It exceeded 1000 days for layers 1 and 2 when a monthly climate resolution was used. The large difference due to the first four months of the monthly climate numerical simulation which are wet, with 56% of the total yearly precipitation falls in January (14%), February (13%), March (15%) and April (14%) (deposition in the numerical simulations starts January 1st) (Table 7.4 and Figure 7.18b). Otherwise, the value of the parameter t_{85} (layers 3 to 6) was also almost the same (around 20 – 40 days) for the three climate resolution simulations. The variability of t_{85} was smaller for the annual climate numerical simulation. The average t_{85} was 27.7±7.8 d for annual data (vs. 542.7±827.0 d and 37.9±14.8 d for the monthly and daily climate data resolutions, respectively).

Table 7.5: Time (in days) to attain a degree of saturation (S_r) of 85%, t_{85}, 1 m below the tailings surface for the three different climate data resolutions (yearly, monthly and daily) (Simulations #1, #2, and #3 - Table 7.1).

Layer	y (m)	t_{85} (days)		
		Baseline (annual data)	**Monthly data**	**Daily measures**
1	1	43.1	1906.6	49.4
2	3	26.2	1244.5	52.5
3	5	24.1	37.3	29.4
4	7	25.4	20.1	23.9
5	9	23.1	18.2	20.6
6	11	23.0	29.4	51.4

The differences between the three climate resolutions (yearly, monthly and daily) in terms of desaturation (i.e. t_{85}), actual evaporation and outflow at y = 0 m are limited. It was therefore decided to use yearly climate resolution in the parametric analyses presented below. Simulations using yearly climate resolution are more stable (better convergence) and made the comparison between the results of the parametric analysis easier than with monthly or daily climate resolutions because seasonal effects are mitigated.

7.2.2 Deposition rate and layer thickness

The thickness of the fresh layers deposited in the facility can be influenced by different factors including the tailings production rate at the mine, the size and position of the active area within the tailings storage facility, and the number of operating deposition points. The effect of fresh layer thickness on the paste tailings hydrogeological behaviour was assessed numerically (see Table 7.1). Several layer thicknesses (between 0.5 m and 12 m) were simulated. The total height of the stack (12 m) and the duration of the deposition (1 year) were kept constant in all the models, so the deposition rate changed (from 0.5 m every two weeks to 12 meters at once; the baseline case is 2 m every 60 days). Paste tailings layers were added instantaneously in the model and then allowed to drain and desaturate by evaporation before the next layer was added. The tailings in the numerical simulations presented in this section had the following thickness values (see Table 7.1 for more

information on the numerical simulation parameters): 0.5 m (Simulation #4), 1 m (Simulation #5), 1.5 m (Simulation #6), 6 m (Simulation #7) and 12 m (Simulation #8) . The number of deposition phases and their duration changed with the layer thickness (as the total deposition period remained constant).

The simulated VWC at y = 5 m remained higher in the models with the thicker layers (Figure 7.24). There was more variability during the deposition period (Days 0 - 330) for 0.5 m layer simulation. The final values of the VWC at the end of the simulation period was comprised between 0.30 and 0.31. Simulations results showed an increase in the VWC at y = 5 m after the deposition of fresh tailings layers above. The results for 1 m and 1.5 m thick layers are not presented here (to keep the Figure 7.24 clearer), but the trends were similar (see Appendix F for all the results).

(a) Days 0 to 500 (b) Days 0 to 2185

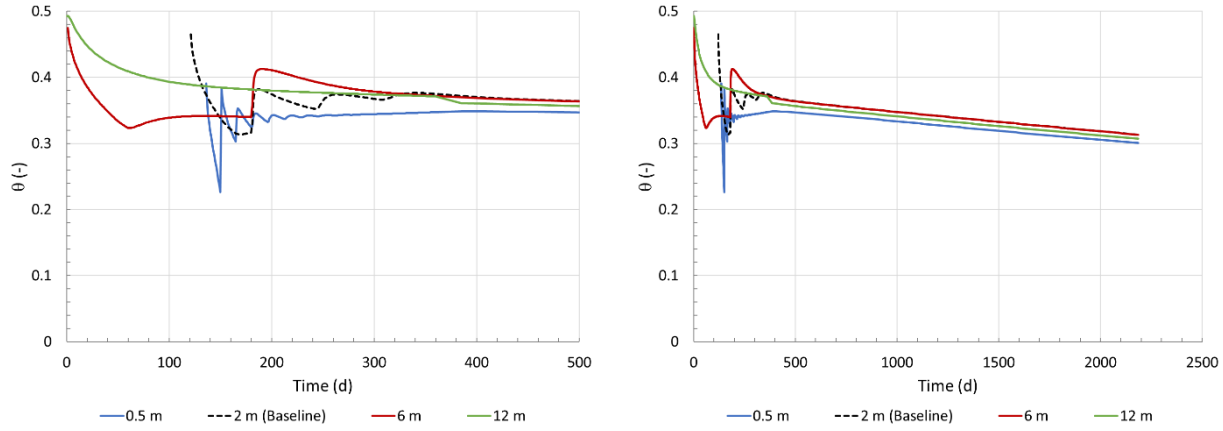

Figure 7.24: Volumetric water content simulated at y = 5 m for varying layer thickness (a) from day 0 to day 500 and (b) from day 0 to day 2185 (deposition + 5 years) (Simulations #1, #4, #5, #6, #7 and #8 - Table 7.1).

The suction in the tailings (y = 5 m) tends to be higher when the layer thickness is smaller since each of the layers is exposed to evaporation before the placement of a fresh tailings layer (Figure 7.25). The exposition time was smaller (more frequent addition of tailings) but sufficient for each layer to lose a significant amount of water to the atmosphere by evaporation (also see Figure 7.26c,

d). The influence of evaporation decreases with depth (as observed also for the baseline model) so thicker layers could protect more efficiently underlying tailings from evaporation (all other things being equal). The simulations for a 12-m thick layer ("instantaneous" deposition in a single layer) showed higher suctions than the other cases (except for 0.5 m thick layers) because there was no regular input of water (through tailings deposition, and apart from precipitation) for one year (see Appendix G for all the results).

(a) Days 0 to 500

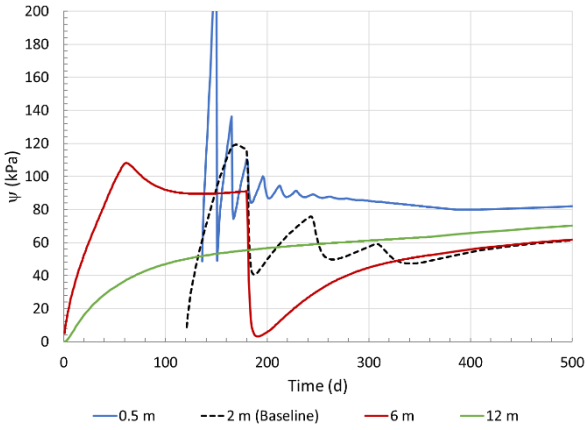

(b) Days 0 to 2185

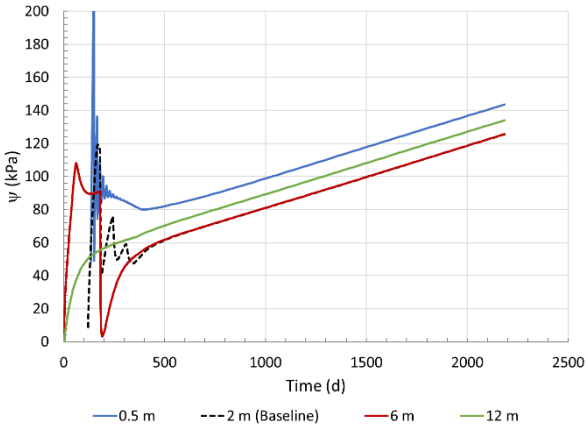

Figure 7.25: Suction simulated at y = 5 m for varying layer thickness (a) from day 0 to day 500 and (b) from day 0 to day 2185 (deposition + 5 years) (Simulations #1, #4, #5, #6, #7 and #8 - Table 7.1).

Flow of water to the underlying subsoil (Σq_y = 0 m) increased when the thickness of the layers increased (Figure 7.26a and b). There was -70 mm infiltration during the active deposition period (< 300 days) for the baseline case (2-m layers). The infiltration into the underlying soil during the active period for the 0.5-m and 1-m layers was 0 mm and -4 mm respectively. Even though the fresh tailings were exposed for a shorter period in the models with thinner layers, it was sufficient to significantly decrease infiltration at the tailings/sand interface (y = 0 m) during the active (deposition) period. The total infiltration for the baseline model (2-m layers) was -164 mm but was -1150 mm for the 12 m thick layer, and only -2 mm, for the 0.5-m layers. The loss of water

due to drainage (Total water outflow at y = 0 m divided by total water (precipitation and pore water) in the model) was 1.5% for the baseline model (2-m layers), 10.3% for the simulation with one 12 m layer, and 0.03% for the simulation with 0.5 m layers after 2185 days of simulation.

The simulated cumulative AE is larger with thinner layers (e.g. 8169 mm in the 1-m layer model vs. 6586 mm in the 12-m layer model). The cumulative AE was 2067 mm during the active deposition period (< 300 days) for the baseline case (2-m). It was 2731 mm and 2563 mm for the 0.5-m and 1-m layer models respectively. When the layer thickness remained 1 m or less, the AE was close to the PE of the model for the duration of the active (deposition) period and drainage could be limited. This could be advantageous if tailings generate contaminated mine drainage since overall drainage into the underlying soil could be minimised by reducing the layer thickness.

(a) Days 0 to 500

(b) Days 0 to 2185

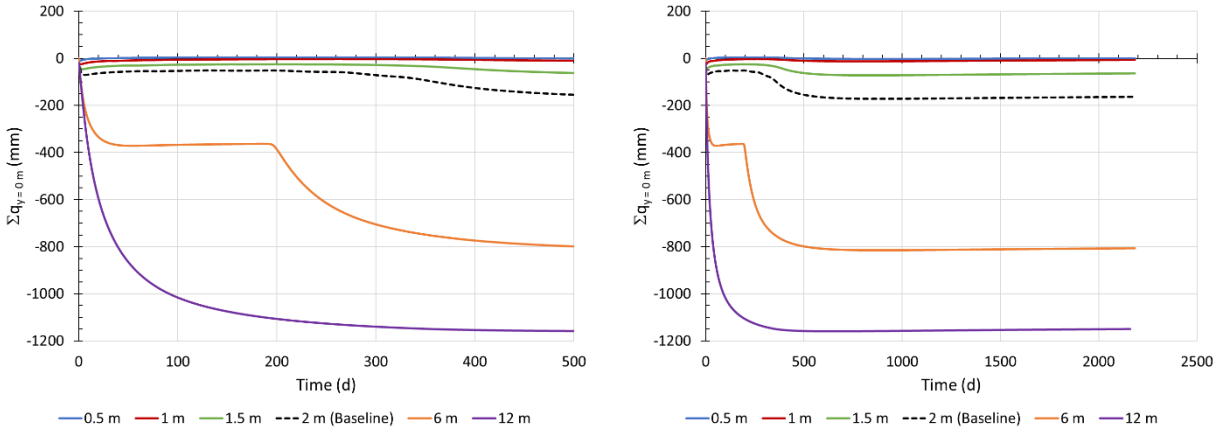

(c) Days 0 to 500

(d) Days 0 to 2185

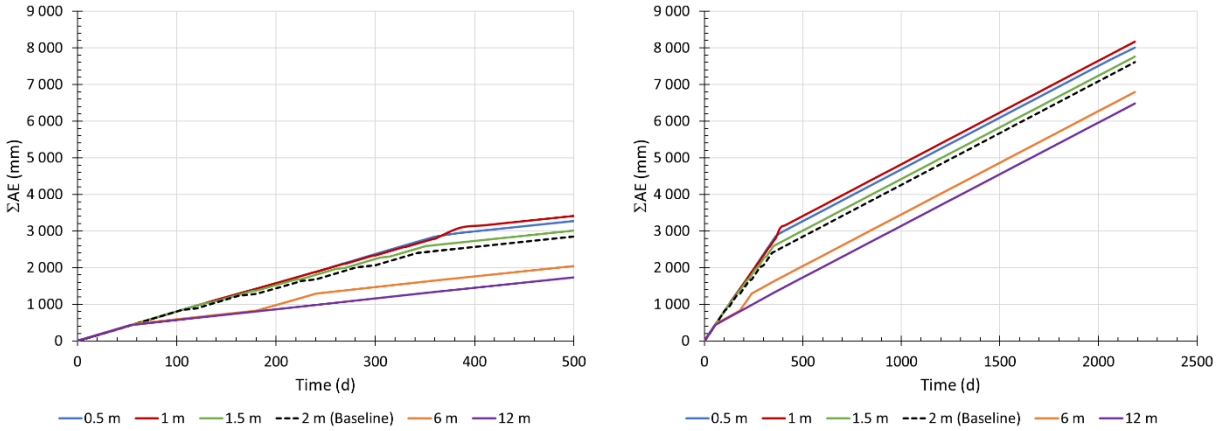

Figure 7.26: (a, b) Total flow and (c, d) total actual evaporation for varying layer thicknesses (Simulations #1, #4, #5, #6, #7 and #8 - Table 7.1).

An increasing layer thickness is associated with a higher desaturation by drainage and a lower total AE at the end of the simulation period (2185 days) (Figure 7.27). Inversely, desaturation through evaporation is greater when the tailings layers were thinner. Drainage was -1150 mm and 0 mm for the 12 m and 0.5 m simulations respectively. The potential cumulative evaporation (ΣPE) is the same for all the numerical simulations (around 1.7×10^4 mm). Most of the desaturation in the

simulations happened by evaporation, and the total AE was between 6486 mm (12-m layer) and 8005 mm (0.5-m layers) (Figure 7.27a).

(a) ΣAE (mm) (b) $\Sigma q_{y = 0\ m}$ (mm)

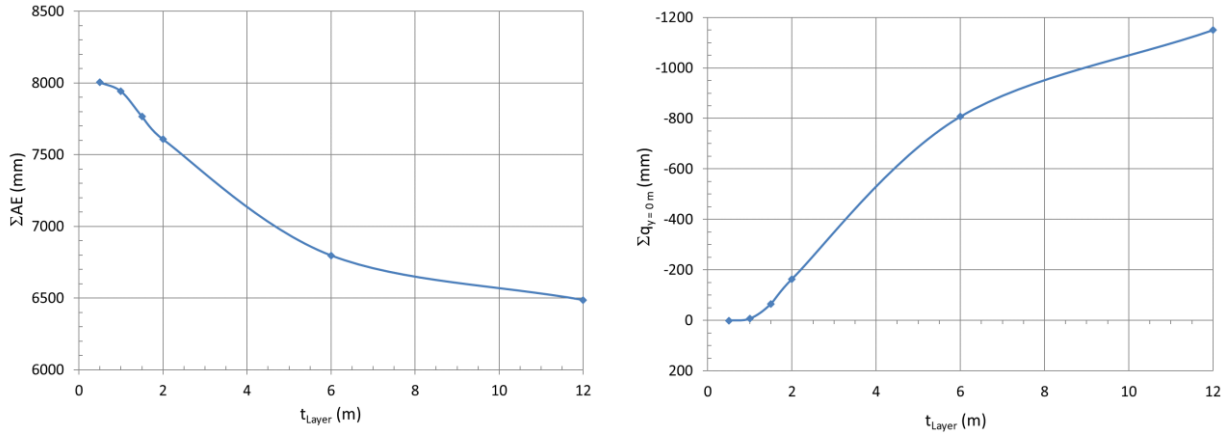

Figure 7.27: (a) Total actual evaporation (ΣAE) and (b) total infiltration into the underlying soil ($\Sigma q_{y = 0\ m}$) for the modelling period (i.e. 2185 days) depending on layer thickness (Simulations #1, #4, #5, #6, #7 and #8 - Table 7.1).

The zero-flux plane (ZFP) in the simulations is located approximately 0.5-1.0 m below the sand/tailings interface at the end of the modelling period (Figure 7.28) for all tailings layer thicknesses. The ZFP position was more variable with thinner tailings layers (0.5 m to 2 m). Because of the longer deposition phases, the position of the ZFP was between the placement of two fresh tailings layers. For example, it is at y = 0.7 m for the 2-m layer simulation after 230 days, and at y = 1.5 m for the 1.5-m layer simulation at the same time.

(a) Days 0 to 500 (b) Days 0 to 2185

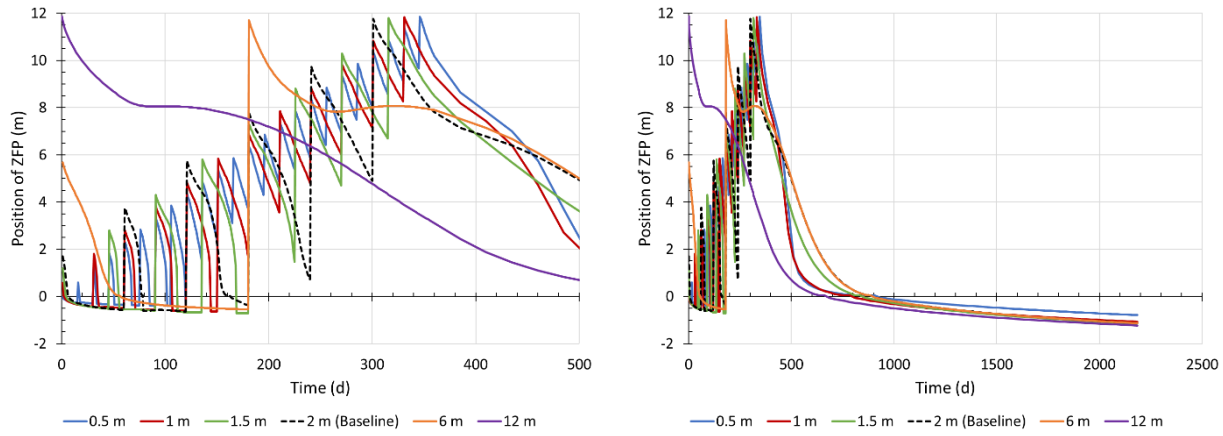

Figure 7.28: Simulated position of the ZFP for the varying layer thickness (a) from day 0 to day 500 (deposition of tailings from day 0 to day 300) and (b) from day 0 to day 2185 (300 days of deposition + 5 years) (Simulations #1, #4, #5, #6, #7 and #8 - Table 7.1).

Table 7.6 gives the time needed for the degree of saturation to attain 85% (t_{85}) in a tailings layer at various elevations (y = 1 m, 3 m, 5 m, 7 m, 9 m and 11 m). The results shown in Figure 7.26(a, b) indicated that the rate of desaturation by drainage increases when the layer thickness increases. It takes less than 10 days to reach a degree of saturation of 85% with the 0.5-m layers model but 35 days or more with the 12-m layer model. In addition, the value of t_{85} decreases as the number of layers increases because the desaturation rate near the surface is more pronounced due to the presence of partially desaturated tailings layers below (as seen in the baseline simulation results, Section 7.1); this increases the overall desaturation rate of a fresh tailings layer placed above.

Table 7.6: Simulated time to attain a degree of saturation (S_r) of 85% (t_{85}) at specific elevations for the varying layer thickness (Simulations #1, #4, #5, #6, #7 and #8 - Table 7.1).

y (m)	t_{85} (d)					
	0.5 m	**1 m**	**1.5 m**	**2 m**	**6 m**	**12 m**
1	9.9	23.1	30.8	43.1	2035.4	1812.2
3	3.6	11.7	23.9	26.2	1448.1	1225.7
5	2.7	10.1	19.0	24.1	37.8	637.7
7	0.0	9.3	13.6	25.4	234.0	263.1
9	0.0	9.4	20.3	23.1	118.5	91.4
11	0.0	9.3	17.2	23.0	39.8	34.8

The influence of the deposition rate on the total oxygen flux (F_{O_2}) is presented in Figure 7.29. The total oxygen flux simulated for each case, over 2000 days, is significantly (several orders of magnitude) higher than the targeted value for the maximum oxygen flux (≈ 40 g/m^2/y or 0.11 g/m^2/d; Aubertin et al., 1999, 2002). The cumulative oxygen flux (e.g. after 500 days – Figure 7.30) slightly increases as the layer thickness increases. It is around 24 kg/m^2 for 0.5-m to 2-m layers, and 34.6 kg/m^2 for the 12-m layer.

(a) Days 0 to 500 (b) Days 0 to 2185

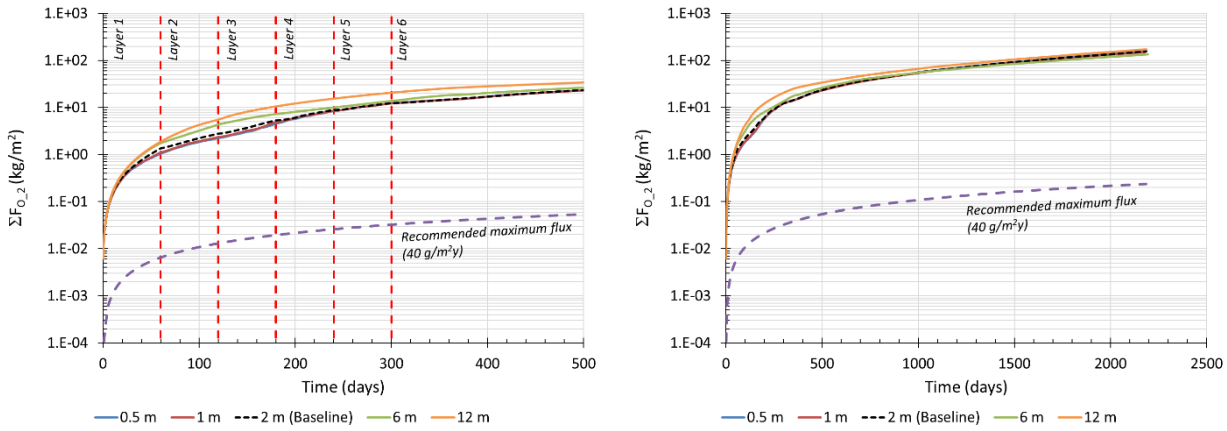

Figure 7.29: Simulated cumulative oxygen flux at the surface of the tailings for varying layer thicknesses (a) from day 0 to day 500 and (b) from day 0 to day 2185 (deposition + 5 years) (Simulations #1, #4, #5, #6, #7 and #8 - Table 7.1).

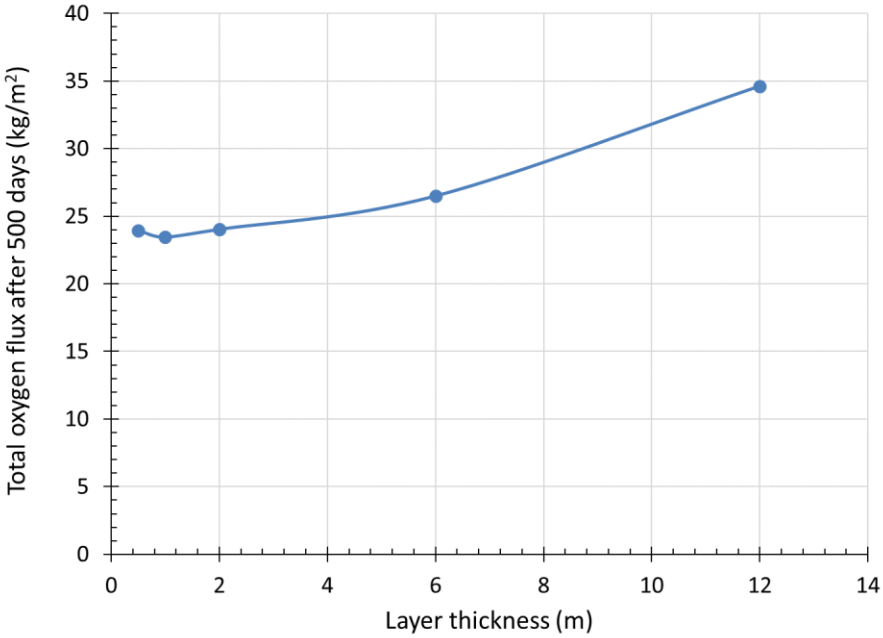

Figure 7.30: Simulated cumulative oxygen flux at the surface of the tailings after 500 days for different tailings layer thicknesses during deposition (Simulations #1, #4, #5, #6, #7 and #8 - Table 7.1).

A higher deposition rate (thinner layers with more frequent depositions) induces a somewhat smaller oxygen flux into the tailings, but this effect is relatively limited for a single year. Shorter deposition cycles contribute to more frequent and regular water addition to the tailings stack, and each fresh (saturated) tailings layer tend to act as a temporary oxygen barrier.

Thinner layers reduce drainage to the underlying sandy soil layer (no drainage with 0.5-m layers, 6-mm drainage with 1 m layers and 164 mm drainage for the baseline, 2-m layers), thus limiting mobility of (contaminated) water. Thinner tailings layers with shorter deposition cycles tend to reduce the average water content and limit drainage into the underlying soil. An operating mine could plan for deposition in thinner layers which would dry by evaporation. By controlling infiltration during the active (deposition) period, generation of contaminated mine drainage could be minimised (for a time, at least). However, this may also favor the production of AMD due to the tailings desaturation near the surface (which could be released following a major precipitation event) and it is preferable to attempt to limit oxidation of the reactive tailings.

7.2.3 Resting time

The time between the deposition of two fresh tailings layers, called herein the resting time, can influence the hydrogeological behaviour of paste tailings. In practice, the resting time depends on the production rate and number of deposition sites (deposition towers in the case of Bulyanhulu mine). A longer resting time promotes drying of the tailings, thus potentially increasing their mechanical strength (e.g. Narvaez et al., 2015). However, this may also expose reactive tailings to oxidation and accelerate AMD generation. The resting time between the deposition of two subsequent layers should therefore be selected to optimize the overall response of the tailings (in terms of strength and oxidation).

The baseline scenario analysed above consisted of six 2-m thick fresh layer of tailings deposited every 60 days (total active period: 300 days). Two alternative cases were also simulated to assess the influence of resting time on the tailings hydrogeological behaviour and risk for AMD generation. The time between the deposition of two layers was reduced to 30 days (total active period: 150 days; Simulation #9; Table 7.1) and doubled to 120 days (total active period: 600 days;

Simulation #10; Table 7.1). The thickness of each new fresh tailings layer remains 2 m in these cases.

The simulated final VWC in the middle of the tailings stack (at y = 5 m) after 6 years is similar (around 0.32) for the three cases, independently of the resting time (Figure 7.31b). However, the VWC during the active deposition phase tends to be higher (around 0.39) when the resting time is shorter (30 days) (average VWC = 0.31). The VWC remained around 0.31 from day 280 to 360 for the longer resting times (120 days) because of a reduction in the positive (evaporation) gradient. Subsequent deposition of fresh tailings layers tends to increase the VWC and reduce the effect of evaporation. Similar results were observed in the tailings at other elevations (Appendix H).

(a) Days 0 to 500 (b) Days 0 to 2185

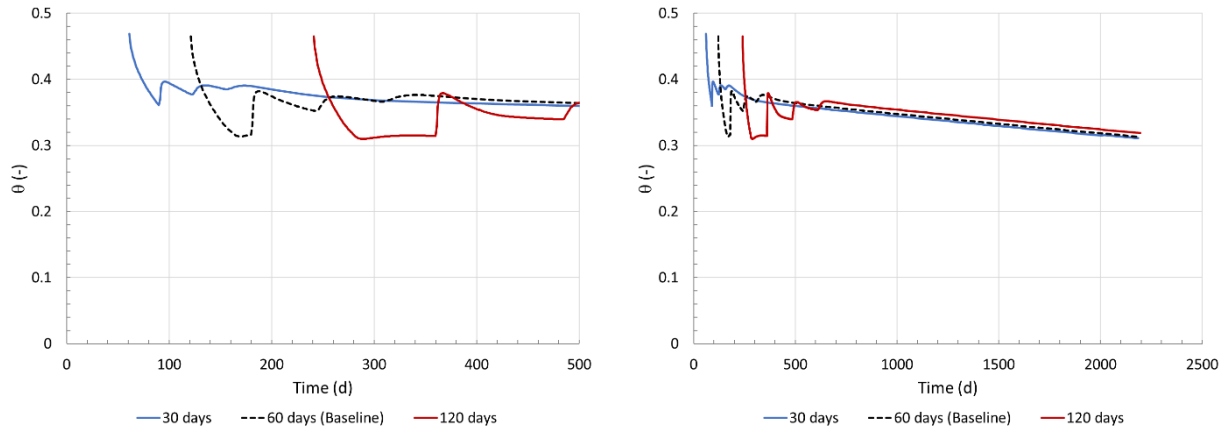

Figure 7.31: Simulated volumetric water content at y = 5 m for varying resting time between the deposition of two layers (a) from day 0 to day 500 and (b) from day 0 to day 2185 (deposition + 5 years) (Simulations #1, #9, and #10 - Table 7.1).

The suction at y = 5 m is between 117 kPa and 128 kPa at the end of the simulations (Figure 7.32). The maximum suction during the active (deposition) period at the beginning of the simulations is similar (around 120-130 kPa) for the two longest resting times (60 days – Active period: 300 days; 120 days – Active period: 600 days). The simulated suction with the 30-day resting time remains below the AEV of the material (ψ_a = 58 kPa) for the complete active (deposition) period (Days 0

to 150) and beyond, i.e. until day 300 (Figure 7.32b). Suction remains above the AEV for most of the other two simulations (60-day and 120-day resting times) (Figure 7.32a) (see Appendix H for all the results).

(a) Days 0 to 500 (b) Days 0 to 2185

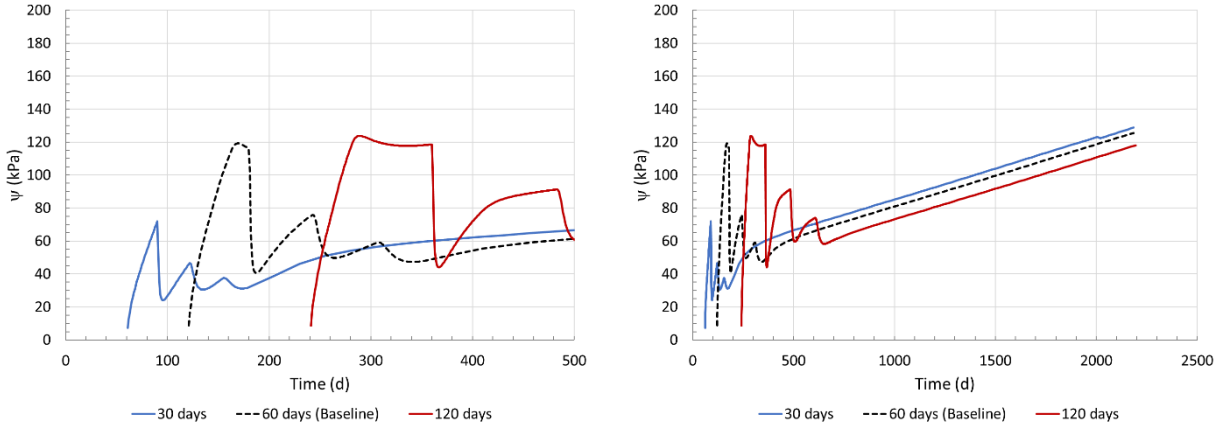

Figure 7.32: Suction at y = 5 m for varying resting time between the deposition of two layers (a) from day 0 to day 500 (deposition of tailings from day 0 to day 300) and (b) from day 0 to day 2185 (deposition + 5 years) (Simulations #1, #9, and #10 - Table 7.1).

The influence of the resting time is more visible when observing the total flow at the tailings/sand interface (Figure 7.33a and b). A total of -457 mm of water drained downward (4.3% of total water) when the resting time was 30 days, and 164 mm and 77 mm (0.6% of total water) of drainage for resting times of 60 and 120 days. The placement of a fresh tailings layer tends to limit the loss of water through evaporation from the underlying tailings layer (Figure 7.33c and d). For example, the cumulative actual evaporation (ΣAE) for the 30-day phase time remained lower than for the 60-day (Baseline) phase time. Limiting loss of water through evaporation (i.e. through shorter phase times) therefore increased the drainage at the bottom of the simulation (at y = 0 m). There is no significant difference in the cumulative AE after day 600 between the 60-day (Baseline) and 120-day resting times.

(a) Days 0 to 500

(b) Days 0 to 2185

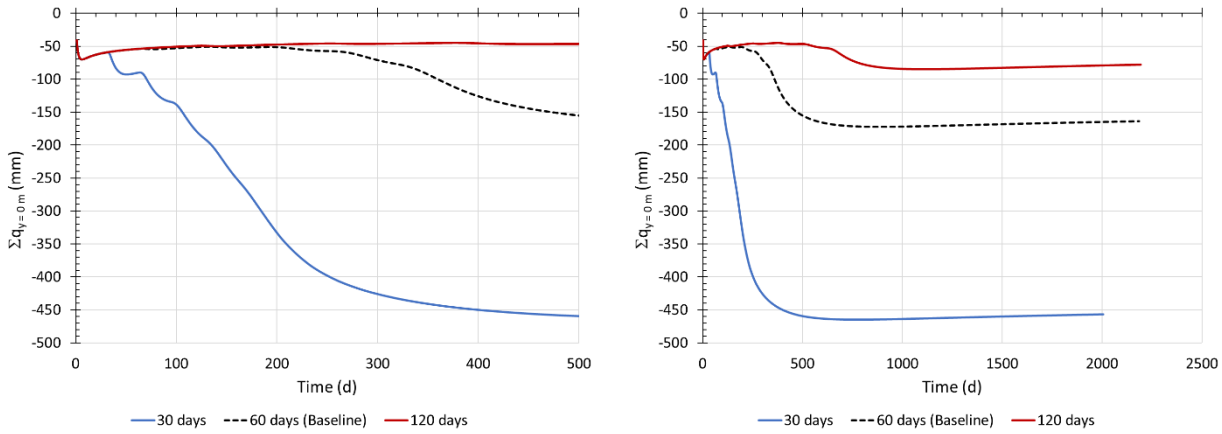

(c) Days 0 to 500

(d) Days 0 to 2185

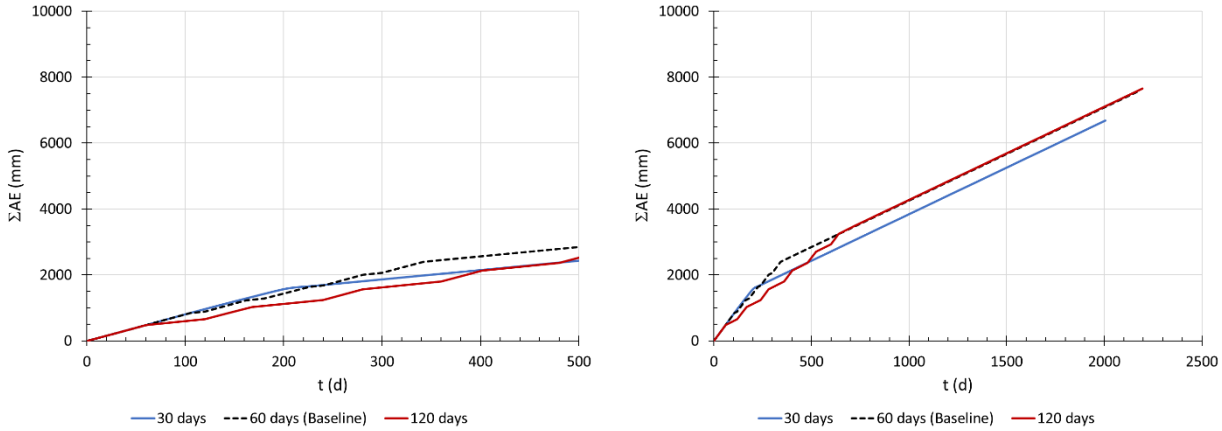

Figure 7.33: (a, b) Cumulative flow and (c, d) cumulative actual evaporation for varying resting time between the deposition of two layers (Simulations #1, #9, and #10 - Table 7.1).

Figure 7.34 presents the cumulative actual evaporation from the tailings stack for each phase. Decreasing the resting time has a major impact on the overall total actual evaporation modeled. The average total actual evaporation per deposition cycle is 409.0±36.2 mm⁄d for the 60-day phase time (Baseline) model. It was 580.0±40.1 mm⁄d and 237.8±6.6 mm⁄d for the 120-day and 30-day resting times simulations respectively.

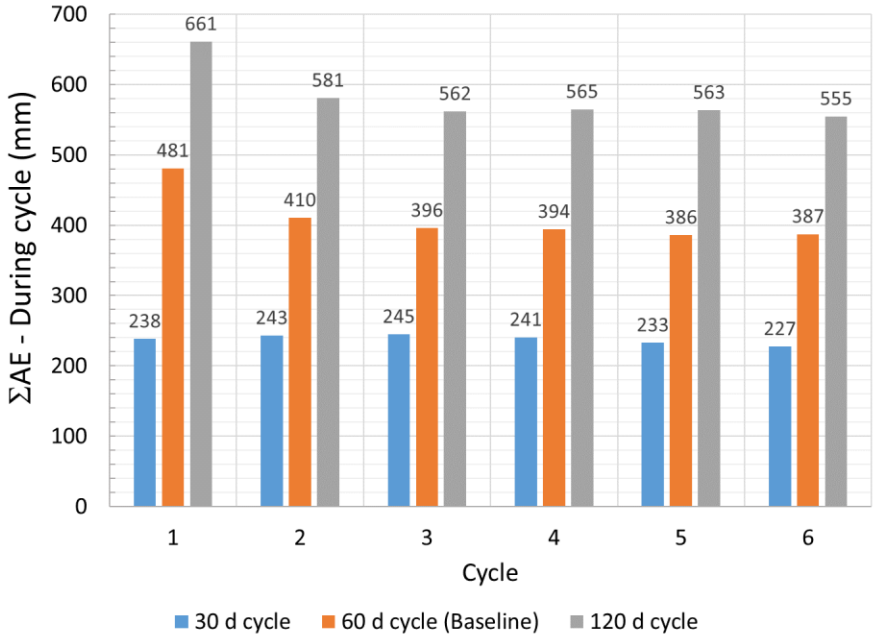

Figure 7.34: Total actual evaporation for each deposition step, for the three studied time intervals (Simulations #1, #9, and #10 - Table 7.1).

The contribution of evaporation to the desaturation of the tailings for the longer resting times is also apparent with respect to the position of the ZFP in the simulation (Figure 7.35). The ZFP is deeper during the active (deposition) period when the phase time is longer. The average elevation (y) of the ZFP within a 30-day resting time was 4.0 m, it was 2.9 m for a 60-day resting time and 1.6 m for a 120-day resting time, during the active period. A deeper ZFP means that a larger volume of tailings is prone to an evaporative gradient and upward flow (which results in a lower outflow from the bottom of the facility).

(a) Days 0 to 500 (b) Days 0 to 2185

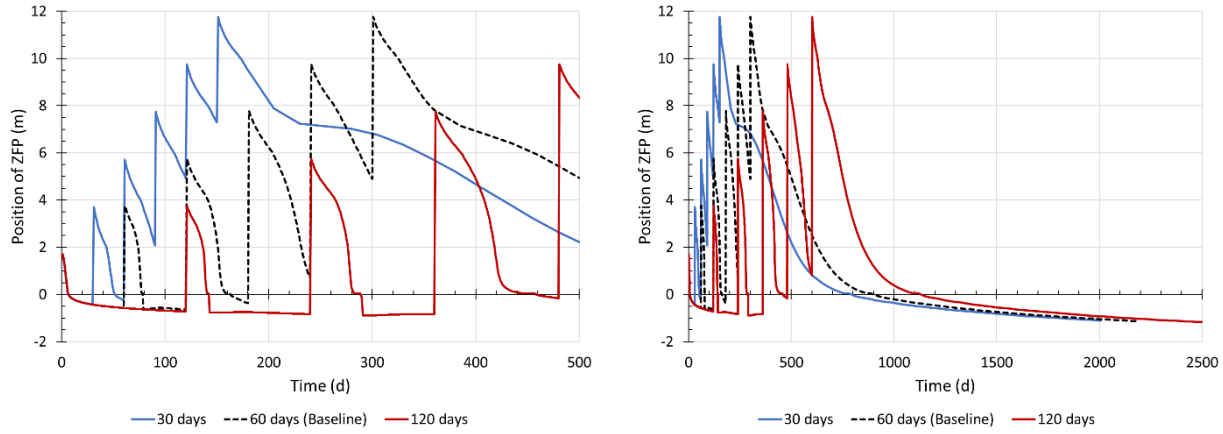

Figure 7.35: Position of the ZFP at y = 5 m for different resting time between the deposition of two layers (a) from day 0 to day 500 (deposition of tailings from day 0 to day 300) and (b) from day 0 to day 2185 (deposition + 5 years) (Simulations #1, #9, and #10 - Table 7.1).

The hydraulic gradient in the baseline simulation was positive (greater than 0, i.e. desaturation is through evaporation) for about 45% of the simulated time after the active deposition phase. The hydraulic gradient was positive 55% of the time in the 120-day resting time simulation and only 23% of the time for the 30-day phase time simulation. Increasing the resting time before the placement of a fresh tailings layer increases desaturation through evaporation (it also tends to decrease infiltration into the underlying subsoil).

The first four layers took more than 200 days to reach a degree of saturation of 85% when the deposition phase was 30 days (Table 7.7). The parameter t_{85} for these phases varied between 1306 days and 30 days (Layers 5 and 6) with 30-day phase times. The parameter t_{85} for the layers 2 to 6 of with 60-day phase times (Baseline simulation) and 120-day phase times was around 25 days.

Table 7.7: Time to attain a degree of saturation (S_r) of 85% (t_{85}) at a depth of 1 m below the tailings surface for different resting times between the deposition of two layers (Simulations #1, #9, and #10 - Table 7.1).

Layer	y (m)	t_{85} (d)		
		30 days	60 days (Baseline)	120 days
1	1	1923.2	43.1	43.1
2	3	1305.9	26.2	24.4
3	5	684.8	24.1	22.7
4	7	217.0	25.4	23.4
5	9	29.9	23.1	22.8
6	11	29.6	23.0	21.7

Figure 7.36 gives the cumulative oxygen flux with respect to the deposition resting time (30, 60, 120 days). The layer thickness is constant for these three simulations (i.e. 2 m). It was observed that a longer phase time would result in a higher cumulative oxygen flux after 500 days.

(a) Days 0 to 500 (b) Days 0 to 2185

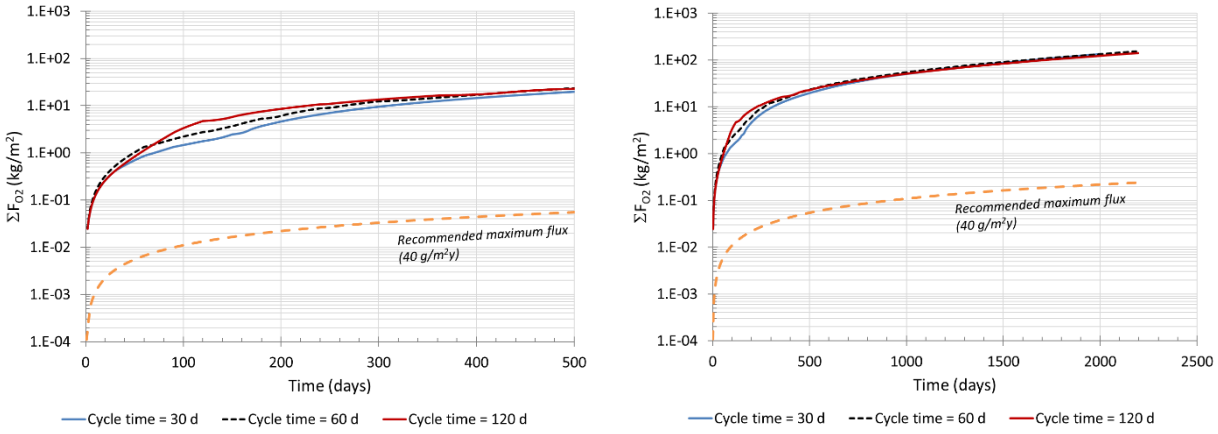

Figure 7.36: Simulated cumulative oxygen flux at the surface for various resting times (a) from day 0 to day 500 (deposition of tailings from day 0 to day 300) and (b) from day 0 to day 2185 (deposition + 5 years) (Simulations #1, #9, and #10 - Table 7.1).

The cumulative oxygen flux tends to be lower for the shorter resting times (Figure 7.37). However, doubling the resting time does not appear to have an important impact on the cumulative oxygen flux, since the tailings already have a sufficiently low degree of saturation in the baseline case (60 days resting time) to allow oxygen fluxes.

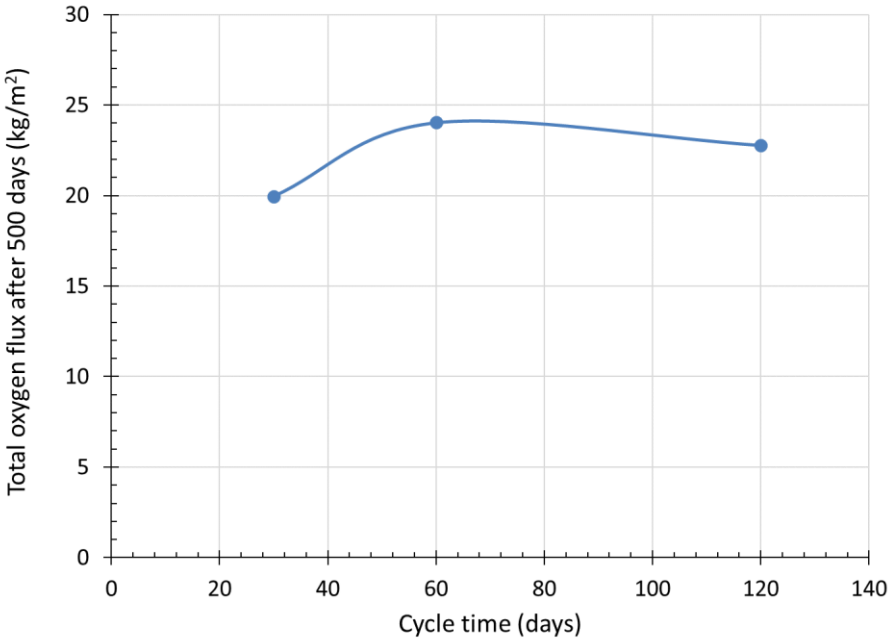

Figure 7.37: Cumulative oxygen flux in the numerical simulations after 500 days depending on the resting time between two layers (Simulations #1, #9, and #10 - Table 7.1).

The shorter resting time tends to increase water drainage at the tailings/sand interface `More frequent addition of fresh tailings layers limits desaturation of the tailings by evaporation during the active (deposition) phase. the shorter resting times also results in lower surface oxygen fluxes (although it was too high in all cases).

7.2.4 Tailings properties

Tailings properties, such as their water retention curve and their hydraulic conductivity, influence the hydrogeological response of a tailings stack. Tailings from two other mining operations were considered in the simulations to assess the effect of their properties on drainage and evaporation in the tailings stack. Tailings from the (former) Osisko mine (now Canadian Malartic mine) (Simulation #11; Table 7.1) and Goldex mine (Simulation #12; Table 7.1) were simulated. Osisko tailings are slightly finer than Bulyanhulu tailings; their characteristics were determined by Narvaez (2013) and Aubertin and Bolduc (2013) (see also Saleh Mbemba, 2010, 2016; L. Bolduc, 2012). Goldex mine tailings are somewhat coarser than Bulyanhulu tailings, based on the properties obtained from Pabst (2011). Table 7.8 presents the parameters of the Fredlund and Xing (1994)

model for these two materials, and Figure 7.38 compares their water retention curves and unsaturated hydraulic conductivity curves; the functions used for the fresh and consolidated tailings used in the baseline simulation are also shown . Simulations were also carried out using consolidated Bulyanhulu tailings (Simulation #13 - Table 7.1) to compare the influence of using two types of tailings (fresh and consolidated, as in the baseline case) to represent the Bulyanhulu tailings in the numerical simulations.

Table 7.8: Fredlund and Xing (1994) CRE model parameters for the Osisko and Goldex tailings used in the numerical simulations; those of the Bulyanhulu tailings are also recalled.

	Bulyanhulu Fresh tailings Simulation #1	**Bulyanhulu Consol. tailings Simulation #11**	**Osisko tailings Simulation #12**	**Goldex tailings Simulation #13**
θ_s (-)	0.49	0.41	0.44	0.38
a_{fx} (kPa)	269	211.8	174	192
n_{fx} (-)	0.8	1.4	1.9	1.0
m_{fx} (-)	2.6	1.9	1.2	2.2
ψ_a (kPa)	23	58	78	31
ψ_r (kPa)	2284	1116	885	1313
k (m/s)	5.2×10^{-7}	1.0×10^{-7}	1.7×10^{-7}	5.0×10^{-7}

The air-entry value (ψ_a) of the Goldex tailings is about 31 kPa, and 78 kPa for the Osisko tailings, which is slightly higher than the value of the consolidated Bulyanhulu tailings (ψ_a = 58.0 kPa determined from the Tempe cell tests -). The WRCs of the Bulyanhulu consolidated and Osisko tailings are similar. The saturated hydraulic conductivity (k_s) of the Osisko and Goldex tailings is 1.7×10^{-7} m⁄s and 5.0×10^{-7} m⁄s respectively (it is 5.2×10^{-7} m⁄s for the fresh Bulyanhulu tailings, and 1.0×10^{-7} m⁄s for the consolidated Bulyanhulu tailings).

(a) Water retention curve (b) Unsaturated hydraulic conductivity

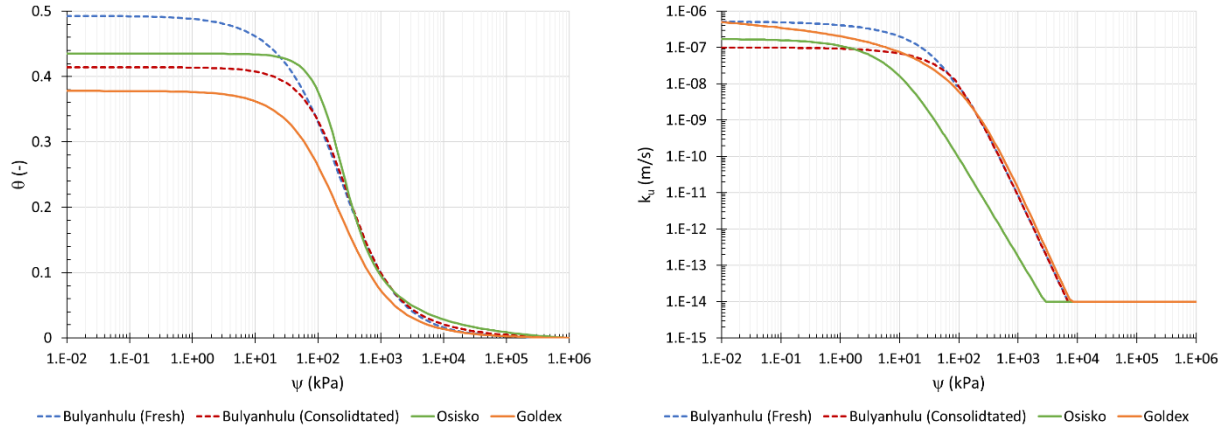

Figure 7.38: (a) Water retention curves and (b) unsaturated hydraulic conductivity functions for the Bulyanhulu, Osisko and Goldex mines tailings (Simulations #1, #11, #12, and #13 - Table 7.1).

The simulated VWC of the baseline and consolidated tailings at y = 5 m is similar and is between (Figure 7.39a). For example, it is 0.34 for the consolidated tailings and 0.37 for the baseline simulation after 500 days. The VWC for the baseline and consolidated tailings simulations also have similar profiles. The VWC at the beginning of the deposition cycles is higher in the baseline simulation because of the higher porosity in the tailings. However, at the end of the simulation phase, the VWC of the baseline simulation was only 0.02 higher than the VWC of the simulation with only the consolidated tailings. There was a significant difference in the VWC for the finer Osisko tailings and coarser Goldex tailings simulations. The VWC of the Osisko tailings was around 0.41 (θ_s = 0.44) at the end of the simulation period. Inversely, the VWC of the Goldex tailings simulation was 0.24 (θ_s = 0.38) (see Appendix J for all the results).

(a) Days 0 to 500 (b) Days 0 to 2185

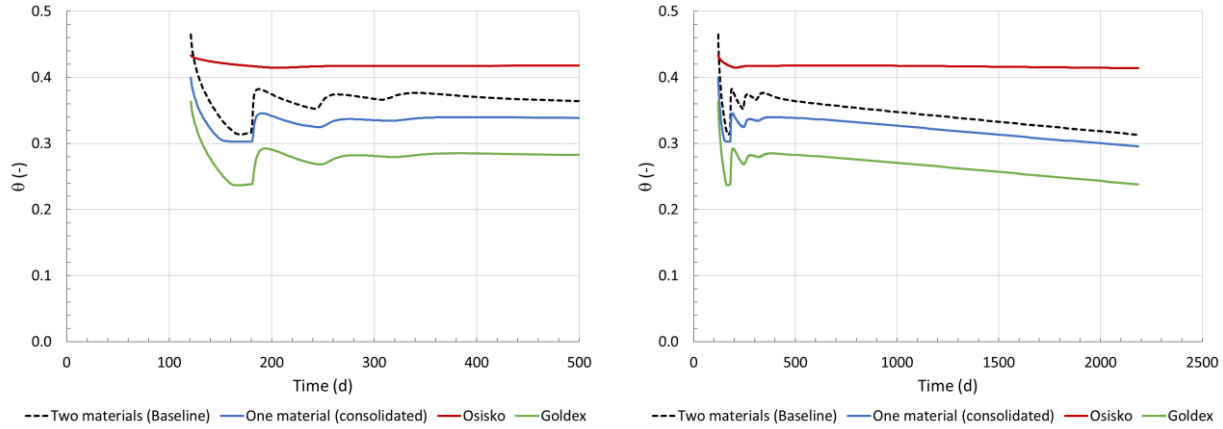

Figure 7.39: Simulated volumetric water content for the different tailings at y = 5 m (a) from day 0 to day 500 (deposition of tailings from day 0 to day 300) and (b) from day 0 to day 2185 (deposition + 5 years) (Simulations #1, #11, #12, and #13 - Table 7.1).

The higher VWC for the Osisko tailings simulation is associated with lower suctions at the end of the simulation period compared to the other three simulated cases (Figure 7.40). The final suction at y = 5 m in the simulation with the Osisko tailings remained constant and below the AEV of the Osisko tailings (ψ_a = 78 kPa). The other three cases (Baseline, consolidated material and Goldex simulations) were more sensitive with a suction that varied during the tailings deposition cycles (decrease at the beginning of the phase and increase afterwards). Except for the Osisko tailings, the suction at y = 5 m in the other three simulations evolved in parallel with the higher suctions being recorded in the Goldex tailings (final suction: 151 kPa) and the lowest suction in the baseline simulation (final suction: 126 kPa) (see Appendix K for all the results).

(a) Days 0 to 500 (b) Days 0 to 2185

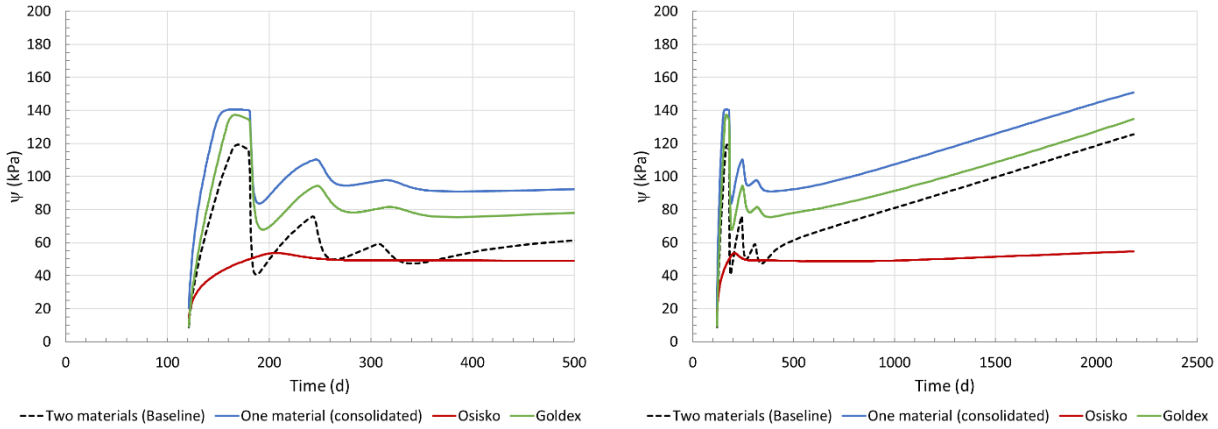

Figure 7.40: Simulated suction for the different tailings properties at y = 5 m (a) from day 0 to day 500 (deposition of tailings from day 0 to day 300) and (b) from day 0 to day 2185 (deposition + 5 years) (Simulations #1, #11, #12, and #13 - Table 7.1).

The cumulative flow at the tailings/sand interface (y = 0 m) is presented in Figure 7.41a. The cumulative flow from the baseline simulation (-164 mm) is much larger than for the other three materials. This is because there is 158 mm more water per layer in the fresh tailings compared to the consolidated tailings (due to the higher porosity of the latter; $n \approx 0.5$ in the fresh tailings vs. $n \approx 0.4$ in the consolidated tailings). The baseline simulation also had more water than the Osisko tailings (986 mm/layer – Baseline simulation vs. 870 mm/layer – Osisko tailings) and the Goldex tailings (756 mm/layer). This underlines the influence of the fresh tailings WRC and the importance of including these tailings in on the infiltration into the underlying soil.

The Osisko tailings (-65 mm) showed higher cumulative infiltration than the Goldex tailings (-12 mm) (Figure 7.41a and b). In addition, there was less evaporation from the finer Osisko tailings (5751 mm after 2185 days), while the other three cases simulated here showed a total AE after 2185 days around 7000 mm (Figure 7.41c and d) (Simulations #1, #11, #12, and #13 - Table 7.1).

(a) Days 0 to 500

(b) Days 0 to 2185

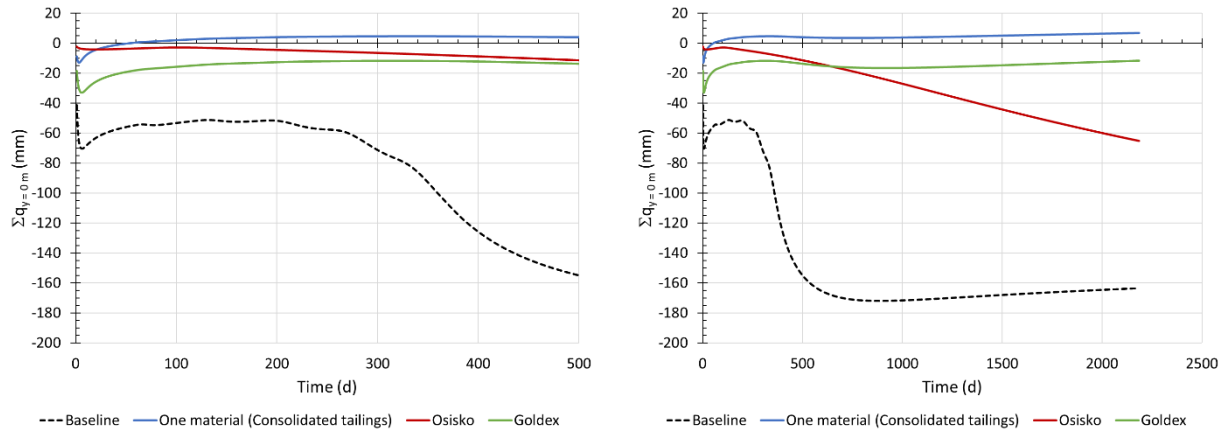

(c) Days 0 to 500

(d) Days 0 to 2185

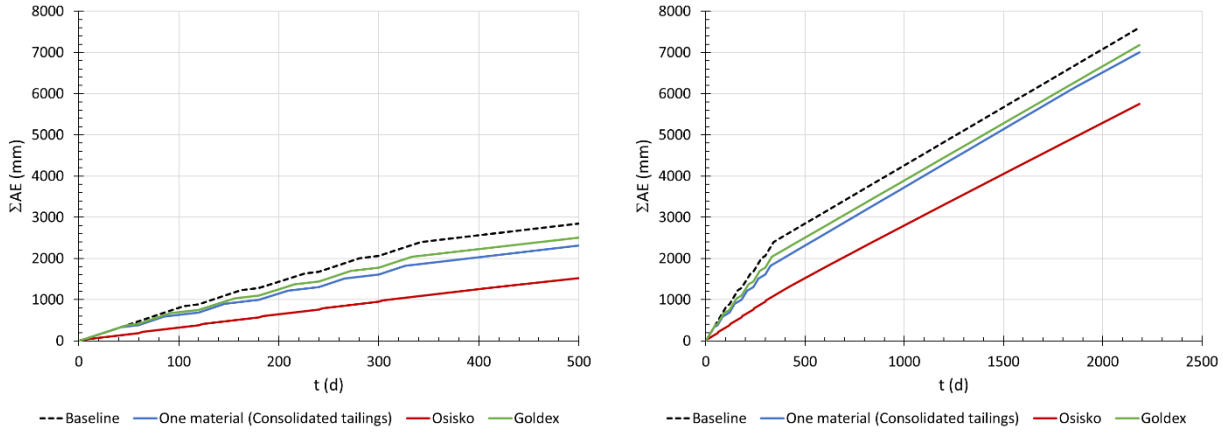

Figure 7.41: (a, b) Cumulative flow at the tailings/sand interface (y = 0 m) and (c, d) total actual evaporation for the varying tailings properties numerical simulations (Simulations #1, #11, #12, and #13 - Table 7.1).

The ZFP of the Osisko tailings is shallower (y ≈ 9 m) (Figure 7.42) because these tailings are less prone to evaporation (Figure 7.41c and d). The position of the ZFP for the three other cases s was similar during the simulation period (Figure 7.42).

(a) Days 0 to 500 (b) Days 0 to 2185

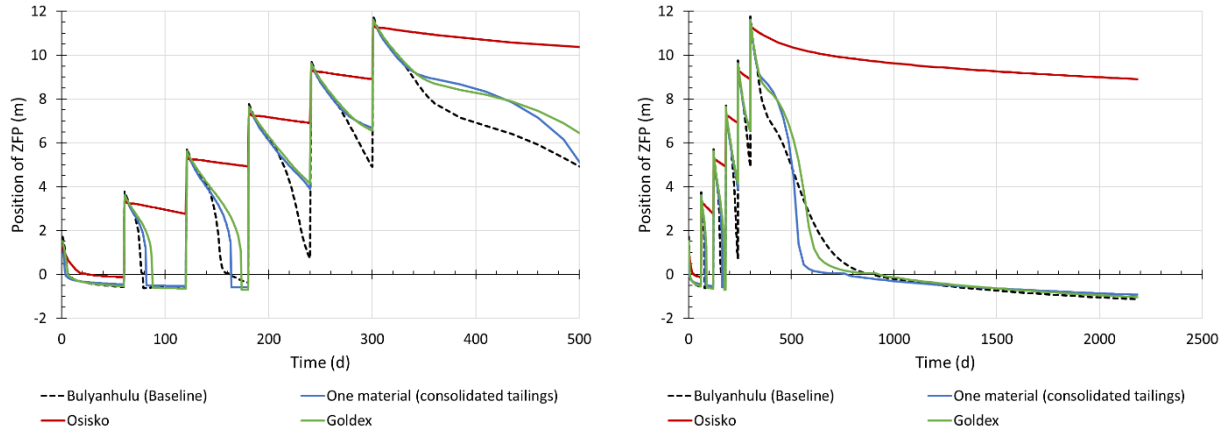

Figure 7.42: Position of the ZFP for the varying tailings properties numerical simulations (a) from day 0 to day 500 (deposition of tailings from day 0 to day 300) and (b) from day 0 to day 2185 (deposition + 5 years) (Simulations #1, #11, #12, and #13 - Table 7.1).

Value of parameter t_{85} was between 10 and 20 days for the simulation with the consolidated Bulyanhulu tailings (compared to 20-40 days for the baseline simulation) (Table 7.9). The simulated degree of saturation 1 m below the surface remained greater than 85% for the first five layers with the Osisko tailings (for 2185 days). Parameter t_{85} (between 5 and 15 days) is slightly lower than that of the baseline simulation for the coarser Goldex tailings.

Table 7.9: Time to attain a degree of saturation (S_r) of 85% (t_{85}) at a depth of 1 m below the tailings surface for the varying tailings properties numerical simulations (Simulations #1, #11, #12, and #13 - Table 7.1).

Layer	y (m)	t_{85} (d)			
		Bulyanhulu	Consolidated tailings	Osisko	Goldex
1	1	43.1	23.5	2185.0[(1)]	17.1
2	3	26.2	8.7	2125.0[(1)]	6.4
3	5	24.1	9.0	2065.0[(1)]	6.8
4	7	25.4	9.3	2005.0[(1)]	6.8
5	9	23.1	8.8	1945.0[(1)]	6.6
6	11	23.0	8.7	1056.6	6.6

[(1)] Layer remains at a degree of saturation (S_r) greater than 85%.

Two parameters appear to influence more significantly the value of parameter t_{85}: the material properties (e.g. the water retention curve) and the amount of pore water in the tailings. When more pore water is in the fresh tailings (i.e. Baseline (fresh Bulyanhulu tailings) simulation) at the beginning of a simulation, the time to attain a degree of saturation of 85% (vs. the consolidated Bulyanhulu tailings scenario) is greater (e.g. the average t_{85} is 24 days for layers 2 to 6 in the baseline simulation and 9 days in the simulation with only the consolidated tailings). Similarly, the WRC also influences the time to reach a degree of saturation of 85%. There is a significant difference in the value of the t_{85} even though the difference between the WRC of the consolidated Bulyanhulu and Osisko tailings is small (the difference between the ψ_a of both materials is roughly 20 kPa). The finer Osisko tailings could remain saturated at higher suctions compared to the Bulyanhulu tailings. Inversely, the coarser Goldex tailings have a lower t_{85} (average of 7 days for layers 2 to 6) The properties of the tailings also influence the outflow at the bottom of the model and the actual evaporation at its surface.

The hydrogeological properties (WRC and k_s) of the tailings thus have a major influence on the desaturation behaviour of a surface paste tailings stack. The water content of the finer tailings tends to remain higher than for the coarser tailings. This can be advantageous if the tailings are reactive

since denser (paste) tailings have a lower initial water content than traditional (slurry) tailings. However, the potentially contaminated porewater from the tailings could eventually drain to the underlying soil (e.g. there was no decrease in the drainage rate from the finer Osisko tailings by the end of the numerical simulation period). To limit this process, an impermeable boundary (with a leachate collection system) could be required at the base of a tailings storage facility

7.2.5 Subsoil properties

The hydrogeological properties of the subsoil can potentially influence infiltration below the tailings storage facility (at y = 0 m), and water distribution in the tailings above. In the baseline scenario, the subsoil is composed of a sandy soil (with $k_{sat} = 10^{-5}$ m⁄s; Section 7.1.1). An alternative scenario is also considered with a subsoil having a lower hydraulic conductivity (Simulation #14 - Table 7.1).

The soil used for this scenario was a Beit Netofa clay. The water retention curve and unsaturated hydraulic conductivity function of this soil are provided by van Genuchten (1980). The air entry value (ψ_a) of the material is 65 kPa ($\alpha_{VG\text{-}Clay} = 0.00152$ cm^{-1}), compared to $\psi_a = 0.8$ kPa for the sand. The saturated hydraulic conductivity (k_s) is 9.5×10^{-9} m⁄s (sand $k_s = 10^{-5}$ m⁄s). Figure 7.43 shows the water retention curves (Figure 7.43a) and the unsaturated hydraulic conductivity curves (Figure 7.43b) for these two materials (used to simulate the underlying soil). The WRC and unsaturated hydraulic conductivity of the clay were defined in Vadose/W using the parameters presented in van Genuchten (1980) ($\alpha_{VG} = 0.00152$ cm^{-1}; $n_{VG} = 1.17$; $m_{VG} = 0.15$).

(a) (b)

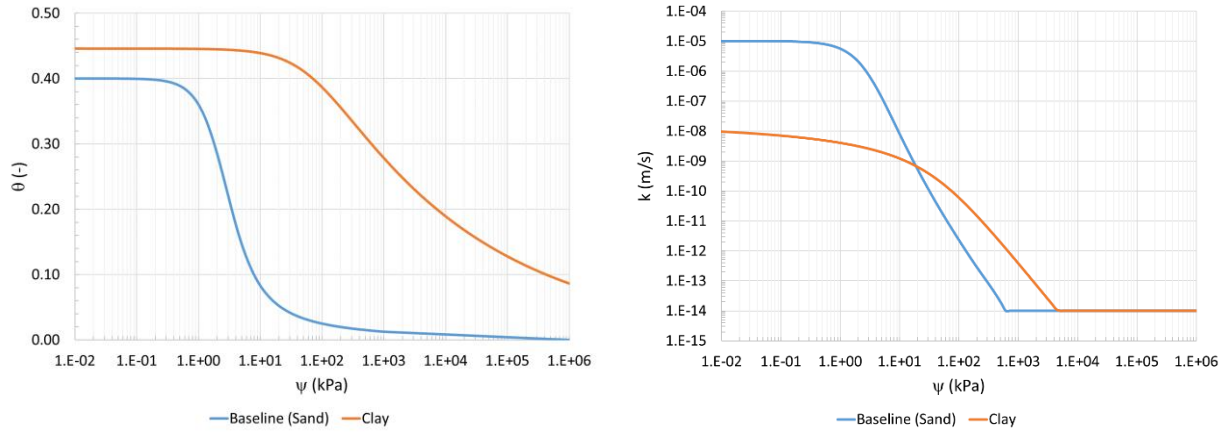

Figure 7.43: (a) Water retention curves and (b) unsaturated hydraulic conductivity functions of the Beit Netofa clay (van Genuchten, 1980) and of the sandy soil (defined with the Fredlund and Xing (1994) model) used in the numerical simulations (Simulations #1 and #14 - Table 7.1).

Simulation results indicate that the VWC (Figure 7.44) and suction (Figure 7.45) in the tailings at y = 5 m during the simulation period were almost identical for both models. There was not a significant difference with a clayey subsoil compared to the baseline simulation (sandy soil) (see Appendices L and M for all the results).

(a) Days 0 to 500 (b) Days 0 to 2185

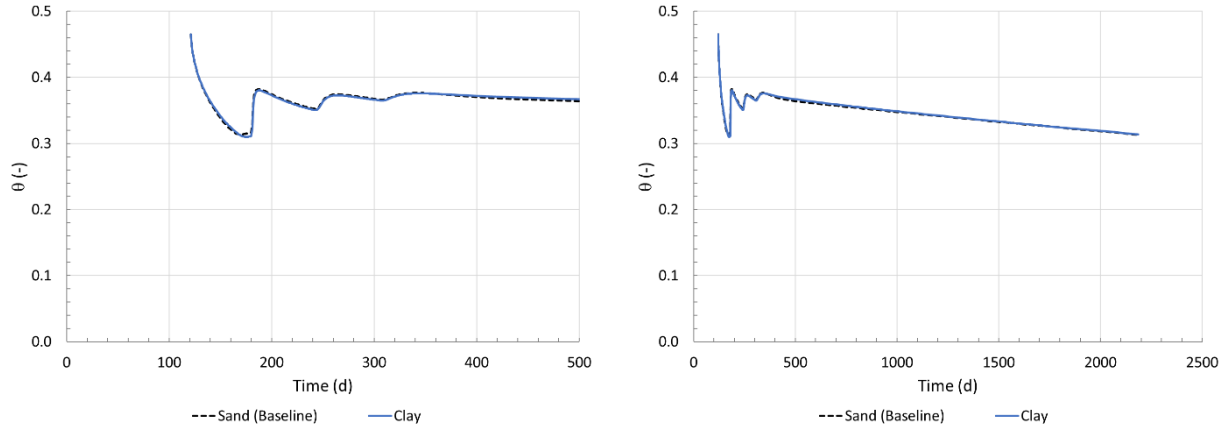

Figure 7.44: Simulated volumetric water content for the two underlying soils at y = 5 m (a) from day 0 to day 500 (deposition of tailings from day 0 to day 300) and (b) from day 0 to day 2185 (deposition + 5 years) (Simulations #1 and #14 - Table 7.1).

(a) Days 0 to 500 (b) Days 0 to 2185

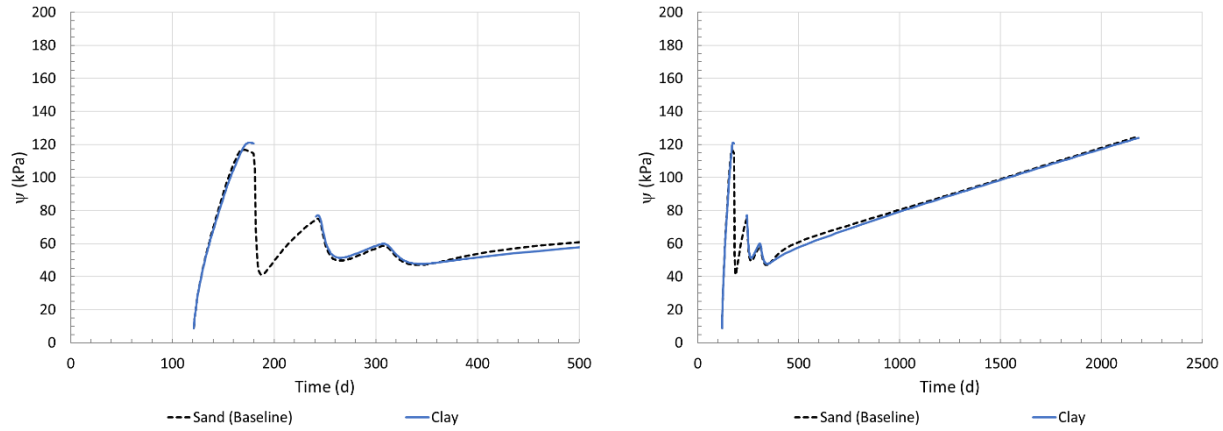

Figure 7.45: Simulated suction for the two underlying soil properties at y = 5 m (a) from day 0 to day 500 (deposition of tailings from day 0 to day 300) and (b) from day 0 to day 2185 (deposition + 5 years) (Simulations #1 and #14 - Table 7.1).

The cumulative flow at y = 0 m in the simulation with the clay foundation (Simulation #14 - Table 7.1) is -132 mm (it is -164 mm for the baseline simulation with the sand); this represents 1.2% of the total water (ratio between cumulative flow at y = 0 m, and cumulative pore water and precipitation during the simulation period) available in the numerical simulation whereas it is 1.5% for the baseline simulation (Figure 7.46a and b). The cumulative actual evaporation (ΣAE) for both simulations is almost the same (Baseline with sand: 7607 mm; clay foundation: 7622 mm) (Figure 7.46c and d).

(a) Days 0 to 500

(b) Days 0 to 2185

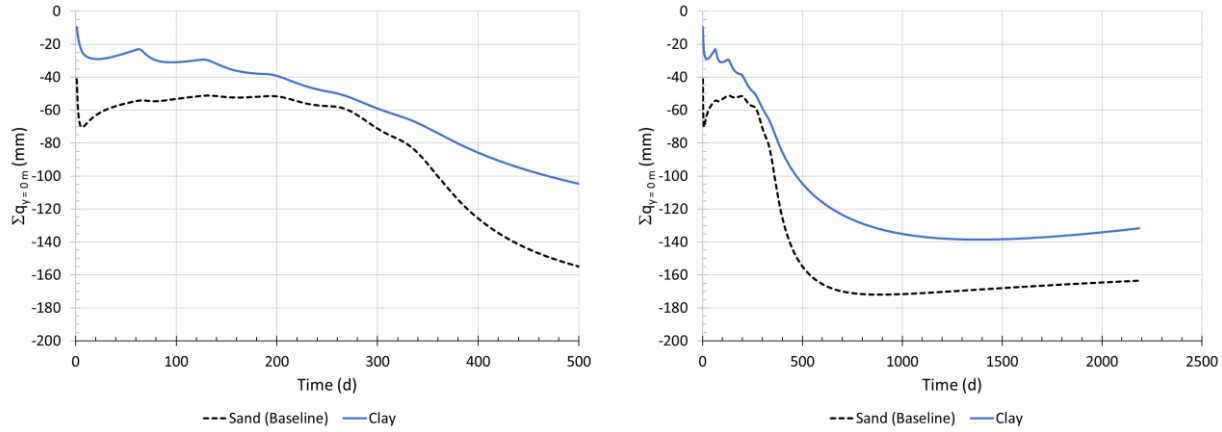

(c) Days 0 to 500

(d) Days 0 to 2185

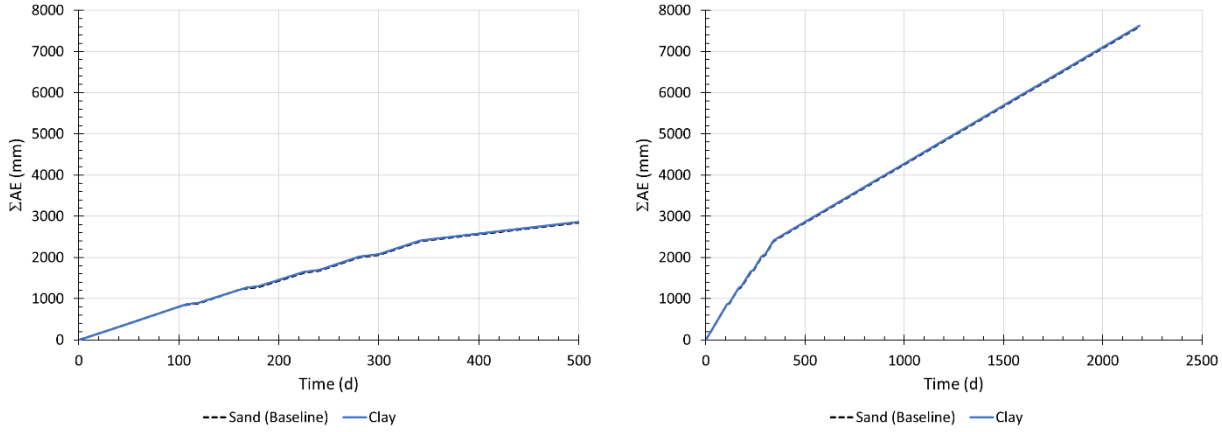

Figure 7.46: (a, b) Simulated cumulative flow and (c, d) cumulative actual evaporation for the two subsoil properties (Simulations #1 and #14 - Table 7.1).

The position of the ZFP given by the simulations is practically identical during the active period (up to day 360) (Figure 7.47). It decreases slightly more rapidly in the baseline simulation but the final position of the ZFP is almost the same at the end of both simulations (Sand: y_{ZFP} = -1.1 m; Clay: y_{ZFP} = -1.0 m).

(a) Days 0 to 500 (b) Days 0 to 2185

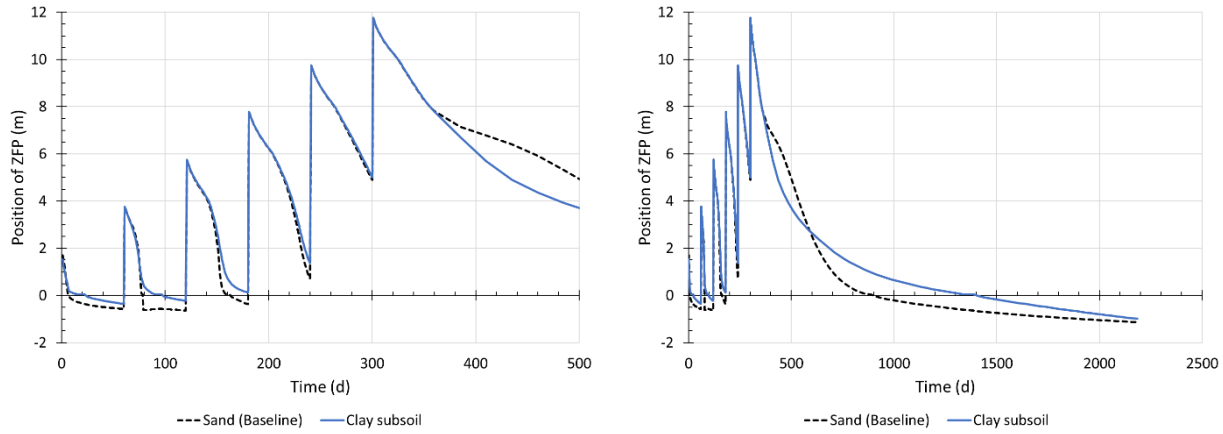

Figure 7.47: Position of the ZFP given by the simulations for both underlying soils numerical simulations (a) from day 0 to day 500 (deposition of tailings from day 0 to day 300) and (b) from day 0 to day 2185 (deposition + 5 years) (Simulations #1 and #14 - Table 7.1).

The values of the parameter t_{85} is about the same in Layers 2 to 6 (Table 7.10). The simulated time to attain a degree of saturation of 85% in Layer 1 is 43.1 days for the sandy subsoil simulation and 48.6 days for the clayey subsoil. The desaturation rate with the clayey subsoil is somewhat smaller because desaturation in Layer 1 in limited by the lower hydraulic conductivity of the clay.

Table 7.10: Time to attain a degree of saturation (S_r) of 85% (t_{85}) at a depth of 1 m below the tailings surface for the two subsoils properties used in the numerical simulations (Simulations #1 and #14 - Table 7.1).

Layer	y (m)	t_{85} (d)	
		Sand (Baseline)	Clay
1	1	43.1	48.6
2	3	26.2	28.7
3	5	24.1	25.1
4	7	25.4	24.6
5	9	23.1	22.9
6	11	23.0	22.8

The simulations presented above confirm that the hydrogeological properties (WRC and k) of the foundation material on which a paste tailings storage facility is built may influence water flow and desaturation t the tailings stack. A clayey subsoil tends to decrease the infiltration of process water from the tailings into the underlying soil (compared to the baseline simulation - sandy subsoil). However, the effect of the hydrogeological properties of the underlying soil is limited in these simulations because moisture flow is largely controlled by the high potential evaporation rate (7.9 mm⁄d or $\Sigma PE = 1.7\times10^4$ mm for the simulation period - 2185 days), which favors desaturation of the tailings (through evaporation). The influence of the underlying soil could be more pronounced for a climate with a lower potential evaporation rate. In any case, an impermeable liner with a leachate collection system should be placed at the bottom of a tailings storage facility that may produce AMD (or CND).

7.2.6 Depth of the water table

Another parameter that may affect moisture distribution and movement in the tailings and underlying soil o is the depth of the water table (WT), which influences the pore water pressure (suction) profile and related hydraulic gradient. The water table is located 12 m below the surface of the soil (y = -12 m) in the baseline simulation (Simulation #1 - Table 7.1). Five alternative

scenarios were simulated also: WT at y = -6 m (Simulation #15), -3 m (Simulation #16), -2 m (Simulation #17), -1 m (Simulation #18) and 0 m (Simulation #19). The position of the water table is fixed (constant) during the whole period (2185 days); there is no seasonal variations in these simulations (as may sometimes be observed in the field).

The simulated VWC and suction in the tailings stack during the simulation is identical for a WT depth varying between -12 m to -2 m (Figure 7.48a, b and Figure 7.49a, b). The VWC in the tailings was somewhat higher, i.e. above 0.3, when the WT is closer to the surface (y = -1 m and 0) (Figure 7.48) (see Appendix N for all the results).

(a) Days 0 to 500

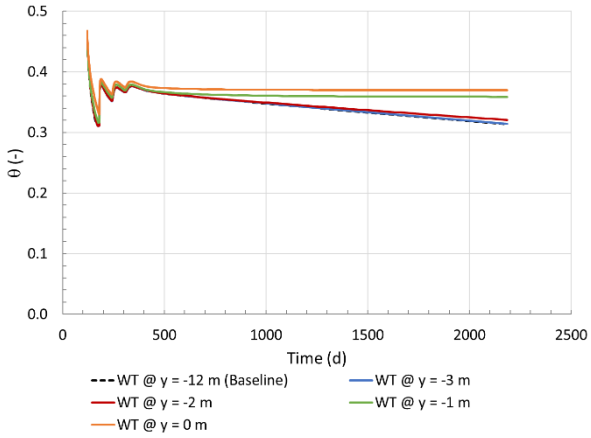

(b) Days 0 to 2185

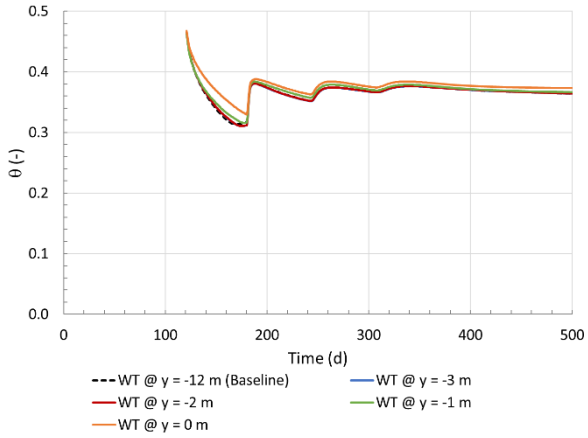

Figure 7.48: Simulated volumetric water content for the varying water table depths at y = 5 m (a) from day 0 to day 500 (deposition of tailings from day 0 to day 300) and (b) from day 0 to day 2185 (deposition + 5 years) (Simulations #1, #15, #16, #17, #18 and #19 - Table 7.1).

The suction at y = 5 m is less than the AEV when the WT is below 1 m from the sand/tailings interface (Figure 7.49). For WT depths of 2 m to 12 m, the suction profile is almost identical (see Appendix O for all the results).

(a) Days 0 to 500 (b) Days 0 to 2185

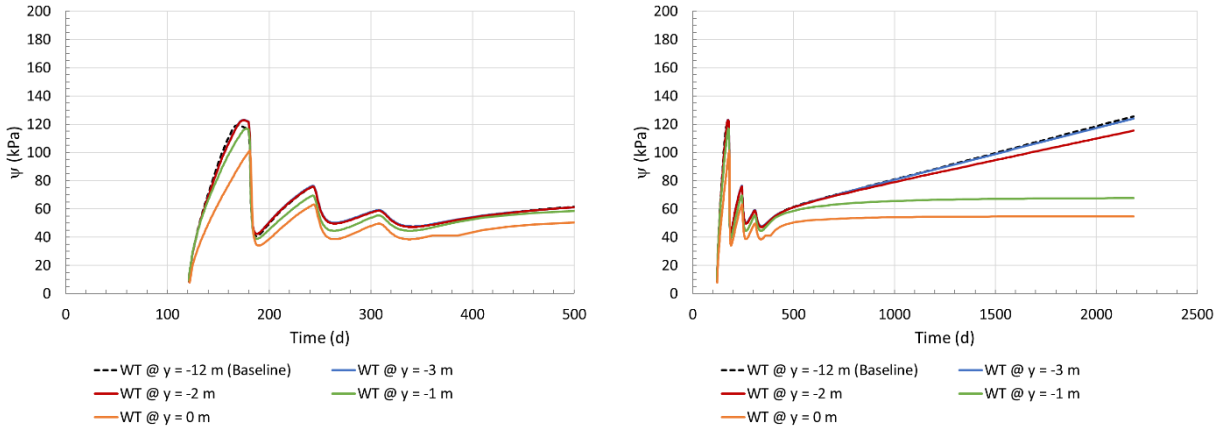

Figure 7.49: Simulated suction for the varying water table depths at y = 5 m (a) from day 0 to day 500 (deposition of tailings from day 0 to day 300) and (b) from day 0 to day 2185 (deposition + 5 years) (Simulations #1, #15, #16, #17, #18 and #19 - Table 7.1).

The simulated total flow (Σq_y = 0 m) is almost the same until day 1000 (Figure 7.50a) when the depth of the water table varies between y = -12 m and y = -2 m, There is upwards flow of +39.0 mm when the water table is 1 m below the ground surface (Simulation WT @ y = -1 m in Figure 7.50a and b) and +442.6 mm at a WT position y = 0 m. The hydraulic gradient (i) is upwards when the total flow is positive, and groundwater from the WT in the soil migrates through the tailings (because of evaporation). The total actual evaporation (Figure 7.50c and d) is almost identical for all cases simulated here.

(a) Days 0 to 500

(b) Days 0 to 2185

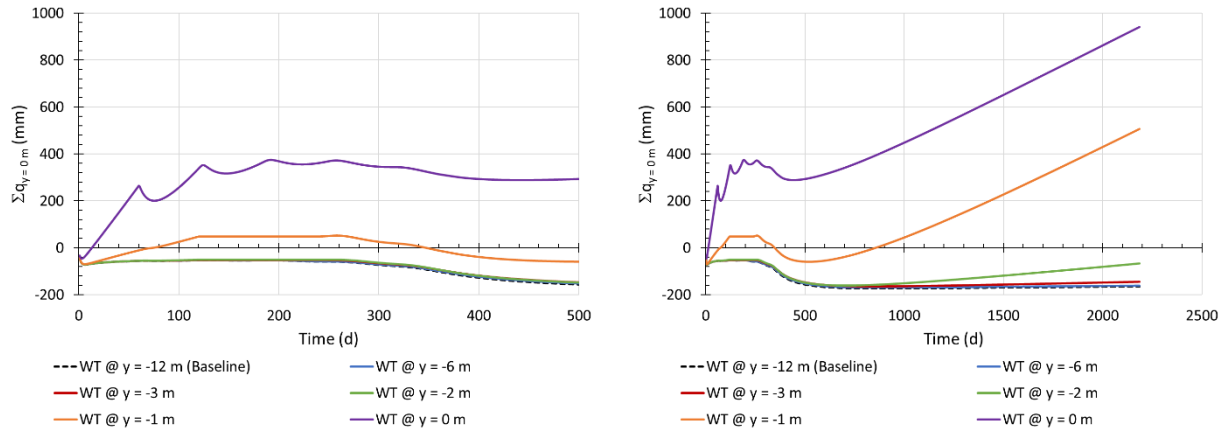

(c) Days 0 to 500

(d) Days 0 to 2185

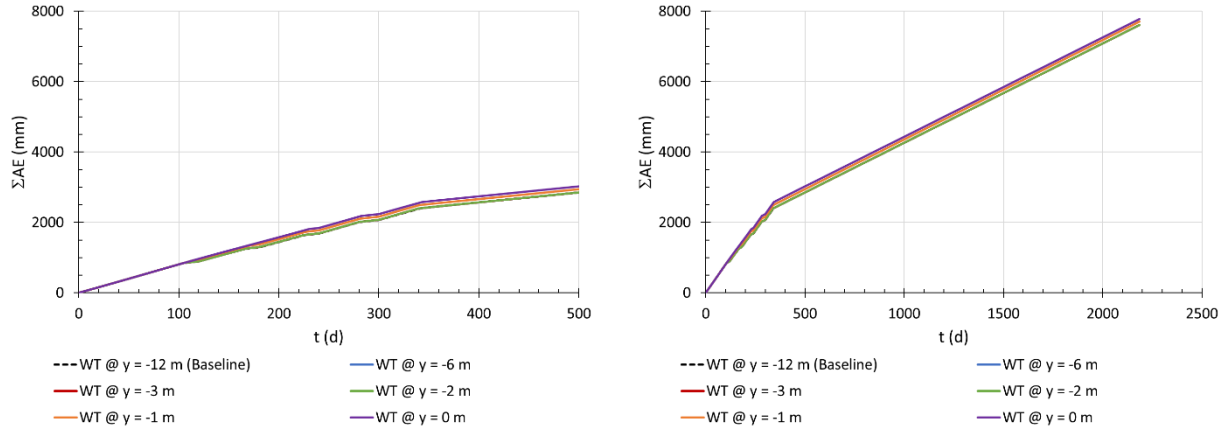

Figure 7.50: (a, b) Simulated total flow and (c, d) total actual evaporation for the varying water table depths (Simulations #1, #15, #16, #17, #18 and #19 - Table 7.1).

The position of the ZFP is about the same for all the simulations and the water table doesn't appear to influence this parameter (Figure 7.51). The ZFP cannot be lower than the WT (e.g. it remains at y = 0 m after day 800 when the WT is at 0 m - Figure 7.51).

(a) Days 0 to 500 (b) Days 0 to 2185

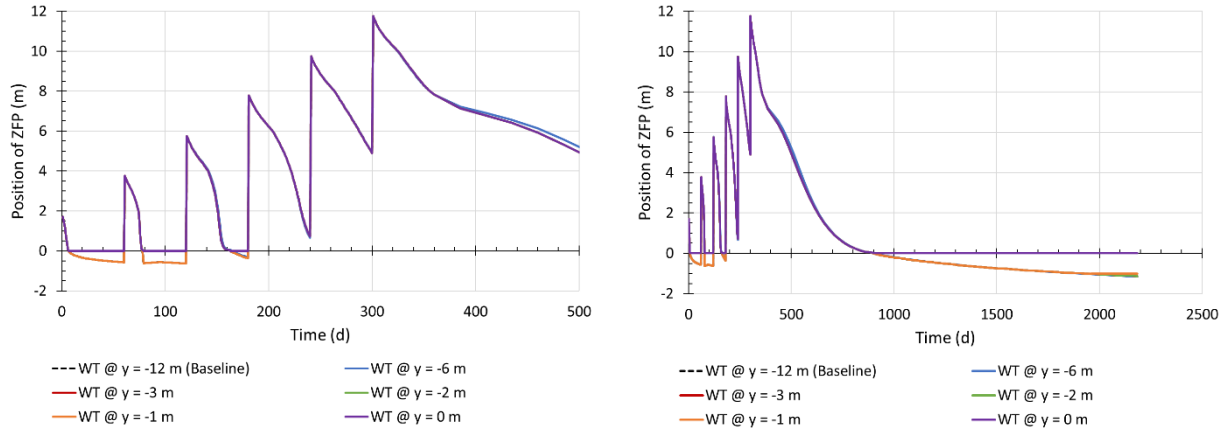

Figure 7.51: Position of the ZFP for the varying water table position given by the simulations (a) from day 0 to day 500 (deposition of tailings from day 0 to day 300) and (b) from day 0 to day 2185 (deposition + 5 years) (Simulations #1, #15, #16, #17, #18 and #19 - Table 7.1).

The value of the parameter t_{85} was almost the same when the position of the water table was at y = -2 m was small, and it was less than 1 day for each of the layers regardless of the elevation of the water table (Table 7.11). The difference becomes more significant when the water table is at the surface of the soil (y = 0 m). In the latter case, the bottom tailings layers (layers 1 and 2) show a degree of saturation (S_r) greater than 85% until the end of the simulation period (for 2185 days for Layer 1 and 2125 days for layer 2). However, the value of parameter t_{85} was less than 5 days between the baseline model for layers 4, 5 and 6. This indicate that when a layer desaturates by drainage (e.g. layer 1 in these simulations), a deeper water table tends to increase the drainage rate (associated with an increased suction at the foundation soil surface). However, when evaporation is the main driver for desaturation, the depth of the water table does not influence desaturation of top tailings layers as significantly (e.g. Layer 6 in these simulations).

Table 7.11: Time to attain a degree of saturation (S_r) of 85% (t_{85}) at a depth of 1 m below the tailings surface for the various simulated water table depths (Simulations #1, #15, #16, #17, #18 and #19 - Table 7.1).

Layer	y (m)	t_{85} (d)					
		WT @ y = -12 m (Baseline)	**WT @ y = -6 m**	**WT @ y = -3 m**	**WT @ y = -2 m**	**WT @ y = -1 m**	**WT @ y = 0 m**
1	1	43.1	43.0	43.0	43.1	49.2	2185.0
2	3	26.2	26.2	26.2	26.2	35.6	2125.0
3	5	24.1	25.2	25.2	25.3	27.9	41.1
4	7	25.4	24.8	24.8	24.9	26.4	29.0
5	9	23.1	23.1	23.1	23.1	23.8	24.6
6	11	23.0	22.5	22.5	22.6	22.9	23.8

(1) Layer remains at a degree of saturation (S_r) greater than 85%.

In summary, the depth of the water table influences the infiltration in the subsoil, and desaturation of a surface paste tailings stack. The depth of the water table has a negligible effect on the tailings desaturation close to the surface when the WT is below a certain depth (i.e. y = -2 m, for the simulations presented above). One of the factors not accounted for in these simulations is that the influence of the TSF on the overall hydrogeological regime and, consequently, on the position of the water table (which may change during and after the operation of a TSF).

7.2.7 Potential evaporation rate

The evaporation rate, related to climatic conditions, can influence the moisture distribution in the tailings and the cumulative flow at the sand/tailings interface ($\Sigma q_{y=0\ m}$). The potential evaporation (PE) rate was estimated by Vadose/W in the models presented in Section 7.1.2. In this section, the PE rate was fixed (Simulation #20: 0.5 mm/d, Simulation #21: 1 mm/d, Simulation #22: 2 mm/d, Simulation #23: 5 mm/d, Simulation #24: 10 mm/d - Table 7.1) to estimate more directly its impact on the field paste tailings simulation. The results from the fixed PE model are compared here with

those from the simulation using Bulyanhulu monthly climatic conditions (Simulation #2 - Table 7.1).

The VWC at y = 5 m is between 0.35 and 0.40 for the simulation period (2185 days) when the PE is 2 mm/d or smaller (Figure 7.52); these values did not seem to be enough to desaturate the column after the active (deposition) period (as was observed in the baseline simulation). The changes in the VWC seems to follow seasonal phases when the PE is lower than 2 mm/d. The VWC at y = 5 m would decrease to a value between 0.31 (PE = 5 mm/d) and 0.33 (PE = 10 mm/d) for the models with a higher PE (i.e. 5 mm/d and larger). It did not appear that the change in the VWC would decrease at the end of the 2185 days simulation period.

(a) Days 0 to 500

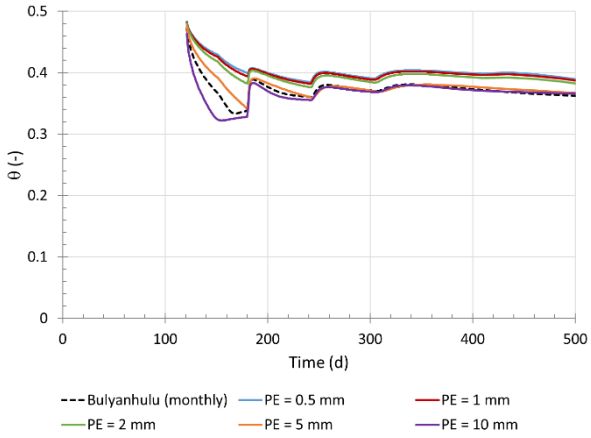

(b) Days 0 to 2185

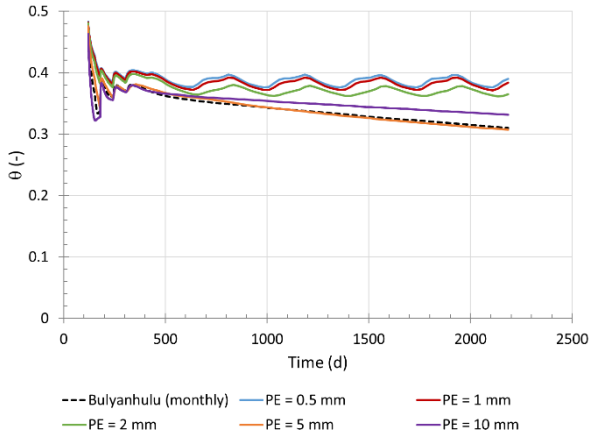

Figure 7.52: Simulated volumetric water content for the varying PE rate numerical simulations at y = 5 m (a) from day 0 to day 500 (deposition of tailings from day 0 to day 300) and (b) from day 0 to day 2185 (deposition + 5 years) (Simulation #2, #20, #21, #22, #23, #24 - Table 7.1).

The suction (ψ) at y = 5 m remained below or close to the AEV when the PE was equal or less than 2 mm/d, and it was constant for the duration of the simulation period (Figure 7.53). The higher PE rates caused a higher suction during the active (deposition) period and an increase with no upper boundary after 2185 days (6 years).

(a) Days 0 to 500 (b) Days 0 to 2185

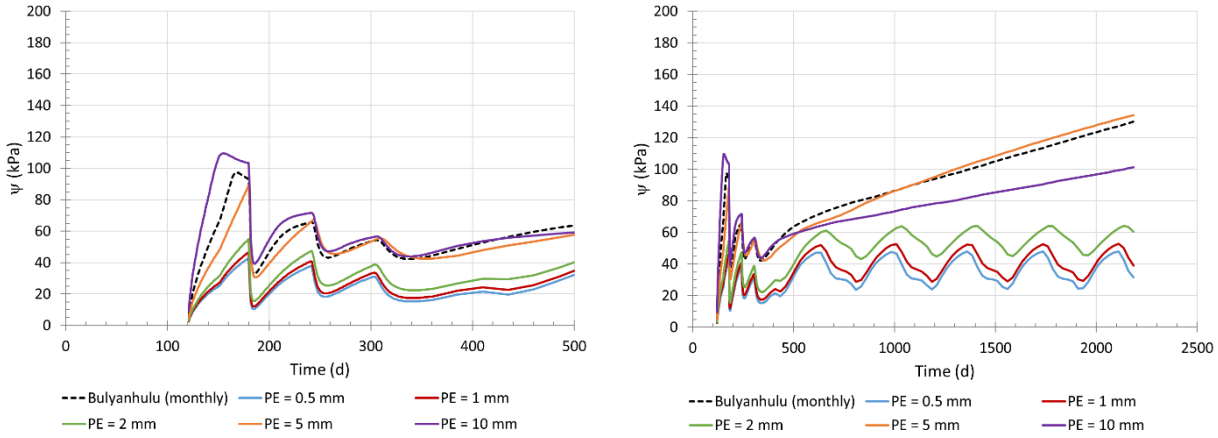

Figure 7.53: Suction for the varying PE rate numerical simulations at y = 5 m (a) from day 0 to day 500 (deposition of tailings from day 0 to day 300) and (b) from day 0 to day 2185 (deposition + 5 years) (Simulation #2, #20, #21, #22, #23, #24 - Table 7.1).

The cumulative outflow at the bottom of the model was higher for the low evaporation models (Figure 7.54a, b). For example, it was -5017 mm for the model with a PE of 0.5 mm/d and -290 mm for the model with a PE of 10 mm/d. When the PE < 2 mm/d, the cumulative flow from the bottom kept increasing after 2185 days. The impact of the PE on the total flow from the bottom of the facility decreases as the PE rate increased. The difference in the cumulative flux after 2185 days between a PE of 2 mm/d and 5 mm/d was 1628 mm and 311 mm between a PE of 5 mm/d and 10 mm/d. A similar pattern is observed with the cumulative AE at the end of the modelling period (Figure 7.54c, d).

(a) Days 0 to 500

(b) Days 0 to 2185

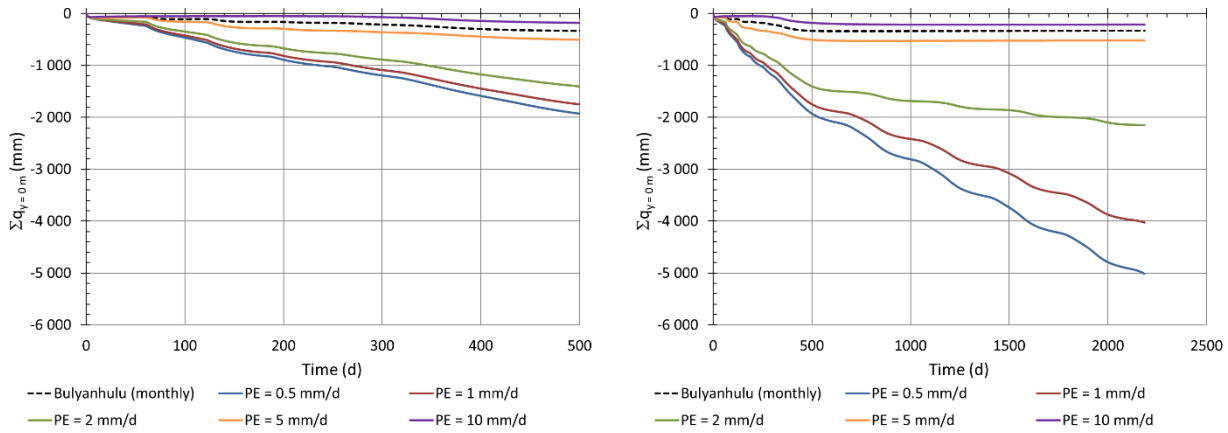

(c) Days 0 to 500

(d) Days 0 to 2185

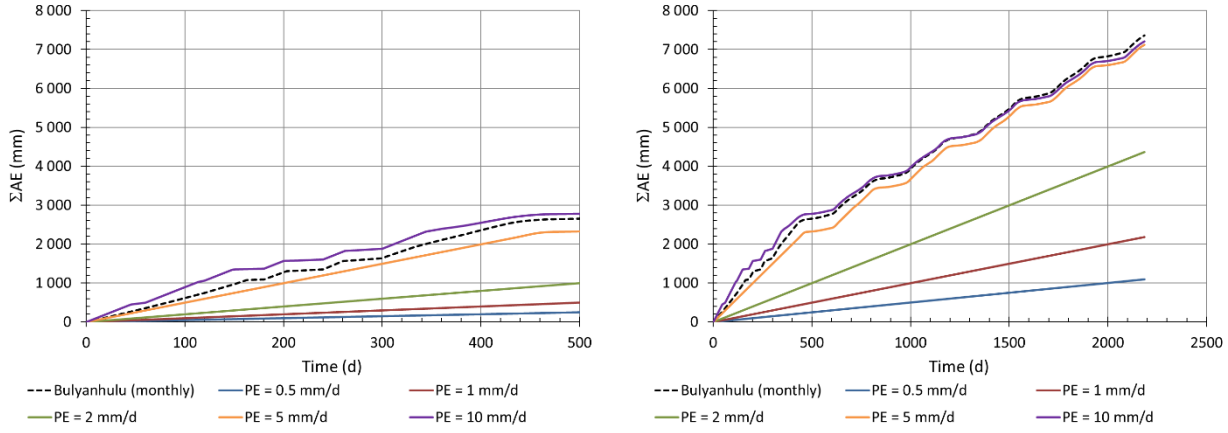

Figure 7.54: (a, b) Total flow and (c, d) total actual evaporation for the varying PE rates numerical simulations (Simulation #2, #20, #21, #22, #23, #24 - Table 7.1).

The daily potential evaporation rate influences the infiltration of water into the underlying soil (at y = 0 m). The flow tends to decrease almost linearly from -1952 mm (17.5% of total water in the simulation) to -511 mm (4.6% of total water in the simulation) when the PE rates increase from 0.5 mm⁄d to 5.0 mm⁄d (after 500 days of simulation). The outflow is -178 mm when the PE was 10 mm/d (Figure 7.55).

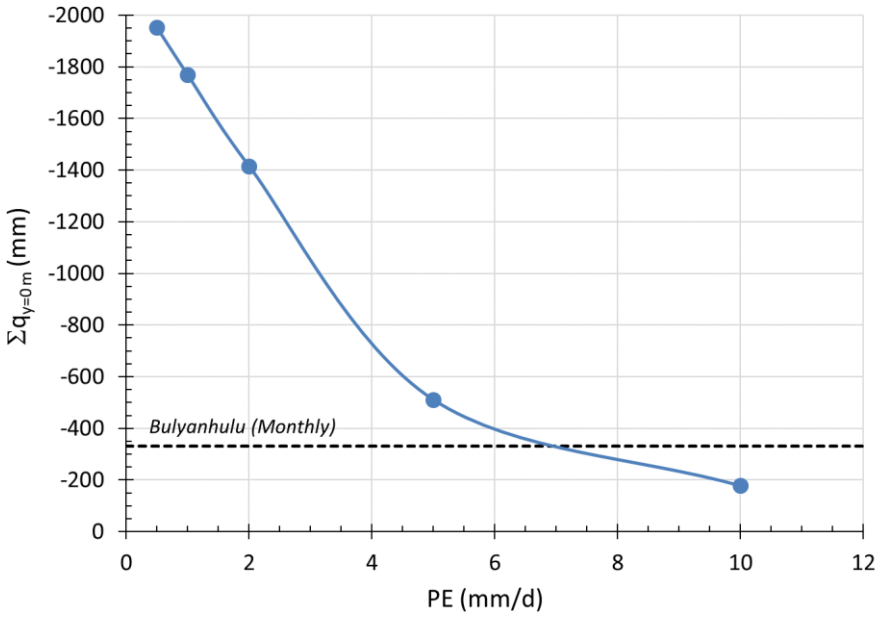

Figure 7.55: Cumulative outflow at the tailings/sand interface (y = 0 m) for different potential evaporation rates (PE) after 500 days of simulation (Simulation #2, #20, #21, #22, #23, #24 - Table 7.1).

The position of the ZFP was influenced by the PE in the models (Figure 7.56). The lower PE rates (2 mm/d and less) would cause rewetting of the column during the wet season (November to April, Table 7.4), and the ZFP would return to the surface of the simulation. The ZFP for the higher evaporation rates (5 mm/d and more) would keep decreasing after the end of the deposition of fresh tailings layers. The position of the ZFP (after 2185 days) was 1 m below the tailings/sand interface.

(a) Days 0 to 500 (b) Days 0 to 2185

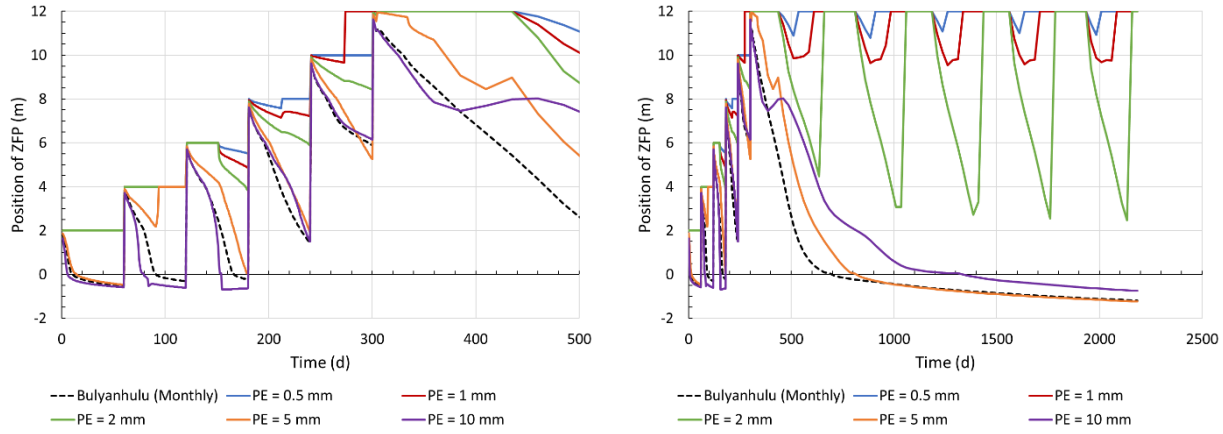

Figure 7.56: Position of the ZFP for the varying PE rates numerical simulations (a) from day 0 to day 500 (deposition of tailings from day 0 to day 300) and (b) from day 0 to day 2185 (deposition + 5 years) (Simulation #2, #20, #21, #22, #23, #24 - Table 7.1).

Figure 7.57 illustrates the influence of the potential evaporation rate (PE) on the simulated total oxygen flux entering the surface of the reactive tailings. A higher flux is recorded when the potential evaporation rate increases. The total flux varies from 8.4 kg/m^2 (PE = 1 mm/d) to 27.7 kg/m^2 (PE = 10 mm/d) for the 500-day simulation period (Figure 7.57b).

(a) Days 0 to 500 (b) Days 0 to 2185

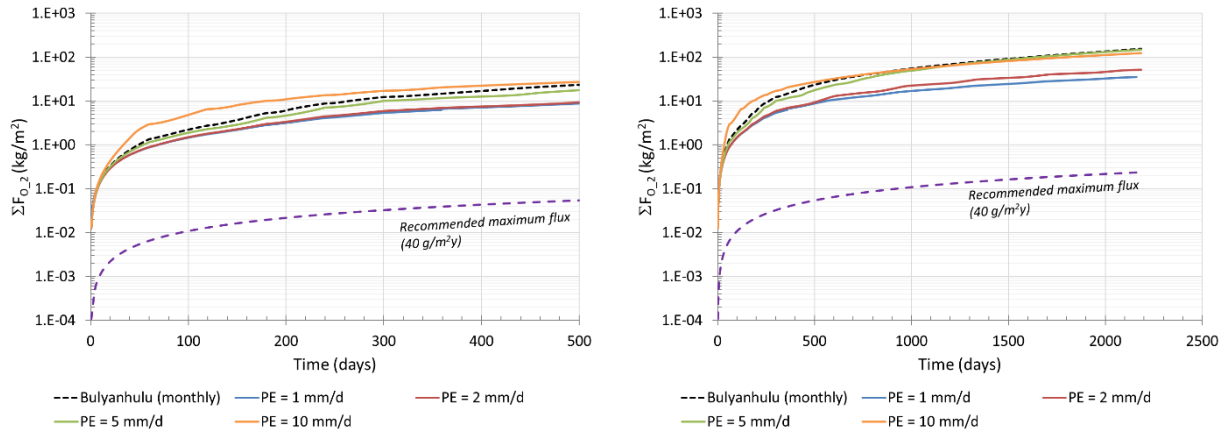

Figure 7.57: Simulated cumulative oxygen flux at the surface for the varying PE rates numerical simulations (a) from day 0 to day 500 (deposition of tailings from day 0 to day 300) and (b) from day 0 to day 2185 (deposition + 5 years) (Simulation #2, #20, #21, #22, #23, #24 - Table 7.1).

A higher PE rate or cumulative AE can be correlated with a more rapid desaturation rate of the tailings, which leads to a higher oxygen flux at the surface (Figure 7.58). Paste tailings tends to desaturate more rapidly than traditional (slurry) tailings because of the lower initial water content.

(a) (b)

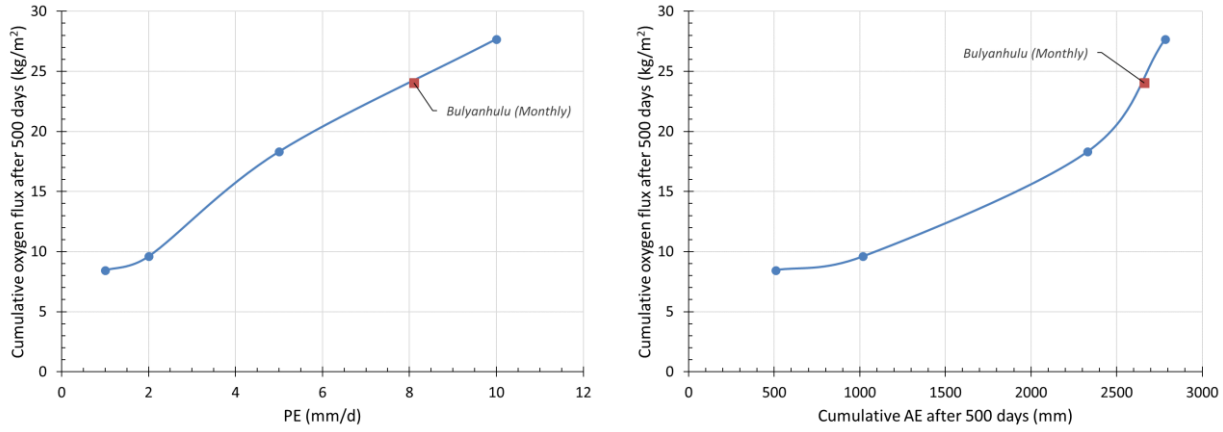

Figure 7.58: Simulated cumulative oxygen flux at the surface after 500 days depending on the (a) PE rate and (b) cumulative AE after 500 days (Simulation #2, #20, #21, #22, #23, #24 - Table 7.1).

A lower PE rate would typically result in a lower oxygen flux at the surface, and to higher infiltration at the base of the TSF.

7.2.8 Other site specific climatic conditions

Simulations presented above highlighted the significant effect of climatic factors on the hydrogeological behaviour of the paste tailings stack. Four other sets of climatic conditions have also been considered in additional simulations with Vadose/W to assess the potential behaviour of paste tailings in other parts of the world (Table 7.5). The geometry, material properties and boundary conditions of the baseline model were used for these simulations (except for climate data resolution; monthly climatic conditions were used here

The four sets of climatic conditions were defined for four mining regions around the world: Central US (Goldstrike Mine), Western Australia (Kalgoorlie Mine), Papua New Guinea (Porgera Mine) and Abitibi region in Quebec (various mines near Val-d'Or). Val-d'Or and Nevada (Goldstrike) have cold winters (average monthly temperature lower than 0ºC); to avoid starting the simulations during the winter, they began on July 1st (instead of January 1st for the other scenarios).

Table 7.12: Alternative climatic conditions introduced in the numerical simulations. Precip.: yearly precipitation; PE: average yearly potential evaporation.

Identification	**Source**	**Climate type (Köppen Classification)[1]**	**Precip (mm/y)**	**PE (mm/y)[2]**
Monthly (Bulyanhulu) Simulation #2	SRK (2002)	Tropical savanna (Aw')	867	2917
Goldstrike Simulation #25	Zhan (2003)	Cold arid steppe (BSk)	267	1506
Kalgoorlie Simulation #26	Australian Bureau of Meteorology	Hot arid steppe (BSh)	264	2407
Porgera Simulation #27	Weather Base	Tropical rainforest (Af)	3296	373
Val-d'Or Simulation #28	Environment Canada	Continental humid (Dfi)	914	1118

[1] Oliver (2005).

[2] Potential evaporation is estimated by Vadose/W.

Figure 7.59 shows the average monthly temperature (°C) (Figure 7.59a) and precipitation rate (mm/d) (Figure 7.59b) for the 4 locations. Monthly averages were used in the simulations, to account for seasons (e.g. winter for Val-d'Or or rain season for Bulyanhulu), on the hydrogeological behaviour of surface tailings stack.

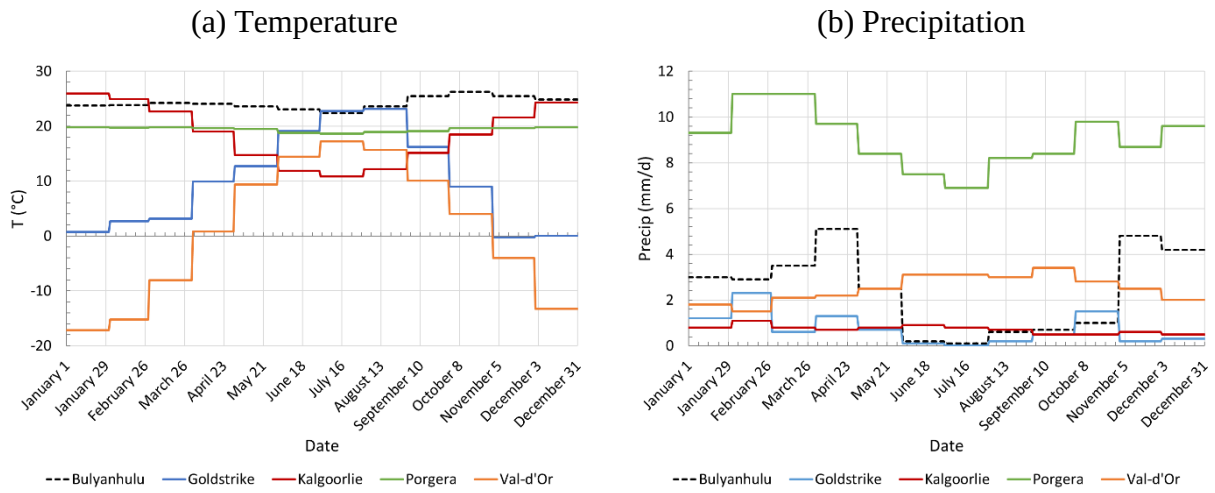

Figure 7.59: Average (a) monthly temperatures (°C) and (b) precipitations (mm/d) for the five locations with climatic conditions used in the simulations.

The VWC fluctuations were relatively similar for drier climates (Bulyanhulu, Goldstrike and Kalgoorlie climatic conditions; Figure 7.60). VWC increased slightly during the rain season but the yearly negative water balance induced a general decrease of the water content over the years. Simulated VWC at y = 5 m was around 0.3 (S_r = 72%) for these three cases after 6 years and seemed to continue to decrease (Figure 7.60b). The high precipitation in Porgera contributed to maintain paste tailings almost saturated (S_r > 99%) at all time. Results with Val-d'Or climatic conditions were somewhat intermediate between the other cases, with a VWC which fluctuated along the years (small increase during spring) but remained relatively constant around 0.38 (S_r = 92%) after the end of the deposition. Results throughout the tailings stack were similar, but variations were slightly more marked closer to the surface (y > 10 m; Appendix P).

(a) Days 0 to 500 (b) Days 0 to 2185

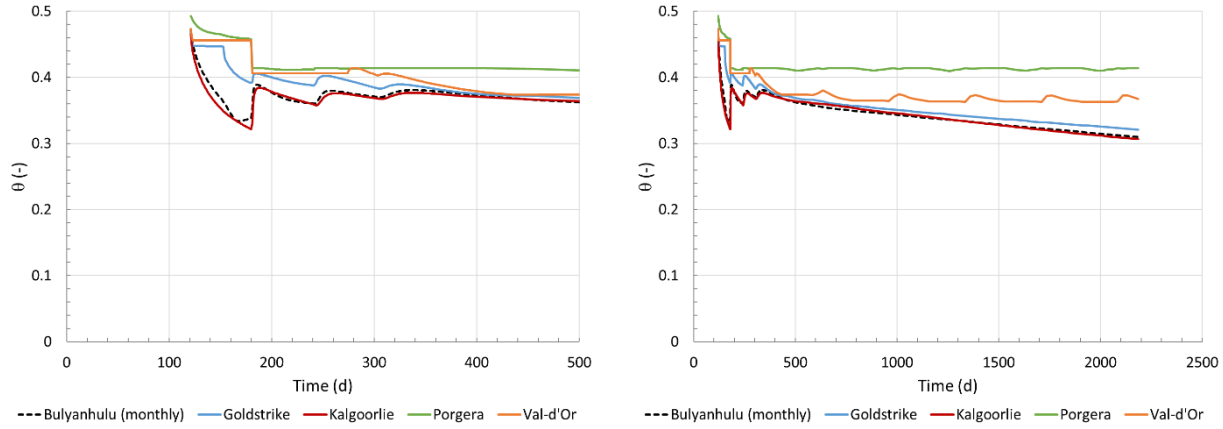

Figure 7.60: Volumetric water content simulated at y = 5 m for varying climatic conditions (a) from day 0 to day 500 and (b) from day 0 to day 2185 (deposition + 5 years) (Simulation #2, #25, #26, #27, #28 - Table 7.1).

The fluctuation of suction with Bulyanhulu, Goldstrike and Kalgoorlie climatic conditions were similar (Figure 7.61), although the suction was slightly lower with the Goldstrike climatic conditions (because of longer and more intense drought periods). Simulations indicated a continuous increase of suction over the years, resulting from the negative water balance at these sites. The simulation with the Porgera climatic conditions showed that tailings were almost saturated and therefore the suction remained close to 0 kPa (maximum +10 kPa which is lower than tailings AEV). The simulated suctions with Val-d'Or climatic conditions were comprised between 20 kPa and 130 kPa. They showed relatively important seasonal variations (up to 20 kPa), with significant decrease of suction during fall rains. Suction in the tailings below y = 7 m remained below the AEV (see Appendix Q for all the results).

(a) Days 0 to 500 (b) Days 0 to 2185

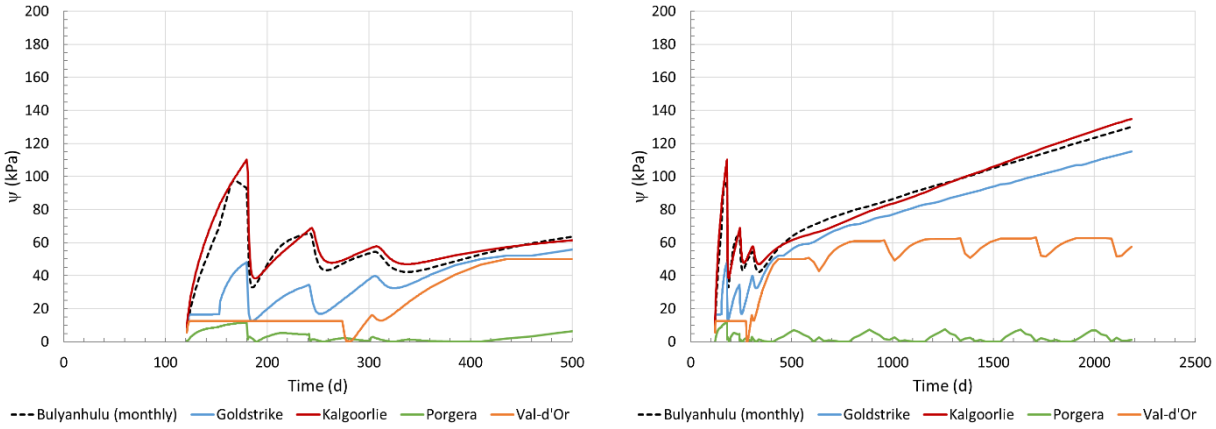

Figure 7.61: Suction simulated at y = 5 m for varying climatic conditions (a) from day 0 to day 500 and (b) from day 0 to day 2185 (deposition + 5 years) (Simulation #2, #25, #26, #27, #28 - Table 7.1).

The quantity of water infiltrating into the sandy subsoil (y < 0 m) depended on the climatic conditions and the water balance on site (Figure 7.62). Cumulative drainage after 6 years in the model with Porgera climatic conditions corresponded for example to 68% ($\Sigma q_{y = 0\ m}$ = -17 391 mm) of precipitation and was significantly larger than in the other cases. Total drainage with Bulyanhulu monthly climatic conditions was -328 mm (3.0% of the total water in the simulation) and only -180 mm with Kalgoorlie conditions (2.4% of the total water in the simulation). Results with Val-d'Or and Goldstrike climatic conditions showed periods with no infiltration because of frost.

The quantity of water infiltrating into the underlying subsoil (y = 0 m) kept increasing when the water balance on site was positive, i.e. when precipitation was greater than evaporation (Porgera, Val-d'Or). On the other hand, the amount of water that infiltrates into the underlying soil tended to become nil after 500 to 1000 days when the water balance was negative (Bulyanhulu, Goldstrike, and Kalgoorlie).

(a) Total flow (from 0 mm to -1000 mm)

Days 0 to 500

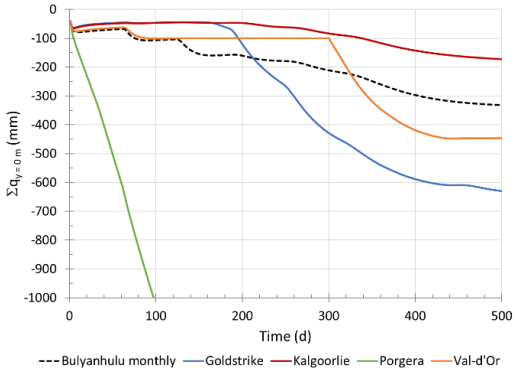

(b) Total flow (from 0 mm to -1000 mm)

Days 0 to 2185

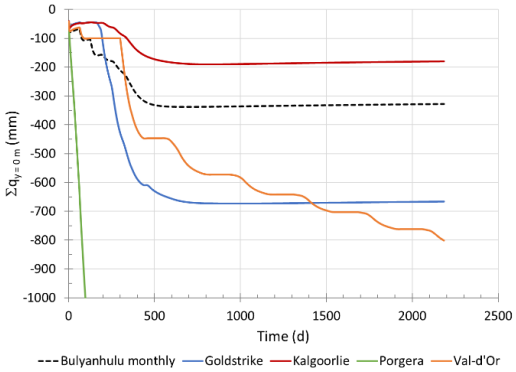

(c) Total flow (complete scale)

Days 0 to 2185

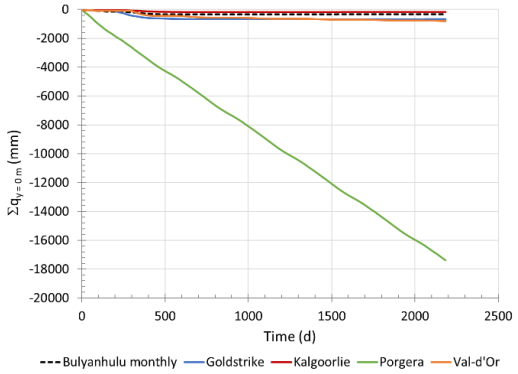

(d) Total actual evaporation

Days 0 to 500

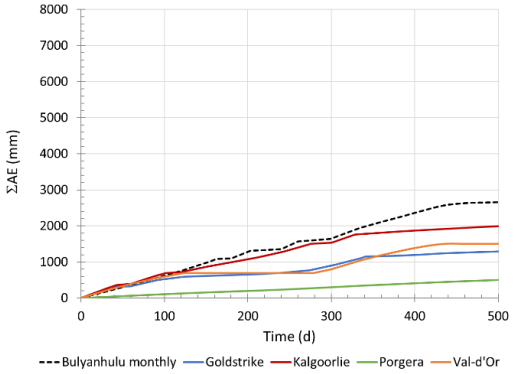

(e) Total actual evaporation

Days 0 to 2185

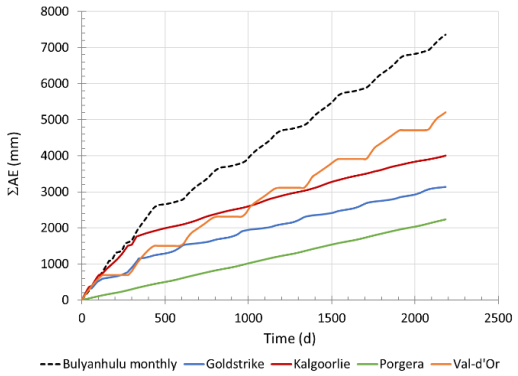

Figure 7.62: (a, b, c) Simulated cumulative flow to the underlying sandy subsoil (y = 0 m) and (d, e) actual evaporation (AE) at the surface (y = 12 m) for varying climatic conditions (Simulation #2, #25, #26, #27, #28 - Table 7.1).

The ratio of the total precipitation over the total potential evaporation (ΣPrecip/ΣPE) during the simulated period is calculated for the models presented above. The ΣPrecip/ΣPE ratio for each of the climatic simulations is presented in Table 7.13. A ratio smaller than 1 indicates that yearly total potential evaporation is greater than yearly total precipitation.

Table 7.13: Climate ratios of the various regional climatic conditions studied.

Simulation	**ΣPrecip/ΣPE**
Bulyanhulu (monthly values) Simulation #2	0.30
Goldstrike Simulation #25	0.18
Kalgoorlie Simulation #26	0.11
Porgera Simulation #27	8.83
Val-d'Or Simulation #28	0.82

Figure 7.63 presents the total infiltration ($\Sigma q_{y = 0\ m}$) with respect to the ΣPrecip/ΣPE ratio for the five simulations presented above, and the simulations with a fixed PE (Section 7.2.7). As the ratio ΣPrecip/ΣPE increases, the cumulative infiltration at y = 0 m also increases.

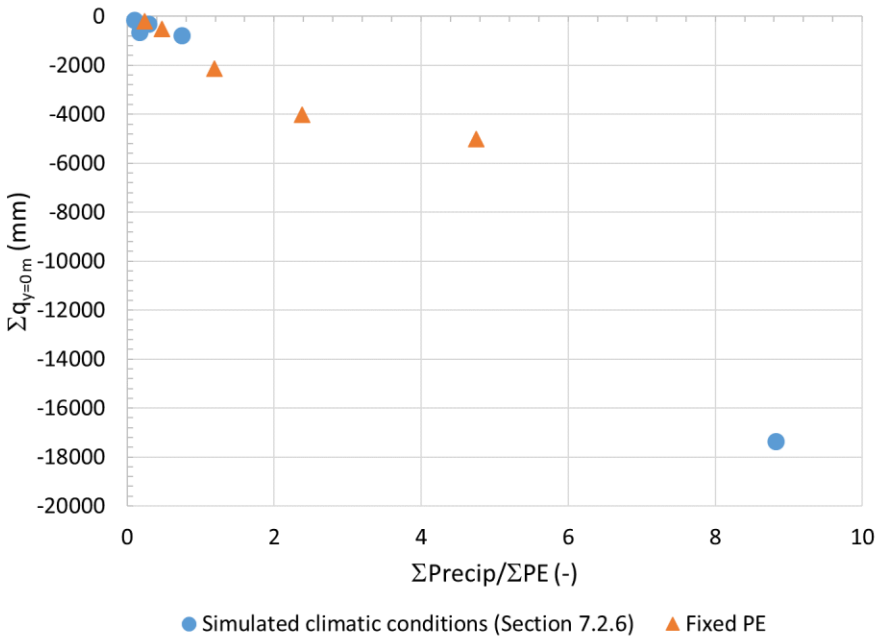

Figure 7.63: Relationship between the ratio ΣPrecip/ΣPE and the total water infiltration into the underlying soil (after 2185 days).

A higher ΣPrecip/ΣPE ratio (Figure 7.63) also results in a ZFP closer to the surface (Figure 7.64). The ZFP remained at the surface for the Porgera climate. The ZFP in the Kalgoorlie and Bulyanhulu climates was at the same location. The position ZFP of the Goldstrike climate (lower evaporation than the Bulyanhulu climate) decreased at a lower rate than the Bulyanhulu or Kalgoorlie numerical simulations. However, it also ends up around the same final value (y = -1 m) than the latter simulation. In the Val-d'Or climate, the potential evaporation rate is not large enough to allow a permanent desaturation of the simulation. The ZFP varies seasonally. It is close to the surface (y > 10 m) in the wet spring and summer, and it decreases (to y = -6 m) during fall and winter.

(a) Days 0 to 500 (b) Days 0 to 2185

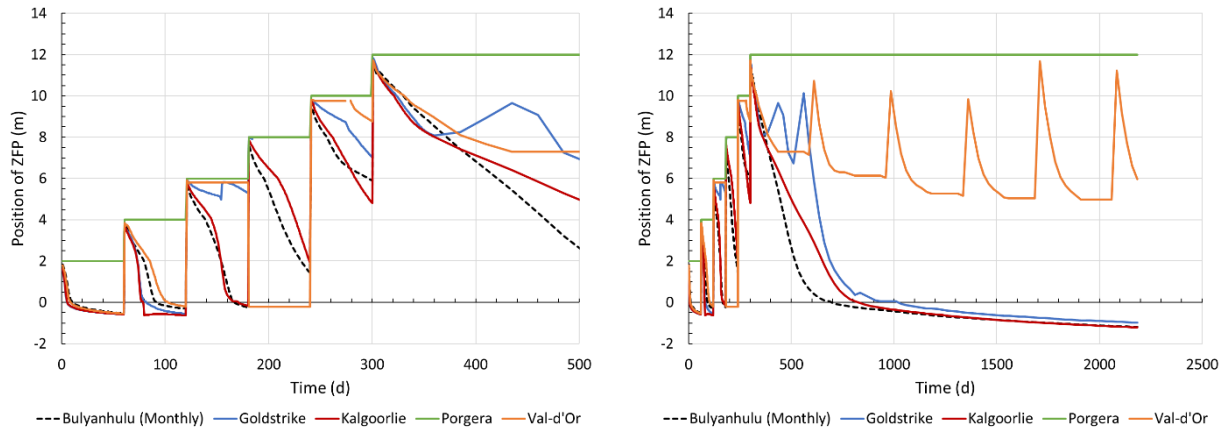

Figure 7.64: Position of the ZFP for the varying climatic conditions numerical simulations (a) from day 0 to day 500 (deposition of tailings from day 0 to day 300) and (b) from day 0 to day 2185 (deposition + 5 years) (Simulation #2, #25, #26, #27, #28 - Table 7.1).

When studying the time required for the degree of saturation of a fresh tailings layer to decrease below 85% (t_{85}), it was observed that a high rain intensity (e.g. Layers 1 to 3 - Val-d'Or) or a temperature below freezing (e.g. Layers 3 and 4 - Goldstrike; and Layers 4 and 5 - Val-d'Or) when the fresh layer is placed on the surface significantly increased the desaturation time. In certain cases (as seen on Table 7.14), the degree of saturation could even remain greater than 85% for the entire duration of simulation (2185 days). Furthermore, the deeper layers of tailings in the Val-d'Or numerical simulation remained saturated since the evaporative gradient (ZFP) never penetrated the totality of the column (Figure 7.64).

Table 7.14: Time to attain a degree of saturation (S_r) of 85% (t_{85}) at a depth of 1 m below the tailings surface for the varying climatic conditions numerical simulations (Simulation #2, #25, #26, #27, #28 - Table 7.1).

Layer	y (m)	t_{85} (d)				
		Bulyanhulu	**Goldstrike**	**Kalgoorlie**	**Porgera**	**Val-d'Or**
1	1	1906.6	30.0	32.7	2185.0[(1)]	2185.0[(1)]
2	3	1244.4	45.3	24.7	2125.0[(1)]	2125.0[(1)]
3	5	37.3	837.1	30.9	2065.0[(1)]	2065.0[(1)]
4	7	20.1	331.9	33.6	2005.0[(1)]	542.2
5	9	18.2	56.3	21.7	1945.0[(1)]	148.8
6	11	29.4	29.7	19.8	1885.0[(1)]	49.0

[(1)] Layer remains at a degree of saturation (S_r) greater than 85%.

The simulations with various climatic conditions presented in this section indicate that infiltration into the underlying soil (at y = 0 m) and desaturation rate of the tailings (as expressed by t_{85}) can be significantly influenced by the climatic boundary conditions at the surface. The ΣPrecip/ΣPE ratio appears as a key parameter in this regard, particularly for infiltration into the underlying soil.

CHAPTER 8 SUMMARY, DISCUSSION, CONCLUSION AND RECOMMENDATIONS

8.1 Summary and discussion

The use of engineered mine tailings has become more common to minimise the impact of mines on the surrounding environment. One of the proposed methods is to decrease the initial water content of mine tailings to a paste-like consistency. The use of paste tailings (with an added binder) has been used for decades in underground mines. Paste tailings are also being considered for surface disposal

Surface paste tailings disposal has several advantages, including a reduction of the quantity of water to manage at the tailings storage facility and a greater geotechnical stability compared to conventional slurry deposition. The method has, however, some limitations that include higher operational costs and a higher risk for acid mine drainage (AMD) generation when the tailings are reactive. The objective of this research project was to assess the hydrogeotechnical response of paste tailings under various conditions. The effect of deposition rate, local natural and climatic conditions and initial water content on the behaviour of the tailings was specifically assessed. The focus was placed on variations of the volumetric water content, pore water pressure, drainage and evaporation rates and oxygen fluxes, which were measured in laboratory and field tests and evaluated using numerical simulations.

The tailings studied in this research were sampled at the Bulyanhulu mine in Tanzania (Barrick Gold Corporation, now Acacia Mining). These paste tailings were deposited for about 15 years at the Bulyanhulu mine at a gravimetric pulp density (P_m) of 74% (water content $w \approx 35\%$). Field work was conducted in 2004 to collect samples for laboratory investigations, perform field observations and carry out several in situ tests.

A thorough laboratory characterization program was conducted in the Polytechnique Montreal (Research institute on mines and the environment) laboratories to determine the hydrogeotechnical properties of the Bulyanhulu mine tailings, including the particle size distribution, grain relative density, Atterberg limits, mineralogy, saturated hydraulic conductivity, water retention curve and consolidation properties. The Bulyanhulu tailings investigated in this project were a non-plastic silt (ML; ASTM D2487, 2006), with an average D_{10} of 3 μm and a D_{60} around 38 μm, for a coefficient

of uniformity ($C_u = D_{60}/D_{10}$) of 13. The relative density of the grains (D_r) was approximately 2.92. The measured saturated hydraulic conductivity (k_s) was comprised between 5×10^{-8} m/s and 2×10^{-7} m/s. The water retention curve (WRC) was determined using both Tempe cell tests (densified tailings with a porosity n = 0.40) and a pressure plate extractor tests (unconsolidated freshly deposited tailings, with n ≈ 0.50). The WRCs were described using the Fredlund and Xing (1994) model. The air entry value (AEV) of the consolidated tailings was approximately 58 kPa and the water entry value (WEV) was close to 1200 kPa. The consolidation properties measured with oedometer tests were comparable to other hard rock mine tailings (e.g. Aubertin et al., 1996; Bussière, 2007; Saleh-Mbemba, 2016). The compression index (C_c) was approximately 6.5×10^{-2}, the coefficient of compressibility (a_v) was comprised between 7.9×10^{-5} kPa^{-1} and 9.5×10^{-5} kPa^{-1}, and the coefficient of volumetric compressibility (m_v) varied from 4.6×10^{-5} kPa^{-1} to 5.7×10^{-5} kPa^{-1}.

Single-layer (SL) and multi-layer (ML) column tests were setup in the laboratory to study the post-deposition behaviour of surface paste tailings. The main objective of the SL tests was to evaluate the effect of layer thickness and initial water content on the movement of water and desaturation of the tailings. The ML tests were conducted to assess paste disposal scenarios, considering more specifically the influence of layer thickness on the moisture distribution and desaturation of the tailings.

Modified oxygen consumption (MOC) tests were carried out at the Bulyanhulu mine tailings storage facility and, on a smaller scale, in the ML columns. Results from the laboratory and the field tests were comparable. These indicate that oxygen flux tends to increase when the degree of saturation of the tailings decreases; similar observations were also reported by others (e.g. Mbonimpa et al. 2003, 2011; Dagenais, 2005; Pabst, 2011). The oxygen diffusion coefficient (D_e) evaluated from field and laboratory tests were well predicted by Aachib et al. (2002, 2004) model. The oxygen reactivity rate coefficient (K_r) was estimated between 0.27 d^{-1} and 2.7 d^{-1}.

Four SL column tests were carried out, with three different tailings thicknesses (SL-01: 10 cm, SL-02: 20 cm, and SL-03: 30 cm) and two different initial water contents (SL-01, 02, 03: P_m = 71%, w = 30%; SL-04: P_m = 66%, w = 51%). Water drainage was collected at the base of the columns and the mass, layer thickness and suction were monitored daily. Drainage took more time (almost twice as much) when the tailings initially contained more water (i.e. column SL-04 vs. column SL-03), but there was almost no difference in the final gravimetric water content after

60 days. Tailings in column test SL-01 (10 cm thick) became almost dry by the end of the testing period, while they remained at a volumetric water content of about 0.1 in the other tests. Cracking at the tailings surface began at a gravimetric water content (w) comprised between 28% and 32%, regardless of the layer thickness or initial water content. Similar observations were made by other authors on different tailings from hard rock mines (e.g. Deschamps, 2009; Saleh-Mbemba et al., 2016). The final void ratio in the tailings was directly affected by the evaporation rate. The results from the numerical simulations carried out with Vadose/W followed the same general behaviour observed in the laboratory tests. However, the simulations with Vadose/W tended to somewhat overestimate desaturation by evaporation and underestimate drainage.

Four ML column tests were also carried out in the laboratory to investigate the effect of the successive deposition of paste tailings layers. The first two column tests, Col-01 and Col-02, were setup with respectively three and four 10 cm thick tailings layers. The other two column tests, Col-03 and Col-04, comprised two 20 cm thick layers. Most of tailings desaturation in the ML columns was caused by evaporation; some drainage was generally observed during the first 24 hours following the deposition of the first layer but stopped afterwards. The placement of a fresh tailings layer above partially saturated tailings layers favored migration of water from the fresh tailings to the underlying tailings. The amount of water flowing into the underlying layers (interlayer flow) was calculated using the volumetric water content variations recorded in each layer; comparable results were obtained from numerical simulations with Vadose/W.

In the ML column tests, the time to attain a constant layer thickness was shorter for lower initial water contents (e.g. Col-02). ML column tests also showed that the final void ratio was influenced by the initial void ratio of the tailings, as observed also by Saleh-Mbemba (2010), and that the final void ratio was also smaller when the actual evaporation rate was larger.

The numerical simulations of the laboratory column tests carried out with Vadose/W generally showed good agreement with experimental results, especially in terms of volumetric water content and suction variations. The simulated potential evaporation was generally overestimated, and the simulated drainage was significantly smaller than measured values. However, the overall behaviour observed in the numerical models was comparable to the laboratory tests (especially in terms of water content variations). Simulated conditions were then extrapolated to assess the hydrogeological behaviour of paste tailings under field conditions. A parametric numerical analysis

was carried out to evaluate the influence of various characteristics (i.e. deposition rate and layer thickness, resting time between two layers, tailings hydrogeological properties, underlying soil hydrogeological properties, position of the water table, potential evaporation rate, and climatic conditions) on water distribution within the paste tailings.

The numerical field model (baseline model) was 12 m high and the water table was fixed 12 m below the tailings surface. Field behavior after deposition was assessed by evaluating tailings desaturation and both drainage (into the soil below the tailings) and evaporation.

Results from the numerical simulations indicated that many parameters may influence the hydrogeological response of a surface paste tailings stack

Figure 8.1 presents a summary of the flow into the underlying subsoil for the cases presented in Chapter 7 including the baseline model (simulations are identified in Table 7.1). For example, in the baseline case (2 m layers with Bulyanhulu annual average climatic conditions), 1.5% of the total water available (i.e. pore water and precipitation) infiltrated into the underlying subsoil (at y = 0 m) during the simulation period (2185 days or 6 years).

The potential evaporation (PE) rate plays a key role in the desaturation of paste tailings. Drainage is limited by the lower hydraulic conductivity and higher AEV associated with the lower initial void ratio (e) in paste tailings (compared to typical slurried tailings).

In all the cases shown in Figure 8.1, the actual evaporation (AE) rate has the greatest impact on the water balance (Figure 8.2). The thickness of the fresh layers deposited on unsaturated tailings affect the overall behaviour of the modelled stack. Infiltration into the underlying soil tends to be greater for a paste tailings stack built with thicker fresh tailings layers (for the same final height and annual rate of rise). A more progressive deposition, with thinner tailings layers, seems to favor desaturation through evaporation, which may help geotechnical stability but could also contribute to increase oxidation of reactive tailings.

Evaporation is also influenced by the resting time between two fresh layers and by the climatic conditions. The hydrogeological properties of the tailings also influence the desaturation of the stack and finer tailings tend to remain saturated for longer periods following deposition because of their higher water retention capacity.

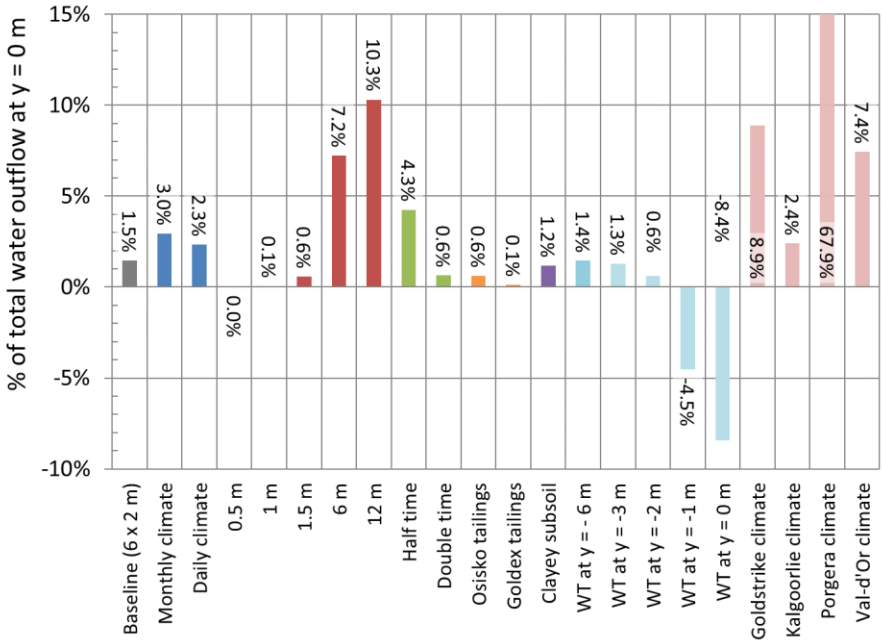

Figure 8.1: Simulated cumulative relative outflow into the underlying subsoil (at y = 0 m) for 1D models of a 12 m (final height) paste tailings stack.

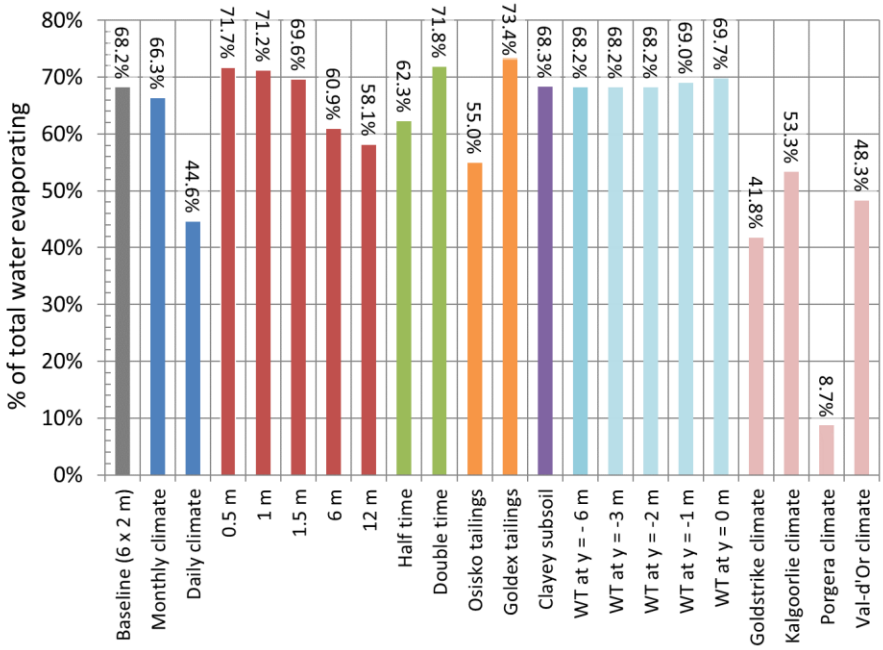

Figure 8.2: Simulated cumulative relative actual evaporation (AE) for 1D models of a 12 m (final height) paste tailings stack.

In general, field simulations showed similar trends to those observed in the ML column tests in the laboratory. Most of the tailings desaturation was through evaporation. The initial desaturation of the fresh tailings layers was also due to drainage into the partially saturated underlying tailings layers. The presence of pore water in the underlying layers could also contribute to the increase of the water content in the tailings surface when evaporation was predominant (Kam et al., 2011; Daliri et al., 2016).

The position of the zero-flux plane (ZFP) tended to decrease following the placement of a fresh tailings layer, and the depth of influence of evaporation increases with time. Eventually the ZFP would reach the tailings/sand interface (at y = 0 m) after the end of the deposition period, and the whole 1D simulation would desaturate through evaporation. In a few cases, however, the ZFP remained in the tailings, which indicated that potentially contaminated water could reach the water table; this was the case for humid climates (i.e. Porgera and Val-d'Or), low PE rates (PE < 2 mm/d) and finer tailings (e.g. Osisko tailings).

Controlling drainage could be critical if tailings are acid generating, to prevent contamination of ground water. Actual evaporation had the greatest influence on limiting drainage from the bottom of the facility. Evaporation rate can be increased for example:

- by disposing thinner tailings layers on the surface;
- by increasing the time between the placement of two fresh tailings layers;
- by having slightly coarser tailings;
- by constructing the tailings storage facility in an area with a higher potential evaporation.

Inversely, thicker layers, longer resting time, small deposition cells inside de TSF, and thinner tailings, for example, could contribute to maintain a higher degree of saturation, and favor the recirculation of water (if collected at the bottom of the TSF).

The simulated oxygen fluxes were generally greater than the usual target of 40 g/m^2y (used for cover systems; Aubertin et al., 2002), especially because of the reactivity of the tailings, the low initial water content of the paste tailings and the high evaporative gradients. This criterion was, however, developed for covers (oxygen barriers; Aubertin et al., 1995, 1999, 2002) and not for

tailings directly exposed to the atmosphere, and it shows that a cover system would be necessary at closure to prevent tailings oxidation and possible contamination. It is also recommended that the tailings remain at a high degree of saturation (e.g. $S_r > 85\%$) at all times to limit oxidation. The actual minimum degree of saturation depends on tailings characteristics (e.g. particle size distribution, oxygen reactivity rate coefficient, *in-situ* porosity).

In summary, the decision to use paste or thickened tailings can be particularly complex for a mine producing tailings that could potentially generate contaminated mine drainage. Under a relatively dry climate with a potential evaporation higher than the precipitation (e.g. Bulyanhulu Mine; Simms et al., 2007; Neves Corvo Mine; Lopes et al., 2015), the operation of a paste tailings facility should aim at controlling water drainage at the base of the facility (as preventing AMD may not be possible due to the risk of desaturation). If the tailings are kept sufficiently dry (at a suction at least greater than the AEV), it may be possible to limit the downward drainage from the bottom of the facility. This behavior can be favored by depositing paste tailings in thin layers (e.g. 50 cm) and letting them rest for a certain time (e.g. at least 2 days for 50 cm thick layers with the simulated conditions, 10 days for 1 m layers). In addition, the slope of the surface paste tailings stack should be controlled to favor runoff and to limit downwards infiltration of precipitation. Controlling infiltration into a large surface (such as a TSF) is technically challenging and such a solution is risky in terms of contaminated drainage control, especially in the long-term.

In a humid climate (e.g. Musselwhite mine; Kam et al., 2011), where the cumulative precipitation is greater than the cumulative potential evaporation, operations of a TSF requires that the paste tailings remain close to saturation at all time. The paste tailings disposal rate should be adjusted so that the top tailings layer does not have time to desaturate, and process water from fresh tailings layers placed on top is regularly added. Simulation results indicate that the paste tailings could be placed in thicker layers.

Reclamation of the filled paste tailings cells should be initiated rapidly after the end of deposition to either limit desaturation (humid climates) or infiltration into the underlying soil (dry climates). Seasonal changes during deposition can also affect mine tailings management. There may be periods in a dry climate area where the precipitation exceeds potential evaporation during a few months (e.g. rainy season at the Bulyanhulu mine) or that evaporation becomes dominant in a

humid climate (e.g. drier summer in Val-d'Or). A tailings management plan must therefore be adaptable to limit the potential for generation of contaminated mine drainage.

Several hypotheses were used in this study which lead to some limitations with regards to the proposed conclusions:

- The measurement of suction due to evaporation is challenging. Sensors that measure both positive and negative pressures may experience desaturation of the porous ceramic tips. It was therefore difficult to record continuously the measured pressure during the laboratory column tests.
- The WRC used in the numerical simulations assumed that there was little or no loss of water due to self-weight consolidation of the tailings (while pore pressure was positive). In practice, it is expected that a significant amount of water would be released during the initial compression phase of the tailings, directly following deposition, while pore water pressure is still positive (Simms et al., 2007; Fisseha et al., 2010; Daliri et al., 2016; Saleh-Mbemba, 2016; Simms et al., 2017; Qi and Simms, 2018). This could explain why the drainage rate simulated with Vadose/W was significantly lower than measured.
- The laboratory study and numerical simulations were conducted in 1D. This simple geometry was considered representative of a surface paste tailings storage facility since the slope is typically low (at least far away from the deposition towers). Surface ponding was not allowed in Vadose/W (any excess water at the surface was eliminated of the numerical simulation), which agrees well with field observations. Using a 1D simulation simplified the modelling and comparison between the various scenarios in the parametric study, but it also created some limitations. For example, in a real operating paste tailings storage facility, the thickness of a paste tailings layer is not constant; it tends to be thicker closer to the deposition point and thinner further away (e.g. Crowder, 2004; Mizani et al., 2013). The effect of evaporation, precipitation, and other climatic factors, and the interlayer fluxes could therefore vary throughout an operating paste tailings storage facility. Additionally, the impact of lateral flow between paste tailings layers could not be addressed in this research.
- Although the study examined drying and rewetting of surface paste tailings layers, it did not include the influence of hysteresis. This phenomenon, which was observed on the WRC

(and unsaturated hydraulic conductivity - k_u - function; Maqsoud et al., 2004, 2012), may play a critical role in the water transfer including rewetting of the underlying (partially saturated) tailings layers after the deposition of a fresh tailings layer above. It could also influence the upwards movement of water (e.g. later phases of the laboratory columns and numerical simulations) when water tends to migrate from the underlying layers to the surface to be evaporated. This is another limitation of the software Vadose/W which does not account for hysteresis.

- The influence of surface evaporation crusts (Fisseha et al., 2010) was not considered but could influence the actual evaporation rate. Both cracks and crusts could have explained, at least in part, the difference between the measured and simulated behaviour of the tailings in the columns.

- Most of the numerical simulations were conducted using the climatic conditions at the Bulyanhulu mine, where the cumulative precipitation is less than the cumulative evaporation. This could influence the desaturation behaviour for the 1D numerical simulation. Reducing the potential evaporation also reduced the influence of evaporation, as was shown for cases where the precipitation was close to or larger than the potential evaporation (e.g. Val-d'Or and Porgera climates). In the latter cases, the infiltration rate at the bottom of the facility would to increase. Water balance in the simulated tailings stack was critical and could be influenced by climate change.

- It was assumed in the numerical simulations that the tailings were incompressible and there was no change in the volume of the tailings layers. The measured settlement in the laboratory columns was, however, between 10% and 20%. The change in porosity (from 0.49 to 0.41) was indirectly accounted for in the numerical simulations by modifying the WRC (of the underlying tailings layers when a fresh tailings layer was placed above. This simplification may have affected the numerical results, especially during the days following deposition.

- The impact of the desiccation cracks on AE was neglected in the laboratory column tests and the numerical simulations. However, the results indicated that the AE rate was generally correlated with the CIF (i.e. a larger CIF yields a higher AE) in the column tests; these results were also consistent with the literature (e.g. Konrad and Ayad, 1997; Fujiyasu

et al., 2000; Benzaazoua et al., 2004; Stewart et al., 2016). Cracks may thus contribute to the actual evaporation by increasing the total exposed area over a given surface. The evolution and impact of cracks is not well understood, despite some recent investigations on this aspect (Saleh Mbemba, 2010, 2016). In the field, crack may also favor runoff and erosion, particularly during wet seasons (and even create preferential flow channels) (e.g. Simms, 2017). In addition, cracks can increase the infiltration of water into the tailings, following a precipitation event or after the placement of a fresh tailings layer (the latter factor was partly considered with the laboratory measurements).

- The concept of the zero-flux plane was used to assess the influence of the evaporative gradient on the tailings response. However, the position of the ZFP does not inform on the magnitude of the gradient in the column. Additionally, there may be more than one ZFP depending on the deposition sequence (Khalil et al., 2003; Healy, 2010; Figure 2.20). For example, after the deposition of a fresh tailings layer, it can be assumed that the ZFP is at the surface since most of the water movement goes downwards. However, the hydraulic gradient can remain positive (upwards) in the bottom part of the column (stack), at least early in wetting period. The deepest ZFP was considered in this research, but it may not be representative of the hydrogeological behaviour throughout the tailings stack.
- The tailings deposition rate (and the corresponding rate of rise) was rapid in the simulations (12 m/year or 1 m/month) and may not be not representative of what is usually observed at an operating mine and especially for Bulyanhulu Mine. For example, the recommended rate of rise for the Bulyanhulu tailings storage facility was between 0.3-0.5 m/month (Metago, 2002; Golder, 2005). Having thinner layers and longer resting times between two fresh tailings layers would have increased the influence of evaporation on the 1D numerical simulation (as shown in the parametric analysis, Section 7.2).
- The simulation software used in this project (Vadose/W) often tends to overestimate the calculated potential evaporation (Chapters 5 and 6), based on data related to the laboratory column tests. Therefore, the PE in the field was also possibly overestimated.

Some recommendations are presented below (Section 8.3) to answer some of the limitations or uncertainties raised during this research.

8.2 Conclusion

The hydrogeological behaviour of surface paste tailings was assessed in the laboratory and using numerical simulations. The objective was to assess the movement of water in a surface paste tailings stack and evaluate the amount of water draining to the underlying soil. Secondary objectives included characterizing the hydrogeological properties of paste tailings from the Bulyanhulu mine (Tanzania), developing hydrogeological conceptual and numerical models for a surface paste tailings (SPT) stack, with a methodology to calculate the inter-layer flow in a variably saturated tailings storage facility. The project also included numerical simulations of the behaviour of a tailings stack under various operational, environmental and climatic conditions.

The main conclusions and contributions of this study can be summarized as follows:

- Deposition of surface paste tailings was studied during a field campaign at the Bulyanhulu mine in Tanzania. Modified oxygen consumption tests were completed on tailings with different degrees of saturation. The results indicate how the oxidation rate of the surface paste tailings is influenced by the water content of the tailings.
- A procedure was developed in the laboratory to measure the water retention curve of a compressible material (such as paste tailings) using a pressure plate extractor and image analysis. By doing so, it was possible to indirectly consider the effect of volume change in the simulations.
- The hydrogeological behaviour of the paste tailings was evaluated using 1D column tests. The experimental results were also used to calibrate and validate numerical simulations. The column tests results indicated that desaturation by drainage was mostly occurring during the first 24 hours following deposition of a fresh paste tailings layer. Afterwards, desaturation of the tailings was mostly through evaporation. The deposition of fresh (saturated) tailings on a partially saturated layer tends to accelerate the drainage into the underlying tailings (while desaturating the top layer). The placement of fresh tailings also fills the cracks in the underlying layer(s). Results further indicate that a higher initial void ratio resulted in a higher final void ratio in the tailings layers. A higher actual evaporation (AE) rate usually produce a greater relative change in the void ratio. Thicker tailings layers also resulted in a greater relative change in the void ratio.

- The presence of partially saturated layers below a fresh paste tailings layer increases significantly the desaturation rate of the surface layer. However, there was a reversal of the gradient and potential resaturation of the surface layer after the drainage of the fresh tailings. The moisture distribution and associated desaturation of surface paste tailings is influenced by the various factors, including tailings properties (i.e. particle size distribution curve and porosity, which influence the water retention curve). A finer grained material tends to retain more water, for longer periods of time, following tailings deposition in the storage facility. Desaturation also depends on field conditions and operational variables such as the suction at the surface before placement of the paste tailings layer, the thickness of the of the paste tailings layers, and the deposition cycle time. Increasing the desaturation of a SPT layer may also expose reactive tailings to oxidation (resulting in the generation of contaminated mine drainage).
- Numerical simulations have also indicated that desaturation of the tailings through evaporation tends to limit deep infiltration of tailings process water.

The research hypothesis stating that the behaviour of paste tailings is highly dependent of the material, operational and site conditions was therefore validated. The lower water content of paste tailings may be problematic when the material is chemically reactive, but it may also limit infiltration into the underlying subsoil, especially if desaturation through evaporation is encouraged (i.e. thin layers, longer resting times between fresh tailings layers).

The use of engineered tailings is gaining in popularity in mining operations throughout the world. Surface paste tailings is one of the solutions available to minimise the environmental impact of mining operations. However, the applicability of the solution varies depending on the site characteristics (e.g. type of mine, production rate, climatic conditions, hydrogeotechnical characteristics of the tailings, etc.), and technical and operational constraints. This project contributed to better understand how water flows through surface paste tailings, and to define areas of applicability of the method.

8.3 Recommendations

Following the limitations raised by this project, some recommendations are proposed for future work regarding surface paste tailings disposal:

- Boundary effects were observed in the SL column tests, which explained (at least in part) the variable potential evaporation (PE) rates observed in Chapter 5. The distance from the tailings surface to the top of the column should be kept to a minimum or fans added to minimise the effect of the column boundaries on the PE rate.
- The yield stress in the paste tailings was not measured nor calculated. The prediction method proposed by Pashias et al. (1996) could also be used in the future to estimate the yield stress and to compare it to the yield stress of similar tailings (e.g. Henriquez and Simms, 2009).
- The use of tensiometers that require resaturation at regular intervals should be limited when studying evaporation because of the desaturation of the ceramics affects the measurements. It would be more appropriate to use positive pore water sensors for the wetting (deposition) phase but to ensure also that some suction sensors are used (e.g. Irrometer Watermark, Meter MPS, Campbell Scientific HDS sensor).
- Some simplified scenarios were evaluated in the laboratory (limited number of layers and only in 1D). It would be useful to evaluate, in the laboratory and in the field, other deposition scenarios (e.g. evolution of the saturated hydraulic conductivity with depth, varying thickness, exposure times, wet/dry cycles) to better understand the behaviour of a variably saturated tailings stack.
- The desaturation and drainage by self-weight compression of the tailings could be considered by modifying the coefficient of volumetric compressibility (mv) when the pore water pressure in the tailings is positive (Simms et al., 2007; Fisseha et al., 2010; Daliri et al., 2016). The actual drainage simulated with Vadose/W would possibly be closer to the value measured in the laboratory.
- Laboratory tests and numerical simulations should be carried out in 2D to account for runoff and lateral groundwater flow. Also, a numerical code that can consider settlement of the tailings would be useful (i.e. a software such as Sigma/W used by e.g. L.-Bolduc, 2012; Saleh Mbemba, 2016; Boudrias, 2018).

- Results obtained here (and reported by others; Pabst, 2011) tends to indicate that evaporation is possibly overestimated with Vadose/W. The aspect could be controlled more efficiently by adapting the climatic boundary conditions in the software.
- Cracking of the tailings surface influences the water flow (actual evaporation, infiltration, runoff). In addition, the impact of evaporation rates on the cracking of paste tailings surfaces, and of cracks on the potential evaporation rate (i.e. desaturation) on the movement of water in a surface paste tailings stack should be examined in greater details.
- 2D laboratory setups and numerical simulations of a surface paste tailings stack (e.g. Mizani et al., 2013; Mizani and Simms, 2016) could also inform on the water flow in surface paste tailings stacks.
- It is also recommended to compare the trends observed in the numerical simulations to actual data from other mining operations using surface paste or thickened tailings disposal such as Kidd Creek (ON), Musselwhite (ON) (Daliri et al., 2016) and Neves Corvo (Portugal) (Lopes et al., 2015).
- Finally, the effect of particle segregation and stratification of layers on the behaviour of a variably saturated surface paste tailings stack should be examined (e.g. laboratory columns with layers having variable tailings properties), as this will also influence water flow and distribution in the tailings.

REFERENCES

Aachib, M. (1997). *Étude en laboratoire de la performance d'un système de recouvrement utilisant le concept de barrière capillaire – Application aux rejets miniers*. (Ph.D. thesis, École Polytechnique de Montréal, Montreal, QC).

Aachib, M., Aubertin, M., & Mbonimpa, M. (2002). Laboratory measurements and predictive equations for gas diffusion coefficient of unsaturated soils. *Proceedings of 55th Canadian Geotechnical Conference and 3rd joint IAH-CNC and CGS Groundwater Specialty Conference*, (p. 163-172). Niagara Falls, ON: Canadian Geotechnical Society.

Aachib, M., Mbonimpa, M., & Aubertin, M. (2004). Measurement and prediction of the oxygen diffusion coefficient in partly saturated media, with applications to soil covers. *Water, Air and Soil Pollution, 156*, 163-193.

Acacia Mining (2018). Bulyanhulu mine overview. From http://www.acaciamining.com/operations/operating-mines/bulyanhulu/overview.aspx

Adu-Wuzu, C., Yanful, E.K., Lanteigne, L., & O'Kane, M. (2007). Prediction of the water balance of two soil cover systems. *Geotechnical and Geological Engineering, 25*(2), 215-237.

Ali, S., Islam, A., Mishra, P.K., & Sikka, A.K. (2016). Green-Ampt approximations: A comprehensive analysis. *Journal of Hydrology, 535*, 340-355.

Alkangas, L., Dagli, D., & Knutsson, S. (2013). *Literature review on potential geochemical and geotechnical effects of adopting paste technology under cold climate conditions*. Luleå, Sweden: University of Technology.

Allen, R.G. (1986). A Penman for all seasons. *Journal of Irrigation and Drainage Engineering, 112*(4), 348-368.

Allen, R.G., Pereira, L.S., Raes, D., & Smith, M. (1998). *Crop evapotranspiration - Guidelines for computing crop water requirements* (FAO Irrigation and Drainage Paper 56). From http://www.fao.org/docrep/X0490E/x0490e00.htm

Alonso, E.E., Gens, A., & Josa, A. (1990). A constitutive model for partially saturated soils. *Géotechnique, 40*(3), 405-430.

Aluwihare, S., & Watanabe, K. (2003). Measurement of evaporation on bare soil and estimating surface resistance. *Journal of Environmental Engineering*, *129*(12). doi:10.1061/(American Society of Civil Engineers)0733-9372(2003)129:12(1157).

Andraski, B.J., & Jacobson, E.A. (2000). Testing a full-range soil-water retention function in modeling water potential and temperature. *Water Resources Research*, 36 (10), 3081-3089.

Annaka, T., & Hanayama, S. (2005). Dynamic water-entry pressure for initially dry glass beads and sea sand. *Vadose Zone Journal*, 4, 127-133.

Arya, L.M., Farrell, D.A., & Blake, G.R. (1975). A field study of soil water depletion patterns in presence of growing soybean roots: I. Determination of hydraulic properties of the soil. *Soil Science Society of America Journal*, 39 (3), 424-430.

Arya, L.M., & Paris, J.F. (1981). A physicoempirical model to predict the soil moisture characteristic from particle-size distribution and bulk density data. *Soil Science Society of America Journal*, 45, 1023-1030.

ASTM International. (2000). *Standard test method for capillary-moisture relationships for fine-textured soils by pressure-membrane apparatus*. ASTM standard D3152-72.

ASTM International. (2002). *Standard test methods for determination of the soil water characteristic curve for desorption using a hanging column, pressure extractor, chilled mirror hygrometer, and/or centrifuge*. ASTM standard D6836-02.

ASTM International. (2003). *Standard test methods for measurement of hydraulic conductivity of saturated porous materials using a flexible wall permeameter*. ASTM standard D5084-03.

ASTM International. (2004). *Standard test methods for one-dimensional consolidation properties of soils using incremental loading*. ASTM standard D2435-04.

ASTM International. (2005). *Standard test methods for specific gravity of soil solids by water pycnometer*. ASTM standard D854-05.

ASTM International. (2005). *Standard test methods for liquid limit, plastic limit, and plasticity index of soils*. ASTM standard D4318-05.

ASTM International. (2006). *Standard practice for classification of soils for engineering purposes (Unified Soil Classification System)*. ASTM standard D2487-06.

ASTM International. (2007). *Standard Test Method for Particle-Size Analysis of Soils*. ASTM standard D422-63.

Aubeny, C., & Long, X. (2007). Moisture diffusion in shallow clay masses. *Journal of Geotechnical and Geoenvironmental Engineering, 133*(10). doi:10.1061/(American Society of Civil Engineers)1090-0241(2007)133:10(1241)

Aubeny, C., Lytton, R., & Tang, D. (2003). Simplified Analysis of Unsteady Moisture Flow through Unsaturated Soil. *Proceedings of 82nd Annual Meeting of the Transportation Research Board*. Washington, DC: Transportation Research Board. From https://ceprofs.civil.tamu.edu/lytton/Spring2003-CVEN646/Simplified.pdf

Aubeny, C.P., & Lytton, R.L. (2004). Shallow slides in compacted high plasticity clay slopes. *Journal of Geotechnical and Geoenvironmental Engineering, 130*(7). doi:10.1061/(American Society of Civil Engineers)1090-0241(2004)130:7(717)

Aubeny, C. & Long, X. (2007). Moisture diffusion in shallow clay masses. *Journal of Geotechnical and Geoenvironmental Engineering, 133*(10). doi:10.1061/(American Society of Civil Engineers)1090-0241(2007)133:10(1241)

Aubertin, M. (2004). *Paste tailings disposal and management at the Bulyanhulu mine: Proposed investigation* (Document prepared for Barrick Gold Corporation). Montreal, QC: École Polytechnique de Montréal

Aubertin, M., Chapuis, R.P., Aachib, M., Bussière, B., Ricard, J.-F., & Tremblay, L. (1995). *Évaluation en laboratoire de barrières sèches construites à partir de résidus miniers* (Report # 2.22.2a). Ottawa, ON: MEND.

Aubertin, M., Bussière, B., & Chapuis, R.P. (1996). Hydraulic conductivity of homogenized tailings from hard rock mines. *Canadian Geotechnical Journal, 33,* 470-482.

Aubertin, M., Ricard, J.-F., & Chapuis, R.P. (1998). A predictive model for the water retention curve: Application to tailings from hard rock mines. *Canadian Geotechnical Journal, 35,* 55-69.

Aubertin, M., Bussière, B., Monzon, M., Joanes, A.-M., Gagnon, D., Barbera, J.-M., Aachib, M., Bédard, C., Chapuis, R.P., & Bernier, L. (1999). *Étude sur les barrières sèches construites à partir de résidus miniers. Phase II: Essais en place* (Report # 2.22.2c). Ottawa, ON: MEND.

Aubertin, M., Aachib, M., & Authier, K. (2000a). Evaluation of diffusive gas flux through covers with a GCL. *Geotextile and Geomembranes*, *18*, 1-19.

Aubertin, M., Mbonimpa, M., & Dagenais, A.-M. (2000b). *Nouvelles procédures d'essais de diffusion et de consommation d'oxygène: Applications au site LTA, Malartic, Québec* (Document prepared for Golder Associates). Montreal, QC: École Polytechnique de Montréal.

Aubertin, M., Bussière, B., & Bernier, L. (2002). *Environnement et gestion des rejets miniers*. Montreal, QC: Les Presses Internationales de Polytechnique.

Aubertin, M., Mbonimpa, M., Bussière, B., & Chapuis, R.P. (2003a). A model to predict the water retention curve from basic geotechnical properties. *Canadian Geotechnical Journal*, *40*, 1104-1122.

Aubertin, M., Mbonimpa, M., Bussière, B., & Chapuis, R.P. (2003b). *Development of a model to predict the water retention curve using basic geotechnical properties* (Report # EPM-RT-2003-01). Montreal, QC: Éditions de l'École Polytechnique.

Aubertin, M., Bussière, B., Pabst, T., James, M., & Mbonimpa, M. (2016). Review of reclamation techniques for acid generating mine wastes upon closure of disposal sites. *Proceedings of Geo-Chicago: Sustainabilty, Energy and the Geoenvironment*. Chicago, IL: American Society of Civil Engineers.

Barnes, H.A., & Walters, K. (1985). The yield stress myth? *Rheologica acta*, *24*(4), 323-326.

Barbour, S.L., Wilson, G.W., & St-Arnaud, L.C. (1993). Evaluation of the saturated-unsaturated groundwater conditions of a thickened tailings deposit. *Canadian Geotechnical Journal*, *30*, 935-946.

Barbour, S.L., Sladen, J., & Wright, I. (2005). The design and construction of a soil vapour barrier in Caerphilly, South Wales, UK. *Proceedings of 58th Canadian Geotechnical Conference and 6th joint IAH-CNC and CGS Groundwater Specialty Conference*. Saskatoon, SK: Canadian Geotechnical Society.

Benson, C.H., & Bareither, C.A. (2012). Designing water balance covers for sustainable waste containment transitioning state of the art to state of the practice. *Geotechnical Engineering State of the Art and Practice* (p. 1–33). doi:10.1061/9780784412138.0001

Benzaazoua, M. (2008). Le contrôle du drainage minier à travers une gestion optimale des rejets miniers et une restauration efficace de sites d'entreposage. *International Congress of Solid Waste Management & Sustainable Development* (p. 215-216). Hammamet, Tunisia.

Benzaazoua, M., Ouellet, J., Servant, S., Newman, P., & Verburg, R. (1999). Cementitious backfill with high sulfur content – Physical, chemical, and mineralogical characterization. *Cement and Concrete Research*, *29*, 719-725.

Benzaazoua, M., Perez, P., Belem, T., & Fall, M. (2004). A laboratory study of the behaviour of surface paste disposal. *Proceedings of Minefill 2004 – The 8th International Symposium of Mining with Backfill* (p. 180-192). Beijing, China: The Nonferrous Metals Society of China.

Benzaazoua, M., Bussière, B., Aubertin, M., Fried, E., & Blier, A. (2008) Integrated sulphidic mine tailings management using environmental desulphurization and cemented paste backfill. *Processing & Disposal of Mineral Industry Waste'07*. Falmouth, UK: Mineral Engineering International.

Benzaazoua, M., Peyronnard, O., Belem, T., Fried, E., Aurore, S., & Dublet, G. (2010). Key issues related to behaviour of binders in cemented paste backfilling. In R.J. Jewell, & A.B. Fourie (eds.), *Paste 2010 – Proceedings of the 13th International Seminar on Paste and Thickened Tailings*. Perth, Australia: Australian Center for Geomechanics.

Blight, G.E. (1997). Interactions between the atmosphere and the earth. *Géotechnique*, *47*(4), 715-767.

Blight, G.E. (2002). Solar radiation on surfaces of tailings dams – Effects of slope and orientation. *Tailings and Mine Waste '02* (p. 333-337). Fort Collins, CO: A.A. Balkema Publishers.

Blight, G.E. (2003). Quantified comparisons of disposal of thickened and unthickened tailings. *Proceedings of Tailings and Mine Waste '03* (p. 63-71). Fort Collins, CO: A.A. Balkema Publishers.

Blight, G.E. (2010). *Geotechnical engineering for mine waste storage facilities*. London, UK: Taylor & Francis Group.

Blight, G.E., Copeland, A., Jardine, P., & MacRobert, C. (2012). Measurements on freshly-deposited surfaces of two platinum tailings dams. In R.J. Jewell, A.B. Fourie, & A. Paterson (eds.),

Paste 2012: Proceedings of the 15th International Seminar on Paste and Thickened Tailings (p.11-24). Perth, Australia: Australian Center for Geomechanics.

Blowes, D.W., Ptacek, C.J., & Jurjovec, J. (2003). Mill tailings: Hydrogeology and geochemistry. In J.L. Jambor, D.W. Blowes, & A.I.M. Ritchie (eds.), *Environmental Aspects of Mine Wastes. Short Course Series: Volume 31* (p. 95-116). Vancouver, BC: Mineralogical Association of Canada.

Boger, D.V. (2012). Personal perspective on paste and thickened tailings: a decade on. *Mining Technology*, *121*(1), 29-36. doi:10.1179/1743286311Y.0000000019

Boger, D.V., Scales, P.J., & Sofra, F. (2002). Section 3: Rheological concepts. In R.J. Jewell, A.B. Fourie, & E.R. Lord (eds.), *Paste and Thickened Tailings: A Guide* (p. 23-34). Nedlands, Australia: Australian Centre for Geomechanics, The University of Western Australia.

Bois, D., Benzaazoua, M., Bussière, B., Kongolo, M., & Poirier, P. (2005). A feasibility study on the use of desulphurized tailings to control acid mine drainage. *CIM Bulletin*, *98*, 74.

Bossé, B., Bussière, B., Hakkou, R., Maqsoud, A., & Benzaazoua, M. (2013). Assessment of phosphate limestone wastes as a component of a store-and-release cover in a semiarid climate. *Mine Water and the Environment*, *32*(2), 152-167.

Bossé, B., Bussière, B., Hakkou, R., Maqsoud, A., & Benzaazoua, M. (2015). Field experimental cells to assess hydrogeological behaviour of store-and-release covers made with phosphate mine waste. *Canadian Geotechnical Journal*, *52*(9), 1255-1269. doi:10.1139/cgj-2014-0263

Boudrias, G. (2018). *Évaluation numérique et expérimentale du drainage et de la consolidation de résidus miniers à proximité d'une inclusion de roches stériles.* (M.A.Sc. Thesis, École Polytechnique de Montréal, Montreal, QC).

Bouwer, H. (1969). Infiltration of water into nonuniform soil. *Journal of the Irrigation and Drainage Division, Proceedings of the American Society of Civil Engineers*, *95*(IR4), 451-462.

Bouwer, H. (2002). Artificial recharge of groundwater: Hydrogeology and engineering. *Hydrogeology Journal*, *10*, 121-142.

Bowles, J.E. (1984). *Physical and geotechnical properties of soils* (2nd ed.). New York, NY: McGraw-Hill, Inc.

Bréard Lanoix, M.-L. (2017). *Caractérisation des propriétés hydrogéologiques de la couche de contrôle des écoulements placée sur la halde à stérile expérimentale à la mine du lac Tio.* (M.A.Sc. Thesis, École Polytechnique de Montréal, Montreal, QC).

Brooks, R.H., & Corey, J.C. (1964). *Hydraulic properties of porous medium* (Hydrology Paper 3). Fort Collins, CO: Colorado State University.

Bruce, R.R., & Klute, A. (1956). The measurement of soil moisture diffusivity. *Soil Science of America Journal*, *20*(4), 458-462.

Brutsaert, W. (1988). *Evaporation into the atmosphere: Theory, history, and applications*. Dordrecht, Netherlands: D. Reidel Publishing Company.

Bryan, R., Simms, P., Verberg, R. (2010). Coupling oxidation to transient drying during multilayer deposition of thickened gold tailings. *Minerals Engineering*, *23*(14), 1101-1112. doi:10.1016/j.mineng.2010.07.003

Burdine, N.T. (1953). Relative permeability calculations from pore-size distribution data. *Transactions American Institute of Mining, Metallurgical and Petroleum Engineers*, *198*, 71-78.

Bussière, B. (1993). *Évaluation des propriétés hydrogéologiques de résidus miniers utilises comme barrières de recouvrement*. (M.A.Sc. Thesis, École Polytechnique de Montréal, Montreal, QC).

Bussière, B. (1999). *Étude du comportement hydrique de couvertures avec effets de barrière capillaire inclinées avec l'aide de modélisations physiques et numériques*. (Ph.D. Thesis, École Polytechnique de Montréal, Montreal, QC).

Bussière, B. (2007). Colloquium 2004: Hydrogeotechnical properties of hard rock tailings from metal mines and emerging geoenvironmental disposal approaches. *Canadian Geotechnical Journal*, *44*(9), 1019-1052. doi:10.1139/T07-040

Bussière, B., Dagenais, A.-M., Mbonimpa, M., & Aubertin, M. (2002). Modification of oxygen-consumption testing for the evaluation of oxygen barrier performance. *Proceedings of the 55th Canadian Geotechnical Conference and 3rd joint IAH-CNC and CGS Groundwater Specialty Conference* (p. 139-146). Niagara Falls, ON: Canadian Geotechnical Society.

Bussière, B., Maqsoud, A., Aubertin, M., Martschuk, J., McMullen, J., & Julien, M. (2003). Results from the monitoring program at the LTA Site: Hydraulic behaviour of the cover. *CIM Conference*. Montreal, QC: Canadian Institute of Mining and Metallurgy.

Bussière, B., Benzaazoua, M., Aubertin, M. & Mbonimpa, M. (2004). A laboratory study of covers made of low-sulphide tailings to prevent acid mine drainage. *Environmental Geology*, *45*(5): 609-622. doi:10.1007/s00254-003-0919-6

Bussière, B., Aubertin, M., Mbonimpa, M., Molson, J.W., & Chapuis, R.P. (2007). Field experimental cells to evaluate the hydrogeological behaviour of oxygen barriers made of silty materials. *Canadian Geotechnical Journal*, *44*, 245-265.

Campbell, G.S. (1985). *Soil Physics with BASIC*. New York, NY: Elsevier.

Carman, P.C. (1937). Fluid flow through granular beds. *Transactions, Institution of Chemical Engineers*, *15*, 150-166.

Chapuis, R.P. (2004). Predicting the saturated hydraulic conductivity of sand and gravel using effective diameter and void ratio. *Canadian Geotechnical Journal*, *41*(5), 787-795. doi:10.1139/t04-022

Chapuis, R.P., & Légaré, P.P. (1992). A simple method for determining the surface area of fine aggregates and fillers in bituminous mixtures. *Effects of aggregates and mineral fillers on asphalt mixture performance*, ASTM STP, 1147, 177–186.

Chapuis, R.P., & Aubertin, M. (2003). On the use of the Kozeny-Carman equation to predict the hydraulic conductivity of soils. *Canadian Geotechnical Journal*, *40*, 616-628.

Childs, E.C. (1969). *An introduction to the physical basis of soil water phenomena*. New York, NY: John Wiley & Sons, Inc.

Cissokho, F. (2008). Études numériques des effets de la configuration des couvertures à effets de barrières capillaires inclinées sur la diffusion de l'oxygène. (M.A.Sc. Thesis, École Polytechnique de Montréal, Montreal, QC).

Clayton, S., Grice, T.G., & Boger, D.V. (2003). Analysis of the slump test for on-site yield stress measurement of mineral suspensions. *International Journal of Mineral Processing*, *70*, 3-21. doi:10.1016/S0301-7516(02)00148-5.

Collin, M. (1987). *Mathematical modeling of water and oxygen transport in layered soil covers for deposits of pyritic mine tailings* (Report # S-10044). Stockholm, Sweden: Department of Chemical Engineering, Royal Institute of Technology.

Collin, M. (1998). *The Bersbo pilot project: numerical simulation of water and oxygen transport in the soil covers at mine waste deposits* (Report # 4763). Stockholm, Sweden: Swedish Environmental Protection Agency.

Collin, M., & Rasmuson, A. (1988). Gas diffusivity models for unsaturated porous media. *Soil Science Society of America Journal*, *52*, 311-333.

Cooper, J.D. (1980). *Measurement of moisture fluxes in unsaturated soils in a Thetford forest* (Institute of Hydrology - Report no. 66). Oxford, UK: National Environment Research Council.

Cooper, J.D., Gardner, C.M.K., & Mackenzie, N. (1990). Soil controls on recharge to aquifers. *Journal of Soil Science, 41*, 613-630.

Coulombe, V. (2012). *Performance de recouvrements isolants partiels pour contrôler l'oxydation de résidus miniers sulfureux.* (M.A.Sc. Thesis, École Polytechnique de Montréal, Montreal, QC).

Coussot, P. (2005). *Rheometry of pastes, suspensions, and granular materials: Applications in industry and environment*. Hoboken, NJ: John Wiley & Sons, Inc. From http://lib.myilibrary.com/Open.aspx?id=27587

Crawford, L. (2014). *Best practices of soil moisture measurements* [Online video]. From http://www.decagon.com/education/virtual-seminar-best-practices-of-soil-moisture-measurements/.

Crowder, J.J. (2004). *Deposition, Consolidation, and Strength of a Non-Plastic Tailings Paste for Surface Disposal*. (Ph.D. Thesis, University of Toronto, Toronto, ON).

Crowder, J.J., & Grabinsky, M.W. (2005). Discussion of 'Assessment of the modified slump test as a measure of the yield stress of high-density thickened tailings'. *Canadian Geotechnical Journal*, *42*, 316-318.

Cui, Y.J., Lu, Y.F., Delage, P., & Riffard, M. (2005). Field simulation of in situ water content and temperature changes due to ground–atmospheric interactions. *Géotechnique, 55*(7), 557-567. doi:10.1680/geot.2005.55.7.557

Cui, Y.J., & Zornberg, J.G. (2008). Water balance and evapotranspiration monitoring in geotechnical and geoenvironmental engineering. *Geotechnical and Geological Engineering*, *26*(6), 783-798. doi:10.1007/s10706-008-9198-z

Cuisinier, O., & Masrouri, F. (2005). Influence de solicitations hydriques et mécaniques complexes sur le comportement d'un sol gonflant compacté. *Canadian Geotechnical Journal*, *42*, 731-741.

Dagenais, A.-M. (2005). *Techniques de contrôle du drainage minier acide basées sur les effets capillaires*. (Ph.D. Thesis, École Polytechnique de Montréal, Montreal, QC).

Dagenais, A.M., Aubertin, M., & Bussière, B. (2006). Parametric study on the water content profiles and oxidation rates in nearly saturated tailings above the water table. *Proceedings of 7th International Conference on Acid Rock Drainage*. St. Louis, MO: The Society for Mining, Metallurgy, and Exploration Inc.

Dagenais, A.M., Mbonimpa, M., Bussière, B., & Aubertin, M. (2012). A modified oxygen consumption test to evaluate gas flux through oxygen barrier cover systems. *Geotechnical Testing Journal*, *35*(1), 150-158. doi:10.1520/GTJ103621

Daliri, F., Simms, P., & Sivathayalan, S. (2013). Shear behaviour of high density tailings sampled from a laboratory simulation of multilayer deposition. *Proceedings of GeoMontreal 2013*. Montreal, QC: Canadian Geotechnical Society.

Daliri, F., Kim, H., Simms, P., & Sivathayalan, S. (2014). Impact of desiccation on monotonic and cyclic shear strength of thickened gold tailings. *Journal of Geotechnical and Geoenvironmental Engineering*, *140*(9). doi:10.1061/(American Society of Civil Engineers)GT.1943-5606.0001147

Daliri, F., Simms, P., & Sivathayalan, S. (2016). Shear and dewatering behaviour of densified gold tailings in a laboratory simulation of multilayer deposition. *Canadian Geotechnical Journal*, *53*(8), 1246-1257. doi:10.1139/cgj-2014-0411

DehghaniSanij, H., Yamamoto, T., & Rasiah, V. (2004). Assessment of evapotranspiration estimation models for use in semi-arid environments. *Agricultural Water Management*, *64*, 91-106.

Delage, P., & Cui, Y.J. (2000). *L'eau dans les sols non saturés* (vol. 1, noC301). Paris, France: Techniques de l'ingénieur.

Demers, I. (2008). *Performance d'une barrière à l'oxygène constituée de résidus miniers faiblement sulfureux pour contrôler la production de drainage minier acide*. (Ph.D. thesis, Université du Québec en Abitibi-Témiscamingue, Rouyn-Noranda, QC).

Demers, I., Bussière, B., Aachib, M., & Aubertin, M. (2010). Repeatability evaluation of instrumented column tests in cover efficiency evaluation for the prevention of acid mine drainage. *Water, Air, & Soil Pollution*, *219*, 113-128. doi:10.1007/s11270-010-0692-6

Deschamps, T. (2009). *Étude du comportement physique et hydrogéochimique d'un dépôt de résidus miniers en pâte dans des conditions de surface*. (Ph.D. thesis, Université du Québec en Abitibi-Témiscamingue, Rouyn-Noranda, QC).

Deschamps, T., Benzaazoua, M., Bussière, B., & Aubertin, M. (2011). Laboratory study of surface paste disposal for sulfidic tailings: Physical model testing. *Minerals Engineering*, *24*(8), 794-806. doi:10.1016/j.mineng.2011.02.013

Dingman, S.L. (1994). *Physical hydrology*. Prentice Hall.

Domenico, P.A., & Schwartz, F.W. (1998). *Physical and Chemical Hydrogeology* (2nd ed.). New York, NY: John Wiley & Sons, Inc.

Dreiss, S.J., & Anderson, L.D. (1985). Estimating vertical soil moisture flux at a land treatment site. *Groundwater*, *23*(4), 503-511.

Dunmola, A. (2012a). *Predicting evaporative fluxes in saline soil and surface-deposited thickened mine tailings*. (Ph.D. thesis, Carleton University, Ottawa, ON).

Dunmola, A. (2012b). Geotechnical and geo-environmental implications of evaporation from sulphidic surface-deposited thickened mine tailings. *Electronic Journal of Geotechnical Engineering*, *17*, 2225-2241. Taken from http://www.ejge.com/2012/Ppr12.187alr.pdf

Dunmola, A., & Simms P. (2010). Solute mass transport and atmospheric drying of high-density gold tailings. In R.J. Jewell, & A.B. Fourie (eds.), *Paste 2010 – Proceedings of the 13th International Seminar on Paste and Thickened Tailings* (pp. 279-289). Perth, Australia: Australian Center for Geomechanics.

Edlefsen, N.E., & Anderson, A.B.C. (1943). Thermodynamics of soil moisture. *Hilgardia*, *15*(2), 31-298.

Elberling, B., Nicholson, R.V., Reardon, E.J., & Tibble, P. (1994). Evaluation of sulphide oxidation rates: A laboratory study comparing oxygen fluxes and rates of oxidation product release. *Canadian Geotechnical Journal*, 31, 375-383.

Elberling, B., & Nicholson, R.V. (1996). Field determination of sulphide oxidation rates in mine tailings. *Water Resources Research*, *32*(6), 1773-1784.

Essayad, K. (2015). *Développement de protocoles expérimentaux pour caractériser la consolidation de résidus miniers saturés et non saturés à partir d'essais de compression en colonne*. (M.A.Sc. thesis, École Polytechnique de Montréal, Montreal, QC).

Éthier, M.-P. (2017). *Évaluation de la performance du système de recouvrement monocouche avec nappe surélevée pour la resturation d'un parc à résidus abandonné*. (Ph.D. thesis, Université du Québec en Abitibi-Témiscamingue, Rouyn-Noranda, QC).

Evett, S.R., Schwartz, R.C., Casanova, J.J., & Heng, L.K. (2012a). Soil water sensing for water balance, ET and WUE. *Agricultural Water Management*, *104*, 1-9. doi:10.1016/j.agwat.2011.12.002

Evett, S.R., Schwartz, R.C., Howell, T.A., Baumhardt, L., & Copeland, K.S. (2012b). Can weighing lysimeter ET represent surrounding field ET well enough to test flux station measurements of daily and sub-daily ET? *Advances in Water Resources*, 50, 79-90. doi:10.1016/j.advwatres.2012.07.023

Fahey, M., Newson, T.A., & Fujiyasu, Y. (2002). Engineering with tailings. *Proceedings of the 4th International Conference on Environmental Geotechnics* (p. 947-973). Rio de Janeiro, Brasil: Balkema Publishers.

Fala, O. (2002). *Étude des écoulements non saturés dans les haldes à stériles à l'aide de simulations numériques*. (M.A.Sc. thesis, École Polytechnique de Montréal, Montreal, QC).

Fala, O. (2008). Analyses des conditions d'écoulement non saturé dans les haldes à stériles. (Ph.D. thesis, École Polytechnique de Montréal, Montreal, QC).

Fank, J. (2011). Lysimeters: A tool for measurements of soil fluxes. In: J. Gliński, J. Horabik, & J. Lipiec (eds.), *Encyclopedia of Agrophysics*. Dordrecht, Netherlands: Springer.

Fernández-Gálvez, J., Verhoef, A. & Barahona, E. (2007). Estimating soil water fluxes from soil water records obtained using dielectric sensors. *Hydrological Processes, 21*(20), 2785-2793. doi:10.1002/hyp.6494

Fisseha, B., Bryan, R., & Simms, P. (2010). Evaporation, unsaturated flow, and salt accumulation in multilayer deposits of "paste" gold tailings. *Journal of Geotechnical and Geoenvironmental Engineering, 136*(12). doi:10.1061/(American Society of Civil Engineers)GT.1943-5606.0000367

Fitton, T. (2017). Avoiding large tailings dams without going underground- Robinsky's thickened tailings concept. *In Paste 2017: Proceedings of the 20th International Seminar on Paste and Thickened Tailings* (pp.243-249). Beijing, China: Australian Center for Geomechanics. From https://papers.acg.uwa.edu.au/p/1752_27_Fitton/

Fourie, A. (2012a). Paste and thickened tailings: has the promise been fulfilled? In R. D. Hryciw, A. Athanasopoulos-Zekkos, & N. Yesiller (eds.), *GeoCongress 2012: State of the Art and Practice in Geotechnical Engineering. American Society of Civil Engineers*, Oakland, CA: American Society of Civil Engineers. doi:10.1061/9780784412121.424

Fourie, A (2012b). Perceived and realised benefits of paste and thickened tailings for surface deposition. In R.J. Jewell, A.B. Fourie, & A. Paterson (eds.), *Paste 2012: Proceedings of the 15th International Seminar on Paste and Thickened Tailings* (p.53-64). Perth, Australia: Australian Center for Geomechanics. From http://www.acg.uwa.edu.au/__data/page/7583/05_Fourie_sample_paper_web.pdf

Fredlund, D.G. (2006). Unsaturated soil mechanics in engineering practice. *Journal of Geotechnical and Geoenvironmental Engineering, 132*(3). doi:10.1061/(American Society of Civil Engineers)1090-0241(2006)132:3(286)

Fredlund, D.G., & Rahardjo, H. (1993). *Soil mechanics for unsaturated soils*. New York, NY: John Wiley & Sons, Inc.

Fredlund, D.G., & Xing, A. (1994). Equations for the soil-water characteristic curve. *Canadian Geotechnical Journal, 31*(4), 521-532.

Fredlund, D.G., Morgenstern, N.R., & Widger, R.A. (1978). The shear-strength of unsaturated soils. *Canadian Geotechnical Journal, 15*(3), 313-321.

Fredlund, D.G., Xing, A., & Huang, S. (1994). Predicting the permeability function for unsaturated soils using the soil-water characteristic curve. *Canadian Geotechnical Journal*, *31*, 533-546.

Fredlund, D.G., Xing, A., Fredlund, M.D., & Barbour, S.L. (1995). The relationship of the unsaturated soil shear strength to the soil-water characteristic curve. *Canadian Geotechnical Journal*, *32*, 440-448.

Fredlund, D.G., Rahardjo, H., & Fredlund, M.D. (2012). *Unsaturated soils in engineering practice*. Hoboken, NJ: John Wiley & Sons, Inc.

Freeze, R.A., & Cherry, J.A. (1979). *Groundwater*. Englewood Cliffs, NJ: Prentice-Hall, Inc.

Fu, B.P. (1981). On the calculation of the evaporation from land surface (in Chinese). *Scientia Atmospherica Sinica*, *5*, 23-31.

Fujiyasu, Y., & Fahey, M. (2000). Experimental study of evaporation from saline tailings. *Journal of Geotechnical and Geoenvironmental Engineering*, *126*(1), 18-27.

Fujiyasu, Y., Fahey, M., & Newson, T. (2000). Field investigation of evaporation from freshwater tailings. *Journal of Geotechnical and Geoenvironmental Engineering*, *126*(6), 556-567.

Gan, J.K.-M., Fredlund, D.G., & Rahardjo, H. (1988). Determination of the shear strength parameters of an unsaturated soil using the direct shear test. *Canadian Geotechnical Journal*, *25*, 500-510.

Gan, J.K.-M., & Fredlund, D.G. (1996). Shear strength characteristics of two saprolitic soils. *Canadian Geotechnical Journal*, *33*, 595-609.

Gardner, W.R. (1958). Some steady state solutions of unsaturated moisture flow equations with application to evaporation from a water table. *Soil Science*, *85*, 228 – 232.

Gawu, S.K.Y., & Fourie, A.B. (2004). Assessment of the modified slump test as a measure of the yield stress of high-density thickened tailings. *Canadian Geotechnical Journal*, *41*, 39-47.

Gawu, S.K.Y., & Fourie, A.B. (2005). Reply to the "Discussion by Crowder and Grabinsky on 'Assessment of the modified Slump Test as a measure of the yield stress of high-density thickened tailings'". *Canadian Geotechnical Journal*, *42*, 319-320.

Geo-Slope International. (2007). GeoStudio [Software]. Calgary, AB: Geo-Slope International Ltd.

Geo-Slope International. (2008). *Vadose Zone Modeling with VADOSE/W 2007: An Engineering Methodology* (3rd ed.). Calgary, AB: Geo-Slope International Ltd.

Geo-Slope International. (2016). GeoStudio [Software]. Calgary, AB: Geo-Slope International Ltd.

Gibson, R.E., England, G.L., & Hussey, M.J.L. (1967). The theory of one-dimensional consolidation of saturated clays. *Géotechnique*, *17*(3), 261-273.

Gibson, R.E., Schifman, R.L., Cargill, K.W. (1981). The theory of one-dimensional consolidation of saturated clays. II. Finite nonlinear consolidation of thick homogeneous layers. *Canadian Geotechnical Journal*, *18*, 280-293.

Golder Associates Ltd. (1998). *Geotechnical Assessment, Tailings Disposal Facility, Bulyanhulu Mining Project, Kahama District, Tanzania* (Report # No. 982-1725/6000). Burnaby, BC: Golder Associates Ltd.

Golder Associates Ltd. (2000). *Interim Report on: Deposition Plan: Surface Paste Tailings Disposal, Bulyanhulu Project, Tanzania* (Report # No. 991-1824 (5500)). Mississauga, ON: Golder Associates Ltd.

Golder Associates Africa (Pty) Ltd. (2005). *Bulyanhulu Tailings Management Optimisation* (Report # No. 5098/6917/6/S). Johannesburg, South Africa: Golder Associates Africa (Pty) Ltd.

Gonzales, V. (2005). Cobriza's Cu Tailings Surface Stacking: A Successful Story. In R. Jewell, & S. Barrera (eds.), *Paste 2005 – Proceedings of the 8th International Seminar on Paste and Thickened Tailings* (pp.261-274). Perth, Australia: Australian Centre for Geomechanics.

Gosselin, M. (2007). *Étude de l'influence des caractéristiques hydrogéochimiques des résidus miniers réactifs sur la diffusion et la consommation de l'oxygène*. (M.A.Sc. thesis, École Polytechnique de Montréal, Montreal, QC).

Grabinsky, M.W., Theriault, J., & Welch, D. (2002). An overview of paste and thickened tailings disposal on surface. *Proceedings of Symposium 2002 on Environment and Mines*. Rouyn-Noranda, QC: Canadian Institute of Mining, Metallurgy and Petroleum.

Gran, M., Carreraa, J., Massanac, J., Saaltinkb, M.W., Olivellab, S., Ayoraa, C., & Lloret, A. (2011). Dynamics of water vapor flux and water separation processes during evaporation from a salty dry soil. *Journal of Hydrology*, *396*(3-4), 215-220. doi:10.1016/j.jhydrol.2010.11.011

Grant, S.A., & Bachmann, J. (2002). Effect of temperature on capillary pressure. In *Environmental Mechanics: Water, Mass and Energy Transfer in the Biosphere - Geophysical Monograph 129* (p. 199-212). Washington, DC: American Geophysical Union.

Gray, N. F. (1997). Environmental impact and remediation of acid mine drainage: A management problem. *Environmental Geology*, *30*, 62-71. doi:10.1007/s002540050133

Green, W.H., & Ampt, G.A. (1911). Studies on soil physics: I. Flow of air and water through soils. Journal of Agricultural Science, *4*, 1-24.

Haigh, S.K. (2012). Mechanics of the Casagrande liquid limit test. *Canadian Geotechnical Journal*, *49*(9), 1015-1023. doi:10.1139/T2012-066.

Haile, G., O'Callanghan, W.B., & Hartney, T.F. (2000). Experience with thickened red mud tailings (paste) stacking in tropical and temperate climates and applicability of the technology to other tailings. *Proceedings of the 53rd Canadian Geotechnical Conference and 1st Joint CGS/IAH-CNC Conference* (p. 683-690). Montreal, QC: Canadian Geotechnical Society.

Harp, D.R., Stormont, J.C., Reda Taha, M.M., Frafan, E. & Coonrod, J. (2006). Estimation of bare soil evaporation using fuzzy modeling. In D.J. DeGroot, J.T. DeJong, D., Frost, & L.G. Baise (eds.), *GeoCongress 2006: Geotechnical Engineering in the Information Technology Age*. Atlanta, GA: American Society of Civil Engineers. doi:10.1061/40803 (187)14

Hart, B., & Boger, D.V. (2005). Tailings waste minimisation, rheology, and the triple bottom line. *Paste 2005 – Proceedings of the 8th International Seminar on Paste and Thickened Tailings* (Vol. 1, p. 5-27). Santiago, Chile: Australian Centre for Geomechanics.

Hassani, F., & Archibald, J.H. (1998). *Mine backfill* [CD-ROM]. Montreal, QC: CIM.

Haverkamp, R., Reggiani, P., Ross, P.J., & Parlange, J.-Y. (2002). Soil water hysteresis prediction model based on theory and geometric scaling. In *Environmental Mechanics: Water, Mass and Energy Transfer in the Biosphere - Geophysical Monograph 129* (p. 213-246). Washington, DC: American Geophysical Union.

Healy, R. (2010). *Estimating groundwater recharge*. Cambridge, UK: Cambridge University Press.

Henriquez, J., & Simms, P. (2009). Dynamic imaging and modelling of multilayer deposition of gold paste tailings. *Minerals Engineering*, *22*(2), 128-139. doi:10.1016/j.mineng.2008.05.010

Herasymuik, G.M. (1996). Hydrogeology of a sulfide waste rock dump. (M.Sc thesis,. University of Saskatchewan, Saskatoon, SK).

Hillel, D. (1980). *Applications to soil physics*. New York, NY: Academic Press.

Hillel, D. (1998). *Environmental soil physics*. San Diego, CA: Academic Press.

Holtz, R.D., & Kovacs, W.D. (1981). *Introduction à la géotechnique*. (trad. J. Lafleur). Montreal, QC: Éditions de l'École Polytechnique de Montréal.

Iyer, K., Jayanth, S., Gurnani, S., & Singh, D.N. (2012). Influence of initial water content and specimen thickness on the SWCC of fine-grained soils. *International Journal of Geomechanics*, *13*(6). doi:10.1061/ (American Society of Civil Engineers)GM.1943-5622.0000265

Jabro, J.D. (2009). Water vapor diffusion through soil as affected by temperature and aggregate size. *Transport in Porous Media, 77*(3), 417-428. doi:10.1007/s11242-008-9267-z

Jambor, J.L. (2003). Chapter 6 - Mine-waste mineralogy and mineralogical perspectives of acid-base accounting. In Jambor, J.L., Blowes, D.W., & Ritchie, A.I.M. (eds.), *Environmental Aspects of Mine Wastes. Short Course Series: Volume 31* (p. 117-145). Vancouver, BC: Mineralogical Association of Canada.

James, M. (2009). *The use of waste rock inclusions to control the effects of liquefaction in tailings impoundments*. (Ph.D. thesis, École Polytechnique de Montréal, Montreal, QC).

Jaynes, R.A., & Gifford, G.F. (1981). An in-depth examination of the Philip equation for cataloging infiltration characteristics in rangeland environments. *Journal of Range Management*, *34*(4), 285-296.

Jewell, R.J., Fourie, A.B., & Lord, E.R. (2002). *Paste and thickened tailings – A guide*. Nedlands, Australia: The Australian Center for Geomecanics.

Johnson, J.M., Vialpando, J., & Lee, C. (2005). Paste tailings management alternative – Study results for Molycorp's lanthanide group operations in Mountain Pass, California. *Mining Engineering*, *57*(2), 50-56.

Jones, H. & Boger, D.V. (2012). Sustainability and waste management in the resource industries. *Industrial & Engineering Chemistry Research, 51*(30), 10057-10065. doi:10.1021/ie202963z

Jones, S.B., Wraith, J.M., & Or, D. (2002). Time domain reflectometry measurement principles and applications. *Hydrological Processes, 16*(1), 141-153. doi:10.1002/hyp.513

Junqueira, F.F., Sanin, M.V., Sedgwick, A., & Blum, J. (2011). Assessment of water removal from oil sands tailings by evaporation and under-drainage, and the impact on tailings consolidation. *Proceedings Tailings and Mine Waste 2011*. Vancouver, BC. From http://www.infomine.com/library/publications/docs/Junqueira2011.pdf

Kalonji Kambabi, A., Bussière, B., & Demers, I. (2017). Hydrogeological behaviour of covers with capillary barrier effects made of mining materials. *Geotechnical and Geological Engineering*, *35*, 1199-1220.

Kam, S., Girard, J., Hmidi, N., Mao, Y., & Longo, S. (2011). Thickened tailings disposal at Musselwhite Mine. In R.J. Jewell, & A.B. Fourie (eds.), *Paste 2011 – Proceedings of the 14th International Seminar on Paste and Thickened Tailings* (p. 225-236). Perth, Australia: Australian Center for Geomechanics.

Kesimal, A., Yilmaz, E., & Ercikdi, B. (2004). Evaluation of paste backfill mixtures consisting of sulphide-rich mill tailings and varying cement content. *Cement and Concrete Research, 34*, 1817-1822.

Khalil, M., Sakai, M., Mizoguchi, M. & Miyazaki, T. (2003). Current and prospective applications of zero-flux plane (ZFP) Method. *Journal of the Japanese Society of Soil Physics*, *95*, 75-90.

Kilborn-SNC Lavallin. (1998). *Bulyanhulu feasibility study, Volume I – Sections 2, 8, 9.* May 1998.

Kim, T.-H., & Sture, S. (2008). Capillary-induced tensile strength in unsaturated sands. Canadian Geotechnical Journal, *45*, 726-737. doi:10.1139/T08-017

Kirsch, S.W. (1993). A field test of a soil-based measure of evapotranspiration. *Soil Science*, 156(6), 396-404.

Kleinmann, R.L.P., Crerar, D.A., & Pacelli, R.R. (1981). Biogeochemistry of acid mine drainage and a method to control acid formation. *Mining Engineering*, *33*(3), 300-305

Knidiri, J., Bussière, B., Hakkou, R., Bossé, B., Maqsoud, A., & Benzaazoua, M. (2017). Hydrogeological behaviour of an inclined store-and-release cover experimental cell made with

phosphate mine wastes. *Canadian Geotechnical Journal*, *54*(1), 102-116. doi:10.1139/cgj-2015-0530

Konrad, J.-M., & Ayad, R. (1997). Desiccation of a sensitive clay: field experimental observations. *Canadian Geotechnical Journal*, *34*, 929-942. doi:10.1139/cgj-34-6-929

Kwak, M., James, D.F., & Klein, K.A. (2005). Flow behaviour of tailings paste for surface disposal. *International Journal of Mineral Processing*, *77*(3), 139-153. doi:10.1016/j.minpro.2005.06.001

Langfelder, L.J. (1964). *An investigation of initial negative pore water pressure in statically compacted cohesive soil*. (Ph.D. thesis, University of Illinois, Urbana, IL).

Landriault, D., Johnson, J.M., & Palkovits, F. (2005). Thickened tailings and paste technology: The future of industrial waste disposal. *Proceedings of SME Annual Meeting* (Pre-print 05-111). Salt Lake City, UT: Society for Mining, Metallurgy and Exploration, Inc.

L.-Bolduc, F. (2012). *Une étude sur l'utilisation des roches stériles comme inclusions drainantes dans les résidus miniers*. (M.A.Sc. thesis, École Polytechnique de Montréal, Montreal, QC).

Leij, F.J., Russel, W.B., & Lesch, S.M. (1997). Closed-form expressions for water retention and conductivity data. *Groundwater*, *35*, 848-858.

Leroueil, S., & Le Bihan, J.-P. (1996). Liquid limits and fall cones. *Canadian Geotechnical Journal*, *33*(5), 793-798. doi:10.1139/t96-104-324

Levenspiel, O. (1972). *Chemical reaction engineering* (2nd ed.) New York, NY: John Wiley & Sons.

Li, H., & Jiao, J.J. (2005). One-dimensional airflow in unsaturated zone induced by periodic water table fluctuations. *Water Resources Research*, *41*(4). doi:10.1029/2004WR003916.

Li, L., & Aubertin, M. (2014). An improved method to assess the required strength of cemented backfill in underground stopes with an open face. *International Journal of Mining Science and Technology*, *24*(4), 549-558. doi:10.1016/j.ijmst.2014.05.020

Li, M., Bernier, L., & Boucher, J.-F. (2002). Rheology of mineral pastes and its implications on underground pipeline delivery. *Proceedings of Symposium 2002 on Environment and Mines*. Rouyn-Noranda, QC: Canadian Institute of Mining, Metallurgy and Petroleum.

Long, X. (2006). *Prediction of shear strength and vertical movement due to moisture diffusion through expansive soils*. (Ph.D. thesis, Texas A&M University, College Station, TX).

Lopes, R., Bahia, R., Jeffries, M., & Oliviera, M. (2015). Upstream stacking of thickened tailings at Nerves Corvo. In R.J. Jewell, & A.B. Fourie (eds.), *Paste 2015 – Proceedings of the 18th International Seminar on Paste and Thickened Tailings* (p. 521-534). Perth, Australia: Australian Center for Geomechanics.

Lowson, L.T. (1982). Aqueous oxidation of pyrite by molecular oxygen. *Chemical reviews*, *82*(5), 461-497. doi:10.1021/cr00051a001

Lu, N., & Likos, W.J. (2004). *Unsaturated soil mechanics*. Hoboken, NJ: John Wiley & Sons, Inc.

Lyell, K.A., Copeland, A.M., & Blight, G.E. (2008). Alternatives to paste disposal with lower water consumption? In A. Fourie, R. Jewell, P. Slatter, & A. Paterson (eds.), *Paste 2008: Proceedings of the Eleventh International Seminar on Paste and Thickened Tailings* (p.171-178). Perth, Australia: Australian Center for Geomechanics.

Maqsoud, A., Bussière, B., Mbonimpa, M., & Aubertin, M. (2004). Hysteresis effects on the water retention curve: A comparison between laboratory results and predictive models. *Proceedings of the 57th Canadian Geotechnical Conference and 5th Joint CGS/IAH-CNC Conference* (p. 8-15). Quebec City, QC: Canadian Geotechnical Society.

Maqsoud, A., Bussière, B., Aubertin, M., & Mbonimpa, M. (2012). Predicting hysteresis of the water retention curve from basic properties of granular soils. *Geotechnical and Geological Engineering*, *30*(5), 1147-1159. doi:10.1007/s10706-012-9529-y

Mabirizi, D., & Bulut, R. (2010). Wetting and drying unsaturated soil moisture diffusivity parameters. *GeoShanghai 2010 Experimental and Applied Modeling of Unsaturated Soils*, (GSP 202). Shanghai, China: American Society of Civil Engineers. doi:10.1061/41103(376)8

Marinho, F.A.M., Take, W.A. & Tarantino, A. (2008). Measurement of matric suction using tensiometric and axis translation techniques. *Geotechnical and Geological Engineering*, *26*, 615-631. doi:10.1007/s10706-008-9201-8

Marinho, F.A.M., Take, W.A. & Tarantino, A. (2009). Measurement of matric suction using tensiometric and axis translation techniques. In Cui, Y.J., Romero, E. & Tarantino, A. (eds.),

Laboratory and field testing of unsaturated soils (p. 3-19). SpringerLink. doi:10.1007/978-1-4020-8819-3

Marshall, T.J., Holmes, J.W., & Rose, C.W. (1996). *Soil physics* (3rd ed.). Cambridge, UK: Cambridge University Press.

Martin, V., Aubertin, M., Bussière, B., & Chapuis, R.P. (2004). Evaluation of unsaturated flow in mine waste rock. *Proceedings of the 57th Canadian Geotechnical Conference and 5th Joint CGS/IAH-CNC Conference*. Quebec City, QC: Canadian Geotechnical Society.

Martin, V., Aubertin, M., Zhan, G., Bussière, B., & Chapuis, R.P. (2005). An investigation into the hydrological behaviour of exposed and covered waste rock dumps. *SME Transactions (2005)* (Vol. 318, p. 139-146). Littleton, CO: The Society for Mining, Metallurgy, and Exploration Inc.

Martin V., Aubertin, M., Bussière, B., Mbonimpa, M., Dagenais, A.-M., & Gosselin, M. (2006a). Measurement of oxygen consumption and diffusion in exposed and covered reactive mine tailings. *Proceedings of 7th International Conference on Acid Rock Drainage*. St. Louis, MO: The Society for Mining, Metallurgy, and Exploration Inc.

Martin, V., Aubertin, M., & McMullen, J. (2006b). Surface disposal of paste tailings. *Proceedings of the 5th International Congress on Environmental Geotechnics*. Cardiff, UK: International Society for Soil Mechanics and Geotechnical Engineering.

Martin, V., Aubertin, M., Benzaazoua, M., & Zhan, G. (2010). Investigation of near-surface exchange processes in reactive paste tailings. In R.J. Jewell, & A.B. Fourie (eds.), *Paste 2010 – Proceedings of the 13th International Seminar on Paste and Thickened Tailings* (p. 265-278). Perth, Australia: Australian Center for Geomechanics.

Martin, V., Aubertin, M., & Benzaazoua, M. (2013). Analysis of the desaturation of paste tailings: Experiments and preliminary simulations. *Proceedings of the 66th Canadian Geotechnical Conference and 15th Joint CGS/IAH-CNC Conference*. Montreal, QC: Canadian Geotechnical Society.

Mayer, K.U., Blowes, D.W., & Frind, E.O. (2003). Chapter 14 - Advances in reactive-transport modelling of contaminant release and attenuation from mine-waste deposits. In Jambor, J.L., Blowes, D.W., & Ritchie, A.I.M. (eds.), *Environmental Aspects of Mine Wastes. Short Course Series: Volume 31* (p. 283-302). Vancouver, BC: Mineralogical Association of Canada.

Mbonimpa, M., Aubertin, M., Chapuis, R.P., & Bussière, B. (2000). Développement de fonctions hydriques utilisant les propriétés géotechniques de base. *Proceedings of the 53rd Canadian Geotechnical Conference and 1st Joint CGS/IAH-CNC Conference* (p. 343-350). Montreal, QC: Canadian Geotechnical Society.

Mbonimpa, M., Aubertin, M., Chapuis, R.P., & Bussière, B. (2002a). Practical pedotransfer functions for estimating the saturated hydraulic conductivity. *Geotechnical and Geological Engineering*, *20*, 235-259.

Mbonimpa, M., Aubertin, M., Aachib, M., & Bussière, B. (2002b). *Oxygen Diffusion and Consumption in Unsaturated Cover Materials* (Report # EPM-RT-02-04). Montreal, QC: Éditions de l'École Polytechnique.

Mbonimpa, M., Aubertin, M., Dagenais, A.-M., Bussière, B., Julien, M., & Kissiova, M. (2002c). Interpretation of field tests to determine the oxygen diffusion and reaction rate coefficients of tailings and soil covers. *Proceedings of the 55th Canadian Geotechnical Conference and 3rd joint IAH-CNC and CGS Groundwater Specialty Conference* (p. 147-154). Niagara Falls, ON: Canadian Geotechnical Society.

Mbonimpa, M., & Aubertin, M. (2003). *Mouvement des gaz en milieux poreux partiellement saturés* (Report # EPM-RT-2003-04). Montreal, QC: Éditions de l'École Polytechnique.

Mbonimpa, M., Aubertin, M., Aachib, M., & Bussière, B. (2003). Diffusion and consumption of oxygen in unsaturated cover materials. *Canadian Geotechnical Journal*, *40*(5), 916-932.

Mbonimpa, M., Aubertin, M., Bussière, B., & Maqsoud, A. (2005). A new equation for the suction induced shrinkage of clayey soils. *Proceedings of the 58th Canadian Geotechnical Conference and 6th Joint CGS/IAH-CNC Conference*. Saskatoon, SK: Canadian Geotechnical Society.

Mbonimpa, M., Aubertin, M., Maqsoud, A., & Bussière, B. (2006). A predictive model for the water retention curve of deformable clayey soils. *Journal of Geotechnical and Geoenvironmental Engineering*, *132*(9), 1121-1132.

Mbonimpa M., Aubertin, M., & Bussière, B. (2011). Oxygen consumption test to evaluate the diffusive flux into reactive tailings: interpretation and numerical assessment. *Canadian Geotechnical Journal, 48*, 878-890.

Mbonimpa, M., Awoh, A.S., & Aubertin, M. (2012). A simple interpretation for the modified oxygen consumption test on sulphide tailings. *Proceedings of the 65th Canadian Geotechnical Conference and 13th Joint CGS/IAH-CNC Conference*. Winnipeg, MB: Canadian Geotechnical Society.

McGowan, M. & Williams, B. (1980). The water balance of an agricultural catchment. I. Estimation of evaporation from soil water records. *Journal of Soil Science*, *31*, 217-230.

McKenn, R.G. (1985). *Validation of procedures for pavement design on expansive soils* (Report # DOT/FAA/PM-85/15). Washington, DC: US Department of Transportation. From http://www.dtic.mil/dtic/tr/fulltext/u2/a160739.pdf

McKeen, R.G., & Johnson, L.D. (1990). Climate controlled soil design parameters for mat foundations. *Journal of Geotechnical Engineering*, *116*(7), 1073-1094.

McWorther, D.B., & Nelson, J.D. (1979). Unsaturated flow beneath tailings impoundments. *Journal of Geotechnical and Geoenvironmental Engineering*, *105*(11), 1317-1334.

Mein, R.G., & Larson, C.L. (1971). *Modeling the infiltration component of the rainfall-runoff process* (Bulletin #43). St. Paul, MN: Water Resources Research Center, University of Minnesota.

Mein, R.G., & Larson, C.L. (1973). Modeling infiltration during a steady rain. *Water Resources Research*, *9*(2), 384-394.

Metago (2002). *Review of the paste tailings disposal operations at Bulyanhulu gold mine* (Project # 164-010, Report no. 1). Sandton, South Africa: Metago Environmental Engineers (Pty) Ltd.

Mi, H. (1995). Kinematic wave formulation for flow through macroporous soil. (Ph.D. thesis, Wayne State University, Detroit, MI).

Mihiretu, W.T., Chlaturnyk, R.J., & Scott, J.D. (2005). Slurry characterization using yield stress measurements. *Proceedings of the 58th Canadian Geotechnical Conference and 6th Joint CGS/IAH-CNC Conference*. Saskatoon, SK: Canadian Geotechnical Society.

Milczarek, M., van Zyl, D., Peng, S., & Rice, R.C. (2006). Saturated and unsaturated hydraulic properties characterization at mine facilities: Are we doing it right? *Proceedings of the 7th International Conference on Acid Rock Drainage*. St. Louis, MO: The Society for Mining, Metallurgy, and Exploration Inc.

Milczarek, M., Orellana, R., Ludwick, W., Zhan, G., Baumann, W., Rice, R.C., Yao, T.M. & Keller, J. (2011). Final results of the cover system test panel trials at the Pierina Mine. *Proceedings Tailings and Mine Waste 2011*. Vancouver, BC: Norman B. Keevil Institute of Mining Engineering, University of British Columbia.

Miller, C.J., Mi, H., & Yesiller, N. (1998). Experimental analysis of desiccation crack propagation in clay liners. *Journal of the American Water Resources Association*, *34*(3), 677-686. doi:10.1111/j.1752-1688.1998.tb00964.x

Mitchell, J.K. (2005). *Fundamentals of soil behaviour* (3rd ed.). Hoboken, NJ: John Wiley & Sons.

Mittal, H.K., & Morgenstern, N.R. (1976). Seepage control in tailings dams. *Canadian Geotechnical Journal*, *13*, 277-293.

Miyazaki, T. (2006). *Water flow in soils* (2nd ed.). CRC Press Taylor & Francis Group.

Mizani, S., He, X., & Simms, P. (2013). Application of lubrication theory to modeling stack geometry of high density mine tailings. *Journal of Non-Newtonian Fluid Mechanics*, *198*, 59-70. doi:10.1016/j.jnnfm.2013.03.002

Mizani, S., & Simms, P. (2016). Method-dependent variation of yield stress in a thickened gold tailings explained using a structure based viscosity model. *Minerals Engineering*, *98*, 40-48. doi:10.1016/j.mineng.2016.07.011.

Mollerup, M. (2007). Philip's infiltration equation for variable-head ponded infiltration. *Journal of Hydrology*, *347*, 173-176.

Molson, J.W., Aubertin, M., Bussière, B., & Joanes, A.-M. (2004). Simulating acid mine drainage through mine wastes constructed with capillary barrier covers. *Proceedings of the 57th Canadian Geotechnical Conference and 5th Joint CGS/IAH-CNC Conference*. Quebec City, QC: Canadian Geotechnical Society.

Molson, J.W., Fala, O., Aubertin, M., & Bussière, B. (2005a). Numerical simulations of pyrite oxidation and acid mine drainage in unsaturated waste rock piles. *Journal of Contaminant Hydrology*, *78*, 343-371.

Molson, J.W., Frind, E.O., Aubertin, M., & Blowes, D. (2005b). *Polymin Version 3.0 – 2D Reactive mass transport model with oxygen diffusion, sulphide oxidation & geochemical speciation: User guide*. Montreal, QC: École Polytechnique.

Molson, J.W., Aubertin, M., Bussière, B. (2012). Reactive transport modelling of acid mine drainage within discretely fractured porous media: Plume evolution from a surface source zone. *Environmental Modelling and Software, 38,* 259-270. doi:10.1016/j.envsoft.2012.06.010.

Morgenstern, N., Vick, S. G., & Van Zyl, D. (2015). *Report on Mount Polley tailings storage facility breach: Report of independent expert engineering investigation and review panel*. Vancouver, BC: Government of British-Columbia. From: https://www.mountpolleyreviewpanel.ca/sites/default/files/report/ReportonMountPolleyTailingsStorageFacilityBreach.pdf

Morgenstern, N., Vick, S. G., Viotti, C.B., & Watts, B. (2016). *Fundão tailings dam review panel: Report on the immediate causes of the failure of the Fundão dam*. From: http://fundaoinvestigation.com/wp-content/uploads/general/PR/en/FinalReport.pdf

Morin, K.A., Gerencher, E., Jones, C.E., & Konasewich, D.E. (1991). *Critical review of acid drainage from waste rock* (Report # 1.11.1). Ottawa, ON: MEND.

Morris, C.E., & Stormont, J.C. (2000). Incorporating near-surface processes in modeling moisture movement in soils. In C.D. Shackelford, S.L. Houston, N.-Y. Cheng (eds.), *Geotechnical Special Publication No. 99: Advances in Unsaturated Geotechnics. Proceedings of Sessions of Geo-Denver* (p. 529-542). Reston, VA: American Society of Civil Engineers.

Morris, P.H., Lockington, D.A., & Apelt, C.J. (2000). Correlations for mine tailings consolidation parameters. *International Journal of Surface Mining, Reclamation and Environment, 14*, 171-182.

Mualem, Y. (1976). A new model for predicting the hydraulic conductivity of unsaturated porous media. *Water Resources Research, 12,* 513-522.

Mualem, Y. (1986). Hydraulic conductivity of unsaturated soils: Prediction and formulas. A. Klute (ed.), *Methods of Soil Analysis, Part I, Agronomy Monograph No. 9* (2nd ed., p.799-823). Madison, WI: ASA and SSSA.

Narvaez, B., Aubertin, M., & Saleh-Mbemba, F. (2015). Determination of the tensile strength of unsaturated tailings using bending tests. *Canadian Geotechnical Journal*, *52*(11), 1874-1885. doi:10.1139/cgj-2014-0156

Nastev, M., Aubertin, M. (2000). Hydrogeological modelling for the reclamation work at the Lorraine mine site Québec. *Proceedings of the 53rd Canadian Geotechnical Conference and 1st Joint CGS/IAH-CNC Conference* (p. 311-318). Montreal, QC: Canadian Geotechnical Society.

Nelson, J.D., Overton, D.D., & Durkee, D.B. (2001). Depth of Wetting and the Active Zone. In C. Vipulanandan, M. B. Addison, & M. Hansen (eds.), *Expansive Clay Soils and Vegetative Influence on Shallow Foundations* (p. 95-109). Reston, VA: American Society of Civil Engineers. doi:10.1061/40592 (270)6

Newson, T.A., & Fahey, M. (2003). Measurement of evaporation from saline tailings storages. *Engineering Geology*, *70*, 217-233.

Nguyen, Q.D., & Boger, D.V. (1998). Application of rheology to solving tailings disposal problems. *International Journal of Mineral Processing*, *54*(3-4), 217-233.

Nicholson, R.V., Gillham, R.W., Cherry, J.A., & Reardon, E.J. (1989). Reduction of acid generation in mine tailings through the use of moisture-retaining cover layers as oxygen barriers. *Canadian Geotechnical Journal*, *26*, 1-8.

Nicholson, R.V., Elberling, B., & Williams, G. (1995). A new oxygen consumption technique to provide rapid assessment of tailings reactivity in the field and laboratory. *Proceedings of Sudbury '95: Conference on Mining and the Environment*. Sudbury, ON.

Öberg, A.-L., & Sällfors, G. (1997). Determination of shear strength parameters of unsaturated silts and sands based on the water retention curve. *Geotechnical Testing Journal*, *20*(1), 40-48.

Oliver, J.E. (2005). Climate classification. In J.E. Oliver (ed.), *Encyclopedia of world climatology* (pp. 218-227). SpringerLink. From http://www.springerlink.com/openurl.asp?genre=book&isbn=978-1-4020-3264-6

Oloo, S.Y., & Fredlund, D.G. (1996). A method for determination of φb for statically compacted soils. *Canadian Geotechnical Journal*, *33*, 272-280.

Olson, R.E., & Langelder, L.J. (1965). Pore water pressure in unsaturated soils. *Journal of the Soil Mechanics and Foundation Division – Proceedings of the American Society of Civil Engineers, 4409*(SM4), 127-150.

Or, D., & Tuller, M. (1999). Liquid retention and interfacial area in variably saturated porous media: Upscaling from single pore to sample-scale model. *Water Resources Research*, *35*(12), 3591-3605. doi:10.1029/1999WR900262

Ouangrawa, M. (2007). *Étude expérimentale et analyse numérique des facteurs qui influencent le comportement hydro-géochimique de résidus miniers sulfureux partiellement saturés*. (Ph.D. thesis, École Polytechnique de Montréal, Montreal, QC).

Pabst, T. (2011). *Étude expérimentale et numérique du comportement hydro-géochimique de recouvrements placés sur des résidus sulfureux partiellement oxydés*. (Ph.D. thesis, École Polytechnique de Montréal, Montreal, QC).

Pabst, T., Aubertin, M., Bussière, B., & Molson, J. (2014). Column tests to characterise the hydrogeochemical response of pre-oxidised acid-generating tailings with a monolayer cover. *Water, Air, and Soil Pollution*, *225*. doi:10.1007/s11270-013-1841-5

Pane, V., & Schiffman, R.L. (1985). A note on sedimentation and consolidation. *Géotechnique, 35*(1), 69-72.

Parlange, J.-Y. (1976). Capillary hysteresis and relationship between drying and wetting curves. *Water Resources Research, 12*, 224-228.

Pashias, N., Boger, D.V., Summers, J., Glenister, D.J. (1996). A fifty cent rheometer for yield stress measurement. *Journal of Rheology, 40*(6), 1179-1189.

Penman, H.L. (1948). Natural evapotranspiration from open water, bare soil, and grass. *Proceedings Royal Society of London, Series A, 193*, 120-145.

Pépin, N. (2010). *Étude du comportement cyclique de résidus miniers avec inclusions drainantes par des essais sur table sismique*. (M.A.Sc. thesis, École Polytechnique de Montréal, Montreal, QC).

Peregoedova, A. (2012) *Étude expérimentale des propriétés hydrogéologiques des roches stériles à une échelle intermédiaire de laboratoire*. (M.A.Sc. thesis, École Polytechnique de Montréal, Montreal, QC).

Philip, J.R. (1957a). The theory of infiltration: 1. The infiltration equation and its solution. *Soil Science, 83*(5), 345-358.

Philip, J.R. (1957b). The theory of infiltration: 2. The profile of infinity. *Soil Science, 83*(6), 435-448.

Philip, J.R. (1957c). The theory of infiltration: 3. Moisture profiles and relation to experiment. *Soil Science, 84*(2), 163-178.

Philip, J.R. (1957d). The theory of infiltration: 4. Sorptivity and algebraic infiltration equations. *Soil Science, 84*(3), 257-264.

Philip, J.R. (1957e). The theory of infiltration: 5. The influence of the initial moisture content. *Soil Science. 84*(4), 329-340.

Philip, J.R. (1958). The theory of infiltration: 6. Effect of water depth over soil. *Soil Science, 85*(5), 278-286.

Plante, B. (2010). *Évaluation des principaux facteurs d'influence sur la prédiction du drainage neutre contaminé*. (Ph.D. thesis, Université du Québec en Abitibi-Témiscamingue, Rouyn-Noranda, QC).

Potvin, Y., Thomas, E., & Fourie, A. (2005). *Handbook on mine fill*. Nedlands, Australia: Australian Centre for Geomechanics.

Prunty, L., & Bell, J. (2007). Soil water hysteresis at low potential. *Pedosphere, 17*(4), 436-444. doi:10.1016/S1002-0160(07)60053-8

Ptacek, C.J., & Blowes, D.W. (2003). Chapter 12 - Geochemistry of concentrated waters at mine-waste sites. In Jambor, J.L., Blowes, D.W., & Ritchie, A.I.M. (eds.), *Environmental Aspects of Mine Wastes. Short Course Series: Volume 31* (p. 239-260). Vancouver, BC: Mineralogical Association of Canada.

Qi, S., & Simms P. (2010). Analysis of dewatering and desaturation of generic field deposition scenarios for thickened tailings. In R.J. Jewell, & A.B. Fourie (eds.), *Paste 2018 – Proceedings of*

the 21th International Seminar on Paste and Thickened Tailings. Perth, Australia: Australian Center for Geomechanics.

Qiu, G., Yano, T., & Momii, K. (1998). An improved methodology to measure evaporation from bare soil based on comparison of surface temperature with a dry soil surface. *Journal of Hydrology, 210*(1-4), 93-105. doi:10.1016/S0022-1694(98)00174-7.

Qiu, Y., & Sego, D.C. (2001). Laboratory properties of mine tailings. *Canadian Geotechnical Journal*, *38*, 183-190.

Rahardjo, H., Lim, T.T., Chang, M.F., & Fredlund, D.G. (1995). Shear-strength characteristics of a residual soil. *Canadian Geotechnical Journal*, *32*, 60-77.

Rassam, D.W. (2002). Variation of evaporative and shear strength parameters along a tailings delta. *Canadian Geotechnical Journal*, *39*, 32-45.

Rassam, D.W., & Williams, D.J. (1999a). A numerical study of steady state evaporative conditions applied to mine tailings. *Canadian Geotechnical Journal, 36*, 640-650.

Rassam, D.W., & Williams, D.J. (1999b). A relationship describing the shear strength of unsaturated soils. *Canadian Geotechnical Journal, 36*, 363-368.

Ravi, V., & Williams, J. R. (1998). *Estimation of infiltration rate in the vadose zone: compilation of simple mathematical models* (Report # EPA/600/R-97/128a). Washington, DC: United States Environmental Protection Agency (EPA).

Ricard, J.-F. (1994). *Étude en laboratoire de la relation capillaire et de la conductivité hydraulique de résidus miniers*. (M.A.Sc. thesis, École Polytechnique de Montréal, Montreal, QC).

Richards, L.A. (1931). Capillary conduction of liquids through porous medium. *Journal of Applied Physics, 1*(5), 318-333.

Richards, L.A. (1941). A pressure-membrane extraction apparatus for soil solution. *Soil Science, 51*(5), 377-386.

Richards, L.A. (1947). Pressure-membrane apparatus - Construction and use. *Agricultural Engineering*, *28*, 451-460.

Richards, L.A., Gardner, W.R., & Ogata, G. (1956). Physical processes determining water loss from soil. *Soil Science Society of America Journal*, *20*(3), 310-314.

Rijtema, P.E. (1965). *An analysis of actual evapotranspiration* (Report # 659). Wageningen, Netherlands: Center for Agricultural Publications and Documents.

Ritcey, G.M. (1989). *Tailings management, problems and solutions in the mining industry*. Amsterdam, Netherlands: Elsevier.

Robinsky, E.I. (1975). Thickened discharge – A new approach to tailings disposal. *CIM Bulletin, 68*(764), 47-53.

Robinsky, E.I. (1999). *Thickened tailings disposal in the mining industry*. Toronto, ON: E.I. Robinsky Associates Ltd.

Rose, D. (1968). Water movement in porous materials III. Evaporation of water from soil. *Journal of Physics D: Applied Physics*, *1*(12). doi:10.1088/0022-3727/1/12/327

Rowe, R.K., Booker, J.R., & Fraser, M.J. (1998). *POLLUTE v6 and POLLUTE-GUI user's guide*. London, ON: GAEA Environmental Engineering Ltd.

Sadeghi, A.M., Scott, H.D., & Ferguson, J.A. (1984). Estimating evaporation: A comparison between Penman, Idso-Jackson, and zero-flux methods. Agricultural and Forest Meteorology, *33*(2-3), 225-238. doi:10.1016/0168-1923(84)90072-8

Saleh-Mbemba, F. (2010). *Évaluation de la dessiccation, du retrait et de la fissuration de matériaux silteux peu plastiques*. (M.A.Sc. thesis, École Polytechnique,Montréal, Montreal, QC).

Saleh-Mbemba, F. (2016). *Évaluation du drainage, de la consolidation et de la dessiccation des résidus miniers fins en présence d'inclusions drainantes*. (Ph.D. thesis, École Polytechnique de Montréal, Montreal, QC).

Saleh-Mbemba, F., Aubertin, M., Mbonimpa, M., & Li, L. (2016). Experimental characterization of the shrinkage and water retention behaviour of tailings from hard rock mines. *Geotechnical and Geological Engineering, 34*(1), 251-266. doi:10.1007/s10706-015-9942-0

Salfate, E.R. (2011). *Predicting Void Ratio for Surface Paste Tailings Deposited in Thin Layers*. (M.A.Sc. thesis, University of British-Columbia, Vancouver, BC).

Scanlon, B.R., Healy, R.W., & Cook, P.G. (2002). Choosing appropriate techniques for quantifying groundwater recharge. *Hydrogeology Journal, 10*(1), 18-39. doi:10.1007/s10040-0010176-2

Senevirathne, N.H., Fahey, M., Newson, T.A., & Fujiyasu, Y. (1996). Numerical modelling of consolidation and evaporation of slurried mine tailings. *International Journal for Numerical and Analytical Methods in Geomechanics, 20,* 647-671.

Seelheim, F. (1880). Methoden zur Bestimmung der Durchlassigkeit des Bodens. Zeitschrif für analytische [In german]. *Chemie*. *19*. 387-402.

Shackelford, C.D. & Benson, C.H. (2006). Selected factors affecting water-balance predictions for alternative covers using unsaturated flow models. *GeoCongress 2006: Geotechnical Engineering in the Information Technology Age*. Atlanta, GA: American Society of Civil Engineers. doi:10.1061/40803(187)223

Sharma, M.L., Bari, M., & Byrne, J. (1991). Dynamics of seasonal recharge beneath a semiarid vegetation on the Gnangara Mound, Western Australia. *Hydrological Processes, 5*, 383-398.

Shuttleworth, J.A., Thomson, B.J., & Wates, J.A. (2005). Surface paste disposal at Bulyanhulu: Practical lessons learned. *Paste 2005 – Proceedings of the 8th International Seminar on Paste and Thickened Tailings* (p. 207-218). Santiago, Chile: Australian Centre for Geomechanics.

Simms, P. (2017). 2013 Colloquium of the Canadian Geotechnical Society: Geotechnical and geoenvironmental behaviour of high-density tailings. *Canadian Geotechnical Journal*, *468*, 455-468.

Simms, P.H., & Grabinsky, M.W. (2004). A simple method for estimating rates of drying and desaturation of paste tailings during surface deposition. *Proceedings of Tailings and Mine Waste '04*. Fort Collins, CO: A.A. Balkema.

Simms, P.H., Grabinsky, M.W., & Zhan, G. (2005). Laboratory evaluation of evaporative drying from surface deposited thickened tailings at the Bulyanhulu gold mine. *Proceedings of the 58th Canadian Geotechnical Conference and 6th Joint CGS/IAH-CNC Conference*. Saskatoon, SK: Canadian Geotechnical Society.

Simms, P., Grabinsky, M.W., & Zhan, G. (2007). Modelling evaporation of paste tailings from the Bulyanhulu mine. *Canadian Geotechnical Journal*, *44*(12), 1417-1432. doi:10.1139/T07-067

Simms, P., Dunmola, A., Fisseha, B., & Bryan, R. (2010). Generic modelling of desiccation for cyclic deposition of thickened tailings to maximise density and to minimise oxidation. In R.J.

Jewell, & A.B. Fourie (eds.), *Paste 2010 – Proceedings of the 13th International Seminar on Paste and Thickened Tailings* (p. 293-301). Perth, Australia: Australian Center for Geomechanics.

Simms, P., Soleimani, S., Mizani, S., Daliri, F., Dunmola, A., Rozina, E., & Innocent-Bernard, T. (2017). Cracking, salinity and evaporation in mesoscale experiments on three types of tailings. *Environmental Geotechnics*. doi:10.1680/jenge.16.00026

Singh, A.K., Singh, H., Singh, S.P. & Sawhney, R.L. (2002). Numerical calculation of psychrometric properties on a calculator. *Building and Environment*, *37*(4), 415-419. doi:10.1016/S0360-1323(01)00032-4

Sivakumar Babu, G.L., & Murthy, D.S.N. (2005). Reliability analysis of unsaturated soil slopes. *Journal of Geotechnical and Geoenvironmental Engineering*, *131*(11), 1423-1428.

Sofra, F. (2005). Understanding feed rheology in nickel laterite processing. In R. Jewell, & S. Barrera (eds.), *Paste 2005 – Proceedings of the 8th International Seminar on Paste and Thickened Tailings* (p. 29-44). Perth, Australia: Australian Centre for Geomechanics.

Sofra, F., & Boger, D.V. (2001). Slope prediction for thickened tailings and pastes. *Proceedings of Tailings and Mine Waste '01* (p. 75-83). Fort Collins, CO: A.A. Balkema.

Sofra, F., & Boger, D.V. (2002). Environmental rheology for waste minimisation in the minerals industry. *Chemical Engineering Journal*, *86*, 319-330.

Soilmoisture Equipment Corp. (1995). *1400/1405 Tempe pressure cell – Operating instructions*. Santa Barbara, CA: Soilmoisture Equipment Corp. From http://www.soilmoisture.com

Soilmoisture Equipment Corp. (2000). *1020 Pressure membrane extractor – Operating instructions*. Santa Barbara, CA: Soilmoisture Equipment Corp. From http://www.soilmoisture.com

Song, W.-K., Cui, Y.-J., Tang, A.M., Ding, W.-Q., & Tran, D.T. (2014). Experimental study on water evaporation from sand using environmental chamber. *Canadian Geotechnical Journal*, *51*(2), 115-128. doi:10.1139/cgj-2013-0155.

Sridharan, A., & Nagaraj, H.B. (2005). Hydraulic conductivity of remolded fine-grained soils versus index properties. *Geotechnical and Geological Engineering*, *23*, 43-60.

SRK (1989). *Acid rock drainage. Technical Guide. Vol. 1. British Columbia Acid Mine Drainage Task Force Report*. Vancouver, BC: Steffen, Robertson, Kirsten in Association with Norecol Environmental Consultants and Gormely Process Engineering.

SRK (2002). *Kahama Mining Corporation Limited, Tanzania, Reclamation and closure plan for the Bulyanhulu mine* (Report # 301581/1). Illovo, South Africa.

Stadler, S.J. (2005). Aridity indices. In J.E. Oliver (ed.), *Encyclopedia of world climatology*. (p. 89-94). SpringerLink. From http://www.springerlink.com/openurl.asp?genre=book&isbn=978-1-4020-3264-6

Stammers, W.N., Igwe, O.C. & Whiteley, H.R. (1973). Calculation of evaporation from measurements of soil water and the soil water characteristic. *Canadian Agricultural Engineering*, *15*, 2-5.

Steward, R.D., Rupp, D.E., Abou Najm, M.R. & Selker, J.S. (2016). A unified model for soil shrinkage, subsidence, and cracking. *Vadose Zone Journal, 15*(3). doi:10.2136/vzj2015.11.0146

Stone, K.J.L., Randolph, M.F., Toh, S., Sales, A.A. (1999). Evaluation of consolidation behavior of mine tailings. *Journal of Geotechnical Engineering*, *120*(3), 473-490.

Stormont, J.C., Farfan, E., Coonrod, J.E.A. (2009). Total soil water evaporation in a riparian environment: Model development and application. *Journal of Hydrologic Engineering*, 14(9). doi:10.1061/(ASCE)HE.1943-5584.0000069

Theriault, J.A., Frostiak, J., & Welch, D. (2003). Surface disposal of paste tailings at the Bulyanhulu gold mine, Tanzania. In G. Spiers, P. Beckett, & H. Conroy (eds.), *Sudbury 2003 - Mining and the Environment* (prof. 149). Sudbury, ON.

Theron, M., Addis, P.C., Wates, J.A., & Martin, V. (2005). Bulyanhulu mine (Tanzania) paste tailings facility: Relating the unsaturated properties of gold tailings to rate of rise. In R. Jewell, & S. Barrera (eds.), *Paste 2005 – Proceedings of the 8th International Seminar on Paste and Thickened Tailings* (p.219-229). Perth, Australia: Australian Centre for Geomechanics.

Thomas, E.G., Nantel, J.H., & Notley, K.R. (1979). *Fill technology in underground metalliferous mines*. Kingston, ON: International Academic Services Ltd.

Thornthwaite, C. W. (1948). An approach toward a rational classification of climate. *Geographical Review*, *38*(1), 55-94.

Tibble, P.A. (1997). *A survey of in situ oxygen consumption rates for sulphide tailings: Investigations on exposed tailings and selected remediation efforts*. (M.Sc. thesis, University of Waterloo, Waterloo, ON).

Tibble, P.A., & Nicholson, R.V. (1997). Oxygen consumption on sulphide tailings and tailings covers: Measured rates and applications. *Proceedings of the 4th International Conference on Acid Rock Drainage* (p. 647-661). Vancouver, BC.

Todd, D.K. (1980). Groundwater hydrology (2nd ed.). New York, NY: John Wiley & Sons.

Toh, S.H., & Fahey, M. (1991). Numerical and centrifuge modelling of large strain consolidation. In Beer, G., Booker, J.R., & Carter, J.P. (eds.), *Computer Methods and Advances in Geomechanics* (Vol. 1, p. 279-284). Cairns, Australia: Balkema.

Toussaint, R. (2016) *Influences des caractéristiques physico-chimiques de résidus miniers sulfureux sur leur réactivité à l'oxygène*. (M.A.Sc. thesis, École Polytechnique de Montréal, Montreal, QC).

Trajkovic, S. (2005). Temperature-based approaches for estimating reference evapotranspiration. *Journal of Irrigation and Drainage Engineering*, *131*(4), 316-323.

Trajkovic, S., Todorovic, B., & Stankovic, M. (2003). Forecasting of reference evaporation by artificial neural networks. *Journal of Irrigation and Drainage Engineering*, *129*(6), 454-457.

Tuller, M., & Or, D. (2005). Water films and scaling of soil characteristic curves at low water contents. *Water Resources Research*, *41*(9). doi:10.1029/2005WR004142

Uhlherr, P.H.T., Guo, J., Fang, T.N., & Tiu, C. (2002). Static measurement of yield stress using a cylindrical penetrometer. *Korea-Australia Rheology Journal*, *14*(1), 17-23. From http://infosys.korea.ac.kr/PDF/KARJ/KR14/KR14-1-0017.pdf

van Genuchten, M. Th. (1980). A closed-form equation for predicting the hydraulic conductivity of unsaturated soils. *Soil Science Society of America Journal*, *44*(5), 892-898.

van Genuchten, M.Th., Leij, F.J., & Yates, S.R. (1991). *The RETC code for quantifying the hydraulic functions of unsaturated soils* (Report # EPA/600/2-91/065). Ada, OK: U.S. Environmental Protection Agency.

Vanapalli, S.K., Fredlund, D.G., Pufahl, D.E., & Clifton, A.W. (1996). Model for the prediction of shear strength with respect to soil suction. Canadian Geotechnical Journal, *33*, 379-392.

Vanapalli, S.K., Wright, A., & Fredlund, D.G. (2000). Shear strength behavior of a silty soil over the suction range from 0 to 1 000 000 kPa. *Proceedings of the 53rd Canadian Geotechnical Conference and 1st Joint CGS/IAH-CNC Conference* (p. 1161-1168). Montreal, QC: Canadian Geotechnical Society.

Vanapalli, S.K., Nicotera, M.V. & Sharma, R.S. (2009). Axis translation and negative water column techniques for suction control. In Y.J. Cui, E. Romero, & A. Tarantino (eds.), *Laboratory and field testing of unsaturated soils* (p. 33-48). SpringerLink, doi:10.1007/978-1-4020-8819-3

Vanapalli, S.K., & Adem, H.H. (2013). A simple modeling approach for estimation of soil deformation behaviour of natural expansive soils using the modulus of elasticity as a tool. *Poromechanics V*, 1695-1704. doi:10.1061/9780784412992.201

Ventura, F., Spano, D., Duce, P., & Snyder, R.L. (1999). An evaluation of common evapotranspiration equations. *Irrigation Science*, 18, 163-170.

Verburg, R. (1997). Envrionmental benefits associated with the use of paste for surface disposal of tailings. *Proceedings of the 50th Canadian Geotechnical Conference* (p. 484-491). Ottawa, ON: Canadian Geotechnical Society.

Verburg, R. (2010). Potential environmental benefits of surface paste disposal. In R.J. Jewell, & A.B. Fourie (eds.), *Paste 2010 – Proceedings of the 13th International Seminar on Paste and Thickened Tailings* (p. 231-240). Perth, Australia: Australian Center for Geomechanics.

Verburg, R., Newman, P., & Fordham, M. (2006). Surface paste disposal of high-sulphide tailings – Field cell monitoring and pilot plant testing. *Proceedings of the 7th International Conference on Acid Rock Drainage*. St. Louis, MO: The Society for Mining, Metallurgy, and Exploration Inc.

Vick, S.G. (1983). *Planning, design, and analysis of tailings dams*. New York, NY: John Wiley & Sons.

Vietti, A.J., Boshoff, J.C.J., & Cope, A. (2011). Does thickening save water? *The Journal of The Southern African Institute of Mining and Metallurgy*, 111(2), 63-66. From http://www.saimm.co.za/Journal/v111n02p063.pdf

Villavicencio, A.G., Breul, P., Bacconnet, C., Boissier, D., & Espinace, A.R. (2011). Estimation of the variability of tailings dams properties in order to perform probabilistic assessment. *Geotechnical and Geological Engineering*, *29*(6), 1073-1084. doi:10.1007/s10706-011-9438-5

Villeneuve, M. (2005). *Évaluation du comportement géochimique à long terme de rejets miniers à faible potentiel de génération d'acide à l'aide d'essais cinétiques*. (M.A.Sc. thesis, École Polytechnique de Montréal, Montreal, QC).

Walvoord, M.A. (2002). *A unifying conceptual model to describe water, vapor, and solute transport in deep arid vadose zones*. (Ph.D. thesis, New Mexico Institute of Mining and Technology, Socorro, NM).

Walvoord, M.A., Plummer, M.A., Phillips, F.M., & Wolfsberg, A.V. (2002). Deep arid system hydrodynamics 1. Equilibrium states and response times in thick desert vadose zones. *Water Resources Research*, 38(12), doi:10.1029/2001WR000824

Walvoord, M.A., & Scanlon, B.R. (2004). Hydrologic processes in deep vadose zones in interdrainage arid environments. *Groundwater Recharge in a Desert Environment: The Southwestern United States. Water Science and Application 9* (p. 15-28). Washington, DC: American Geophysical Union.

Wang, Q., Shao, M., & Horton, R. (1999). Modified Green and Ampt models for layered soil infiltration and muddy water infiltration. *Soil Science, 164*(7), 445-453.

Weeks, B., & Wilson, G.W. (2003). The influence of solar radiation on evaporation for three-dimensional flux boundary modelling of soil cover systems on waste rock dumps. *Proceedings of the 6th International Conference on Acid Rock Drainage* (p. 711-717). Cairns, Australia: AusIMM.

Weiss, A. (1982). An experimental study of net radiation, its components and prediction. *Agronomy Journal*, 74, 871-874.

WEGS Consultants. (2002). *Hydrogeological review and assessment of groundwater monitoring and contamination risk at Bulyanhulu gold mine.* Arusha, Tanzania: WEGS Consultants.

Wheeler, S.J., Sharma, R.S., & Buisson, M.S.R. (2003). Coupling of hydraulic hysteresis and stress–strain behaviour in unsaturated soils. *Géotechnique, 53*(1), 41-54.

Williams, D.J. (2012). Some mining applications of unsaturated soil mechanics. Geotechnical *Engineering Journal of the SEAGS & AGSSEA, 43*(1), 89-98. From http://www.seags.ait.ac.th/83-98%20Williams%20-Some%20mining%20applications%20of%20Unsaturated%20SM%20-%20A.pdf

Williams, J. R., Ouyang, Y., & Chen, J. S. (1998). *Estimation of infiltration rate in the vadose zone: Application of selected mathematical models* (Report # EPA/600/R-97/128b). Washington, DC: United States Environmental Protection Agency (EPA).

Wilson, G.W. (1990). *Soil evaporative fluxes for geotechnical engineering problems*. (Ph.D. thesis, University of Saskatchewan, Saskatoon, SK).

Wilson, G.W., Fredlund, D.G., & Barbour, S.L. (1994). Coupled soil-atmosphere modelling for soil evaporation. *Canadian Geotechnical Journal, 31,* 151-161.

Wilson, G.W., Fredlund, D.G., & Barbour, S.L. (1997). The effect of soil suction on evaporative fluxes from soil surfaces. *Canadian Geotechnical Journal, 34,* 145-155.

Wilson, G.W., Wickland, B., & Fines, P. (2002). Concepts for co-mixing waste rock and tailings. *Proceedings of Symposium on Mines and the Environment*. Rouyn-Noranda, QC: Canadian Institute of Mining, Metallurgy and Petroleum.

Wilson, L.G. (1982). Monitoring in vadose zone: Part II. *Ground Water Monitoring & Remediation, 2*(1), 31-42. doi:10.1111/j.1745-6592.1982.tb00822.x

Yazdani, J. (1995). *Soil water characteristic curve for mine waste rock containing coarse material*. (M.Sc. thesis, University of Saskatchewan, Saskatoon, SK).

Yoder, R.E., Odhiambo, L.O., & Wright, W.C. (2005). Effects of vapor-pressure deficit and net-irradiance calculation methods on accuracy of standardized Penman-Monteith equation in a humid climate. *Journal of Irrigation and Drainage Engineering, 131*(3), 228-237.

Zhan, G. (2000). *Experimental and theoretical studies on leach pad hydraulics and transport behavior during rinsing*. (Ph.D. thesis, University of Nevada, Reno, NV).

Zhan, G. (2003). *Cover design: Bazza waste dump facility*. Elko, NV: Barrick Goldstrike Mines.

Zhang, L., Hickel, K., Dawes, W.R., Chiew, F.H.S., Western, A.W., & Briggs, P.R. (2004). A rational function approach for estimating mean annual evapotranspiration. *Water Resources Research*, *40*(2). doi:10.1029/2003WR002710.

Zhou, Z., Scales, P.J., & Boger, D.V. (2001). Chemical and physical control of the rheology of concentrated metal oxide suspensions. *Chemical Engineering Science*, *56*, 2901-2920.

APPENDIX A – VOLUMETRIC WATER CONTENT PROFILES: FIELD CLIMATIC DATA SIMULATIONS

(a) Annual climate

(Simulation #1)

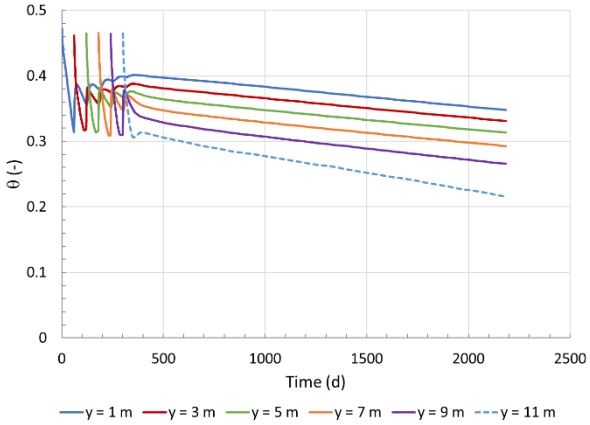

(b) Monthly climate

(Simulation #2)

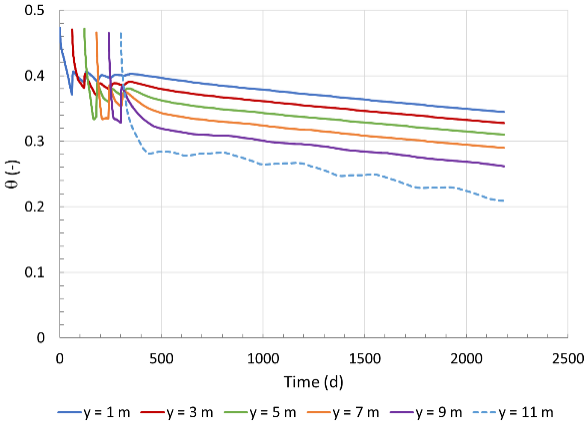

(c) Daily climate

(Simulation #3)

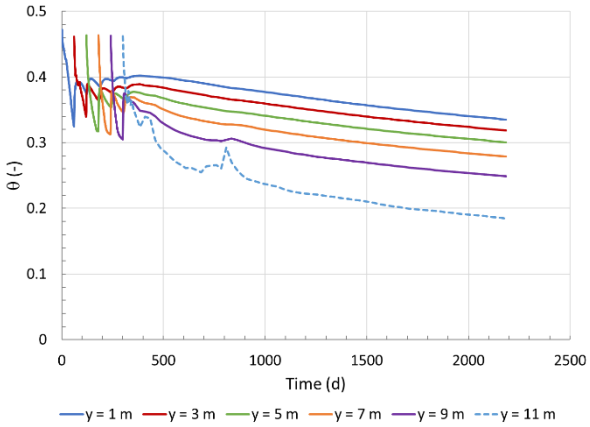

APPENDIX B – SUCTION PROFILES: FIELD CLIMATIC DATA SIMULATIONS

(a) Annual climate

(Simulation #1)

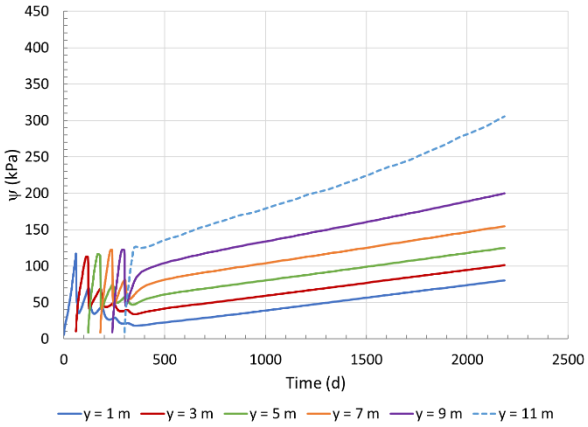

(b) Monthly climate

(Simulation #2)

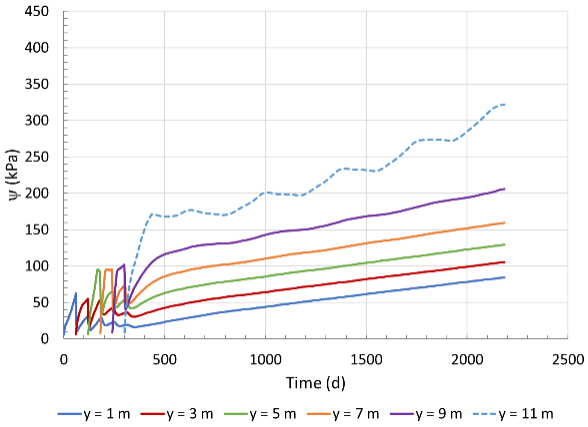

(c) Daily climate

(Simulation #3)

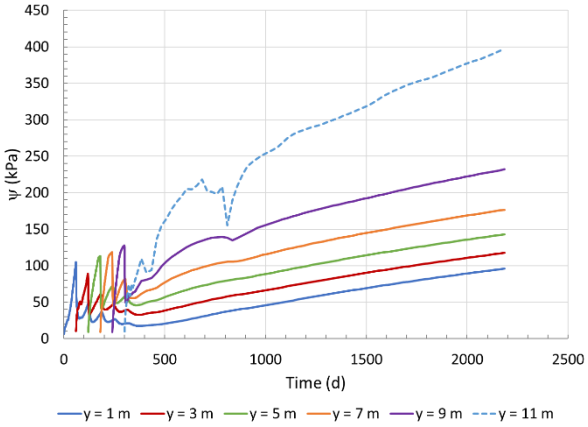

APPENDIX C – VOLUMETRIC WATER CONTENT PROFILES: DEPOSITION RATE AND LAYER THICKNESS SIMULATIONS

(a) 50 cm layers

(Simulation #4)

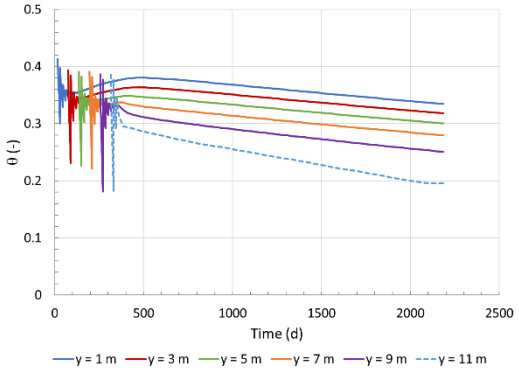

(b) 1 m layers

(Simulation #5)

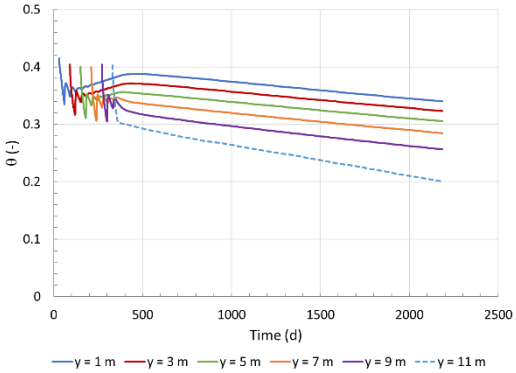

(c) 1.5 m layers

(Simulation #6)

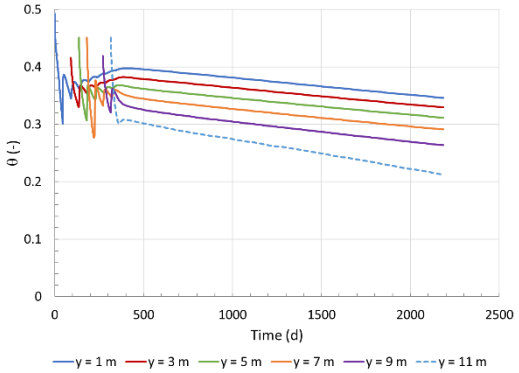

(d) 2 m layers

(Simulation #1)

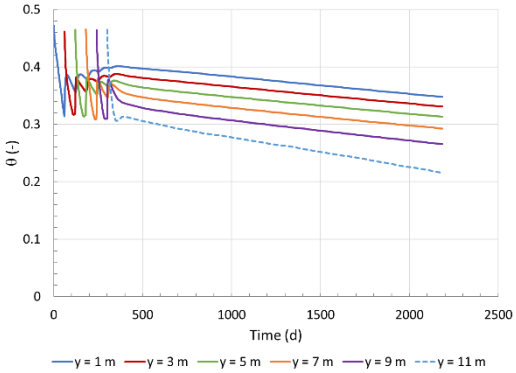

(e) 6 m layers

(Simulation #7)

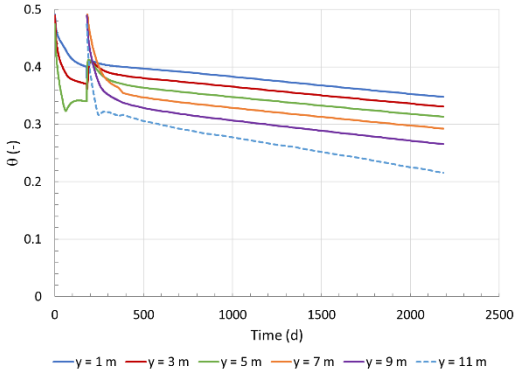

(d) 12 m layer

(Simulation #8)

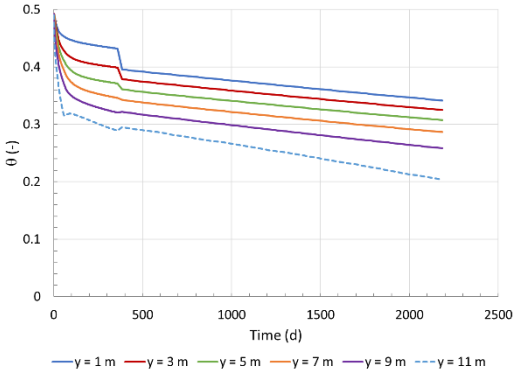

APPENDIX D – SUCTION PROFILES: DEPOSITION RATE AND LAYER THICKNESS SIMULATIONS

(a) 50 cm layers

(Simulation #4)

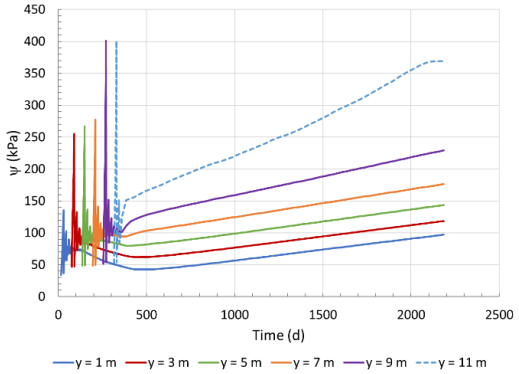

(b) 1 m layers

(Simulation #5)

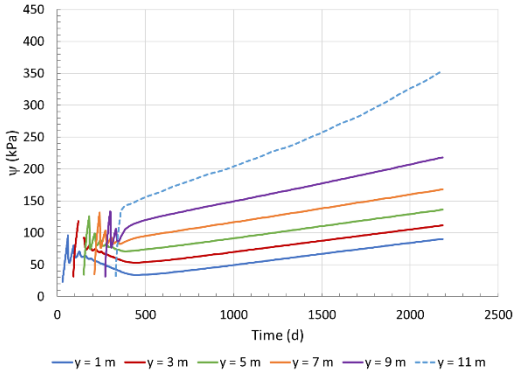

(c) 1.5 m layers

(Simulation #6)

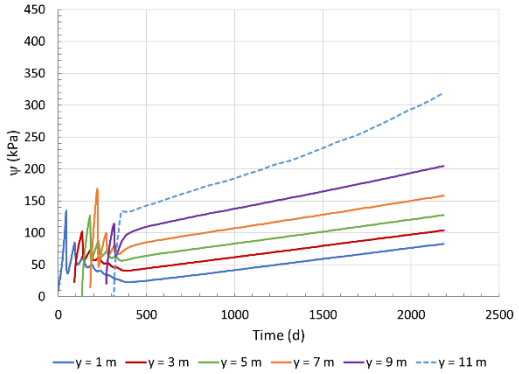

(d) 2 m layers

(Simulation #1)

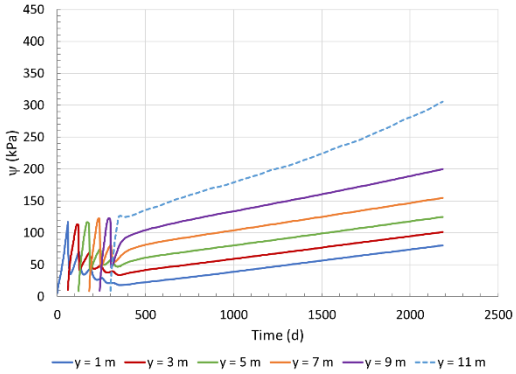

(e) 6 m layers

(Simulation #7)

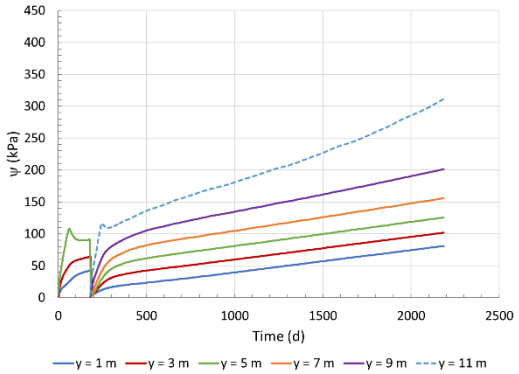

(d) 12 m layer

(Simulation #8)

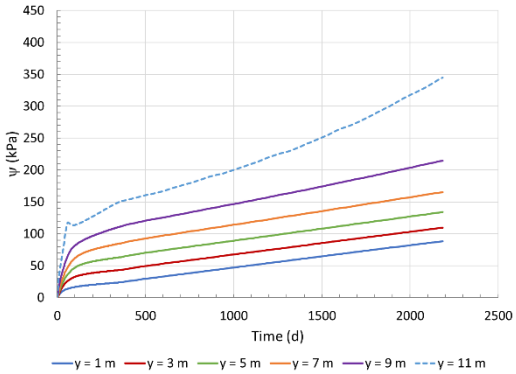

APPENDIX E – VOLUMETRIC WATER CONTENT PROFILES: RESTING TIME SIMULATIONS

(a) 30 days

(Simulation #9)

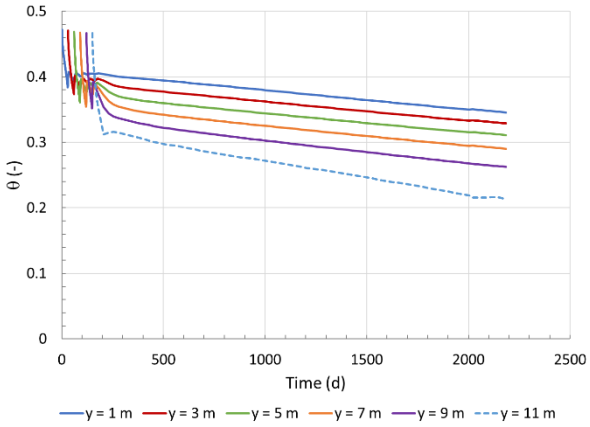

(b) 60 days (Baseline)

(Simulation #1)

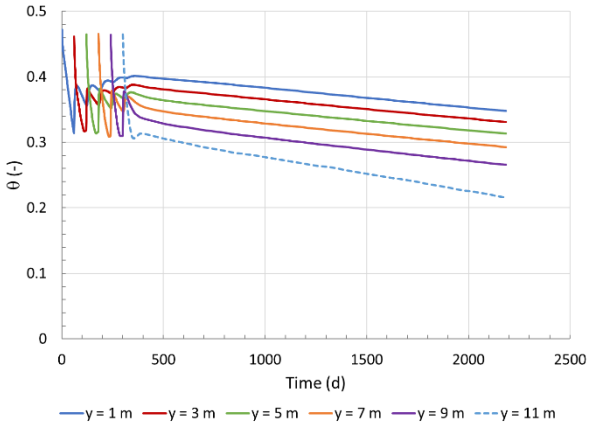

(c) 120 days

(Simulation #10)

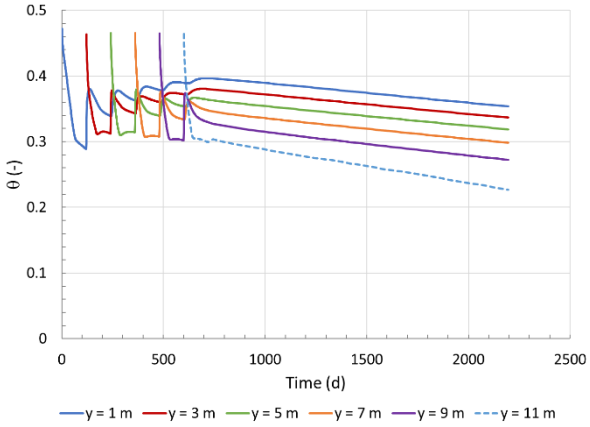

APPENDIX F – SUCTION PROFILES: RESTING TIME SIMULATIONS

(a) 30 days

(Simulation #9)

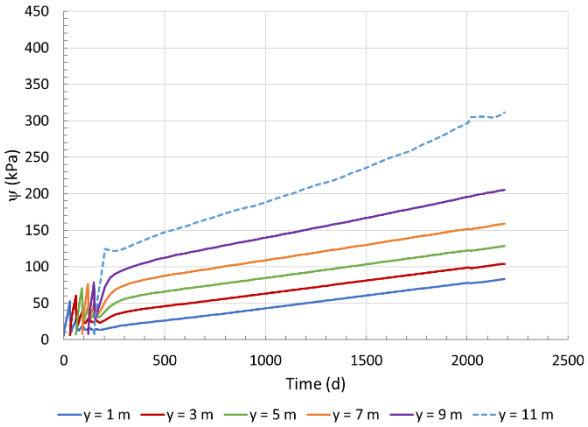

(b) 60 days (Baseline)

(Simulation #1)

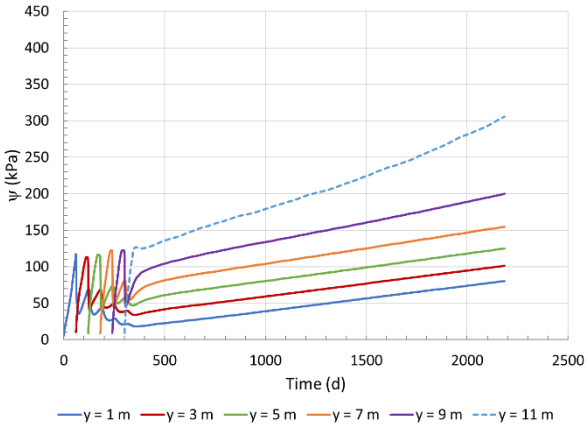

(c) 120 days

(Simulation #10)

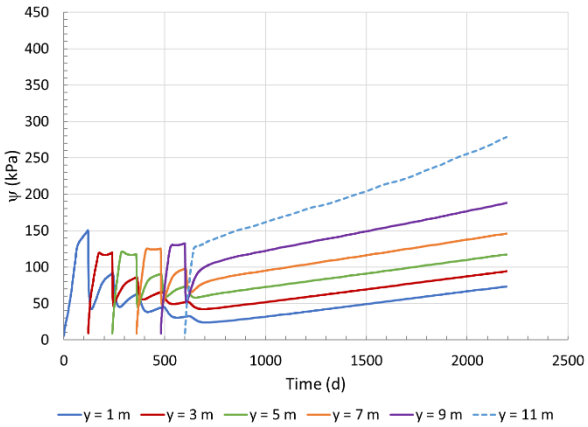

APPENDIX G – VOLUMETRIC WATER CONTENT PROFILES: TAILINGS PROPERTIES SIMULATIONS

(a) Baseline (Two materials)

(Simulation #1)

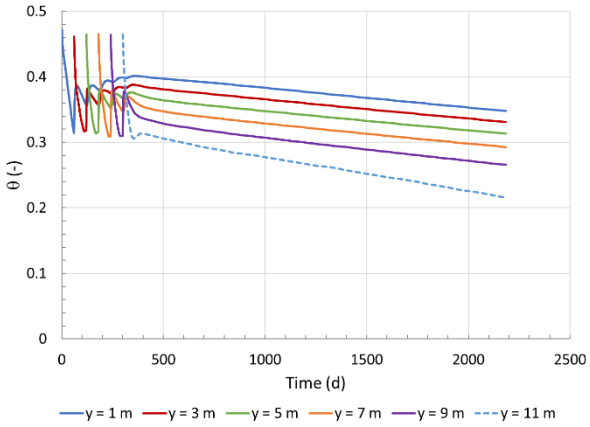

(b) One material (consolidated tailings)

(Simulation #11)

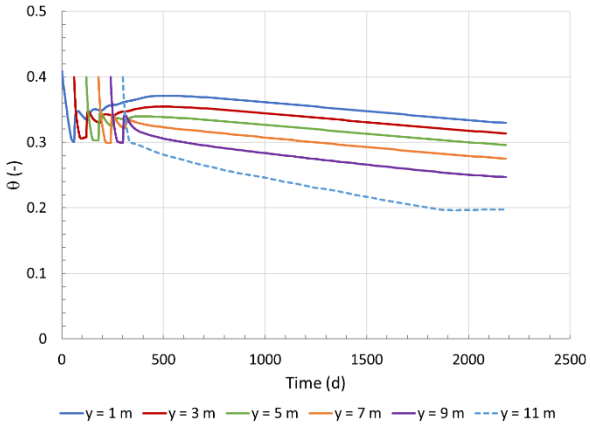

(c) Osisko

(Simulation #12)

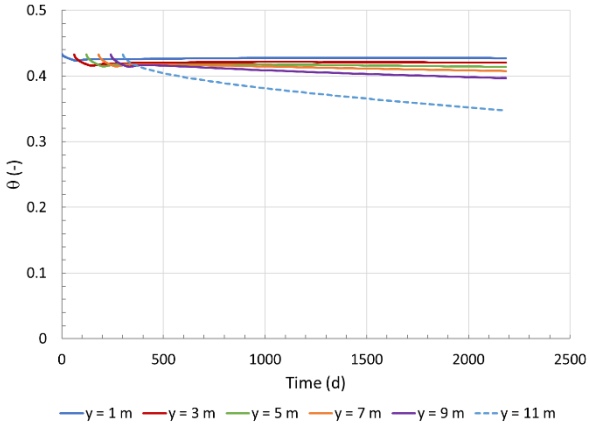

(d) Goldex

(Simulation #13)

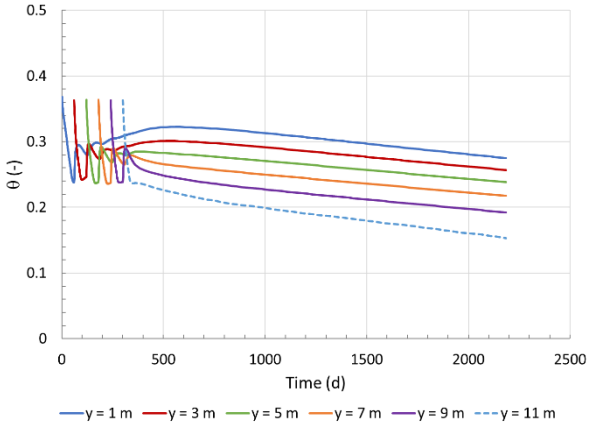

APPENDIX H – SUCTION PROFILES: TAILINGS PROPERTIES SIMULATIONS

(a) Baseline

(Simulation #1)

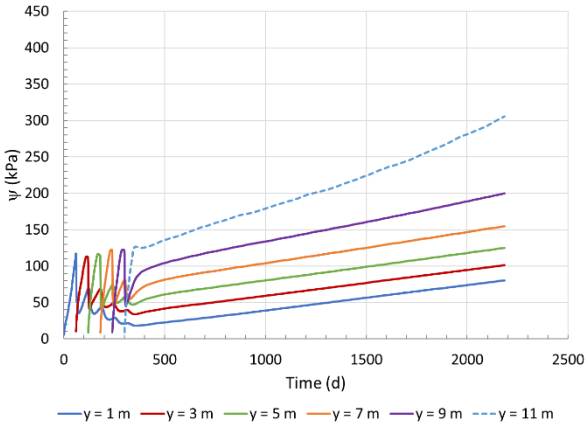

(b) One material (partially saturated tailings)

(Simulation #11)

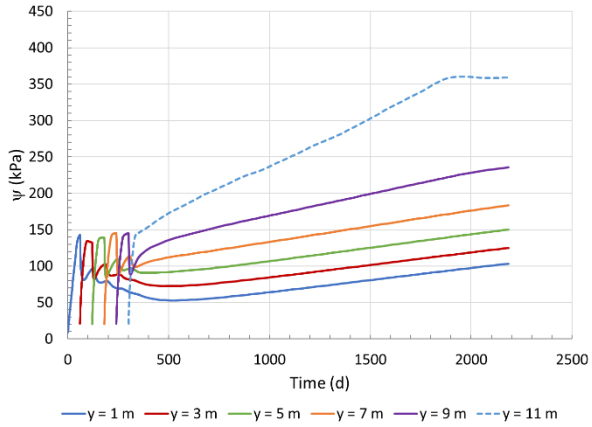

(c) Osisko

(Simulation #12)

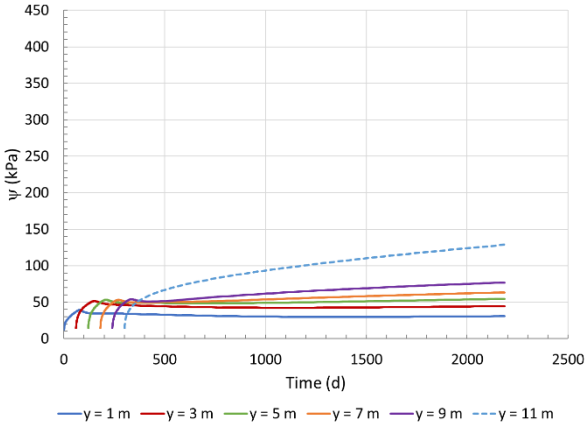

(d) Goldex

(Simulation #13)

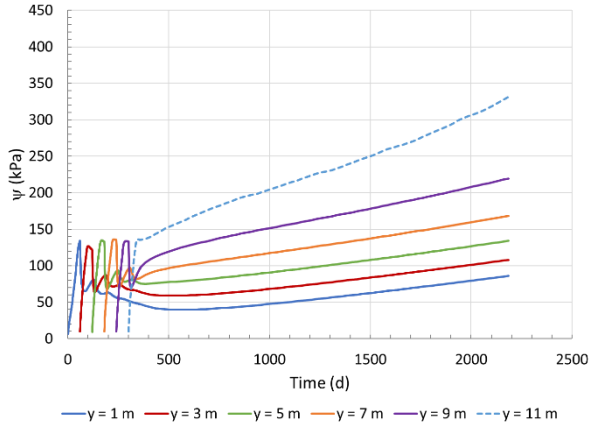

APPENDIX I – VOLUMETRIC WATER CONTENT PROFILES: SUBSOIL PROPERTIES SIMULATIONS

(a) Baseline

(Simulation #1)

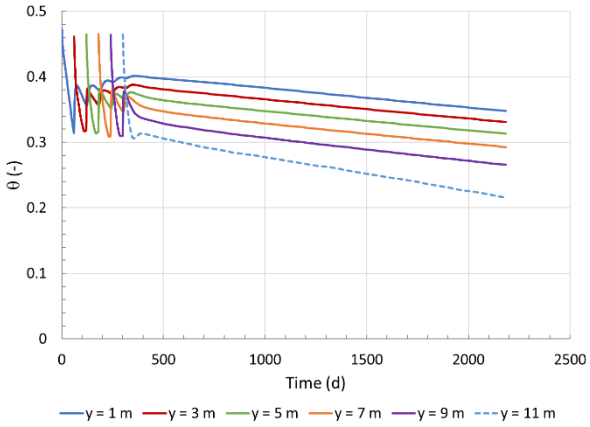

(b) Clay

(Simulation #14)

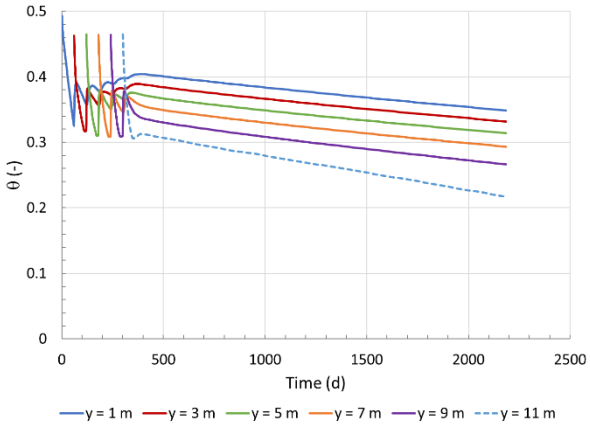

APPENDIX J – SUCTION PROFILES: SUBSOIL PROPERTIES SIMULATIONS

(a) Sand (Baseline)

(Simulation #1)

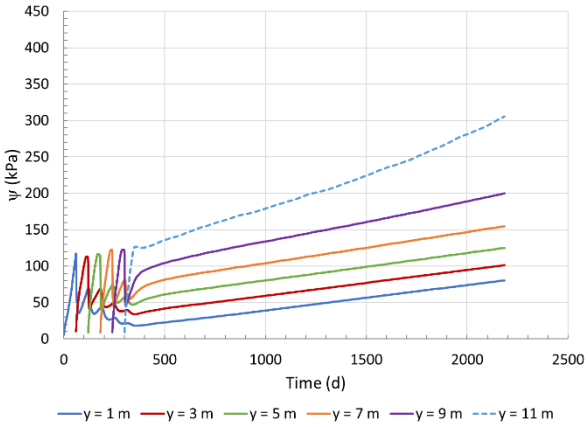

(b) Clay

(Simulation #14)

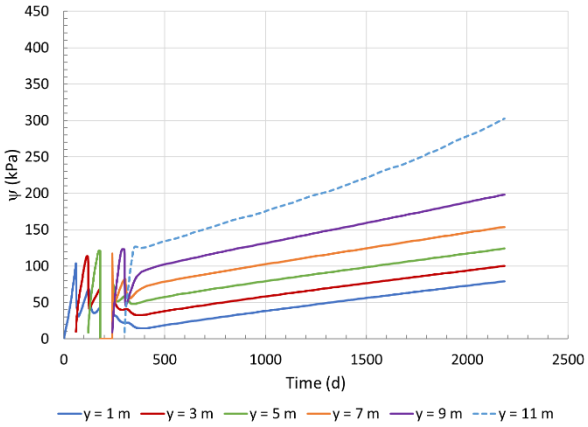

APPENDIX K – VOLUMETRIC WATER CONTENT PROFILES: WATER TABLE DEPTH SIMULATIONS

(a) WT @ y = -12 m (Baseline)

(Simulation #1)

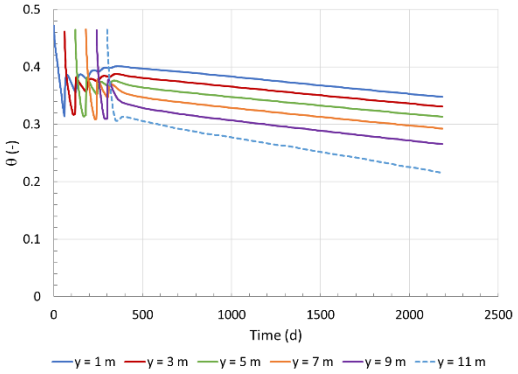

(b) WT @ y = -6 m

(Simulation #15)

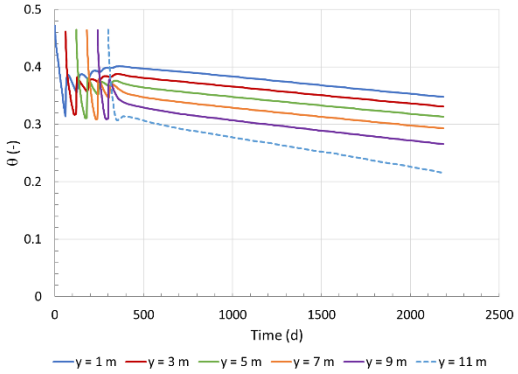

(c) WT @ y = -3 m

(Simulation #16)

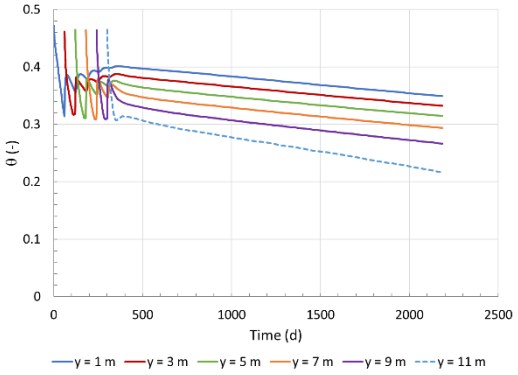

(d) WT @ y = -2 m

(Simulation #17)

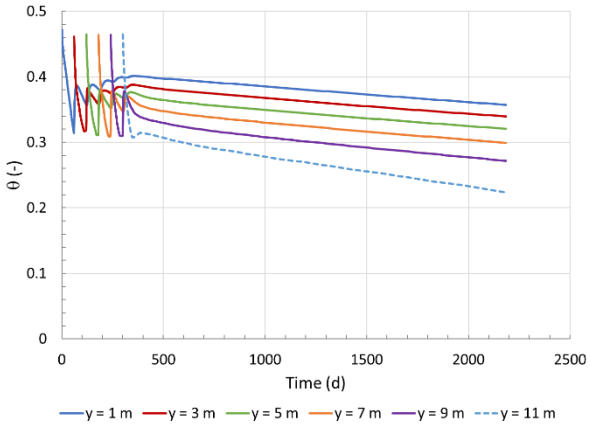

(e) WT @ y = -1 m

(Simulation #18)

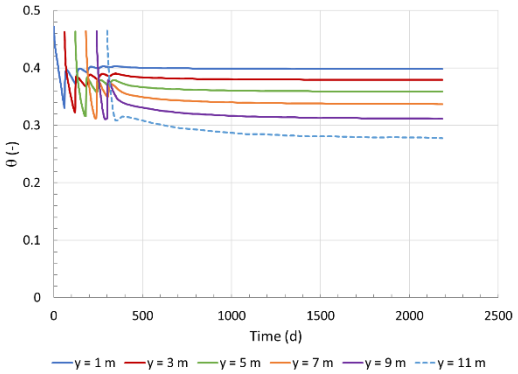

(f) WT @ y = 0 m

(Simulation #19)

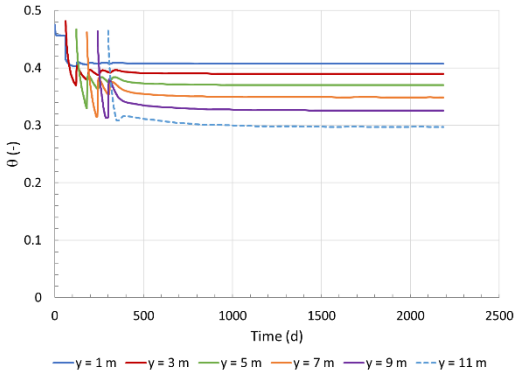

APPENDIX L – SUCTION PROFILES: WATER TABLE DEPTH SIMULATIONS

(a) WT @ y = -12 m (Baseline)

(Simulation #1)

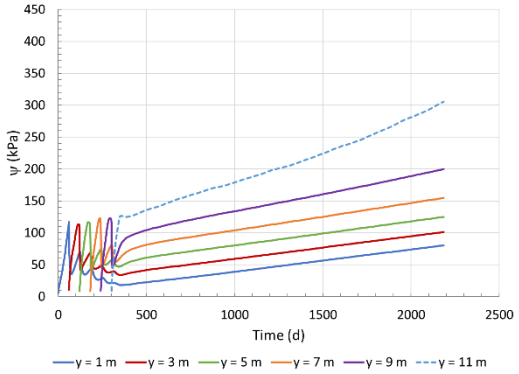

(b) WT @ y = -6 m

(Simulation #15)

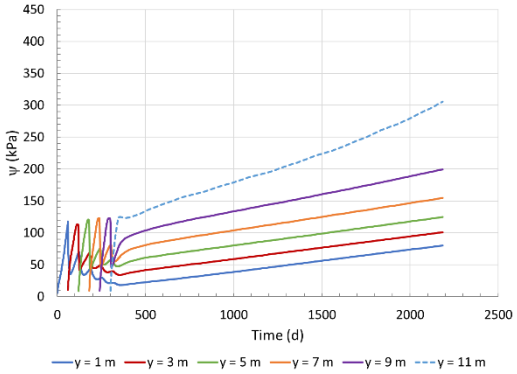

(c) WT @ y = -3 m

(Simulation #16)

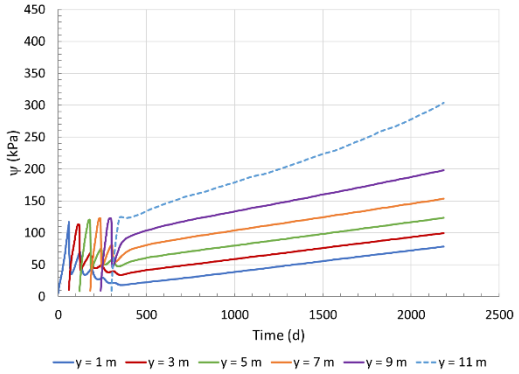

(d) WT @ y = -2 m

(Simulation #17)

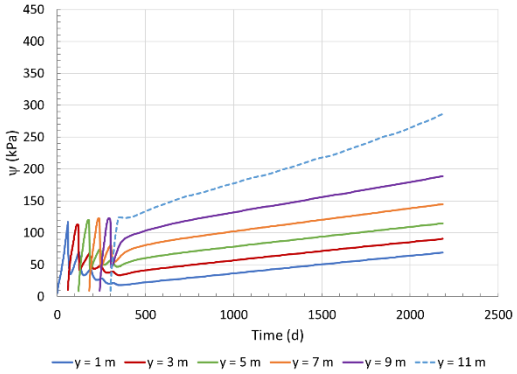

(e) WT @ y = -1 m

(Simulation #18)

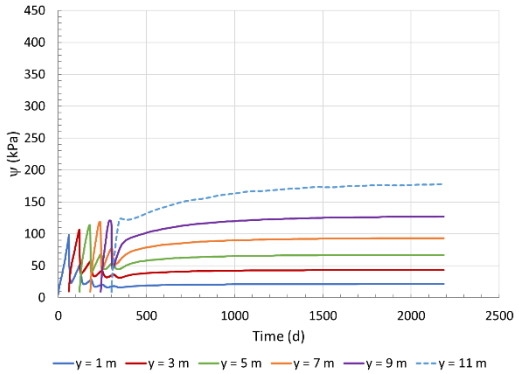

(f) WT @ y = 0 m

(Simulation #19)

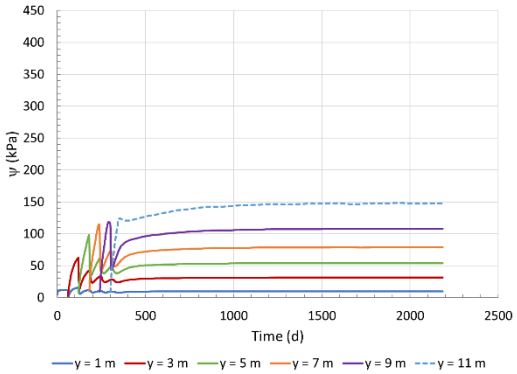

APPENDIX M – VOLUMETRIC WATER CONTENT: OTHER SITE SPECIFIC CLIMATIC CONDITIONS SIMULATIONS

(a) Bulyanhulu

(Simulation #2)

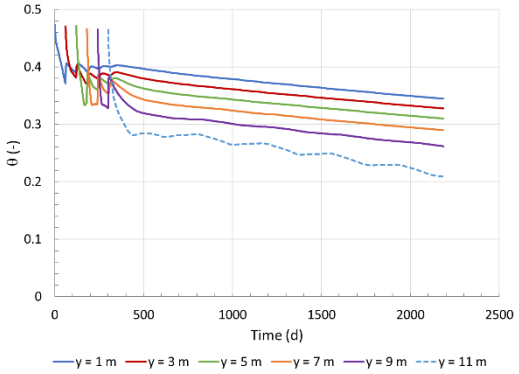

(b) Goldstrike

(Simulation #25)

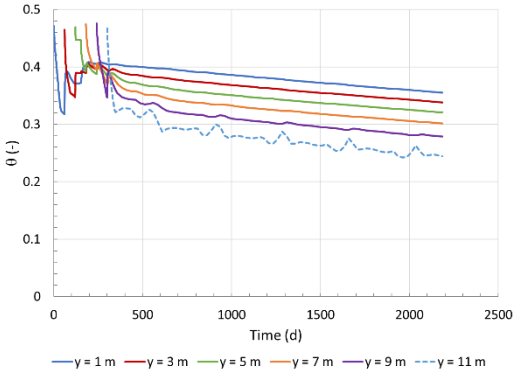

(c) Kalgoorlie

(Simulation #26)

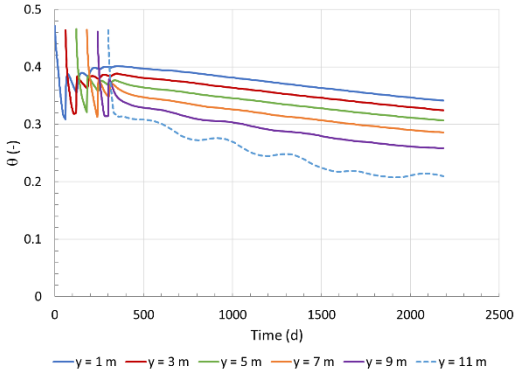

(d) Porgera

(Simulation #27)

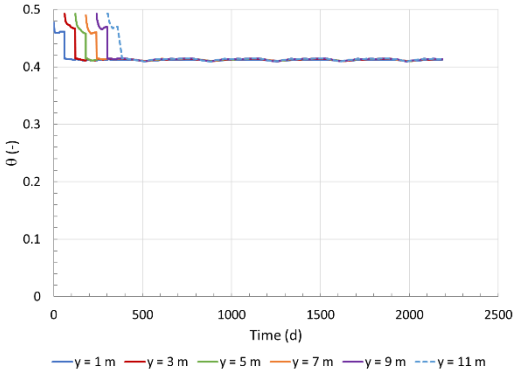

(e) Val-d'Or

(Simulation #28)

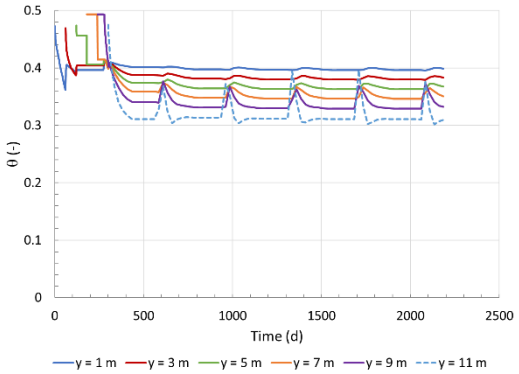

APPENDIX N – SUCTION PROFILES: OTHER SITE SPECIFIC CLIMATIC CONDITIONS SIMULATIONS

(a) Bulyanhulu

(Simulation #2)

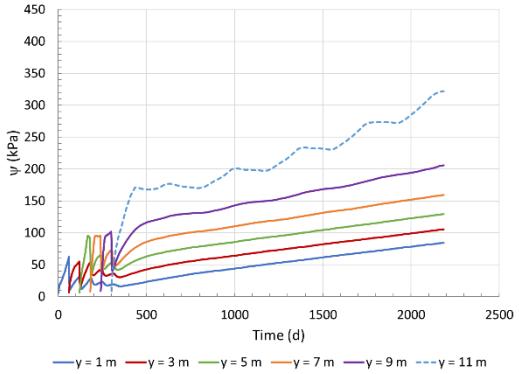

(b) Goldstrike

(Simulation #25)

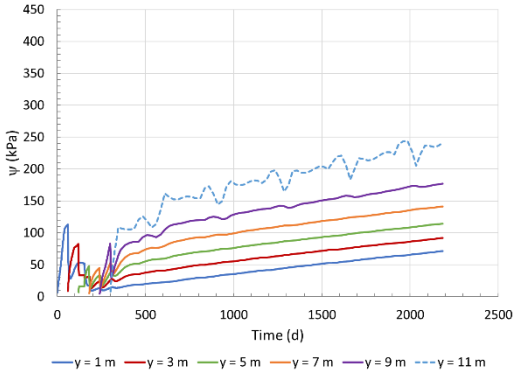

(c) Kalgoorlie

(Simulation #26)

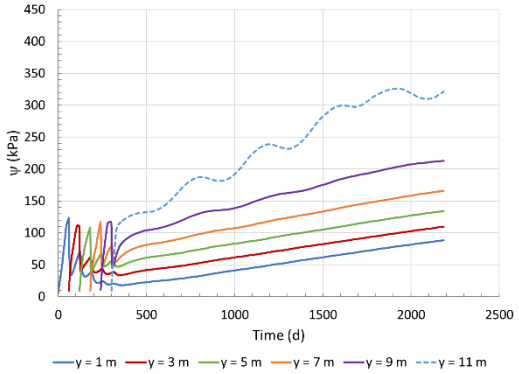

(d) Porgera

(Simulation #27)

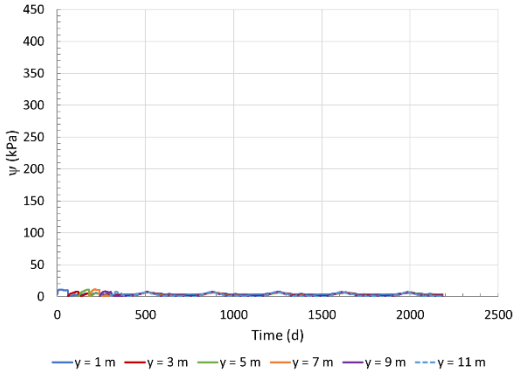

(e) Val-d'Or

(Simulation #28)